GLOBAL MODELING OF SECONDARY ORGANIC AEROSOL FORMATION: FROM ATMOSPHERIC CHEMISTRY TO CLIMATE

By

Guangxing Lin

A dissertation submitted in partial fulfillment
of the requirements for the degree of
Doctor of Philosophy
(Atmospheric, Oceanic and Space Sciences)
in the University of Michigan
2013

Doctoral Committee:
Professor Joyce E. Penner, Co-Chair
Assistant Professor Mark G. Flanner, Co-Chair
Assistant Professor Valeriy Y. Ivanov
Research Professor Sanford Sillman

ACKNOWLEDGEMENTS

Looking back my six years at University of Michigan, I owe a debt of gratitude to many people, without whom this work would not have been possible. They all made my studies at Michigan an enjoyable and memorable time of my life.

I would like to start by thanking my major advisor, Dr. Joyce Penner, for helping to guide and shape my graduate experience. Thanks to her for leading me to the amazing area in atmospheric chemistry, aerosol and climate. She has a sharp and ahead-of-others vision in this field, always giving me a "big picture" for my work, so that I didn't get lost in the tiny coding and plotting things. Thanks for her "infinite" questions, letting me look at a problem deeper and more thoroughly, and ensuring the quality of my work. Her enthusiasm and passion on science sets up a good example for me to follow in my future career.

Most graduate students are lucky to have one advisor care about their research. I have been very fortunate to have Dr. Sandy Sillman as my co-advisor, and Dr. Mark Flanner as my third advisor. Sandy has taught me a lot in atmospheric chemistry. In my first year's study, he even taught me hand by hand how to use, check and debug his chemistry solver. Every time I had a problem with chemistry, I always turned to Sandy for help and never got disappointed. As he has retired, I would like to take this opportunity to wish him best luck in the future. Dr. Mark Flanner has given me many advise on the radiative effect of organic aerosol on snow and ice. I was amazed that he replied to my emails very quickly

when I have questions for him. Dr. Valeriy Ivanov is the cognate member. I am grateful to him for his critical suggestions and comments on my thesis.

I want to thank all other members in Joyce's group: Minghuai, Luis, Roy, Li, Erika, Yuxing, Xi and Cheng. They all gave me valuable suggestions on my research. I would also like to give many thanks to all other AOSS friends who shared my daily life and work here. In addition, I would like to thank AOSS staffs for all their assistance and support.

My parents and my elder sister deserve special thanks for their caring and love. It has been 18 years since I left home to another town for study. Wherever I go, I know they are and will always there for me.

Finally, my wife, Ran, has been wonderful, possessing an abundance of patience throughout this journey. I am grateful for her support and for her encouragements.

TABLE OF CONTENTS

LIST OF TABLES

LIST OF FIGURES

LIST OF APPENDICES

CHAPTER 1

Introduction

Aerosols are small liquid or solid particles suspended in the atmosphere (excluding cloud droplets and ice crystals), consisting of mineral dust, sea salt, sulfate, nitrate, ammonium, soot and organic aerosol. They can be either emitted as primary aerosols (e.g., dust or soot) or formed by the conversion of sulfur dioxide, nitrogen oxides, ammonia and hydrocarbons in atmospheric chemical reactions to sulfates, nitrates and ammonium compounds, and secondary organic aerosol (SOA). Aerosols represent a relatively small fraction of atmosphere mass but are important components of the earth system.

1.1 The importance of aerosols

Aerosols have a large impact on air pollution & air quality, biogeochemistry, and climate.

Aerosols with an aerodynamic diameter smaller than 2.5 μm ($PM_{2.5}$) as well as ozone are mostly responsible for hazardous air pollution with serious health impacts on cardiovascular and respiratory disease and lung cancer, and their increased concentration could cause an extra mortality (Lelieveld et al., 2013). For instance, anthropogenic $PM_{2.5}$ has been showed to be connected with 3.5 ± 0.9 million cardiopulmonary and 220,000 ± 80,000 lung cancer mortalities annually (Susan et al., 2010) by using the health impact function to relate changes in mortality to change in $PM_{2.5}$ concentrations between present

day (year 2000) and preindustrial times, as simulated by a global chemical transport model.

Aerosol can affect the biogeochemistry either in a direct way through its deposition of nutrients (e.g., carbon, nitrogen, phosphorus, and iron) on land or ocean or indirectly by changing climate (Mahowald et al., 2011). First of all, tens of Tg (tera-grams) of carbon can be deposited to ecosystems from atmospheric organic aerosol. Secondarly, nitrate aerosol due to human activities through fossil fuel combustion and the application of artificial nitrogen fertilizer to soils can change the deposition of nitrogen into the surface, which further increases the productivity and thus decreases carbon in ecosystems (Galloway et al, 2008). In addition, the input of phosphorus from atmospheric dust aerosols might play a major role in many ecosystems on a 1,000- to 100,000- year time scale in maintaining soil fertility (Okin et al., 2004). Finally, the dust aerosol can also supply the most important nutrient (i.e., iron) for ocean biogeochemistry (Boyd, 1998).

Aerosol particles can influence climate by changing the earth energy budget in several ways: they can scatter and absorb the radiation directly (direct effects). They can also act as cloud condensation nuclei (CCN), around which clouds can form, and hence modify the radiative properties (e.g., reflectivity), amount and lifetime of clouds (indirect effects). Light-absorbing aerosols (e.g., soot) can have another indirect effect on climate by depositing into land snow or sea ice and further changing their albedo.

Key parameters determining the direct effects of aerosols are their optical properties (Penner et al, 2001). These optical properties can be summarized in terms of aerosol extinction coefficient (the fraction of the light lost from aerosol scattering and absorption

per unit thickness of aerosol, with a unit of m^{-1}), of single scattering albedo (the ratio of reflected light to the total intercepted (absorbed and reflected) light), and of scattering phase function (the chances of a photon of light being scattered in a particular direction) (Liou, 2002). These optical properties depend on aerosol particles' size distribution. To a first approximation, the aerosol extinction coefficient of an aerosol is maximized when the wavelength of incoming light and the size of the particle are about the same according to mie scattering theory. Given the different wavelength between short-wave radiation (e.g., sun light) and long-wave radiation (e.g., infrared), the particles with different sizes have different efficiencies for light extinction. Incoming solar radiation (where most energy is present at wavelengths between 0.4 and 1 micrometer) is effectively scattered or reflected by particles in the size range of 0.1 to 1 micrometer (mostly fine particles) (Liou, 2002), whereas the long-wave radiation is only likely scattered by particles of roughly an order magnitude larger size (Liou, 2002). In addition to the size, the composition of aerosol is also important to determine the direct effects of aerosol on climate. First, the aerosol composition determine how much water it can absorb from the ambient atmosphere (the hygroscopicity), which sometimes can dominate the aerosol mass (Chuang et al., 1997). Secondly, the aerosol composition controls the "color" of the aerosol: the ability to absorb the solar radiation (the refractive index of the aerosol). Generally, dark color particles (e.g., soot) absorb more solar radiation and heat the atmosphere, while the light color particles (e.g., sulfate) mainly scatter the sunlight back to space and thus cool the atmosphere.

The indirect effect of aerosol particles on climate depends on their capacity to act as CCNs, which is a function of aerosol size distributions, aerosol number concentrations,

aerosol composition, and ambient environment conditions (Penner et al., 2001). A solution droplet grows by condensation of water vapor onto one particle in a vapor pressure equilibrium relationship described by the Köhler theory (Rogers and Yau, 1989). Once the droplet size reaches a threshold value (critical size), the droplet enters into an unstable growth regime and will automatically grow to cloud droplet size if the ambient water vapor pressure is still lager than the equilibrium vapor pressure, and the particle is activated to a CCN (Rogers and Yau, 1989). This critical size depends on the initial particle size and also its hygroscopicity, a function of the particle composition. In general, if more aerosols are emitted into the atmosphere (e.g., fossil fuel emissions) acting as CCN, liquid clouds with the total cloud water content held constant will consist of more, but smaller, droplets, causing the cloud to be more reflective (first indirect effect). Due to the smaller size of cloud droplets, the formation of precipitation may be suppressed, resulting in a longer cloud lifetime and larger cloud cover or cloud height (second indirect effect).

Even a small amount of absorbing aerosols deposited into snow and sea ice can reduce albedo because the reflectivity of snow and ice is extremely high and because multiple scattering in the snow pack greatly increases the chances that the absorbing aerosols will intercept the light (Wiscombe et al., 1980; Warren et al., 1980).

1.2 Uncertainty of aerosol's effect on climate

Despite the importance of aerosol in determining the earth's radiation budget, its effect still remains the least understood part according to the IPCC 2007 fourth assessment

report (Foster et al., 2007). Figure 1-1 shows changes in the anthropogenic aerosols since 1750 have resulted in a globally averaged net radiative forcing of roughly -1.2 W/m^2, in comparison to the overall average CO_2 forcing of +1.66 W/m^2 (Forster et al., 2007). This figure also shows the level of scientific understanding of aerosols climate influence is "low" to "medium-low", although they are contributing the largest negative forcing.

The low understanding of aerosol climate impact hinders our ability to assess the result of emission control, to constrain the climate sensitivity of CO_2, and thus to further project the future climate change. As we are reducing the fossil fuel use to improve the air quality and to slow down the global warming, we need to understand how this decreases the aerosol formation and might hide the effect of decreasing CO_2, since the aerosol cools the earth, counter balancing the warming effect of CO_2. The climate sensitivity of CO_2 represents how the earth surface temperature changes given a doubling of CO_2. The deficient understanding of aerosol's climate effect confounds the interpretation of the climate sensitivity. Thus, a better understanding of aerosol's climate effect might improve the accuracy of future climate prediction.

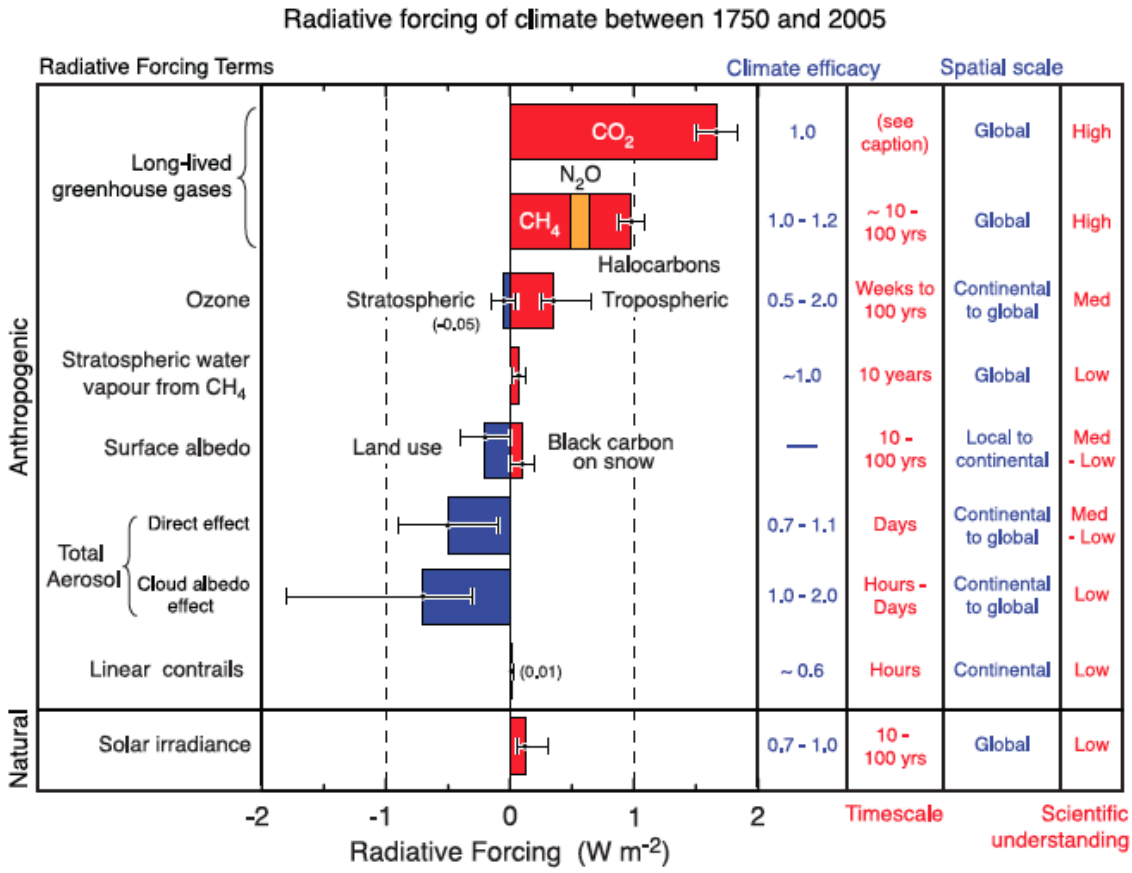

Figure 1-1 Radiative forcing of climate between 1750 and 2005 caused by different agents (Forster et at., 2007).

To narrow the error bars in Figure 1-1, we need to accurately represent aerosols' source, atmospheric evolution, and properties in the model. Organic aerosol (OA) explains about 45% the atmospheric aerosol mass (Zhang et al., 2007; Jimenez et al., 2009), and sometimes the fraction can be up to 90% (Kanakidou et al., 2005). Organic aerosol can be either directly emitted into the atmosphere as primary organic aerosol (POA) from biomass burning, fossil fuel and biofuel use, sea spray, and biological organisms (e.g., fungi, spores, pollen, etc.), or are formed by atmospheric oxidation of volatile organic compounds (VOCs) as secondary organic aerosol (SOA). Up to 95% of the total OA is shown to be secondary in rural region (Zhang et al., 2007;Jimenez et al., 2009). However,

SOA remains the least understood aerosol component because organics (gas + particle) comprises of a mixture of hundreds of thousands of organic compounds (Goldstein and Galbally, 2007), with each compound further undergoing a number of atmospheric reactions to produce a range of oxidized products (Hallquist et al., 2009). Due to the complexity of SOA, very few radiative forcing estimates of SOA exist, and SOA was included in the AeroCom exercise in an extremely simple way- as primary organic aerosol (Forster et al., 2007). Moreover, all of it was assumed to be natural and thus the radiative effect of anthropogenic SOA was neglected. One purpose of this thesis, therefore, is to estimate the radiative effect of SOA in a more realistic way. In addition, Figure 1-1 only gave us the effect of BC on snow on the surface albedo, but didn't include the effect of another light-absorbing agent – organic aerosol. Thus, this thesis will also try to examine the effect of organic aerosol on snow surface albedo.

1.3 Secondary organic aerosol formation

SOA can be formed from the oxidation of both natural emissions of VOCs from plants and vegetation (i.e. biogenic VOCs,) and anthropogenic VOCs (e.g., aromatics and alkanes). On a global basis, isoprene (2-methyl-1,3-butadiene, C_5H_8) is the most abundant non-methane biogenic VOC (Guenther et al., 1995) and it is thought to make great contribution to SOA formation (Henze et al. 2008). Most of SOA formation was shown to be associated with isoprene as well as monoterpene ($C_{10}H_{16}$) both in the model simulation (Tsigaridis et al., 2006; Henze et al., 2008) and measurements (Szidat et al., 2009; Goldstein et al., 2009). VOCs emitted by anthropogenic sources may produce a minor fraction of global SOA (Tsigaridis and Kanakidou, 2003). However, on the regional scale, they can contribute to the SOA formation significantly (Vutukuru et al.,

2006). Among these anthropogenic VOCs, aromatic compounds account for the majority of ambient SOA formation, followed by alkanes and alkenes (Vutukuru et al., 2006).

In the traditional theory of SOA formation (Pankow 1994), VOCs were oxidized in the gas phase to form several generations of products with different volatilities. The highly volatile products remained in the gas phase and might further undergo reactions with other gaseous species, while the semi-volatile products would condense on the pre-existing aerosols (e.g. POA) to form SOA. The gaseous semi-volatile VOCs were in equilibrium with their condensed part through so called gas-particle partitioning. In addition to the gas-particle partitioning of semi-volatile VOCs, the low volatile compounds formed from the condensed phase reactions of organic compounds has also been established as a major component of SOA over the last 5–10 years. Condensed-phase reactions can cause the vapor pressure of organics to be lowered by several orders of magnitude, either by oxidation or formation of high-molecular-weight species (e.g., through oligomerization) (Hallquist et al., 2009). The rate of formation of these low volatile compounds increases in the presence of inorganic acid seed aerosol, at least for the products formed in the ozonolysis of alpha-pinene (Jang et al., 2006; Czoschke et al., 2003; Iinuma et al., 2004; Gao et al., 2004). Additionally, in regions where isoprene is present under low NO_x conditions, epoxydiols can form (Paulot et al., 2009) and their reactive uptake on acidic sulphate aerosols (Minerath and Elrod, 2009) may lead to a 20-fold increase in OA mass yields from isoprene (Surratt et al., 2010). Similarly, the aqueous phase reactions of organic compounds in both cloud droplets and aqueous ammonium sulfate particles have been suggested as a potentially important source of SOA (Blando and Turpin, 2000; Lim et al., 2005; Carlton et al., 2007; Ervens et al.,

2011; Kroll et al., 2005; Liggio et al., 2005). Another potential source of SOA is through the oxidation of evaporated primary organic aerosol (POA) vapors (Robinson et al., 2007). The non-volatile primary organic aerosol (POA) from diesel exhaust and biomass burning is known to include low-volatility compounds that partition between the gas and aerosol phase. These can then undergo gas-phase oxidation to form species of different volatilities that form SOA (Robinson et al., 2007; Huffman et al., 2009).

To predict ambient SOA growth correctly requires an accurate model of SOA formation mechanism. Traditionally, SOA formation was described by an absorptive model including only the gas-particle partitioning process with empirical parameters derived from laboratory measurements. However, this simple equilibrium model cannot represent the full complexity and the dynamics of SOA production (e.g., the SOA formation through aerosol phase and aqueous phase reactions described in the paragraph above). Indeed, recent measurements have also shown that models with this simple scheme substantially under-estimate the amount of SOA in the atmosphere, often by an order of magnitude or more (e.g., Volkamer et al., 2006; Kleinman et al., 2008; Simpson et al., 2007; Heald et al., 2005). To close the gap between the measured SOA and predicted SOA, this thesis fully accounts for the up to date SOA formation mechanisms using an explicit photochemical model with detailed gaseous and aqueous photochemical reactions.

The objectives of this thesis are to develop an SOA module with explicit gas-phase reactions and new aqueous-phase and aerosol-phase chemistry, then to incorporate this SOA module into the 3-D chemical and transport model (IMPACT) to simulate global SOA production, and finally to assess the radiative effect of SOA. To achieve these

objectives, this thesis is organized as follows. In Chapter 2, an explicit model based on detailed gas-phase photochemical reactions is introduced as a basic framework to include SOA formation from organic nitrates and peroxide, the formation of low-volatility SOA from the reactive uptake of glyoxal and methylglyoxal on aqueous aerosols and cloud droplets as well as from the uptake of epoxides on aqueous aerosols. In Chapter 3, the SOA formation from glyoxal and methylglyoxal is examined by using different uptake processes and different photochemical reactions in cloud droplets and aqueous aerosol. In Chapter 4, the change in SOA since pre-industrial times is calculated and its resulting radiative forcing is assessed using an offline radiative transfer model. In addition, the radiative forcing of present-day OA in snow and ice is estimated.

1.4 References

Blando, J. D. and Turpin, B. J.: Secondary organic aerosol formation in cloud and fog droplets: a literature evaluation of plausibility, Atmospheric Environment, 34(10), 1623–1632, 2000.

Boyd, P. W., Wong, C. S., Merrill, J., Whitney, F., Snow, J., Harrison, P. J. and Gower, J.: Atmospheric iron supply and enhanced vertical carbon flux in the NE subarctic Pacific: Is there a connection? Global Biogeochem. Cycles, 12(3), 429–441, doi:10.1029/98GB00745, 2012.

Carlton, A. G., Turpin, B. J., Altieri, K. E., Seitzinger, S., Reff, A., Lim, H. J. and Ervens, B.: Atmospheric oxalic acid and SOA production from glyoxal: Results of aqueous photooxidation experiments, Atmospheric Environment, 41(35), 7588–7602, doi:10.1016/j.atmosenv.2007.05.035, 2007.

Chuang, P. Y., Seinfeld, J. H., and Charlson, R. J.: Kinetic limitations on droplet formation in clouds, Nature, 390(6660), 594–596, doi:10.1038/37576, 1997.

Czoschke, N. M., Jang, M. and Kamens, R. M.: Effect of acidic seed on biogenic secondary organic aerosol growth, Atmospheric Environment, 37(30), 4287–4299, doi:10.1016/s1352-2310(03)00511-9, 2003.

Ervens, B., Turpin, B. J. and Weber, R. J.: Secondary organic aerosol formation in cloud droplets and aqueous particles (aqSOA): a review of laboratory, field and model studies, Atmos. Chem. Phys., 11, 11069-11102, doi:10.5194/acp-11-11069-2011, 2011.

Forster, P., V. Ramaswamy, P. Artaxo, T. Berntsen, R. Betts, D.W. Fahey, J. Haywood, J. Lean, D.C. Lowe, G. Myhre, J. Nganga, R. Prinn, G. Raga, M. Schulz and R. Van Dorland : Changes in Atmospheric Constituents and in Radiative Forcing. In: Climate Change 2007: The Physical Science Basis. Contribution of Working Group I to the Fourth Assessment Report of the Intergovernmental Panel on Climate Change [Solomon, S., D. Qin, M. Manning, Z. Chen, M. Marquis, K.B. Averyt, M.Tignor and H.L. Miller (eds.)]. Cambridge University Press, Cambridge, United Kingdom and New York, NY, USA, 2007.

Galloway, J. N., Townsend, A. R., Erisman, J. W., Bekunda, M., Cai, Z., Freney, J. R., Martinelli, L. A., Seitzinger, S. P. and Sutton, M. A.: Transformation of the Nitrogen Cycle: Recent Trends, Questions, and Potential Solutions, Science, 320(5878), 889–892, doi:10.1126/science.1136674, 2008.

Gao, S., Keywood, M., Ng, N. L., Surratt, J., Varutbangkul, V., Bahreini, R., Flagan, R. C. and Seinfeld, J. H.: Low-molecular-weight and oligomeric components in secondary organic aerosol from the ozonolysis of cycloalkenes and alpha-pinene, Journal of Physical Chemistry A, 108(46), 10147–10164, doi:10.1021/jp047466e, 2004.

Goldstein, A. H. and Galbally, I. E.: Known and unexplored organic constituents in the earth's atmosphere, Environ. Sci. Technol., 41(5), 1514–1521, 2007.

Goldstein, A. H., Koven, C. D., Heald, C. L. and Fung, I. Y.: Biogenic carbon and anthropogenic pollutants combine to form a cooling haze over the southeastern United States, Proceedings of the National Academy of Sciences of the United States of America, 106(22), 8835–8840, doi:10.1073/pnas.0904128106, 2009.

Guenther, A., Hewitt, C. N., Erickson, D., Fall, R., Geron, C., Graedel, T., Harley, P., Klinger, L., Lerdau, M., McKay, W. A., Pierce, T., et al.: A global-model of natural volatile organic-compound emissions, J. Geophys. Res., 100(D5), 8873–8892, 1995.

Hallquist, M., Wenger, J. C., Baltensperger, U., Rudich, Y., Simpson, D., Claeys, M., Dommen, J., Donahue, N. M., George, C., Goldstein, A. H., Hamilton, J. F., et al.: The formation, properties and impact of secondary organic aerosol: current and emerging issues, Atmos. Chem. Phys., 9(14), 5155–5236, 2009.

Heald, C. L., Jacob, D. J., Park, R. J., Russell, L. M., Huebert, B. J., Seinfeld, J. H., Liao, H. and Weber, R. J.: A large organic aerosol source in the free troposphere missing from current models, Geophys. Res. Lett., 32(18), doi:10.1029/2005gl023831, 2005.

Henze, D. K., Seinfeld, J. H., Ng, N. L., Kroll, J. H., Fu, T. M., Jacob, D. J. and Heald, C. L.: Global modeling of secondary organic aerosol formation from aromatic hydrocarbons: high- vs. low-yield pathways, Atmos. Chem. Phys., 8(9), 2405–2420, 2008.

Huffman, J. A., Docherty, K. S., Aiken, A. C., Cubison, M. J., Ulbrich, I. M., DeCarlo, P. F., Sueper, D., Jayne, J. T., Worsnop, D. R., Ziemann, P. J. and Jimenez, J. L.: Chemically-resolved aerosol volatility measurements from two megacity field studies,

Atmos. Chem. Phys., 9(18), 7161–7182, 2009.

Iinuma, Y., Boge, O., Gnauk, T. and Herrmann, H.: Aerosol-chamber study of the alpha-pinene/O-3 reaction: influence of particle acidity on aerosol yields and products, Atmospheric Environment, 38(5), 761–773, doi:10.1016/j.atmosenv.2003.10.015, 2004.

Jang, M., Czoschke, N. M., Northcross, A. L., Cao, G. and Shaof, D.: SOA formation from partitioning and heterogeneous reactions: Model study in the presence of inorganic species, Environ. Sci. Technol., 40(9), 3013–3022, doi:10.1021/es0511220, 2006.

Jimenez, J. L., Canagaratna, M. R., Donahue, N. M., Prevot, A. S. H., Zhang, Q., Kroll, J. H., DeCarlo, P. F., Allan, J. D., Coe, H., Ng, N. L., Aiken, A. C., et al.: Evolution of Organic Aerosols in the Atmosphere, Science, 326(5959), 1525–1529, doi:10.1126/science.1180353, 2009.

Kanakidou, M., Seinfeld, J. H., Pandis, S. N., Barnes, I., Dentener, F. J., Facchini, M. C., Van Dingenen, R., Ervens, B., Nenes, A., Nielsen, C. J., Swietlicki, E., et al.: Organic aerosol and global climate modeling: a review, Atmos. Chem. Phys., 5, 1053–1123, 2005.

Kleinman, L. I., Springston, S. R., Daum, P. H., Lee, Y. N., Nunnermacker, L. J., Senum, G. I., Wang, J., Weinstein-Lloyd, J., Alexander, M. L., Hubbe, J., Ortega, J., et al.: The time evolution of aerosol composition over the Mexico City plateau, Atmos. Chem. Phys., 8(6), 1559–1575, 2008.

Kroll, J. H., Ng, N. L., Murphy, S. M., Varutbangkul, V., Flagan, R. C. and Seinfeld, J. H.: Chamber studies of secondary organic aerosol growth by reactive uptake of simple carbonyl compounds, J. Geophys. Res., 110(D23), D23207, doi:10.1029/2005JD006004, 2005.

Lelieveld, J., Barlas, C., Giannadaki, D. and Pozzer, A.: Model calculated global, regional and megacity premature mortality due to air pollution, Atmos. Chem. Phys. Discuss., 13(3), 7737–7766, doi:10.5194/acpd-13-7737-2013, 2013.

Liggio, J., Li, S. M. and McLaren, R.: Heterogeneous reactions of glyoxal on particulate matter: Identification of acetals and sulfate esters, Environ. Sci. Technol., 39(6), 1532–1541, 2005.

Lim, H. J., Carlton, A. G. and Turpin, B. J.: Isoprene Forms Secondary Organic Aerosol through Cloud Processing: Model Simulations, *Environ. Sci. Technol.*, *39* (12), 4441–4446, doi: 10.1021/es048039h, 2005.

Liou, K. N.: An introduction to atmospheric radiation, 2nd Ed. Academic Press, 583 pages, 2002.

Mahowald, N., Ward, D. S., Kloster, S., Flanner, M. G., Heald, C. L., Heavens, N. G., Hess, P. G., Lamarque, J.-F. and Chuang, P. Y.: Aerosol Impacts on Climate and Biogeochemistry, Annu. Rev. Environ. Resourc., 36(1), 45–74, doi:10.1146/annurev-environ-042009-094507, 2011.

Minerath, E. C. and Elrod, M. J.: Assessing the Potential for Diol and Hydroxy Sulfate Ester Formation from the Reaction of Epoxides in Tropospheric Aerosols, Environ. Sci. Technol., 43(5), 1386–1392, doi:10.1021/es8029076, 2009.

Okin, G. S., Mahowald, N. and Chadwick, O. A.: Impact of desert dust on the biogeochemistry of phosphorus in terrestrial ecosystems Global Biogeochemical Cycles, 18(2), 2004.

Pankow, J. F.: An absorption model of gas/particle partitioning of organic compounds in the atmosphere, Atmospheric Environment, 28(2), 185–188, doi:10.1016/1352-2310(94)90093-0, 1994.

Paulot, F., Crounse, J. D., Kjaergaard, H. G., Kurten, A., St Clair, J. M., Seinfeld, J. H. and Wennberg, P. O.: Unexpected Epoxide Formation in the Gas-Phase Photooxidation of Isoprene, Science, 325(5941), 730–733, doi:10.1126/science.1172910, 2009.

Penner, J.E., et al.: Aerosols, their direct and indirect effects. In: Climate Change 2001: The Scientific Basis. Contribution of Working Group I to the Third Assessment Report of the Intergovernmental Panel on Climate Change [Houghton, J.T., et al. (eds.)]. Cambridge University Press, Cambridge, United Kingdom and New York, NY, USA, pp. 289– 348, 2001.

Robinson, A. L., Donahue, N. M., Shrivastava, M. K., Weitkamp, E. A., Sage, A. M., Grieshop, A. P., Lane, T. E., Pierce, J. R. and Pandis, S. N.: Rethinking organic aerosols: Semivolatile emissions and photochemical aging, Science, 315(5816), 1259–1262, doi:10.1126/science.1133061, 2007.

Rogers, R. R. and Yau M. K.: A Short Course in Cloud Physics, 3rd Ed. Pergamon Press. 293 pp, 1989.

Simpson, D., Yttri, K. E., Klimont, Z., Kupiainen, K., Caseiro, A., Gelencsér, A., Pio, C., Puxbaum, H. and Legrand, M.: Modeling carbonaceous aerosol over Europe: Analysis of the CARBOSOL and EMEP EC/OC campaigns, J. Geophys. Res., 112(D23), D23S14, doi:10.1029/2006JD008158, 2007.

Surratt, J. D., Chan, A. W. H., Eddingsaas, N. C., Chan, M. N., Loza, C. L., Kwan, A. J., Hersey, S. P., Flagan, R. C., Wennberg, P. O. and Seinfeld, J. H.: Reactive intermediates revealed in secondary organic aerosol formation from isoprene, Proceedings of the National Academy of Sciences of the United States of America, 107(15), 6640–6645, doi:10.1073/pnas.0911114107, 2010.

Susan C Anenberg, L. W. H. D. Q. T. J. J. W.: An Estimate of the Global Burden of Anthropogenic Ozone and Fine Particulate Matter on Premature Human Mortality Using Atmospheric Modeling, Environ Health Perspect, 118(9), 1189, doi:10.1289/ehp.0901220, 2010.

Szidat, S., Jenk, T. M., Synal, H.-A., Kalberer, M., Wacker, L., Hajdas, I., Kasper-Giebl, A. and Baltensperger, U.: Contributions of fossil fuel, biomass-burning, and biogenic

emissions to carbonaceous aerosols in Zurich as traced by 14C, J. Geophys. Res., 111(D7), D07206, doi:10.1029/2005JD006590, 2006.

Tsigaridis, K. and Kanakidou, M.: Global modelling of secondary organic aerosol in the troposphere: a sensitivity analysis, Atmos. Chem. Phys., 2003.

Tsigaridis, K., Krol, M., Dentener, F. J., Balkanski, Y., Lathiere, J., Metzger, S., Hauglustaine, D. A. and Kanakidou, M.: Change in global aerosol composition since preindustrial times, Atmos. Chem. Phys., 6, 5143–5162, 2006.

Volkamer, R., Jimenez, J. L., San Martini, F., Dzepina, K., Zhang, Q., Salcedo, D., Molina, L. T., Worsnop, D. R. and Molina, M. J.: Secondary organic aerosol formation from anthropogenic air pollution: Rapid and higher than expected, Geophys. Res. Lett., 33(17), doi:10.1029/2006gl026899, 2006.

Vutukuru, S., Griffin, R. J. and Dabdub, D.: Simulation and analysis of secondary organic aerosol dynamics in the South Coast Air Basin of California, J. Geophys. Res., 2006.

Warren, S. G. and Wiscombe, W. J.: A model for the spectral albedo of snow. II: Snow containing atmospheric aerosols, J. Atmos. Sci., 1980.

Wiscombe, W. J. and Warren, S. G.: AMS Journals Online - A Model for the Spectral Albedo of Snow. I: Pure Snow, J. Atmos. Sci., 1980.

Zhang, Q., Jimenez, J. L., Canagaratna, M. R., Allan, J. D., Coe, H., Ulbrich, I., Alfarra, M. R., Takami, A., Middlebrook, A. M., Sun, Y. L., Dzepina, K., et al.: Ubiquity and dominance of oxygenated species in organic aerosols in anthropogenically-influenced Northern Hemisphere midlatitudes, Geophys. Res. Lett., 34(13), L13801, doi:10.1029/2007GL029979, 2007.

CHAPTER 2

Global modeling of SOA formation from dicarbonyls, epoxides, organic nitrates and peroxides

2.1 Introduction

Atmospheric particles have important impacts on human health, air quality as well as regional and global climate and climate change. Organic aerosols represent a large fraction of the particulate mass at both urban and remote locations (Kanakidou et al., 2005; Zhang et al., 2007; Jimenez et al., 2009). They are often categorized as either "primary organic aerosol (POA)", a class of organic compounds that is emitted directly into the atmosphere in particulate form, or "secondary organic aerosols (SOA)", which are formed by atmospheric oxidation of volatile organic compounds (VOCs). The distinction between these two categories, however, is changing as a result of recent studies which show that the volatility of emitted particles can change as a result of the oxidation of primary emissions which can subsequently provide an extra source of SOA (Robinson et al, 2007). Previously unrecognized low-volatility compounds (LV-OOA) are also present in measured SOA (Jimenez et al., 2009)

Despite the importance of organic aerosols (OA) in the environment, data sets to constrain models are limited. Nevertheless, based on available data sets it appears that models tend to underestimate SOA concentrations in the boundary layer (e.g., Johnson et al., 2006; Volkamer et al., 2006; Kleinman et al., 2008; Simpson et al., 2007) as well as in the free troposphere (Heald et at., 2005). Johnson et al. (2006) studied SOA formation in the UK using a fully explicit chemical scheme in the modified Master Chemical Mechanism (MCM v3.1), and found that they had to increase all partitioning coefficients of SOA precursors by a factor of 500 in order to capture observed OA levels. Volkamer et al. (2006) employed aerosol mass spectrometer (AMS) measurements to analyze the

surface concentrations of oxidized organic aerosol (OOA) in Mexico City. The measured SOA was about 8 times larger than a conservative (high end) estimate from an SOA model based on an empirical parameterization of chamber experiments. Their results were corroborated by Kleinman et al. (2008) who reported a discrepancy of an order of magnitude between the measured SOA taken in aircraft data from the MILAGRO 2006 campaign and that computed by a model. Simpson et al. (2007) found that their SOA modeling framework under-predicted SOA concentrations at Southern European sites, but predicted SOA levels that were within the range of observations in Northern Europe. Heald et al (2005) compared free tropospheric OA measurements from the Asia Pacific Regional Aerosol Characterization Experiment (ACE-Asia) field campaign with predictions from the global chemical transport model GEOS-Chem and concluded that a significant source of SOA was missing in the free troposphere.

Although these regional and global models showed a tendency to under-predict organic carbon (OC) concentrations in polluted regions, there is no universal underestimation for regions in which biogenic sources dominate (Capes et al., 2009; Chen et al., 2009; Slowik et al., 2010). Capes et al (2009) presented measurements of OA over subtropical West Africa during the wet season using data from the UK Facility for Airborne Atmospheric Measurements (FAAM) aircraft. Their theoretical SOA estimates which were based on smog-chamber aerosol yields together with estimates of the amount of isoprene and monoterpenes present at their site under-represented the measured organic matter (OM) by about a factor of 4. Chen et al. (2009) presented loadings of organic aerosols using the GEOS-Chem model that were 35% lower than measurements in the Amazon Basin taken using a high-resolution AMS during the wet season of 2008. In contrast, Slowik et al. (2010) obtained very good agreement between measurements in an eastern Candian forest region and simulations using a regional air quality model

The reasons for the differences between measured vs. modeled SOA in different regions remain unclear due to the numerous and complex chemical and physical phenomena involved in SOA formation (Hallquist et al., 2009; Pankow and Barsanti, 2009). One major uncertainty relates to the formation of gaseous secondary organics. It has been estimated that there are many hundreds of thousands of different organic compounds in

the atmosphere (Goldstein and Galbally, 2007), with each compound further undergoing a number of atmospheric reactions to produce a range of oxidized products (Hallquist et al., 2009). Therefore, the atmosphere contains a highly complex mixture with a myriad of structurally different organic oxygenates having a wide range of physico-chemical properties and different gas-to-particle-transfer potentials (Utembe et al., 2011; Lee-Talor et al., 2011). The complexity of the emitted VOC mixture and the oxidation chemistry requires a rigorous and thorough gas-phase chemical mechanism that describes SOA formation. Donahue et al (2009) argues that the complexity of SOA cannot be followed in detail and requires an approach where species are lumped into individual "volatility basis sets". Although the development of a "rigorous" mechanism may not be completely possible given that there are many species and reactions that we still do not know, we prefer to tie the formation of SOA to an explicit chemical mechanism, so that the contribution of the specific reaction mechanism and the specific individual species to SOA formation is known. Without this, it may not be possible to compare specific species with measurements (though, admittedly few are available now). Also, we think this approach can be easily updated as chemical mechanisms are further developed. Isoprene emissions (~500 Tg C/year) (Guenther et al., 2006) constitute around one third of total VOC emissions to the atmosphere (Goldstein and Galbally, 2007). In addition, SOA derived from biogenic VOCs dominate model-predicted global atmospheric SOA burdens (Tsigaridis et al., 2006; Henze et al., 2008) and many measured data also suggest that most of the SOA is associated with biogenic emissions (Lewis et al, 2004; Kleindienst et al, 2007; Szidat et al. 2009; Goldstein et al., 2009). However, the precise mechanisms of the SOA formation are not known. Further, field studies in forested environments have found much higher OH radical concentrations than those predicted by models that are based on traditional mechanisms in which isoprene peroxy radicals react mainly with HO_2 to form organic hydroperoxides in low NO_x conditions (Lelieveld et al., 2008; Pugh et al., 2010). This indicates that the isoprene oxidation mechanisms traditionally used in chemistry-transport models may require substantial revision.

In addition to the oxidation mechanisms for VOCs, other efforts have focused on the gap between measured and modeled SOA. The non-volatile primary organic aerosol (POA) from diesel exhaust and biomass burning is known to include low-volatility compounds

that partition between the gas and aerosol phase. These can then undergo gas-phase oxidation to form species of different volatilities that form SOA (Robinson et al. 2007; Huffman et al. 2009). This previously neglected SOA source has been explored using box (Dzepina et al., 2009), regional (Hodzic et al., 2010) and global (Pye and Seinfeld, 2010) models, which indicate that this may be an important source of SOA. These studies show that adding this new SOA source can bring the model simulation into better agreement with the observations in Mexico City (Li et al., 2011), or can even over-predict the observations (Dzepina et al., 2011; Hodzic et al., 2010). However, there is still substantial uncertainty in the emissions, reaction rates, and SOA yields of the traditional primary emitted aerosols (Pye and Seinfeld, 2010; Spracklen et al., 2011).

The propensity of VOC oxidation products to undergo further reactions within or on the condensed phase has also been established as playing a key role in the formation and growth of SOA over the last 5-10 years. Condensed-phase reactions can cause the vapor pressure of organics to be lowered by several orders of magnitude either by oxidation or formation of high-molecular-weight species (e.g., through oligomerization) (Hallquist et al., 2009). The rate of formation of these low volatile compounds increases in the presence of inorganic acid seed aerosol, at least for the products formed in the ozonolysis of alpha-pinene (Jang et al., 2006; Czoschke et al, 2003; Iinuma et al., 2004; Gao et al., 2004a, 2004b). Additionally, in regions where isoprene is present under low NO_x conditions, epoxydiols can form (Paulot et al., 2009) and their reactive uptake on acidic sulphate aerosols (Minerath and Elrod, 2009) may lead to a 20-fold increase in OA mass yields from isoprene (Surratt et al., 2010). Similarly, the uptake of gas-phase glyoxal into aqueous ammonium sulfate particles has been observed (Jang and Kamens, 2001; Hastings et al., 2005; Kroll et al., 2005b; Liggio et al., 2005a). Following these observations, the production of SOA by reactive uptake of glyoxal as well as methylglyoxal was examined in a global model (Fu et al., 2008).

In this paper, we begin with a short description of the model in section 2.2, followed by a description of the gas-phase chemical mechanisms for the oxidation of VOCs and the formation of SOA from gas-particle partitioning of semi-volatile organic compounds (SVOCs). We describe our treatment for the formation of low-volatility or oligomeric

compounds, and for irreversible uptake of glyoxal, methylglyoxal and epoxydiols. Our model results using different chemical mechanisms for HO_x recycling are presented in section 2.3. Section 2.4 compares our results with both surface and free tropospheric observations, followed by sensitivity tests in which we vary the oligomer formation rate in section 2.5. A summary is presented in section 2.6.

2.2 Model Description

Here, we use the Integrated Massively Parallel Atmospheric Chemical Transport (IMPACT) model that was developed at the Lawrence Livermore National Laboratory (LLNL) (Rotman et al., 2004) and at the University of Michigan (Penner et al., 1998; Liu and Penner, 2002; Liu et al., 2005; Ito et al., 2007). The IMPACT model was developed using massively parallel computer architecture and was extended by Liu and Penner (2002) to treat the mass of sulfate aerosol as a prognostic variable. It was further extended by Liu et al. (2005) to treat the microphysics of sulfate aerosol and the interactions between sulfate and non-sulfate aerosols based on the aerosol module developed by Herzog et al. (2004). Ito et al. (2007) investigated the effect of non-methane volatile organic compounds on tropospheric ozone and its precursors using the IMPACT model, with a modified numerical solution for photochemistry (Sillman, 1991; Barth et al., 2003) and a modified chemical mechanism (Ito et al., 2007). In this paper, we used the same microphysics module described in Liu et al. (2005). We prescribed the SOA size distribution to be the same as that for biomass burning OM in Liu et al. (2005), but allowed it to interact with sulfate through condensation of sulfuric acid, through coagulation with pure sulfate aerosols, and through aqueous formation of sulfate. We use the 1997 meteorological fields from the National Aeronautics and Space Administration (NASA) Data Assimilation Office (DAO) GEOS-START (Goddard EOS Assimilation System-Stratospheric Tracers of Atmospheric Transport) model (Coy and Swinbank, 1997; Coy et al., 1997). The meteorology was defined on a 4° latitude × 5° longitude horizontal grids with 46 vertical layers. The model was run for a 1-year time period with a 1-month spin up time.

2.2.1 Atmospheric oxidation mechanisms for SOA precursors

2.2.1.A Chemical mechanism by Ito et al. (2007)

We used the chemical mechanism published by Ito et al. (2007) to represent the basic photochemistry of O_3, OH, NO_x and volatile organic compounds (VOC). The Ito et al. (2007) mechanism uses surrogate species to represent classes of VOC, so that (for example) the chemistry of toluene is also used to represent ethyl benzene. Representation of the chemical reaction pathways to form SOA described below, are all incorporated in the Ito et al. (2007) gas-phase mechanism. In certain cases we have used modified reaction sequences (e.g. Peeters et al., (2009), for the first stages of isoprene oxidation) as replacements for the original sequences from Ito et al. (2007). In these cases the subsequent reaction products (e.g. methylvinyl ketone) react as in Ito et al. (2007), unless otherwise specified. The gas-phase oxidation is initiated by reaction with hydroxyl (OH) radicals, O_3, nitrate (NO_3) radicals or via photolysis, leading to the formation of organic peroxy radicals (RO_2). In the presence of nitrogen oxides (NO_x = NO +NO_2), RO_2, oxy radicals (RO) and the hydroperoxy radical (HO_2) can act as chain propagating species, leading to the regeneration of OH (e.g., Kroll and Seinfeld, 2008). The reactions of RO_2 and HO_2 with NO play a key role in these catalytic cycles, since the associated oxidation of NO to NO_2 leads to the formation of ozone by the subsequent photolysis of NO_2:

$$\mathrm{RO_2 + NO \rightarrow RO + NO_2} \qquad (R1)$$

$$\mathrm{HO_2 + NO \rightarrow OH + NO_2} \qquad (R2)$$

At low levels of NO_x, RO_2 will instead react with HO_2 and then form a hydroperoxide, leading to a general suppression of the concentrations of the free radical species:

$$\mathrm{RO_2 + HO_2 \rightarrow ROOH + O_2} \qquad (R3)$$

2.2.1.B Epoxide formation following Paulot et al. (2009)

The gas-phase formation of epoxides (IEPOX) has been characterized by Paulot et al. (2009). These compounds are formed in the OH-initiated oxidation of isoprene

hydroperoxide (RIP) under low-NO_x conditions. IEPOX formation is accompanied by OH regeneration and is implemented in the model as shown below:

$$\mathrm{RIP} + \mathrm{OH} \rightarrow \mathrm{IEPOX} + \mathrm{OH} \qquad (R4)$$

The subsequent oxidation of IEPOX is as follows:

$$\mathrm{IEPOX} + \mathrm{OH} \rightarrow \mathrm{IEPOXO2} \qquad (R5)$$

$$\mathrm{IEPOX} + \mathrm{NO} \rightarrow \mathrm{NO2} + 0.725\,\mathrm{HAC} + 0.275\mathrm{GLYC} + 0.275\mathrm{GLYX} + 0.275\mathrm{MGLY} + 0.375\mathrm{HCHO} + 0.074\mathrm{ACO2} + 0.251\mathrm{CO} \qquad (R6)$$

$$\mathrm{IEPOX} + \mathrm{HO2} \rightarrow 0.825\mathrm{HO2} + 0.125\mathrm{OH} + 0.725\,\mathrm{HAC} + 0.275\mathrm{GLYC} + 0.275\mathrm{GLYX} + 0.275\mathrm{MGLY} + 0.375\mathrm{HCHO} + 0.074\mathrm{ACO2} + 0.251\mathrm{CO} \qquad (R7)$$

The short names used here (e.g., HAC) are adopted from Ito et al. (2007). The full species and chemical formulas can be found in Table S2 in the supplementary material.

2.2.1.C HO_x regeneration in isoprene oxidation

As described in the Introduction, analysis of recent direct measurements of HO_x (OH and HO_2) over the Amazonian rainforest (Lelieveld et al., 2008) and the tropical forests of Borneo (Pugh et al., 2010) showed that the traditional chemistry used in numerical model studies cannot explain the high measured OH concentrations, which suggested that there is a yet unknown recycling mechanism for OH. To address this, Peeters et al. (2009) proposed and theoretically quantified a novel HO_x-regenerating pathway for the OH-initiated oxidation of isoprene. This oxidation mechanism has the following main features. The isoprene hydroxyl alkyl radicals first react with O_2 to form three isoprene peroxyradicals, which are in near-equilibrium steady-state. Some of the isoprene peroxy radicals, i.e. β-peroxys, are proposed to undergo 1,5-H shifts, that compete with the conventional reaction channels through HO_2, RO_2 and NO, leading to OH and HCHO along with either methacrolein (MACR) or methylvinylketone (MVK). Similarly, the Z-δ-OH-peroxys may undergo fast 1,6-H shifts leading to the formation of HO_2 and hydroperoxy aldehydes, which can rapidly photo-dissociate, initiating a reaction cascade

that can yield 1-3 OH radicals. Our simplified representation of the HO_x recycling mechanism is detailed in Table S3 in the supplementary material.

Although the chemical mechanism framework proposed by Peeters et al. (2009) provides a significant potential for addressing the atmospheric OH recycling issue, some atmospheric field measurements (e.g., Karl et al., 2009) and laboratory data (e.g., Paulot et al. 2009) indicate that it does not fully capture all observations. Karl et al. (2009) pointed out that the Peeters et al. (2009) mechanism overestimates MVK/MACR ratios and under-predicts the sum of MVK and MACR relative to isoprene when compared to field measurements conducted during the Amazonian Aerosol Characterization Experiment (AMAZE-08). Unrealistically high ratios of MVK/MACR and peroxyacetyl nitrate (PAN)/ peroxymethacryloyl nitrate (MPAN) were also reported by Archibald et al. (2010) using the Peeters et al. (2009) mechanism. In addition, Paulot et al. (2009) carried out a chamber experiment and found a lower yield (<10%) for the formation of the hydroperoxy-methyl-butenal isomers (HPC41CHO and HPC42CHO) than that proposed by Peeters et al. (2009). Moreover, Da Silva et al. (2010) used density functional theory (DFT) methods to calculate the 1,5-H atom shift isomerization rates for the isoprene-derived β-peroxy radicals and obtained an order of magnitude lower rates than those reported by Peeters et al. (2009). To reconcile the differences between Peeters et al. (2009) and the atmospheric observations or laboratory data mentioned above, both Karl et al. (2009) and Archibald et al. (2010) decreased the 1,5-H shift, 1,6-H shift rates by a factor of 10 as a sensitivity test. However, Peeters and Mueller (2010) showed that Paulot et al. (2009) did not account for 25% of the isoprene peroxy radicals produced during the experiments. During the preparation of this manuscript, an experimental estimate for 1,6-H shift was published (Crounse et al., 2011) and was a factor of 50 ±25 lower than the estimate of Peeters and Müller (2010). In this paper, we carried out three different simulations with different gas-phase chemical mechanisms (see Table 2-1). Simulation A only employs the Ito et al. (2007) chemical mechanism together with the epoxide formation mechanism from Paulot et al. (2009). Simulation B includes the HO_x recycling mechanism during isoprene oxidation from Peeters et al. (2009) and the mechanism in Simulation A with some reactions modified in accordance with the recent literature (Table S4 in the supplementary material). Simulation C uses the same chemical

mechanism as Simulation B, but with the 1,5-H and 1,6-H shift rates reduced by a factor 10.

Table 2-1 Description of three runs and four SOA components performed in this paper.

Name of runs or SOA components	Description
Simulation A	Bases on Ito et al. (2007) chemistry mechanism and epoxide formation from isoprene from Paulot et al. (2009), without HO_x recycling. It uses emissions for year 2000, and meteorology for 1997.
Simulation B	Includes the mechanism in Simulation A with some reactions modified in accord with the recent literature and HO_x regeneration through isoprene oxidation proposed by Peeters et al. (2009).
Simulation C	The same chemistry mechanism as Simulation B, but with a reduced rate for the 1,5-H and 1,6-H shifts in isoprene radicals by a factor of 10.
sv_oSOA	SOA formed from the traditional gas-particle partitioning of SVOCs produced by oxidation of VOCs. There are 23 SVOC species in Simulation A, and 26 SVOC species in Simulation B and C (see the Table S1).
ne_oSOA	Low-volatility SOA formed from irreversible aerosol-phase reactions of sv_oSOA (i.e. oligomer formation), assuming a fixed lifetime for the oligomer formation.
ne_GLYX	Glyoxal SOA formed from the irreversible uptake of gas-phase glyoxal into aqueous sulfate and clouds following the methods used in Fu et al. (2008, 2009).
ne_MGLY	Methylglyoxal SOA formed from the irreversible uptake of gas-phase methylglyoxal into aqueous sulfate and clouds following the methods used in Fu et al. (2008, 2009).
ne_IEPOX	Epoxide SOA formed from the irreversible uptake of gas-phase epoxide into aqueous sulfate aerosol with the same uptake coefficient as glyoxal and methylglyoxal.

2.2.2 SOA formation

2.2.2.A Gas-particle partitioning of semi-volatile organic compounds

Traditionally, SOA is thought to be formed from gas-particle partitioning of semi-volatile organic compounds which are derived from the oxidation of VOCs. The gas-particle partitioning of organics produced during gas-phase oxidation is based on the absorptive model described by Pankow (1994), which assumes thermodynamic equilibrium between the gas and particulate phase. According to this model, partitioning of each semi-volatile organic compound between the gas and aerosol phases can be described by an equilibrium partitioning coefficient K_i (m^3 μg^{-1}), or equivalently, its inverse, the effective saturation vapor concentration, C_i^* (μg m^{-3}), (Donahue et al., 2006),

$$\frac{[A_i]}{[G_i]} = K_i C_{OM} = \frac{C_{OM}}{C_i^*} \quad (1)$$

where C_{OM} (μg m^{-3}) is the mass concentration per unit volume of air of the total absorbing particle phase, which may include the pre-existing organic aerosol into which semi-volatile organics partition and possibly the aqueous portion of the organics if the semi-volatile organics are water-soluble; $[A_i]$ (μg m^{-3}) and $[G_i]$ (μg m^{-3}) are the concentrations of species *i* in the aerosol and gas phases, respectively. Here, we define,

$$C_{OM} = [POA] + \sum_{i=1}^{n} [A_i] \quad (2)$$

In this equation *n* is the number of species that can partition to the aerosol phase; [POA] (μg m^{-3}) is the concentration of primary organic aerosols, though the inclusion of the hydrophobic un-oxidized POA in the estimate of $[POA]$ may tend to overestimate the yield of SOA (Song et al., 2007).

In the first basic model of SOA formation using partitioning theory, Odum et al. (1996), used the measured yields of SOA obtained from smog chamber studies together with partitioning theory and was able to fit these yields by assuming that different amounts of two semi-volatile products were formed. This two-product model has been employed in a number of regional and global models (Chung and Seinfeld, 2002; Tsigaridis and Kanakidou, 2003; Liao et al., 2007; Carlton et al., 2010). These types of models can

include the effect of changes in NO_x emissions on O_3, and the effects of NO_x on the abundance of reaction products by fitting to smog chamber results in high and low NO_x environments (Tsidigaris et al., 2006; Henze et al., 2008). They can also be extended to include more than two volatility products (Donahue, 2009).

However, this simple approach cannot account for the full complexity and the dynamics of SOA production. First, SVOC formation strongly depends on ambient conditions, e.g. temperature, photolysis, and most notably on the fate of RO_2, which can react with NO_x, HO_2, and other RO_2. This is usually described as a VOC: NO_x dependence. This dependence was parameterized in a simple way for aromatics by Henze et al. (2008) based on two different SOA product yields in low and high NO_x conditions (specifically, a high yield in low-NO_x conditions and a low yield in high NO_x conditions). But SOA formation is more complex and cannot be represented by these simple parameterizations. SOA formation from isoprene at high NO_x is also reduced (Kroll et al., 2005a, 2006), while SOA formation is broadly similar at all NO_x levels in the ozonolysis of limonene (Zhang et al., 2006). Moreover, unlike aromatics and isoprene, SOA formation is increased at high NO_x in the photo-oxidation of sesquiterpenes (Ng et al., 2007). In addition, the SVOC products may be formed from first generation or higher generation products, and these products may undergo further reactions in the gas phase or aerosol phase (Ng et al., 2006; Camredon et al., 2007; Chan et al., 2007; Hallquist et al., 2009). As a consequence of these complexities and dynamics, the use of simple SOA yields from laboratory data may not account for the actual SOA system without a significant increase in the availability of these data and the complexity of the parameterizations.

In contrast to this empirical Odum-type model, a second type of model uses an explicit photochemical mechanism to form SVOC (e.g. Griffin et al., 2002; Zhang et al., 2004; Pun et al. 2006; Johnson et al., 2006; Camredon et al., 2007; Xia et al., 2008; Utembe et al., 2011), but may be limited in its ability to form SOA if the product distribution of SVOCs and their properties are incorrect. Nevertheless, we follow this philosophy here because this type of mechanism (1) is more explicit in its description of the oxidation products that lead to SOA formation, (2) handles the VOC:NO_x dependence in SVOC formation based on first principles as deduced in the explicit mechanism, (3) is easily

extended as more knowledge of VOC oxidation schemes becomes available, and (4) predicts products that can be explicitly compared to observations.

In this explicit model, a detailed gas-phase mechanism is used to predict the formation of semi-volatile products, with gas-particle partitioning computed from an explicit calculation of K_i for each semi-volatile compound. To determine the semi-volatile compounds that might partition into the aerosol phase, we used the following criteria suggested by Griffin et al., (2002): (1) partially soluble; (2) an aromatic acid; (3) an aromatic compound with two functional groups that are not aldehydes; (4) 12 or more carbon atoms; (5) at least 10 carbon atoms and two functional groups; (6) at least six carbon atoms and two functional groups, one of which is an acid; (7) tri-functional. From the above criteria, 26 species from the chemical mechanism described above that have the potential to produce SOA were selected (Table S1 in the supplementary material). All the species were oxygenated derivatives from aromatics, isoprene, alpha-pinene, limonene and carbonyls.

The partitioning coefficient K_i for each compound listed in Table S1 in the supplementary material is calculated explicitly according to:

$$K_i = \frac{R\,T}{10^6 MW\,\zeta_i p^0_{L,i}} \quad (3)$$

Where R (8.206 x 10^{-5} atm m^3 mol^{-1} K^{-1}) is the ideal gas constant, T (K) the temperature, MW (g mol^{-1}) the average molecular weight of the absorbing aerosol phase, ζ_i (dimensionless) the activity coefficient of the compound in the organic aerosol phase, $p^o_{L,i}$ (atm) the compound vapor pressure (sub-cooled if necessary) and 10^6 is a unit conversion factor (g g^{-1}).

Since experimentally determined vapor pressures are not available for many species, we used the method of Myrdal and Yalkowsky (1997) to determine $p^o_{L,i}$, with some changes added to include the particular chemical structure of the SOA forming compounds (Camredon and Aumont, 2006). The Myrdal and Yalkowsky method estimates the boiling point of a given organic compound based on the Joback group contribution method (Reid et al., 1987), and then estimates the vapor pressure at a given temperature.

Similar methods have been used previously by Griffin et al. (2002), Zhang et al. (2004) and Pun et al. (2006). Camredon and Aumont (2006) showed that the Myrdal and Yalkowsky method provides good estimates of vapor pressure for a set of organic species of importance for SOA formation. There are, however, many methods in the literature that have been developed to estimate vapor pressure. Barley and McFiggans (2010) assessed the ability of different vapor pressure methods to predict vapor pressures of lower volatility compounds. As noted by Barley and McFiggans (2010), the Joback method for estimating boiling points tends to underestimate the amount of material that can partition to the aerosol phase. Nevertheless, Booth et al. (2010, 2011) used some new room temperature low vapor pressure data for polyfunctional compounds, especially acids and diacids, and showed that other methods (e.g. the method of Nannoolal et al. (2008)) do not predict the data as well. Therefore, we should keep in mind uncertainties in the vapor-pressure estimates when drawing conclusions regarding the ability of this mechanism to reproduce observations. For example, Simpson et al. (2007) showed that the total modeled carbonaceous aerosol over Europe was very sensitivity to the choice of vapor pressures. Valorso et al. (2011) tested the sensitivity of SOA formation from α-pinene photo-oxidation to three different vapor pressure estimation methods (i.e., Myrdal and Yalkowsky (1997), Nannoolal et al. (2008), and the SIMPOL-1 method from Pankow and Asher (2008)), and found that the predicted SOA mass concentrations varied significantly from 8 to 28 μ g/m^3 in "high NO_x" experiments. Despite the sensitivity of SOA formation to different vapor pressure estimation methods, Camredon et al. (2010) found the best agreement with experimental aerosol yields of α-pinene dark ozonolysis experiments using the Myrdal and Yalkowsky method. Thus, we use this method here.

In the model represented by Eq. (3), the value of ζ_i is also uncertain. Several authors (e.g. Pankow, 1994a and Kamens et al., 1999) have assumed a value of one for oxidation products in an aerosol particle composed of a mixture of similar species. Although methods have been proposed to estimate the activity coefficient (Bowman and Karamalegos, 2002), we set ζ_i to one for simplicity.

The effect of temperature was taken into account according to the Clausius-Clapeyron equation using enthalpies of vaporization. However, the values for the enthalpy for most

compounds are highly uncertain (Bilde and Pandis, 2001; Chung and Seinfeld, 2002; Donahue et al., 2006; Stanier et al., 2007; Saathoff et al., 2009; Epstein et al., 2010). In this paper, following other recent studies, we assume a value of 42 *k*J mol^{-1} for all organic species for simplicity (Chung and Seinfeld, 2002; Liao et al., 2007; Heald et al., 2008). Table S1 shows the compounds that are allowed to partition to the aerosol phase, their parent VOC and the partitioning coefficients at a temperature of 298K.

2.2.2.B Formation of oligomers

Oligomer formation has been seen in both laboratory and atmospheric observations of SOA (Decesari et al., 2000; Gelencsér et al., 2002; Gross et al., 2006; Dommen et al., 2006; Iinuma et al., 2007). To incorporate this formation and other heterogeneous reactions that form low-volatility products in the aerosol phase into our model, we assumed that these compounds form with a time constant of 1 day following the reversible gas-particle partitioning process. This 1-day time scale is somewhat arbitrary, but is consistent with the Paulsen et al. (2006) laboratory study of oligomer formation. Support for the low-volatility of these products is provided by Vaden et al. (2011) who studied the evaporation kinetics of laboratory and ambient SOA, and found that SOA evaporation is very slow, lasting more than a day, and Perraud et al. (2012) reported irreversible SOA formation from the oxidation of α-pinene by ozone and NO_3, which seems to contradict equilibrium gas-particle partitioning Evidence for ambient low-volatility compounds was provided by Cappa and Jimenez (2010) who analyzed a thermodenuder dataset and concluded that a significant fraction of the atmospheric OA consisted of non-evaporative components. Since we do not have information on the volatility of these compounds, we make the expedient assumption that the oligomers which form do not evaporate. We note that the presence of oligomers within SOA would be expected to increase its MW, which typically ranges from 200-900 g/mol in laboratory observations (Gross et al., 2006; Sato et al., 2007; Dommen et al., 2006; Iinuma et al., 2007). This increase would be expected to decrease the partitioning coefficient, K_i. However, since we do not actually follow the chemical form of the oligomers in our model, we assumed that the molecular weight (MW) of the low-volatility products is equal to the MW of the absorbing semi-volatile compounds.

We note that the formation of oligomers in heterogeneous reactions within or on aerosols may be reversible or irreversible. Liggio et al. (2005a) had an experimental set up designed to look at kinetics and demonstrated that the reactions in the aerosol phase after uptake of glyoxal were irreversible on the 4 hour time scale of their experiments. The experimental setup for Kroll et al. (2005b) was designed to look at equilibrium products. They examined the possible heterogeneous uptake and irreversible transformation of a number of simple carbonyl species (formaldehyde, octanal, trans-2, 4-hexadienal, glyoxal, methylglyoxal, 2,3-butanedione, 2,4-pentanedione, glutaraldehyde, and hydroxyacetone) onto inorganic seed aerosols. Only glyoxal was reported to substantially increase in the particle phase. Moreover, the lack of particle growth while gas phase glyoxal was still present in their system indicated that the uptake was fully reversible. These results are at odds with those of other researchers (Jang and Kamens, 2001; Jang et al., 2002, 2003a, 2003b, 2005) who observed significant aerosol growth when inorganic seed was exposed to a wide variety of organic species. The compounds studied included simple C4–C10 aldehydes, unsaturated carbonyl compounds, and dicarbonyl compounds.

The rate of formation of oligomers used in our simple treatment is uncertain, and may vary with different compounds. While some laboratory studies showed that at least some of the oligomers are formed quite rapidly on a time scale of one minute (e.g. Heaton et al., 2007), several chamber studies of the chemical composition, volatility and hygroscopicity of SOA indicated that accretion reactions also take place on longer time scales (Gross et al., 2006; Paulsen et al., 2006; Dommen et al., 2006, Kalberer, et al., 2006). Gross et al. (2006) demonstrated that high MW oligomeric species could be detected within 1 to 2 hours (after turning the lights on) due to oligomerization reactions within the aerosol phase. Formation of these low volatility compounds continued for up to 20 hours, with about 50 – 60% of the SOA particle volume non-volatile at 100°C for 1,3,5-trimethylbenzene after 5-6 hrs and 80 to 90% of the SOA particle volume non-volatile for α-pinene generated SOA after 25 hours (Paulsen et al., 2006). The rate of formation of oligomers in the Paulsen et al. study was of order 1 day for 1,3,5-trimethylbenzene and 3 days for a-pinene generated SOA, but might be slower in ambient

aerosols, since the oligomer-forming compounds might be more dilute within ambient aerosol mixtures. The rate of formation of oligomers follows a chain growth polymerization model, wherein most of the molecular size develops rapidly followed by a continuous growth in the fraction of SOA that consists of oligomers (Kalberer, et al. 2006). For isoprene in a low NO_x environment, the time constant for formation of low volatility products within the aerosol phase is about 2.3 days (Chan et al., 2007). In contrast to the Chan et al. (2007) study, Dommen et al. (2006) observed that particles grew steadily within 8 hours mainly due to oligomers formed in the aerosol phase from isoprene photo-oxidation at high NO_x.

Smog chamber experiments have also shown that polymerization within the aerosol phase can be catalyzed by semi-volatile acidic reaction products (Kalberer et al., 2004). The smog-chamber study by Iinuma et al. (2005) examined the effect of acidic seed particles on α-pinene ozonolysis and suggested that acidity promotes SOA formation and increases aerosol yields by up to 40%. Surratt et al. (2007) examined SOA formation from isoprene and demonstrated that for low relative humidities (30%), the range of acidities observed in atmospheric aerosols could increase SOA concentrations by a factor of two.

The above discussion demonstrates that oligomer formation seems ubiquitous, but the rate of formation may vary with compound and concentration. In addition, the possibility of reversible oligomerization should be considered as well in light of the dependence of condensed phase reactions on the acidity of the existing aerosols. Nevertheless, our simple 1-day formation rate together with the assumption of irreversibility seems justified at this point in time, though we acknowledge the need to refine this part of model when additional experimental data become available. We note that oligomers contribute most of the SOA formed after gas-particle partitioning (see Table 2-4). We test the response of the model to an increase and a decrease in the time constant for formation in Section 2.5.

In summary, we use an explicit gas-phase mechanism to predict the formation of SVOCs, which can condense onto pre-existing aerosols through gas-particle partitioning. These condensed SVOCs are assumed to further react to form low-volatility compounds (i.e., oligomers) with a one-day time constant. Due to the lack of any detailed knowledge of

their volatility, we assume that these compounds do not evaporate once they are formed. For convenience, we refer these condensed SVOCs and their reaction products (oligomers), formed through the mechanism above, as sv_oSOA and ne_oSOA, respectively, (see Table 2-1). "sv" indicates "semi-volatile", "ne" stands for "non-evaporative", since this is how the low-volatility compounds are treated in the model. "oSOA" stands for "other oxygenated SOA" to differentiate it from SOA formed from the uptake of glyoxal, methylglyoxal and epoxide which is described in the next section.

2.2.2.C Uptake of glyoxal, methylglyoxal and epoxide

In addition to examining the formation of SOA from the basic Ito et al. (2007) mechanism, we added the formation of SOA from glyoxal and methylglyoxal which form as a result of the oxidation of several VOCs. We also included the formation of SOA from epoxide formed in the oxidation of isoprene. Hereafter, we refer to these SOAs as ne_GLYX, ne_MGLY and ne_IEPOX, respectively (see Table 2-1). Over the past few years, glyoxal and methylglyoxal have gained great attention because of their potential importance to form SOA through aqueous phase reactions due to their high water solubility, their ability to form oligomers via acid catalysis, and their reactivity with OH radicals (Blando and Turpin, 2000; Volkamer et al., 2007; Carlton et al., 2007). Generally, these aqueous-phase reactions can be categorized as radical or non-radical reactions (Lim et al., 2010). Radical reactions can involve a variety of atmospheric oxidants, including OH radicals, NO_3 radicals, O_3, and can be initiated by photolysis. The chamber study of Volkamer et al. (2009) demonstrated that SOA formation through aqueous photooxidation of glyoxal was dramatic during daytime when the gas-phase OH radical concentration is about 10^7 molecules cm^{-3}. Non-radical reactions include hemiacetal formation (Liggio et al, 2005a; Loeffler et al., 2006), aldol condensation (Jang et al., 2002), imine formation (Galloway et al., 2009), anhydride formation (Gao et al., 2004), esterification via condensation reactions (Gao et al., 2004), and organosulfate formation (Liggio et al., 2005b; Surratt et al., 2007).

Here, we treat the SOA formation from glyoxal, methylglyoxal and epoxide following the basic methods described by Fu et al. (2008, 2009) for glyoxal and methylglyoxal. Based

on early laboratory evidence for irreversible surface-controlled uptake of glyoxal to aerosols (Liggio et al., 2005a, b), Fu et al. (2008, 2009) parameterized the loss of gas phase glyoxal and methylglyoxal on aqueous particles using the following equation:

$$\frac{d\,C_g}{d\,t} = \frac{1}{4} \cdot \gamma \cdot A \cdot < \upsilon > \cdot C_g \qquad (4)$$

Where A is the total surface area of aqueous sulfate aerosols, m^2], and C_g is the concentration of gas phase glyoxal or methylglyoxal. The production of aqueous phase products can be directly equated to the loss of gas phase species. The parameter γ is the reactive uptake coefficient, representing the probability that a collision between a gas molecule and the aqueous particle surface will result in irreversible uptake considering processes such as diffusion, mass accommodation, dissolution and chemical reaction. The value of γ used in the Fu et al. (2008, 2009) studies was assumed, 2.9×10^{-3}, for both glyoxal and methylglyoxal, and we use the same value for epoxide here. In addition to treating uptake on aqueous particles, Fu et al. (2008, 2009) also included uptake by cloud droplets in a similar fashion, but accounting for diffusion limitation. Here, we also account for the uptake of glyoxal and methylglyoxal by cloud droplets in the same way as that in Fu et al. (2008, 2009).

It should be noted, however, that this simple treatment of irreversible surface-controlled uptake might be misleading if there is competition between reversible vs. irreversible uptake and bulk reactions vs. surface processes (Ervens and Volkamer, 2010). While aqueous photooxidation (e.g., aqueous-phase reactions of glyoxal with OH radical) of glyoxal can lead to products that are clearly formed through irreversible processes, Kroll et al. (2005b) and Galloway et al. (2009) report that glyoxal oligomers formed through acid catalyzed pathways are reversible. Furthermore, Ervens and Volkamer (2010) fit the observed glyoxal loss rates or observed SOA mass formation rates from different literature studies (i.e. Hastings et al., 2005; Liggio et al., 2005a; Volkamer et al., 2009) to a bulk-limitation equation expressing the SOA formation rate, and showed that the surface area of the aerosol population did not control the uptake of glyoxal and its conversion to SOA mass. In spite of the high uncertainty associated with the processes leading to the formation of SOA from glyoxal and methylglyoxal, we use the compact

and simplified representation adopted by Fu et al. (2008) to obtain a first order estimate of the significance of glyoxal and methylglyoxal uptake for secondary organic aerosol formation.

Paulot et al. (2009) demonstrated that isoprene photooxidation under low-NO_x conditions can generate high concentrations of gas-phase epoxydiols, which are observed to be a key gas-phase intermediate in the formation of SOA from isoprene at low-NO_x conditions (Surratt et al., 2010). The reaction kinetics for the formation of epoxydiols have recently been reported (Minerath et al., 2009a, b; Eddingsaas et al., 2010). These studies showed that acid-catalyzed ring-opening reactions of epoxides in the particle phase were kinetically favored under typical tropospheric conditions, leading to the formation of known isoprene SOA tracers (e.g., 2-methyltetrols and their corresponding organosulfates) (Claeys et al., 2004; Surratt et al., 2010). Also, these isoprene-derived epoxydiols and organosulfates were identified in ambient aerosols during several aircraft measurement campaigns (Froyd et al., 2010; Chan et al., 2010). Therefore, we added the uptake of epoxydiols by aqueous sulfate aerosols using the same formulation as that for glyoxal and methylglyoxal.

2.2.3 Emissions

Table 2-2 summarizes the global emissions of gas, aerosols and aerosol precursors used in the model. The emissions of gas-phase species are based on the paper by Ito et al. (2007, 2009) and the POA emissions on the paper by Wang et al. (2009) with some additions. We include both terrestrial and marine isoprene sources. Terrestrial isoprene emissions are based on a modified version of the inventory of Guenther et al. (1995) by Wang et al. (1998) and Bey et al. (2001), with a total biogenic isoprene source of 470.8 Tg C/yr. The total marine isoprene emission, with a value of 0.92 Tg C/yr, is from the estimate by Gantt et al. (2009) based on satellite observations. This total marine isoprene flux is scaled by monthly mean MODIS chlorophyll concentrations and surface wind speeds to determine the spatial and time variation of the flux (Palmer and Shaw 2005). The biogenic terpene source is 117.6 Tg C/year and is based on the work of Guenther et al. (1995) as modified by Wang et al. (1998). The other temperature-dependent BVOC

emissions for ethane, propene, acetone, and methanol are distributed according to emissions of isoprene following Ito et al. (2007).

Sources of primary organic emissions in the model include organics from sea spray (35 Tg/yr), fossil fuel and biofuel emissions (16 Tg/yr), and open biomass burning (47 Tg/yr). The primary sea spray organic source was estimated using the correlation between chlorophyll-a and the fractional water insoluble organic mass of sea salt following O'Dowd et al. (2008) where the chlorophyll concentrations were those measured by MODIS Aqua averaged for the 5 years from 2004 to 2008**.** The total marine organic aerosol is 35 Tg/yr, which is very close to the value given by Gantt et al. (2009) based on remote sensing (i.e. 22.3 Tg C/yr or 35.6 Tg/yr if the ratio of OM to OC is 1.6). Water soluble organic carbon (WSOC) is also present in marine aerosols and makes up 20-25% of the total submicron mass (Yoon et al., 2007). It is likely produced through photochemical aging of volatile organic compounds, so has not been included in our primary marine source. We note that there is a large difference in the source strengths estimated from "bottom-up" and "top-down" methods (Gantt et al., 2009; Luo and Yu, 2010).

The concentration of the organic portion of the sea salt source was lumped together with the concentration of MSA produced from the oxidation of DMS within the code. For this source, we assumed a pathway based on the reaction of DMS with OH that produced only SO_2 (with a rate coefficient $9.6\times10^{-12}\exp\left(-\frac{234}{T}\right)$; and a pathway that forms 0.75 moles of SO_2 and 0.25 moles MSA, with a rate coefficient $\frac{k_1 M}{1+2k_2 M}$, where $k_1 = 1.7\times10^{-42}\exp\left(\frac{7810}{T}\right)$, $k_2 = 5.5\times10^{-31}\exp\left(\frac{7460}{T}\right)$ and M = O_2 (molecules cm^{-3}) following Gondwe et al. (2003) and references therein. The total annual average source of MSA is 8.23 Tg/yr.

Table 2-2 Global emissions of gases, aerosols and aerosol precursors.

Species	Emission Rate
SO_2 or precursor	92.2 Tg S/yr
Fossil fuel and industry	61.3 Tg S/yr
Volcanoes	4.8 Tg S/yr
DMS	26.1 Tg S/yr
NO	42.1 Tg N/yr
Fossil Fuel	22.7 Tg N/yr
Biomass burning	9.3 Tg N/yr
Soil	5.5 Tg N/yr
Lighting	3.0 Tg N/yr
Aircraft	0.9 Tg N/yr
Ship	0.7 Tg N/yr
CO	426.0 Tg C/ yr
MEK(>C3 ketones)	5.8 Tg C/yr
PRPE(>=C4 alkenes)	11.3 TgC/yr
C_2H_6	9.3 Tg C/yr
C_3H_8	7.3 Tg C/yr
ALK4(>=C4 alkanes)	15.3 Tg C/yr
Acetaldehyde	3.3 Tg C/yr
CH_2O	2.4Tg C/yr
ALK7(C6-C8 alkanes)	11.3Tg C/yr
Benzene	3.2 Tg C/yr
Toluene	5.8 Tg C/yr
Xylene	3.9 Tg C/yr
trans-2-butene	6.6 Tg C/yr
HCOOH	2.6 Tg C/yr

acetic acid	12.4 Tg C/yr
Phenol	4.3Tg C/yr
Ocean source of POA	34.5 Tg/yr
DMS source of MSA	8.2 Tg/yr
Fossil fuel+biofuel POA[a]	15.7 Tg OM/yr
Fossil fuel+biofuel BC	5.8 Tg BC/yr
Biomass burning OM[a]	47.4 Tg OM/yr
Biomass burning BC	4.7Tg BC/yr
Isoprene	472.0 Tg C/yr
a-pinene	78.8 Tg C/yr
Limonene	38.8 Tg C/yr
PRPE(>=C4 alkenes)	24.2 Tg C/yr
Methanol	42.9 Tg C/yr
Acetone	44.5 Tg C/yr
Ethane	28.2 Tg C/yr

[a]Half of these POA emissions are assumed to be composed of low-volatility compounds that may have undergone reactions and partitioned back into the aerosol form as SOA.

Fossil fuel and biofuel emissions total 16 Tg/yr. These emissions were estimated by Ito and Penner (2005) for the year 2000, but Wang et al. (2009) adjusted the fossil fuel emissions to fit observed surface BC concentration and we use their adjusted emissions here. Open biomass burning emissions total 47.4 Tg/yr and were developed based on using the Ito and Penner (2005) emissions for BC as an a priori estimate together with the inverse model approach of Zhang et al. (2005). The POM associated with open burning was then similarly scaled. While we have not considered primary emissions of semi-volatile organics or organics with intermediate volatility, we assume that half of our POA emissions are SOA. This assumption is simpler than the detailed modeling of semi-

volatile emissions by Pye and Seinfeld (2010), but is generally consistent with their findings. The budget for these compounds follows that given in Table 2-3 for total POA, but the burden is only half the quantities shown there.

2.2.4 Dry and wet deposition

We treat the dry deposition of gas phase species in the same manner as Ito et al. (2007), which uses the dry deposition algorithm described in Wang et al. (1998). Bessagnet et al. (2010) demonstrated the importance of dry deposition of semi-volatile organic compounds to the estimate of SOA concentrations, and Karl et al. (2010) showed that a model with a small value of reactive factor f_0 (i.e., f_0=0 or 0.1) for oxygenated VOCs may underestimate their dry deposition remove rate as measured by ecosystem-scale flux measurements. In this paper, we use the same dry deposition loss rate for SVOCs as that for PAN, i.e. a reactive factor f_0 of 0.1. Gravitational settling is taken into account for aerosol species. The settling velocity and the slip correction factor for Stokes law are calculated from Seinfeld and Pandis (1998) using the mass-weighted average radius in each size bin for each aerosol component based on the assumed dry size distribution and it's growth with relative humidity. Wet deposition is calculated using the scavenging module developed by Mari et al. (2000) and Liu et al. (2001) which includes scavenging in convective updrafts and first-order rainout and washout in precipitating columns. The horizontal fractional area of each grid box experiencing precipitation is based on the work by Giorgi and Chameides (1986) assuming a cloud liquid water content of 1.5 g m^{-3} for stratiform cloud and 2.0 g m^{-3} for convective cloud. Wet removal of gas-phase organic compounds is calculated based on the Henry's law constant. We adopted Henry's law coefficients for gas-phase species from Ito et al. (2007). The scavenging efficiencies of OA as well as other aerosol types are equal to the mass fraction of OA that is activated to cloud droplets in liquid clouds. The calculation of the mass fraction is based on the cloud droplet activation parameterization of Abdul-Razzak and Ghan (2000, 2002). The detailed description of the cloud activation parameterization may be found in Wang and Penner (2009).

Table 2-3 Global budgets for organic aerosols from oceans and primary sources (Tg/yr)[a].

	This Work
POA from oceans	
Formation of MSA from DMS	8.2
Primary organics from sea spray	34.9
Dry deposition	5.1
Wet deposition	38.0
Burden	0.25
Lifetime (days)	2.1
Anthropogenic POA	
Fossil/bio fuel emission	15.7
Dry deposition	1.5
Wet deposition	14.2
Burden	0.13
Lifetime	3.0
Open burning emission	47.4
Dry deposition	3.7
Wet deposition	43.7
Burden	0.64
Lifetime	4.9

[a]Half of the anthropogenic POA emissions are assumed to be composed of low-volatility compounds that may have undergone reactions and partitioned back into the aerosol form as SOA.

Table 2-4 Global budgets for organic aerosols from oceans and primary sources (Tg/yr)[a].

		sv_oSOA	ne_oSOA	ne_GLYX	ne_MGLY	ne_IEPOX	Total SOA
Burden (Tg)	Simulation A	0.06	0.54	0.15	0.34	0.56	1.65
	Simulation B	0.04	0.39	0.19	0.26	0.20	1.08
	Simulation C	0.07	0.62	0.20	0.30	0.35	1.54
Total production (Tg/yr)	Simulation A	7.0	24.5	13.5	38.3	37.2	120.5
	Simulation B	5.8	17.8	22.2	32.1	12.9	90.8
	Simulation C	8.1	26.6	22.6	36.9	25.1	119.3
Anthropogenic production (Tg/yr)	Simulation A	1.1	3.7	2.5	5.9	0.0	13.2
	Simulation B	1.1	3.4	2.7	6.6	0.0	13.8
	Simulation C	1.1	3.6	2.6	6.4	0.0	13.7
Biogenic production (Tg/yr)	Simulation A	5.9	20.8	11.0	32.4	37.2	107.3
	Simulation B	4.7	14.4	19.5	25.6	12.9	77.0
	Simulation C	7.0	23.0	20.0	30.5	25.1	105.6
Lifetime (days)	Simulation A	3.1	8.1	4.1	3.2	5.5	5.0
	Simulation B	2.5	8.0	3.1	3.0	5.7	4.3
	Simulation C	3.1	8.5	3.2	3.0	5.1	4.7

2.3 Results

Here we summarize our model predictions for SOA and OM and compare these to measurements. Liu et al. (2005) provided a thorough evaluation of the model-predicted sulfate, black carbon, dust, and sea salt so this is not repeated here.

2.3.1 Budget calculation

The budget of POA from ocean sources and fossil fuel and biomass burning is shown in Table 2-3. The atmospheric burden of organics from the oceans is 0.25 Tg, with a lifetime of 2.1 days. This lifetime is somewhat shorter than the lifetime for the average over all organics in the standard version of the IMPACT model (Liu et al. 2005), which is 3.2 days, and may reflect the fact that most of the current source only injects POA into the lowest model layer over the oceans. The total atmospheric burden of fossil and biofuel POA is 0.13 Tg, while that for biomass burning is 0.64 Tg. The lifetime for the surface-based fossil and biofuel emissions is 3.0 days, while that for open burning is 4.9 days. The average lifetime computed here differs somewhat from that in Liu et al. (2005) because our scavenging treatment has been adjusted to reflect the mass fraction of OM that acts to form cloud droplets as a cloud condensation nuclei.

Table 2-4 summarizes the production and the burden for the three simulations performed in this study (i.e. Simulation A without HO_x recycling, Simulation B with Peeters et al. (2009) HO_x regeneration, and Simulation C with reduced HO_x recycling rate). The total production rate of SOA in Simulation A is 120 Tg/yr. A little more than 62% of the production rate is approximately evenly split between sources associated with methylglyoxal and epoxide while 26% is associated with sv_oSOA and ne_oSOA and 11% with glyoxal. The introduction of the HO_x recycling mechanism of Peeters et al. (2009) has a large impact on the global average SOA burden and production rate. Both the total burden and production rate decrease by about 30% in comparison to that of Simulation A, whereas the burden in Simulation C is only 5% smaller than that in Simulation A. This reduction is caused by the competition of the 1, 5- and 1, 6-H shift reactions of the isoprene peroxy radicals with their traditional bimolecular reactions (e.g. reactions with NO and HO_2), which reduces the epoxide formation rate more than it is increased due to the increase in OH and HO_2. A detailed analysis of this competition will be described below. The burden and source strength in Simulation C lies between those in Simulation A and Simulation B.

The global budget of SOA is very uncertain. Recent top-down estimates based either on the mass balance of VOCs or on scaling to the sulfate budget suggest a global source strength ranging from 140-910 Tg C/yr (Goldstein and Galbally, 2007; Hallquist et al., 2009) corresponding to 280-1820 Tg/yr if the ratio of total OA to OC is 2.0 (Tupin and Lim, 2001). A more recent top-down estimate of the total OA budget using satellite observations of aerosol optical depth and a global model (Heald et al., 2010) was consistent with an SOA source of 150±120 Tg C/yr corresponding to 300 ±240 Tg/yr if one assumes an OA:OC ratio of 2:1. In addition, Spracklen et al. (2011) estimate a SOA source ranging from 50 to 230 Tg/year, based on fitting the results of a global chemical transport model to aerosol mass spectrometer (AMS) observations. In contrast to these top-down estimates, traditional bottom-up estimates from global models that use known or inferred biogenic and/or anthropogenic VOC precursor fluxes together with laboratory data from oxidation experiments give much lower SOA production rates of 14-82 Tg/yr (Hallquist et al., 2009).

When comparing with some other global chemical transport model bottom-up estimates (Table 2-5), our SOA production rates are larger in all simulations, but are well within the range deduced by Heald et al. (2010) and Spracklen et al. (2011). This higher source of SOA formation mainly comes from the irreversible uptake of gas phase glyoxal, methylglyoxal and IEPOX which are not taken into account in traditional two-product models. Actually, our source of sv_oSOA and ne_oSOA as indicated in Table 2-4 is comparable to the SOA sources reported for other models. Table 2-5 also breaks down the sources into those from anthropogenic emissions and those from biogenic emissions. The dominance of biogenic SOA production also agrees well with previous global model results. The fraction of biogenic production in our simulations, 84.8%-89.0%, is similar to that from previous models, i.e. typically 80-95%. The lifetime of total SOA in the model (4-5 days) is somewhat shorter than that from other models, except for the results reported by Utembe et al. (2011). This shorter lifetime is mainly due to the larger removal rate coefficients from wet scavenging. One reason for the larger wet removal rates in our model is that most carbonaceous aerosols are internally mixed with sulfate and are generally hygroscopic except very close to source regions (Liu et al., 2005).

Table 2-5 Global modeling studies of SOA precursor emissions, SOA production, burden and lifetime (Eb: emissions of biogenic species (i.e. isoprene and monoterpenes); Ea: emissions of anthropogenic species (i.e. aromatics); Pb: SOA production from biogenic species; Pa: SOA production from anthropogenic species; Pt and Bt: total SOA production and SOA burden).

References	Global Model	SOA model	Eb (Tg/yr)	Ea (Tg/yr)	Pb Tg/yr)	(Pa (Tg/yr)	Pt (Tg/yr)	Bt (Tg)	Lifetime (day)
O'Donnell et al. 2011	ECHAM5-HAM	2-product	537	17	21.0	5.6	26.6	0.83	11.4
Heald et al. 2008	CAM3	2-product	539[a]	16[a]	22.9[a]	1.4[a]	24.3[a]	0.59[a]	8.9
Farina et al. 2010	GISS II	Volatility basis	736	49	27.28	1.62-11.02[b]	28.9-38.3[b]	0.54-0.98[b]	6.8-9.4[b]
Utembe et al. 2011	STOCHEM	explicit chemistry	628	60	21.1	1.4	22.5	0.23	3.7
Hoyle et al.2009	Oslo CTM3	2-product	386[a]	21.6[a]	-	-	53.4-68.8[c]	0.50-0.7[c]	3.4-3.7[c]
Tsigaridis and Kanakidou, 2007	TM3	2-product	747.2	15.8	16.8	1.8	18.6	0.82	16.0
Henze et al. 2008	GEOS-Chem	2-product	635.2	18.8	26.8	3.5	30.3	0.81	9.8
Fu et al. 2008	GEOS-Chem	2-product[d]	570	9.8	26.7[a]	2.3[a]	29[a]	0.62[a]	7.8
This work	IMPACT	explicit chemistry	589.6[a]	12.9[a]	77.0-107.3	13.3-13.8	90.8-120.5	1.08-1.65	4.3-5.0

[a]:reported in Tg carbon and converted here using a 2:1 ratio of OM:OC

[b]: high estimate assumes chemical aging of anthropogenic SOA

[c]: high estimate assumes partitioning with sulfate

[d]: includes irreversible uptake of glyoxal and methlyglyoxal

The oligomer formation rates for SVOCs that partition to the aerosol phase are summarized in Table S1 in Appendix A, as well as the relative contribution (annual mean) of various biogenic and anthropogenic species to the total ne_oSOA. Among these precursors, PRN2, or isoprene-hydroxy-nitrate, makes the greatest contribution to total ne_oSOA (54%, 45% and 39% in Simulation A, B, and C, respectively). The global average source of PRN2 is mainly from the reaction of RIO_2 (RO2 from isoprene) with NO, although it also comes from some other reactions (e.g. the reaction of RO2 from

monoterpenes with NO). The reaction of RIO_2 with NO competes with the isomerization through the 1,5-H shift or 1,6-H shift. This competition reduces the PRN2 formation rate from the reaction of RIO_2 with NO. As a result, the PRN2 SOA production rate is decreased to 8.1 Tg/year in Simulation B from 13.4 Tg/year in Simulation A. Not surprisingly, the PRN2 production rate in Simulation C is higher than that in Simulation B.

The total anthropogenic source of sv_oSOA and ne_oSOA in Simulation A is 4.8 Tg/yr, while that from biogenics is 26.7 Tg/yr (Table 2-4). The lifetime of ne_oSOA is 8.1 days. This lifetime is much longer than that of the other SOA components. One reason for this longer lifetime is the longer lifetime of the precursors, which make them more likely to be transported to higher altitudes prior to the formation of SOA, where dry and wet deposition are less efficient. The lifetime of gas-phase PRN2, which contributes the most to ne_oSOA, is about 9 hours, which is longer than that of glyoxal and methylglyoxal (see Table 2-6). Another reason for the longer lifetime of ne_oSOA can be related to the temperature dependence of the gas-aerosol partition coefficients (Tsigaridis and Kanakidou, 2003; Hoyle et al., 2007). The lower temperature in the upper atmosphere favors condensation to form sv_oSOA on pre-existing aerosols thereby also forming more ne_oSOA.

Table 2-6 shows the budget for the glyoxal, methylglyoxal, and epoxide SOA precursors. For simulation A, the model predicts a total methylglyoxal formation rate of 156 Tg/yr from biogenic sources, with 26 Tg/yr from anthropogenic sources and 2.2 Tg/yr from acetone (which is a mixture of anthropogenic and biogenic sources). These may be compared to the source strengths reported by Fu et al. (2008) of 116 Tg/yr, 16 Tg/yr and 10 Tg/yr, respectively. Loss is primarily through photolysis (97 Tg/yr) and reaction with OH (43 Tg/yr), followed by the uptake by cloud drops (30 Tg/yr) and sulfate aerosols (8 Tg/yr). Our reaction with OH and on sulfate aerosols and clouds is a somewhat larger proportion of the total loss rate than that in Fu et al. (2008), and photolysis is somewhat less efficient than in Fu et al. (2008). If we add the HO_x recycling mechanism for isoprene oxidation, we produce less methylglyoxal (Simulation B), which is close to that reported by Fu et al. (2008). More methylglyoxal is again predicted in Simulation C when

the rates of the 1,5-H and 1,6-H shifts in isoprene peroxy radicals are reduced.

The inclusion of the Peeters et al. (2009) HO_x recycling mechanism in Simulation B increases the rate of production of glyoxal by about 34% compared to that in simulation A, while decreasing the rates of the 1,5-H and 1, 6-H shift increases the glyoxal production rate by about 6%. The total source of glyoxal from Simulation A is 49 Tg/yr. This is similar to the total source in Fu et al. (2008), but the proportion of our source from biogenics (89%) is much higher than that in Fu et al. (2008) (i.e. 54%). This source is significantly smaller, however, than the estimate of Stavrakou et al. (2009), 95 – 105 Tg/yr, which was based on inverse modeling to fit satellite observations of glyoxal. Because our lifetime of glyoxal is similar to that of Stavrakou et al. (2009) (i.e. 3.0 hours vs. 2.5 hours), we conclude that our glyoxal production rate may be too low to reproduce the satellite observations. The production rate of glyoxal is also relatively low in the other two simulations. The proportion of our sink from the reaction of glyoxal with OH and from the formation of aerosols is higher than that by Fu et al. (2008) in all three simulations.

The only pathway to produce epoxides is reaction of RIO with HO_2. The introduction of the Peeters et al. (2009) HO_x recycling pathway decreases the production of epoxides in spite of the increase in RIO_2 and HO_2 concentrations. Most of the epoxides are lost by reaction with OH, and about 20% reacts on sulfate aerosol to form organic aerosols.

The above secondary organic source gases result in total secondary organic aerosol burdens of 0.15, 0.34, and 0.56 Tg for ne_GLY, ne_MGLY and ne_IEPOX, respectively, in Simulation A. The lifetimes of these components are 4.1, 3.2 and 5.5 days. The inclusion of the Peeters et al. (2009) HO_x recycling mechanism makes the lifetime of ne_GLYX and ne_MGLY slightly shorter while slightly increasing the lifetime of ne_IEPOX. The reason for the shorter aerosol lifetime is related to the shorter lifetimes of the corresponding gas-phase precursors (Table 2-6). Higher OH concentrations in Simulation B consume glyoxal and methylglyoxal more efficiently so that they have shorter lifetimes. For ne_IEPOX, although its precursor epoxide also has a shorter lifetime when the HO_x recycling mechanism is included, the geographical distribution has changed (Figure 2-1), with its peak concentration shifting from tropical regions with

frequent precipitation to North America and East Asia with less precipitation. This change causes a smaller wet deposition flux of ne_IEPOX.

Table 2-6 Budgets for secondary organic aerosol precursors reacting on acidic aerosols and cloud drops (Tg/yr)

Glyoxal				
	Simulation A	Simulation B	Simulation C	Other work
Total sources	48.97	65.72	70.12	95-105 (Stavrakou et al. 2009)
Biogenic sources	39.95	57.78	62.16	24.28 (Fu et al. 2008)
Anthropogenic sources	9.02	7.94	7.96	20.47 (Fu et al. 2008)
Sinks				
Reaction with OH	9.97	15.28	14.79	6.5 (Fu et al. 2008)
Reaction with NO3	0.02	0.03	0.03	<0.1 (Fu et al. 2008)
Photolysis	23.05	22.89	27.57	28 (Fu et al. 2008)
Aerosol formation on cloud drops	10.35	16.90	17.84	5.5 (Fu et al. 2008)
Aerosol formation on sulfate aerosols	3.19	5.32	4.82	0.94 (Fu et al. 2008)
Wet deposition	1.57	3.21	3.14	1.9 (Fu et al. 2008)
Dry deposition	0.86	2.11	1.93	2.2 (Fu et al. 2008)
Burden	0.0170	0.020	0.022	0.015 (Fu et al. 2008)
Lifetime (hour)	3.0	2.7	2.8	2.9 (Fu et al. 2008)
Methylglyoxal				
	Simulation A	Simulation B	Simulation C	Fu et al. 2008
Total sources	184.5	143.2	167.6	131.8
Biogenic sources	156.3	114.3	138.7	115.6
Anthropogenic sources	26.0	25.6	25.9	16.2
Acetone	2.2	3.3	3.0	10
Sinks				

Reaction with OH	43.0	43.6	45.5	15
Reaction with NO3	9.6E-02	7.0E-02	8.3E-02	<0.1
Photolysis	97.2	62.7	80.0	100
Aerosol formation on cloud drops	30.4	24.6	29.1	14
Aerosol formation on sulfate aerosols	7.9	7.5	7.8	1.4
Wet deposition	3.1	2.8	3.2	1.8
Dry deposition	1.8	1.9	2.0	1.7
Burden	0.037	0.027	0.032	0.025
Lifetime (hours)	1.8	1.7	1.7	1.6

Epoxides from isoprene

	Simulation A	Simulation B	Simulation C
Formation of IEPOX	195.2	78.5	150.7
Sinks			
reaction with OH	157.9	65.8	125.5
Converted to SOA	37.2	12.9	25.1
Burden	0.259	0.063	0.145
Lifetime (hour)	11.6	7.0	8.4

2.3.2 Global and vertical distributions

Figure 2-1 and Figure 2-2 show the annual mean simulated concentrations of POA and SOA at the surface, respectively. The surface distribution of POA shows high concentrations in areas where significant biomass burning occurs. This pattern is consistent with the global average source from biomass burning which contributes 75.1% of the global average primary organic aerosols from combustion sources. The geographical distribution of SOA also reflects precursor emissions, with large concentrations of biogenic (isoprene) SOA in the tropics and in the southeastern United States. The SOA from gas to particle partitioning (sv_oSOA and ne_oSOA) shows a surface peak over Africa, which tracks POA to a certain extent. This correspondence

between POA and sv_oSOA is related to the fact that the formation of sv_oSOA depends on both the supply of SOA precursors and oxidants and the presence of POA as a partitioning medium. On the other hand, the formation of ne_MGLY, ne_GLYX and ne_IEPOX are related to the sulfate concentration to some extent, which is reflected in the strong peaks in their surface concentrations near polluted areas in the Northern Hemisphere.

The change of each SOA component and total SOA between Simulation A and Simulations B and C is also shown in Figure 2-2. Generally, the introduction of the Peeters et al. (2009) isoprene mechanism decreases sv_oSOA, ne_oSOA and ne_IEPOX surface concentrations and increases ne_GLYX surface concentrations, which is consistent with the change in global sources as described above. ne_MGLY surface concentrations change very little between Simulation A and Simulations B and C. Most regions show a decrease in the total SOA between Simulation B and A, consistent with the decreases in sv_oSOA, ne_oSOA and ne_IEPOX. Slowing the rates of the 1,5-H and 1,6-H shifts in isoprene radicals in Simulation C causes all the surface SOA component surface concentrations to increase compared to Simulation B and the total SOA at the surface is larger than in simulation A.

The zonal average vertical distribution of POA and SOA is shown in Figure 2-1 and Figure 2-3. The high concentrations of POA and SOA in the tropics near the surface (below 700 hPa) are consistent with the biomass burning sources and the significant SOA formation from biogenic precursors, respectively, as described above. One obvious feature of the ne_oSOA plot is that there is sustained SOA production in the free troposphere due to the relatively long lifetimes of ne_oSOA precursors and the colder temperatures in the free troposphere compared to those at the surface, causing a maximum in its concentration near 750 hPa.

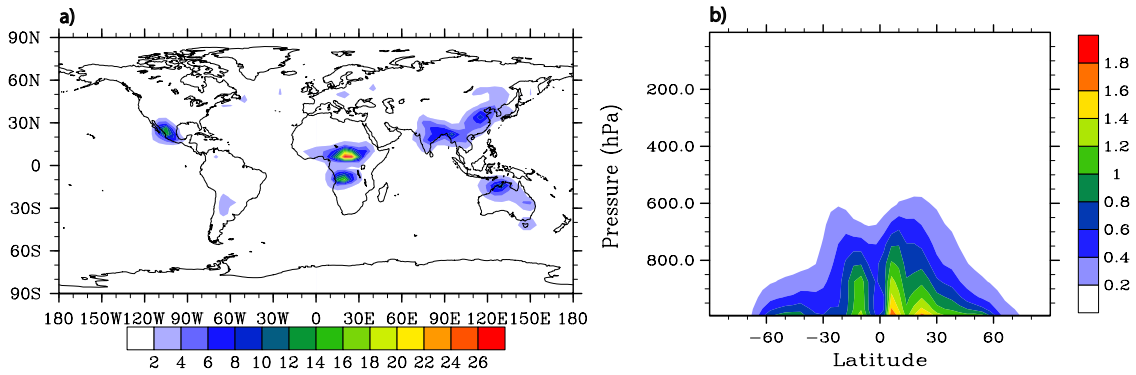

Figure 2-1 Annual mean simulated surface POA concentrations (left) and zonal distrutubion of POA concentrations (right).Units: $\mu g/m^3$.

Table 2-7 Normalized mean bias (NMB) and correlation coefficient (R) between the predicted SOA for the simulation and observations. The number of sites in the comparison is in parentheses.

Simulation name	AMS measurements (Zhang et al., 2007)					
	Urban sites (N=14)		Urban downwind sites (N=6)		Rural sites (N=17)	
	NMB	R	NMB	R	NMB	R
Simulation A	-15.2%	0.75	5.8%	0.85	15.7%	0.33
Simulation B	-23.0%	0.74	-8.9%	0.86	6.5%	0.34
Simulation C	-12.5%	0.72	8.9%	0.86	20.0%	0.30
	IMPROVE network (N=48)					
	Annual average		Summer		Winter	
	NMB	R	NMB	R	NMB	R
Simulation A	-2.4%	0.35	10.1%	0.37	-15.0%	0.38
Simulation B	-9.3%	0.39	-4.8%	0.44	-14.2%	0.40
Simulation C	1.7%	0.41	16.8%	0.44	-13.8%	0.40

2.4 Comparison with measurements

2.4.1 Surface measurements

Figure 2-4 shows a comparison of annual mean model predicted and measured OA concentrations (from March 1996 to February 1999) in the United States for the 48 sites of the Interagency Monitoring of Protected Visual Environments (IMPROVE) network (Malm et al., 2000). Measurement data are reported as organic carbon (OC) in micrograms of carbon per cubic meter, while the model predicts organic mass (OM) concentrations. To convert OM to OC, we use a factor of 1.4 for POA and 1.8 for ne_oSOA. These factors are based on Tupin and Lim (2001) who suggested an average of 1.6± 0.2 for OM:OC ratio for urban OA and 2.1±0.2 for more-oxygenated background aerosol. For other SOA components, we converted OM to OC based on their molecular mass and carbon number (i.e. 2.4 for ne_GLYX, 2.0 for ne_MGLY and 1.9 for ne_IEPOX). As shown in Figure 2-4(a), the simulated concentrations for most of the IMPROVE sites are generally within a factor of 2 of the observed concentrations. The annual mean OA concentrations have a mean bias (MB) of -0.04 ug C/m^3 and a normalized mean bias (NMB) of -2.4% for Simulation A, a MB of -0.16 ugC/m^3 and NMB of -9.3% for Simulation B, and a MB of 0.03 ugC/m^3 and NMB of 1.7% for Simulation C (Table 2-7). The correlation coefficients (R) between observations and simulations for these three simulations are around 0.40 (Table 2-7), which indicates that the model does not capture the observed spatial variability well in North America. Figure 2-5 shows the simulated versus measured seasonal mean OA concentrations for the IMPROVE sites in summer and winter and the values of NMB and R for these comparisons are shown in Table 2-7. While the model slightly over-estimates the observations in the summer, the comparison in the winter has a NMB of around -15%. The correlation coefficients for the summer and winter are similar to that in the annual mean comparison.

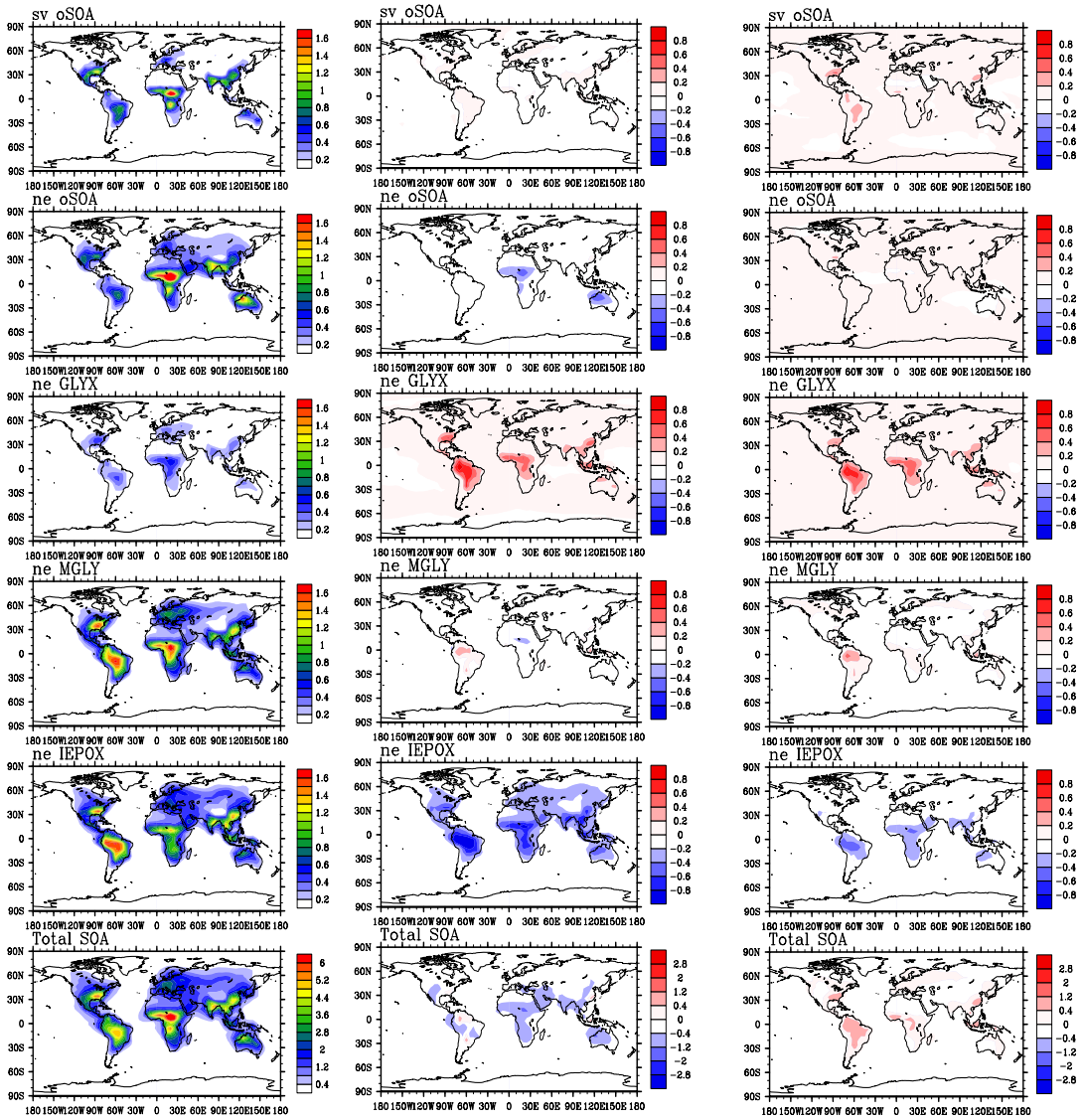

Figure 2-2 Annual mean simulated surface SOA concentrations in Simulation A (first column) and the changes in surface SOA concentrations from Simulation A after including the new HO_x recycling mechanism (Simulation B-Simulation A) in the second column, and reducing the reaction rates of 1,5-H and 1,6-H shifts by a factor 10 (Simulation C- Simulation A) in the third column for each SOA component (the first 5 rows) and the total SOA (the sixth row). The maximum and minimum values for color scales in the second and third column are set to half the maximum values of those in the first column (Simulation A). Units: $\mu g/m^3$.

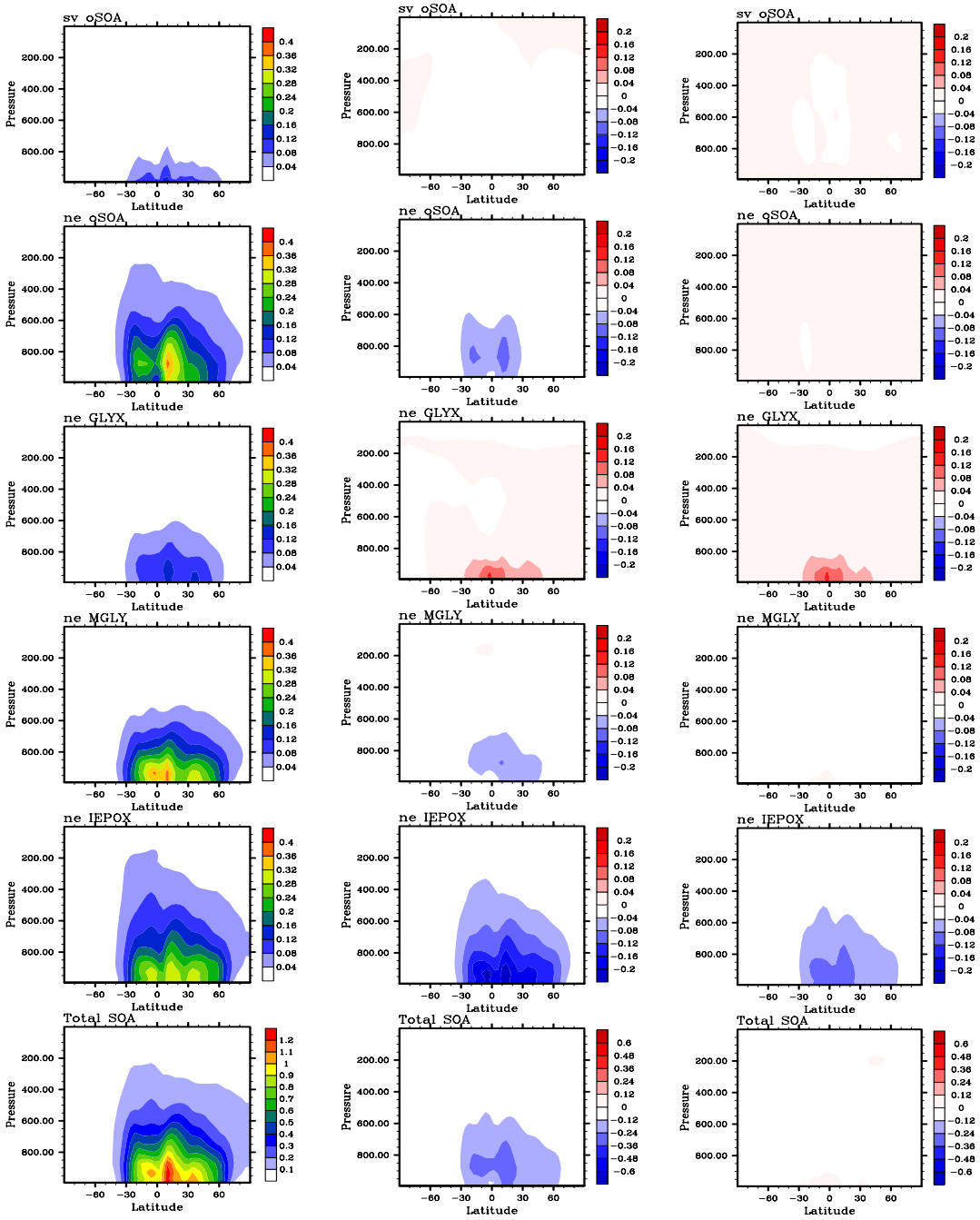

Figure 2-3 Annual zonal mean simulated SOA concentrations in Simulation A (first column) and the changes in vertical distributions of SOA concentrations from Simulation A after including the new HO_x recycling mechanism (Simulation B-Simulation A) in the second column, and reducing the reaction rates of 1,5-H and 1,6-H shifts by a factor 10 (Simulation C- Simulation A) in the third column for each SOA component (the first 5 rows) and the total SOA (the sixth row). The maximum and minimum values for color scales in the second and third column are set to half the maximum values of those in the first column (Simulation A). Units: $\mu g/m^3$.

Chung and Seinfeld (2002) compared their results with observations from the IMPROVE network and reported that OM concentrations were consistently under-predicted by a factor of 3 or more. Park et al. (2003) showed a small bias (~20%) in predicted OC concentrations when compared to IMPROVE sites for the year 1998. Liao et al. (2007) under-predicted OM relative to measurements over the United States with a NMB of -34.2%. Farina et al. (2010) found that their model under-predicted OM by ~ 26% when compared to the IMPROVE network. This model included the chemical aging of anthropogenic SOA by gas-phase reaction of the SOA component with the hydroxyl radical. Both Park et al. (2003) and Farina et al. (2010) reported spatial pattern correlation coefficients R of around 0.65. Liao et al. (2007) compared to observed seasonal mean surface OA concentrations in the IMPROVE network and obtained correlation coefficients (R) in different seasons that ranged from 0.4 to 0.7.

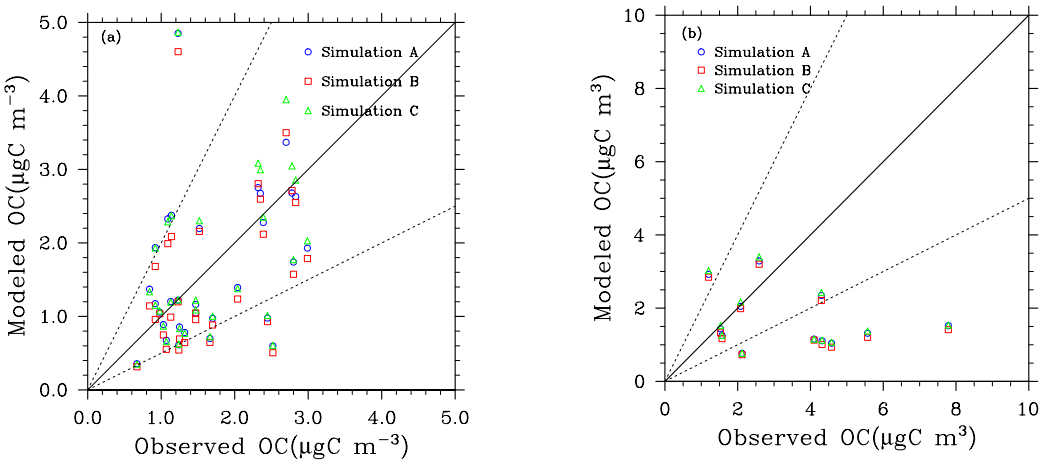

Figure 2-4 Total annual averaged organic aerosol model comparison with the IMPROVE (a) and EMEP (b) observation networks. The solid lines represent ideal agreement (1:1 ratio), and the dashed lines are the 2:1 and 1:2 ratios, i.e. indicating agreement within a factor of 2. The IMPROVE network data are from 1996 to 1999, and the EMEP measurements were made in 2002-2003. The meteorology data used to run the model were for 1997.

Figure 2-4(b) compares the model results to measurements taken in Europe during a one-year campaign, performed in 2002-2003 and focused on elemental and organic carbon, as part of the European Monitoring and Evaluation Program (EMEP) (Yttri et al., 2007). Again, we used a scaling factor of 1.4 for POA and 1.8 for ne_oSOA to covert from units of OM to units of OC. In contrast to the comparison with the IMPROVE stations, the results of the model are significantly lower than all of the corresponding observations. The average concentrations observed at EMEP sites, however, are much higher than in the IMPROVE data set, as PM10 measurements were reported at the EMEP sites vs. PM2.5 in the IMPROVE network. These large particles are not captured in the model, because we assume that all organics are only present as sub-micron particles. To gain further insight into the reasons for the difference between the model and observations, we examined the results for the summer and winter, respectively (Figure 2-6). From the figure, it can be seen that SOA dominates OM in the summer and POA dominates in the winter when POA sources are larger (e.g. biomass burning) and isoprene emissions are low, consistent with other studies (Szidat et al., 2006; Simpson et al., 2007). Gelencsér et al. (2007) analyzed the PM2.5 organic aerosol over Europe from the CARBOSOL project and concluded that biomass burning primary emissions were a significant contributor to OC in winter. Therefore a possible reason for the wintertime discrepancy is that the emissions from domestic wood combustion are not fully represented in our emission database. To examine this hypothesis, we compared the model results with the corresponding components from the source-apportionment analysis of CARBOSOL in Gelencsér et al. (2007) for two surface sites (Aveiro, K-Puszta) (Table 2-8), as did Simpson et al. (2007). It may be of interest to also include the other two mountain sites, but surface sites reflect the boundary layer sources of OA (e.g. biomass burning) more directly. In addition, the comparisons with these surface sites are more comparable to evaluations that use the EMEP network for which most observations are near the surface. Recently, Gilardoni et al. (2011b) specifically distinguished primary and secondary biomass burning organic carbon from primary and secondary fossil organic carbon as well as biogenic organic carbon by using a combined ^{14}C – macro tracer analysis in Ispra, a site in northern Italy. Here we also compare our model results with their analysis in Table 2-8. Obviously, the primary biomass burning organic carbon is significantly under-

represented in the model. This may be due to the coarse resolution of the model, which cannot resolve the effects of local emissions. Another possible reason for the wintertime discrepancy is that the emissions from domestic wood combustion are too low in our emission database, which was also found in other model comparisons in Alpine Valleys (Szidat et al., 2007) and Ispra (Gilardoni et al., 2011b) during winter. For SOA, the model generally underestimates the observations. The SOA at the other European sites, therefore, is likely also underestimated in the model. The underestimation of SOA in Europe may be caused by the underestimation of biogenic VOC emissions in these regions, by the low value of enthalpy that is used to represent the temperature dependence of gas-particle partitioning efficiency, by a wet scavenging rate that is too high, or by an underrepresentation of SOA formation from anthropogenic sources. It should nevertheless be emphasized that some of the EMEP stations, notably Ispra, are located in topographically pronounced terrain and represent rather localized conditions, which are difficult to quantitatively capture with a global model.

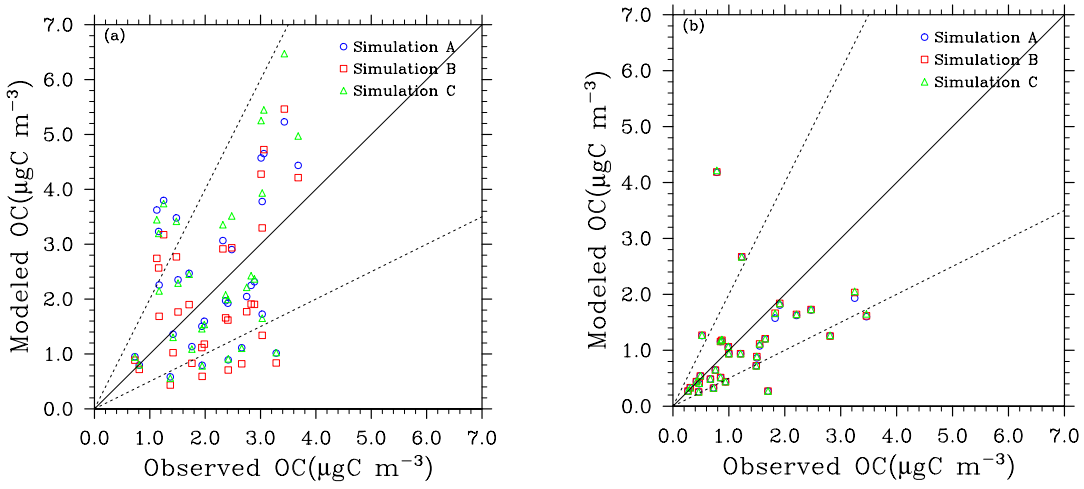

Figure 2-5 Simulated versus observed seasonal mean OC concentrations for the IMPROVE network. (a) summer (JJA) and (b) winter (DJF). The solid lines represent ideal agreement (1:1 ratio), and the dashed lines are the 2:1 and 1:2 ratios. The IMPROVE network data are from 1996 to 1999. The meteorology data used to run the model were for 1997.

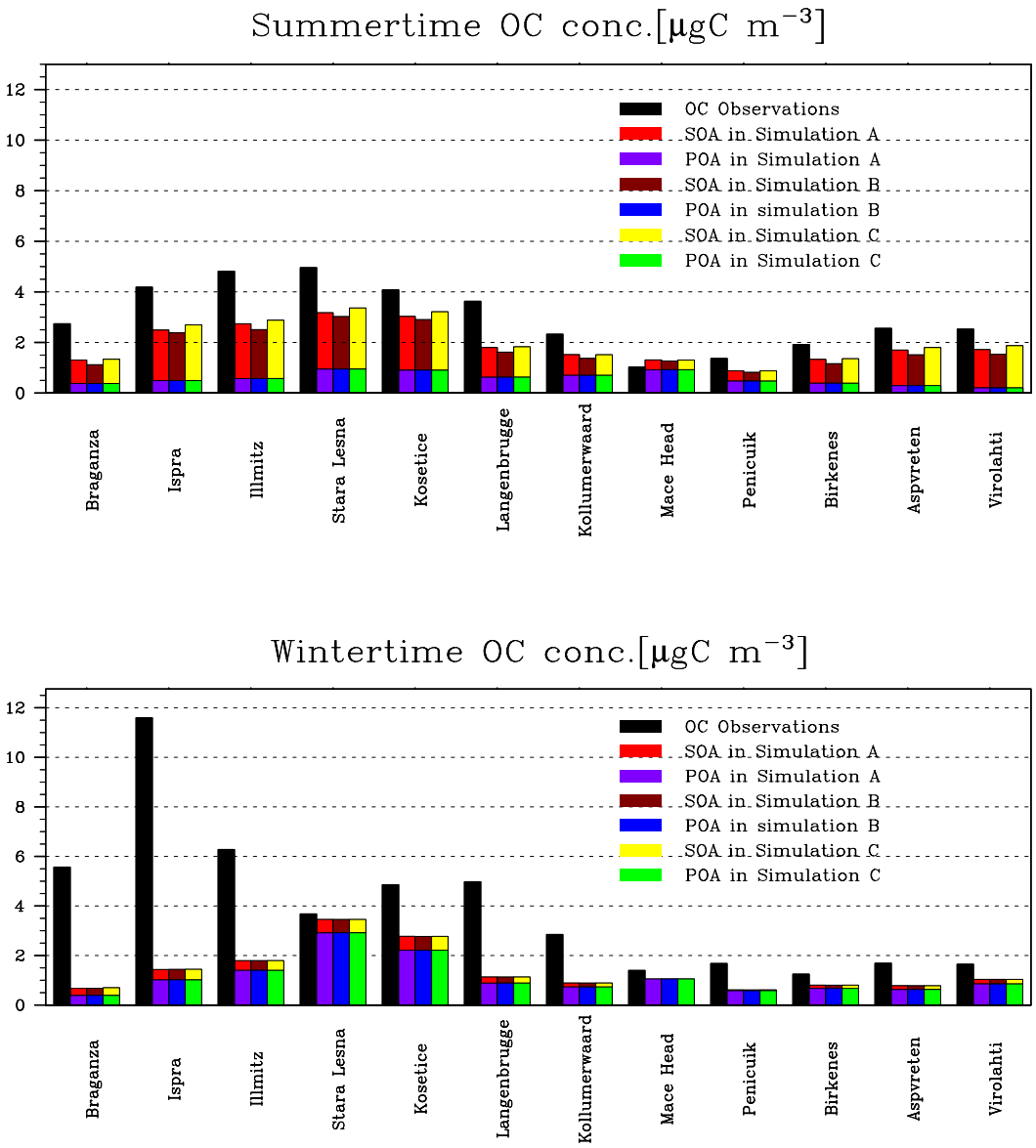

Figure 2-6 OC concentrations in summer (July 2002-October 2002 and April 2003-July 2003) and winter (October 2002-April 2003) for 12 rural sites in the EMEP network. Y axis: OC concentration; X axis: site names (the sites are ordered according to latitude from the most southern station (left) to the the most northern station (right).

Table 2-8 Comparison of simulated seasonal average carbon concentrations (in µg C/m3) with the observations made in Aveiro and K-Puszta from Gelencsér et al. (2007) and in Ispra from Gilardoni et al. (2011b).

Station Name	Source	Winter				Summer			
		Observation	Simulation A	Simulation B	Simulation C	Observations	Simulation A	Simulation B	Simulation C
Aveiro	POC_bb[a]	8.96	0.02	0.02	0.02	0.28	0.06	0.06	0.06
	POC_ff[a]	0.18	0.08	0.08	0.08	0.30	0.02	0.02	0.02
	SOC_bio[a]	0.70	0.10	0.10	0.11	2.54	0.29	0.22	0.29
	SOC_ff[a]	2.27	0.04	0.04	0.04	0.30	0.01	0.01	0.01
K-Puszta	POC_bb	4.30	0.01	0.01	0.01	0.32	0.03	0.03	0.03
	POC_ff	0.59	1.75	1.75	1.75	0.27	0.56	0.56	0.56
	SOC_bio	2.24	0.04	0.04	0.04	3.48	2.29	1.94	2.44
	SOC_ff	1.63	0.24	0.24	0.24	0.19	0.20	0.14	0.15
Ispra	POC_bb	11.9	0.02	0.02	0.02	0.5	0.04	0.04	0.04
	POC_ff	1.2	0.82	0.82	0.82	0.6	0.34	0.34	0.34
	SOC_bio	2.0	0.19	0.20	0.21	3.1	1.83	1.78	2.10
	SOC_ff	2.3	0.26	0.25	0.25	1.3	0.23	0.20	0.21

[a]POC_bb: primary organic carbon from biomass burning; POC_ff: primary organic carbon from fossil fuel and biofuel burning; SOC_bio: secondary organic carbon from the oxidation of biogenic species; SOC_ff: secondary organic carbon from fossil fuel and biofuel burning. Half of the POC burden is assumed to be composed of low-volatility compounds that may have undergone reactions and partitioned back into the aerosol form as SOA after emission.

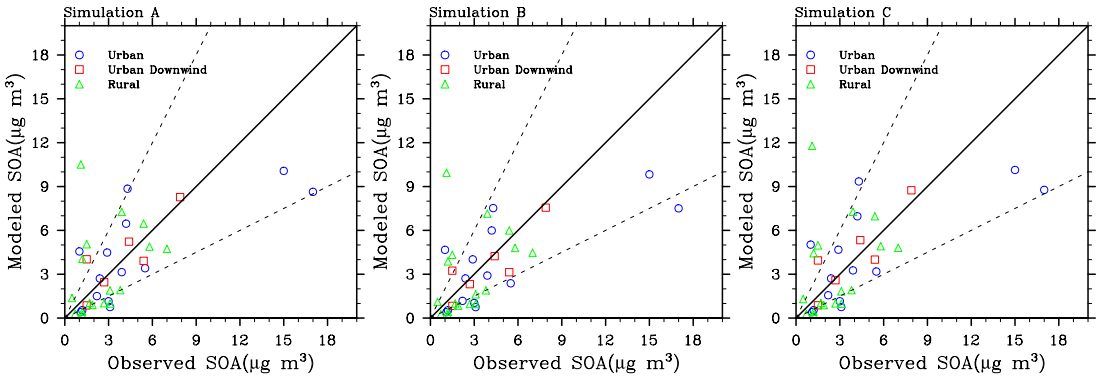

Figure 2-7 Comparison of SOA mass concentrations observed at the urban, urban-downwind and rural sites reported in Zhang et al. (2007) with those simulated in Simulation A (a), Simulation B(b) and Simulation C(c). Solid lines show the 1:1 ratio, and dashed lines show the 1:2 and 2:1 ratios. The measurements at the various sites were made in different seasons and different years between 2000 and 2006 and were reported for the average of varying durations spanning from 8 to 36 days. The model results are the average values over the same months as the observations.

Zhang et al. (2007) present observational SOA data (measured by aerosol mass spectrometry, AMS) from a series of surface measurements at multiple sites in the Northern Hemisphere. The measurements at the various sites were made in different seasons and different years between 2000 and 2006 and were reported for the average of varying durations spanning from 8 to 36 days. In addition, most of the reported measurements were performed in urban locations. However, because of the unique nature of these measurements, all sites are included in our comparison though we differentiate the urban and downwind urban sites from rural sites. Figure 2-7 shows that the model underestimates the observations in urban locations, while it overestimates the measurements for rural sites and urban downwind sites. We do not expect the model with its low horizontal resolution to capture the POA emissions at urban sites, nor would we capture high local VOC and NO_x emissions, which have a very complex effect on SOA formation due to non-linear chemistry (Stroud et al., 2011). Nevertheless, the model-predicted SOA is subject to longer formation times than is POA, and is in reasonable agreement with the AMS observations. The NMB for Simulation A is -0.152, 0.058 and 0.157 for urban, urban downwind and rural sites, respectively (see the Table 2-7). The

introduction of the Peeters et al. (2009) isoprene mechanism improves the agreement between predicted and observed SOA concentrations at rural sites giving an NMB of 0.065, but under-estimates the urban observations even more. The correlation coefficient for the rural sites in the AMS data set is small, similar to the correlation coefficient for the IMPROVE sites.

The Zhang et al. (2007) database is limited to the Northern Hemisphere extra-tropics, which are influenced by both anthropogenic and biogenic sources. Observations from more remote forested regions may provide a more stringent test of the biogenic sources represented in the model. Table 2-9 shows measurements from three different campaigns in tropical forested areas in comparison with the model simulations corresponding to the location and time of measurements. While typical measurements in Northern mid latitudes indicate an average of about 2~3 $\mu g/m^3$ for remote sites (Zhang et al., 2007), these forested regions show a relatively low loading of OM of only ~1 $\mu g/m^3$. In contrast, the model predicts OM that is about a factor of 3 too high over both West Africa and the Amazon basin and a factor of 2 too high over Borneo, Malaysia. Chen et al. (2009) indicated that biogenic SOA dominated the submicron organic aerosol during the AMAZE 2008 experiment, consistent with our model findings. Therefore it seems likely that either the production rate of SOA in the model is too large or the biogenic sources are too strong, although the prediction of POA at this site explains around 10% of the total predicted OM. The introduction of the Peeters et al. (2009) HO_x-recycling mechanism improves the model estimate of isoprene, but actually degrades the comparison of OM by a small amount. It appears from these comparisons that the SOA formation mechanism (from, for example, the uptake of glyoxal, methyglyoxal and epoxide) in tropical forests needs to be improved. Amazon basin OC concentrations were also overestimated in the recent study of Gilardoni et al. (2011a), who investigated the composition of fine and coarse aerosols in a Brazilian forest site from February through September 2008. Gilardoni et al. (2011a) reported average $PM_{2.5}$ OM concentrations during the wet season (February-June) of 1.7 $\mu g /m^3$, larger than the wet season concentrations measured at the same site by Chen et al. (2009) by about 60-80%. In comparison with these measurements, our simulated concentrations are high by a factor of 2. The Gilardoni et al. (2011a) simulations were based on the TM5 global chemistry

transport model and treat SOA as a primary species (i.e., they assumed that 15% of natural terpene emissions form SOA and are directly emitted into the model atmosphere). Thus, these simulations also cannot capture observed OM in tropical regions.

Table 2-9 Comparison of simulated OA with observed OA measured in tropical forested regions.

		Observations	Simulation A	Simulation B	Simulation C
West Africa (below 2km)	Total OM (μg m^{-3})	1.18 (Capes et al., 2009)	5.20	4.53	5.59
	POA[a] (μg m^{-3})	-	0.57	0.57	0.57
	sv_oSOA (μg m^{-3})	-	0.42	0.41	0.55
	ne_oSOA (μg m^{-3})	-	0.70	0.51	0.79
	ne_GLYX (μg m^{-3})	-	0.49	1.08	1.03
	ne_MGLY (μg m^{-3})	-	1.59	1.45	1.63
	ne_IEPOX (μg m^{-3})	-	1.43	0.51	1.02
	Isoprene (ppt)	620 (Capes et al., 2009)	1734	845	1126
	NOx (ppb)	0.21 (Capes et al., 2009)	0.34	0.37	0.35
Amazon basin (surface)	Total OM (μg m^{-3})	0.70 (Chen et al., 2009)	3.55	3.82	4.45
		1.70 (Gilardoni et al., 2011a)			
	POA[a] (μg m^{-3})	-	0.36	0.36	0.36
	sv_oSOA (μg m^{-3})	-	0.28	0.36	0.46
	ne_oSOA (μg m^{-3})	-	0.31	0.26	0.37

	ne_GLYX (µg m^{-3})	-	0.24	0.95	0.87
	ne_MGLY (µg m^{-3})	-	1.20	1.49	1.57
	ne_IEPOX (µg m^{-3})	-	1.12	0.40	0.82
	Isoprene (ppb)	2.0 (Chen et al., 2009)	4.4	1.9	2.7
Malaysian Borneo (surface)	Total OM (µg m^{-3})	0.74 (Robinson et al., 2011)	1.53	1.21	1.57
	POA[a] (µg m^{-3})	-	0.25	0.25	0.25
	sv_oSOA (µg m^{-3})	-	0.07	0.05	0.08
	ne_oSOA (µg m^{-3})	-	0.08	0.06	0.09
	ne_GLYX (µg m^{-3})	-	0.15	0.32	0.34
	ne_MGLY (µg m^{-3})	-	0.45	0.40	0.47
	ne_IEPOX (µg m^{-3})	-	0.53	0.13	0.34

[a] Half of the POA burden is assumed to be composed of low-volatility compounds that may have undergone reactions and partitioned back into the aerosol form as SOA after emission.

The comparisons with the measurements reported above provide an evaluation of the model's ability to predict OA or OC mass distributions, but they do not evaluate the predicted chemical composition of the organic aerosol. There are very few speciated compounds that can be compared to the model, but organic functional groups in atmospheric particles have been measured by proton nuclear magnetic resonance (^{1}H-NMR) spectroscopy (Decesari et al., 2000) which provide some insight into the OA composition. Therefore we compiled the data for measured functional groups reported in the literature, and compare these to the relative contributions of different functional groups in the model predictions. We included the ^{1}H-NMR data measured in mid-

latitudes in the warm season (Po Valley in spring and summer (Decesari et al., 2001), Mace Head (Ireland) from April to October for submicron WSOC (Cavalli et al., 2004), Jeju Island (Korea) during ACE-Asia (Decesari et al., 2005), and Hyyttiälä (Finland) in spring (Cavalli et al., 2006)), i.e., under conditions in which SOA are expected to dominate. These data all show compositions with a high H-C (unfunctionalized alkyls) and HC-C=O (aliphatic carbons bound to an unsaturated carbon atom) content, which roughly accounts for 50% and 35% of the total WSOC mass, respectively. The model underestimates the contributions of these two functional groups in Simulation A which predicts that the total SOA predicted in these regions consists of approximately 35% of H-C, 10% of HC-C=O, and 35% of H-C=O (aldehyde). The introduction of the Peeters et al. (2009) HO_x recycling mechanism does not improve the prediction by very much and increases the fraction of the H-C=O group to about 40%. Most of H-C=O group in the model comes from ne_GLYX and ne_MGLY, which we assumed had the same chemical structural as their gas-phase precursors for this comparison. This assumption may overestimate the contribution of H-C=O group and underestimate the contribution of HC-C=O group, because many laboratory studies have suggested that dissolved glyoxal and methylglyoxal will be oxidized by dissolved OH to carboxylic acids (e.g., glyoxylic, oxalic and pyruvic acid) in cloud and aerosol water (Ervens and Volkamer, 2010; Lim et al., 2010; Tan et al., 2010). Overall, the model can predict the measured H-C group to some extent, but, without further defining the chemistry of dissolved glyoxal and methylglyoxal, underestimates the relative abundance of the HC-C=O group and over-predicts the contribution of the H-C=O group.

2.4.2 Vertical profiles

Figure 2-8 (a) compares the simulated mean vertical profile of OC concentrations and the observed mean profile measured by aircraft off the Coast of Japan during the ACE-Asia campaign from April to May 2001. The measurements were made by two methods (thermal optical analysis and Fourier Transform infrared transmission spectroscopy) and were in excellent agreement (Maria et al., 2003). Heald et al. (2005) compared these measurements with the simulation from the GEOS-Chem global 3-D chemical transport model, and deduced that a large source of organic aerosol in the free troposphere is

missing from current models. Here, we show the results of our model for the same month that the measurements were made, but for a different year and consequently with different meteorology than during the measurements. Figure 2-8 (a) shows that there are still large discrepancies between the model and the measurements in the free troposphere, although the magnitude of the discrepancy is smaller than that reported by Heald et al. (2005) (10-100 times). Dunlea et al. (2009) examined the evolution of Asian aerosols during transpacific transport in the INTEX-B campaign and found no evidence for significant SOA formation in the free troposphere. The AMS aircraft measurements for Asian pollution layers in the INTEX-B campaign were about an order of magnitude lower than those measured during the ACE-Asia campaign, and our results compare favorably with the INTEX-B results at altitudes higher than 3 km. Similarly, the aircraft observations during the ITCT-2K4 aircraft campaign, conducted from 9 July to 15 August 2004 out of Portsmouth, New Hampshire, did not suggest a major SOA source in the free troposphere either (Heald et al., 2006). An illustrative comparison of the vertical profile of values from our model for aerosol OC with the measured water-soluble organic carbon (WSOC) from the Particle-Into-Liquid Sampler (PILS) instrument on board the NOAA WP3 aircraft is shown in Figure 2-8 (b). The model performs reasonably well in the boundary layer (below 2 km), but still underestimates OC in the free troposphere (2-6 km). The mean observed concentration was $0.900 \pm 0.187 \mu g\ C/m^3$ in the free troposphere (Heald et al., 2006), while the corresponding mean model value in Simulation A is $0.574 \pm 0.172 \mu g\ C/m^3$.

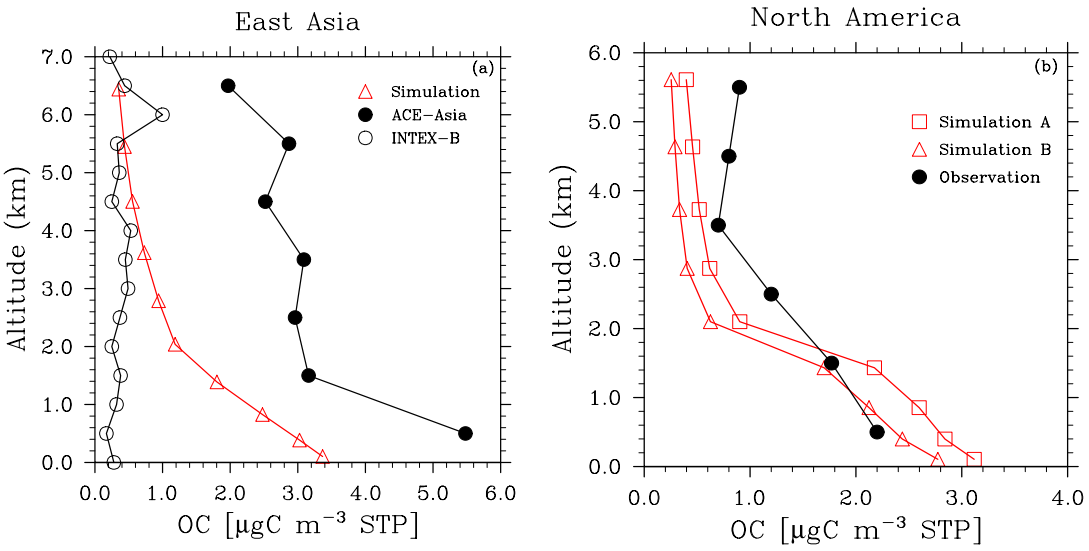

Figure 2-8 Mean vertical profiles of total organic carbon at standard conditions of temperature and pressure. Observed mean profiles (black solid circle) were measured during the ACE-Asia campaign at Fukue Island off the coast of Japan in April/MAY 2001 (left plot) and during the ITCT-2K4 aircraft campaign over NE North America which took place in the Summer (July to August) 2004 (right plot). The black empty circles in the left plot represent average vertical profile of aerosol species for Asian pollution layers measured during the INTEX-B campaign made during April to May in 2006. The model results are the average values over the months of the campaigns. Three simulations produce very similar profiles over East Asia, thus only one simulated profile is shown in (a). The vertical profile over North America produced in Simulation C is omitted because it is almost identical to that of Simulation A.

2.5 Sensitivity tests of the oligomer formation rate

As discussed in Sec. 2.2.2.A, the rate formation of oligomers in heterogeneous reactions within aerosols may vary with different compounds and with the concentration of semi-volatile compounds within the aerosols. Therefore, two extra simulations were performed using the same chemical mechanism as used in Simulation C but with a lifetime for oligomer formation of 2 days and 0.5 days, respectively. As expected, the shorter lifetime enhances the transfer from condensed SVOCs to oligomers, which increases the burden of ne_oSOA by 0.15 Tg (23%) in comparison with the burden obtained in Simulation C. Correspondingly, the burden of ne_oSOA in the simulation using a lifetime for the formation of oligomers of 2 days is decreased by 0.19 Tg (28%). The short lifetime of 0.5

days increases the gap between the annual mean simulation and the observations in IMPROVE network, and results in a normalized mean bias (NMB) of 10.3% compared to the NMB of 1.7% in Simulation C. In addition, the shorter lifetime increases the NMB between the simulation and AMS observations slightly, i.e., from -12.5% to -5.5% at urban sites, from 8.9% to 20.9% at urban downwind sites, and from 20.0% to 27.0% at rural sites. In contrast, the 2-day lifetime decreases the NMB to -16.5% at urban sites, to 1.9% at urban downwind sites and to 15.0% at rural sites, and produces a simulation with a NMB of -3.4% compared to the annual mean observations from IMPROVE network. The 0.5-day lifetime brings the simulation slightly closer to the EMEP observations in terms of NMB compared to the 1-day lifetime, but the simulation still under-estimates the observations by over 50%. While the change of the lifetime has an effect on the NMB values, there are only small changes to the correlation coefficients (R) between the simulations and various observations. At the three tropical sites, the ne_oSOA component only explains a small part of the total OA, so the change in the lifetime for the formation of oligomers causes only a very small change in the total OA (4%). Therefore, these simulations still over-predict the measurements by more than a factor of 2. Similarly, the vertical profiles of OC off of East Asia and over North America are almost the same as those shown above.

2.6 Discussion and conclusions

The IMPACT model was used to simulate global SOA formation using three different mechanisms. We accounted for SOA formation from traditional gas-particle partitioning using an explicit full chemistry scheme instead of a 2-product model which has been used in a number of previous studies. These condensed SVOCs are assumed to go undergo further aerosol-phase reactions to form oligomers with a fixed time constant (assumed to be 1 day in the baseline model). We also included SOA formation from the uptake of gas-phase glyoxal and methlyglyoxal onto clouds and aqueous sulfate aerosol following the work of Fu et al. (2008, 2009), and from the uptake of gas-phase epoxides onto aqueous sulfate aerosol following the work of Paulot et al. (2009). In addition, we examined the influence of including the HO_x recycling mechanism proposed by Peeters et al. (2009) for the oxidation of isoprene. Our SOA formation mechanisms were evaluated by comparing

our global chemical transport model simulations with surface observations from the IMPROVE network in North America, the EMEP network in Europe and from a collection of AMS measurements. We also compared our results with vertical profiles of OC from aircraft measurements off of East Asia and over North America.

The total SOA source in Simulation A was 115.7 Tg/yr, much larger than that estimated by previous global chemical transport models (see Table 2-5), but is within the range of recent top-down estimates that use satellite observations and AMS measurements (Heald et al., 2010; Spracklen et al., 2011). The SOA formation from biogenic precursors (e.g., isoprene, monoterpenes and etc.) dominates that from anthropogenic sources by a large margin, i.e., the fraction of biogenic SOA is 88%. However, the production of "biogenic" SOA is strongly linked with anthropogenic components through a variety of mechanisms. Thus, anthropogenic POA emissions provide an absorptive medium for the condensation of semivolatile species of biogenic origin, and anthropogenic sulfate aerosols facilitate the conversion of glyoxal, methlyglyoxal and epoxides of biogenic origin to SOA. The formation of SOA from biogenic VOCs is also influenced by anthropogenic emissions of NO_x, not only because these biogenic VOCs react with anthropogenic NO_x or NO_3 to form SVOCs (e.g. isoprene-hydroxy-nitrate), but also because NO_x competes with HO_2 for peroxy radicals formed in the initial stages of VOC oxidation (e.g., reactions R1 and R3), leading to changes in functional groups and affecting subsequent reactions. The feedback between anthropogenic emissions and the formation of SOA from biogenic VOCs could have significant implications for future emissions regulations and for predicting the change of organic aerosol in response to future climate change. In order to control emissions contributing to the organic aerosol burden, it is necessary to separate the anthropogenic contribution to SOA formation from the natural background OA (Hoyle et al. 2011).

The introduction of the Peeters et al. (2009) HO_x recycling mechanism into the isoprene oxidation scheme has a strong impact on global SOA formation. It decreases the production rate of ne_oSOA, ne_MGLY and ne_IEPOX by about 28%, 16% and 65%, respectively, as a result of the competition between the unimolecular isomerization pathway and the traditional oxidation pathways, i.e. isoprene RO_2 + NO and isoprene

$RO_2 + HO_2$. On the other hand, it increases the SOA production rates from glyoxal by about 65%. The combination of these effects causes the total SOA source to only decrease by 25%. When the reaction rates for the 1,5-H and 1,6-H shifts in isoprene radicals are decreased by a factor of 10, the total SOA production rate increases from 87 Tg/yr to 113 Tg/yr, very close to that from simulation A which does not consider the HO_x recycling mechanism. The large difference between the simulations B and C is indicative of the discrepancy between state-of-the-art density functional theories (Peeters et al., 2009) and laboratory measurements (Crounse et al., 2011). These different SOA production rates imply that further laboratory studies, field measurements and theoretical studies are needed to better constrain the budgets of the SOA components.

Comparison with the IMPROVE network and with AMS surface measurements in the Northern Hemisphere shows that the model can predict the surface organic aerosol concentrations reasonably well with low normalized mean biases ranging from -15% to 15% in rural regions. The low normalized mean biases for the IMPROVE network and AMS surface measurements contrasts with the under-predictions of observations by other models (Chung and Seinfeld, 2002; Liao et al., 2007; Farina et al., 2010; Utembe et al., 2011; Yu, 2011). The low correlation coefficients R (varying from 0.3 to 0.5) between the simulations and observations, however, indicate that the model does not capture the spatial variability of the measurements very well. These may be compared to the correlation coefficients R of around 0.65 between simulations and observations for the IMPROVE network reported in other models (Park et al., 2003; Liao et al., 2007; Farina et al., 2010). The comparison with the EMEP measurements demonstrates that the model under-predicts surface OC concentrations in Europe, which may be the result of an underestimation of POA in winter and of SOA in summer. In pristine tropical forest regions, the model over-estimates the OM burden by roughly a factor of three compared to three surface AMS measurements made in West Africa, Amazon and Malaysia. This overestimate is present both with and without the HO_x recycling mechanism in the isoprene oxidation scheme. Our overestimation in the Amazon basin differs significantly from predictions of the GEOS-Chem model, which underestimated OM (Chen et al., 2009), but is consistent with the TM5 model over-prediction (Gilardoni et al., 2011a). Because the ne_GLYX, ne_MGLY and ne_IEPOX components account for the major

fraction of total OM predicted at these sites (Table 2-9), it is important to improve the formation of these compounds in the model. Trainic et al. (2011) conducted experiments to study the uptake of glyoxal on ammonium sulfate seed aerosols under hydrated conditions over a wide range of relative humidities, (RH from 35% to 90%) and found that the reactive uptake rate decreased with increasing RH. The ratio of the final organic aerosol mass to the seed mass at the 50% RH condition was similar to that found by Liggio et al. (2005a) (who conducted their studies at 49% RH), but decreased by 57% when the RH increased to 90%. This trend was attributed to the slower glyoxal oligomerization rate caused by the dilution of the ammonium sulfate aerosol at the higher RH values (Liggio et al., 2005a; Trainic et al., 2011). Thus, the work of Trainic et al. (2011) may indicate that the uptake coefficient adopted here for sulfate aerosols (which was based on Liggio et al. (2005a)) as well as its application to cloud water is too high in much of the tropics where typical RH values are around 90%. In addition, the simple treatment of irreversible surface controlled uptake might be misleading if there is a competition between reversible vs. irreversible uptake and of bulk reactions vs. surface processes (Ervens and Volkamer 2010). Furthermore, the same uptake coefficient for both cloud droplets and aqueous aerosols cannot account for the differences in the chemistry of carbonyl compounds between cloud water and aerosol water (Lim et al., 2010; Ervens and Volkamer 2010). Therefore it may be that improvements to the processes responsible for the formation of SOA from glyoxal, methylglyoxal and epoxide would improve the model. Given the sparse amount of data, however, the conclusion that the model overestimates surface OM concentrations observed at 3 sites in the tropical forest regions may not necessarily lead to the conclusion that the model is in error. It would be valuable to have more measurements and model studies to examine the properties of organic aerosols in the tropics. In the free troposphere, the model reproduces the OC observed during the ITCT-2K4 aircraft campaign over North America relatively well, but clearly underestimates OC observations during ACE-Asia campaign off the coast of Japan. However, the model simulates Asian pollution layers above 3 km during the INTEX-B campaign very well.

2.7 References

Abdul-Razzak, H., and Ghan, S. J.: A parameterization of aerosol activation 2. Multiple aerosol types, J. Geophys. Res., 105, 6837-6844, 2000.

Abdul-Razzak, H., and Ghan, S. J.: A parameterization of aerosol activation - 3. Sectional representation, J. Geophys. Res., 107(D3), 4026, doi:10.1029/2001JD000483, 2002.

Archibald, A. T., Cooke, M. C., Utembe, S. R., Shallcross, D. E., Derwent, R. G., and Jenkin, M. E.: Impacts of mechanistic changes on HO_x formation and recycling in the oxidation of isoprene, Atmos. Chem. Phys., 10, 8097-8118, doi:10.5194/acp-10-8097-2010, 2010.

Barley, M. H., and McFiggans, G.: The critical assessment of vapour pressure estimation methods for use in modelling the formation of atmospheric organic aerosol, Atmos. Chem. Phys., 10, 749-767, 2010.

Barth, M. C., Sillman, S., Hudman, R., Jacobson, M. Z., Kim, C.-H., Monod, A., Liang, J.: Summary of the cloud chemistry modeling intercomparison: Photochemical box model simulation, J. Geophys. Res., 108, 4214, doi:10.1029/2002JD002673, 2003.

Bessagnet, B.; Seigneur, C. & Menut, L. Impact of dry deposition of semi-volatile organic compounds on secondary organic aerosols Atmos. Environ., 44, 1781 -1787, 2010.

Bey, I., Jacob, D., Yantosca, R., Logan, J., Field, B., Fiore, A., Li, Q., Liu, H., Mickley, L., and Schultz, M.: Global modeling of tropospheric chemistry with assimilated meteorology: Model description and evaluation, J. Geophys. Res., 106(D19), 23,073 – 23,096, doi:10.1029/2001JD000807, 2001.

Bilde, M., and Pandis, S. N.: Evaporation rates and vapor pressures of individual aerosol species formed in the atmospheric oxidation of alpha- and beta-pinene, Environ. Sci. Technol., 35, 3344-3349, 2001.

Blando, J. D., and Turpin, B. J.: Secondary organic aerosol formation in cloud and fog droplets: a literature evaluation of plausibility, Atmos. Environ., 34, 1623-1632, 2000.

Booth, A. M., Barley, M. H., Topping, D. O., McFiggans, G., Garforth, A., and Percival, C. J.: Solid state and sub-cooled liquid vapor pressures of substituted dicarboxylic acids using Knudsen Effusion Mass Spectrometry (KEMS) and Differential Scanning Calorimetry, Atmos. Chem. Phys., 10, 4879–4892, doi:10.5194/acp-10-4879-2010, 2010.

Booth, A. M., Montague, W. J., Barley, M. H., Topping, D. O., McFiggans, G., Garforth, A., and Percival, C. J.: Solid state and sub-cooled liquid vapor pressures of cyclic aliphatic dicarboxylic acids, Atmos. Chem. Phys., 11, 655–665, doi:10.5194/acp-11-655-2011, 2011.

Bowman, F. M., and Karamalegos, A. M.: Estimated effects of composition on secondary organic aerosol mass concentrations, Environ. Sci. Technol., 36, 2701-2707, 2002.

Butler, T. M., Taraborrelli, D., Fischer, C. B. H., Harder, H., Martinez, M., Williams, J., Lawrence, M. G., and Lelieveld, J.: Improved simulation of isoprene oxidation chemistry with the ECHAM5/MESSy chemistry-climate model: lessons from the GABRIEL airborne field campaign, Atmos. Chem. Phys., 8, 4529-4546, 2008.

Camredon, M., and Aumont, B.: Assessment of vapor pressure estimation methods for secondary organic aerosol modeling, Atmos. Environ., 40, 2105-2116, 2006.

Camredon, M., Aumont, B., Lee-Taylor, J., and Madronich, S.: The SOA/VOC/NOx system: an explicit model of secondary organic aerosol formation, Atmos. Chem. Phys., 7, 5599-5610, 2007.

Camredon, M., Hamilton, J. F., Alam, M. S., Wyche, K. P., Carr, T., White, I. R., Monks, P. S., Rickard, A. R., and Bloss, W. J.: Distribution of gaseous and particulate organic composition during dark α-pinene ozonolysis, Atmos. Chem. Phys., 10, 2893–2917, doi:10.5194/acp-10-2893-2010, 2010.

Capes, G., Murphy, J. G., Reeves, C. E., McQuaid, J. B., Hamilton, J. F., Hopkins, J. R., Crosier, J., Williams, P. I., and Coe, H.: Secondary organic aerosol from biogenic VOCs over West Africa during AMMA, Atmos. Chem. Phys., 9, 3841-3850, 2009.

Cappa, C. D., and Jimenez, J. L.: Quantitative estimates of the volatility of ambient organic aerosol, Atmos. Chem. Phys., 10, 5409-5424, 2010.

Carlton, A. G., Pinder, R. W., Bhave, P. V., and Pouliot, G. A.: To what extent can biogenic SOA be controlled?, Environ. Sci. Technol., 44, 3376-3380, 2010.

Carlton, A. G., Turpin, B. J., Altieri, K. E., Seitzinger, S., Reff, A., Lim, H. J., and Ervens, B.: Atmospheric oxalic acid and SOA production from glyoxal: Results of aqueous photooxidation experiments, Atmos. Environ., 41, 7588-7602, 2007.

Cavalli, F., Facchini, M. C., Decesari, S., Mircea, M., Emblico, L., Fuzzi, S., Ceburnis, D., Yoon, Y. J., O'Dowd, C., Putaud, J.-P., and Dell'Acqua, A.: Advances in characterization of size-resolved organic matter in marine aerosol over the North Atlantic, J. Geophys. Res., 109, D24215, doi:10.1029/2004JD005137, 2004.

Cavalli, F., Facchini, M. C., Decesari, S., Emblico, L., Mircea, M., Jensen, N. R., and Fuzzi, S.: Size-segregated aerosol chemical composition at a boreal site in southern Finland, during the QUEST project, Atmos. Chem. Phys., 6, 993–1002, doi:10.5194/acp-6-993-2006, 2006.

Chan, A. W. H., Kroll, J. H., Ng, N. L., and Seinfeld, J. H.: Kinetic modeling of secondary organic aerosol formation: effects of particle- and gas-phase reactions of semivolatile products, Atmos. Chem. Phys., 7, 4135-4147, 2007.

Chan, M. N., Surratt, J. D., Claeys, M., Edgerton, E. S., Tanner, R. L., Shaw, S. L., Zheng, M., Knipping, E. M., Eddingsaas, N. C., Wennberg, P. O., and Seinfeld, J. H.: Characterization and quantification of isoprene-derived epoxydiols in ambient aerosol in

the southeastern United States, Environ. Sci. Technol., 44, 4590–4596, doi:10.1021/es100596b, 2010.

Chen, Q., Farmer, D. K., Schneider, J., Zorn, S. R., Heald, C. L., Karl, T. G., Guenther, A., Allan, J. D., Robinson, N., Coe, H., Kimmel, J. R., Pauliquevis, T., Borrmann, S., Poschl, U., Andreae, M. O., Artaxo, P., Jimenez, J. L., and Martin, S. T.: Mass spectral characterization of submicron biogenic organic particles in the Amazon Basin, Geophys. Res. Lett., 36, L20806,doi:10.1029/2009gl039880, 2009.

Chung, S. H., and Seinfeld, J. H.: Global distribution and climate forcing of carbonaceous aerosols, J. Geophys. Res., 107, , D19, doi:10.1029/2001jd001397, 2002.

Claeys, M., Graham, B., Vas, G.,Wang,W., Vermeylen, R., Pashynska, V., Cafmeyer, J., Guyon, P., Andreae, M. O., Artaxo, P., and Maenhaut, W.: Formation of secondary organic aerosols through photooxidation of isoprene, Science, 303, 1173–1176, 2004.

Coy, L., Nash, E. R., and Newman, P. A.: Meteorology of the polar vortex: Spring 1997, Geophys. Res. Lett., 24, 2693-2696, 1997.

Coy, L., and Swinbank, R.: Characteristics of stratospheric winds and temperatures produced by data assimilation, J. Geophys. Res., 102, 25763-25781, 1997.

Crounse, J. D., Paulot, F., Kjaergaard, H. G., and Wennberg, P. O.,: Peroxy radical isomerization in the oxidation of isoprene, Phys. Chem. Chem. Phys., 13, 13607–13613, 2011.

Czoschke, N. M., Jang, M., and Kamens, R. M.: Effect of acidic seed on biogenic secondary organic aerosol growth, Atmos. Environ., 37, 4287-4299, 2003.

Da Silva, G., Graham, C., and Wang, Z.-F.: Unimolecular β-hydroxyperoxy radical decomposition with OH recycling in the photochemical oxidation of isoprene, Environ. Sci. Technol., 44, 250–256, 2010.

Decesari, S., Facchini, M. C., and Fuzzi, S.: Characterization of water-soluble organic compounds in atmospheric aerosols: a new approach, J. Geophys. Res., 105, 1481–1489, 2000.

Decdsari, S., Facchini, M. C., Matta, E., Lettini, F., Mircea, M., Fuzzi, S., Tagliavini, E., and Pautaud, J.-P.: Chemical features and seasonal variation of fine aerosol water-soluble organic compounds in the Po Valley, Italy, Atmos. Environ., 35, 3691-3699, 2001.

Decesari, S., Facchini, M. C., Fuzzi, S., McFiggans, G. B., Coe, H., and Bower, K. N.: The water-soluble organic component of sizesegregates aerosol, cloud water and wet depositions from Jeju Island during ACE-Asia, Atmos. Environ., 39, 211–222, 2005.

de Gouw, J. A., Middlebrook, A. M., Warneke, C., Goldan, P. D., Kuster, W. C., Roberts, J. M., Fehsenfeld, F. C., Worsnop, D. R., Canagaratna, M. R., Pszenny, A. A. P., Keene, W. C., Marchewka, M., Bertman, S. B., and Bates, T. S.: Budget of organic carbon in a polluted atmosphere: Results from the New England Air Quality Study in 2002, J. Geophys. Res., 110, D16, doi:10.1029/2004jd005623, 2005.

Dommen, J., Metzger, A., Duplissy, J., Kalberer, M., Alfarra, M. R., Gascho, A., Weingartner, E., Prevot, A. S. H., Verheggen, B., and Baltensperger, U.: Laboratory observation of oligomers in the aerosol from isoprene/NOx photooxidation, Geophys. Res. Lett., 33, 2006.

Donahue, N. M., Robinson, A. L., and Pandis, S. N.: Atmospheric organic particulate matter: From smoke to secondary organic aerosol, Atmos. Environ., 43, 94-106, 2009.

Donahue, N. M., Robinson, A. L., Stanier, C. O., and Pandis, S. N.: Coupled partitioning, dilution, and chemical aging of semivolatile organics, Environ. Sci. Technol., 40, 2635-2643, 2006.

Dunlea, E. J., DeCarlo, P. F., Aiken, A. C., Kimmel, J. R., Peltier, R. E., Weber, R. J., Tomlinson, J., Collins, D. R., Shinozuka, Y., McNaughton, C. S., Howell, S. G., Clarke, A. D., Emmons, L. K., Apel, E. C., Pfister, G. G., van Donkelaar, A., Martin, R. V., Millet, D. B., Heald, C. L., and Jimenez, J. L.: Evolution of Asian aerosols during transpacific transport in INTEX-B, Atmos. Chem. Phys., 9, 7257-7287, 2009.

Dzepina, K., Volkamer, R. M., Madronich, S., Tulet, P., Ulbrich, I. M., Zhang, Q., Cappa, C. D., Ziemann, P. J., and Jimenez, J. L.: Evaluation of recently-proposed secondary organic aerosol models for a case study in Mexico City, Atmos. Chem. Phys., 9, 5681-5709, 2009.

Eddingsaas, N. C., VanderVelde, D. G., and Wennberg, P. O.: Kinetics and products of the acid-catalyzed ring-opening of atmospherically relevant butyl epoxy alcohols, J. Phys. Chem. A, 114, 8106-8113, 2010.

Ervens, B., and Volkamer, R.: Glyoxal processing by aerosol multiphase chemistry: towards a kinetic modeling framework of secondary organic aerosol formation in aqueous particles, Atmos. Chem. Phys., 10, 8219-8244, 2010.

Epstein, S., Riipinen, I., and Donahue, A. M.: A semiempirical correlation between enthalpy of vaporization and saturation concentration for organic aerosol, Environ. Sci. Technol., 44, 743–748, 2010.

Farina, S. C., Adams, P. J., and Pandis, S. N.: Modeling global secondary organic aerosol formation and processing with the volatility basis set: Implications for anthropogenic secondary organic aerosol, J. Geophys. Res., 115, D09202, doi:10.1029/2009JD013046, 2010.

Froyd, K. D., Murphy, S. M., Murphy, D. M., de Gouw, J. A., Eddingsaas, N. C., and Wennberg, P. O.: Contribution of isoprene-derived organosulfates to free tropospheric aerosol mass, Pro. Natl. Acad. Sci. USA., 107, 21360-21365, 2010.

Fu, T. M., Jacob, D. J., and Heald, C. L.: Aqueous-phase reactive uptake of dicarbonyls as a source of organic aerosol over eastern North America, Atmos. Environ., 43, 1814-1822, 2009.

Fu, T. M., Jacob, D. J., Wittrock, F., Burrows, J. P., Vrekoussis, M., and Henze, D. K.: Global budgets of atmospheric glyoxal and methylglyoxal, and implications for formation of secondary organic aerosols, J. Geophys. Res., 113, D15303, doi:10.1029/2007JD009505,2008.

Galloway, M. M., Chhabra, P. S., Chan, A. W. H., Surratt, J. D., Flagan, R. C., Seinfeld, J. H., and Keutsch, F. N.: Glyoxal uptake on ammonium sulphate seed aerosol: reaction products and reversibility of uptake under dark and irradiated conditions, Atmos. Chem. Phys., 9, 3331-3345, 2009.

Gantt, B., Meskhidze, N., and Kamykowski, D.: A new physically-based quantification of marine isoprene and primary organic aerosol emissions, Atmos. Chem. Phys., 9, 4915-4927, 2009.

Gao, S., Keywood, M., Ng, N. L., Surratt, J., Varutbangkul, V., Bahreini, R., Flagan, R. C., and Seinfeld, J. H.: Low-molecular-weight and oligomeric components in secondary organic aerosol from the ozonolysis of cycloalkenes and alpha-pinene, J. Phys. Chem. A, 108, 10147-10164, 2004a.

Gao, S., Ng, N. L., Keywood, M., Varutbangkul, V., Bahreini, R., Nenes, A., He, J. W., Yoo, K. Y., Beauchamp, J. L., Hodyss, R. P., Flagan, R. C., and Seinfeld, J. H.: Particle phase acidity and oligomer formation in secondary organic aerosol, Environ. Sci. Technol., 38, 6582-6589, 2004b.

Gelencsér, A., Hoffer, A., Krivacsy, Z., Kiss, G., Molnar, A., and Meszaros, E.: On the possible origin of humic matter in fine continental aerosol, J. Geophys. Res., 107, 4137, doi:10.1029/2001JD001299, 2002.

Gelencsér, A., May, B., Simpson, D., Sánchez-Ochoa, A., Kasper-Giebl, A., Puxbaum, H., Caseiro, A., Pio, C., and Legrand., M.: Source apportionment of PM2.5 organic aerosol over Europe: Primary/secondary, natural/anthropogenic, and fossil/biogenic origin, J. Geophys. Res., 112, D23S04, doi:10.1029/2006JD008094, 2007.

Gilardoni, S., Vignati, E., Cavalli, F., Putaud, J. P., Larsen, B. R., Karl, M., Stenström, K., Genberg, J., Henne, S., and Dentener, F.: Better constraints on sources of carbonaceous aerosols using a combined ^{14}C – macro tracer analysis in a European rural background site, Atmos. Chem. Phys., 11, 5685-5700, doi:10.5194/acp-11-5685-2011, 2011a.

Gilardoni, S., Vignati, E., Marmer, E., Cavalli, F., Belis, C., Gianelle, V., Loureiro, A., and Artaxo, P.: Sources of carbonaceous aerosol in the Amazon basin, Atmos. Chem. Phys., 11, 2747-2764, 2011b.

Giorgi, F., and Chameides, W. L.: Rainout lifetimes of highly soluble aerosols and gases as inferred from simulations with a g general-circulation model, J. Geophys. Res., 91, 14367-14376, 1986.

Goldstein, A. H., and Galbally, I. E.: Known and unexplored organic constituents in the earth's atmosphere, Environ. Sci. Technol., 41, 1514-1521, 2007.

Goldstein, A. H., Koven, C. D., Heald, C. L., and Fung, I. Y.: Biogenic carbon and anthropogenic pollutants combine to form a cooling haze over the southeastern United States, Proc. Natl. Acda. Sci. USA., 106, 8835-8840, 2009.

Griffin, R. J., Dabdub, D., and Seinfeld, J. H.: Secondary organic aerosol - 1. Atmospheric chemical mechanism for production of molecular constituents, J. Geophys. Res., 107, D17, doi:10.1029/2001JD000541, 2002.

Gross, D. S., Galli, M. E., Kalberer, M., Prevot, A. S. H., Dommen, J., Alfarra, M. R., Duplissy, J., Gaeggeler, K., Gascho, A., Metzger, A., and Baltensperger, U.: Real-time measurement of oligomeric species in secondary organic aerosol with the aerosol time-of-flight mass spectrometer, Analytical Chemistry, 78, 2130-2137, 2006.

Guenther, A., Hewitt, C. N., Erickson, D., Fall, R., Geron, C., Graedel, T., Harley, P., Klinger, L., Lerdau, M., McKay, W. A., Pierce, T., Scholes, B., Steinbrecher, R., Tallamraju, R., Taylor, J., and Zimmerman, P.: A global-model of natural volatile organic-compound emissions, J. Geophys. Res., 100, 8873-8892, 1995.

Guenther, A., Karl, T., Harley, P., Wiedinmyer, C., Palmer, P. I., and Geron, C.: Estimates of global terrestrial isoprene emissions using MEGAN (Model of Emissions of Gases and Aerosols from Nature), Atmos. Chem. Phys., 6, 3181-3210, 2006.

Hallquist, M., Wenger, J. C., Baltensperger, U., Rudich, Y., Simpson, D., Claeys, M., Dommen, J., Donahue, N. M., George, C., Goldstein, A. H., Hamilton, J. F., Herrmann, H., Hoffmann, T., Iinuma, Y., Jang, M., Jenkin, M. E., Jimenez, J. L., Kiendler-Scharr, A., Maenhaut, W., McFiggans, G., Mentel, T. F., Monod, A., Prevot, A. S. H., Seinfeld, J. H., Surratt, J. D., Szmigielski, R., and Wildt, J.: The formation, properties and impact of secondary organic aerosol: current and emerging issues, Atmos. Chem. Phys., 9, 5155-5236, 2009.

Hastings, W. P., Koehler, C. A., Bailey, E. L., and De Haan, D. O.: Secondary organic aerosol formation by glyoxal hydration and oligomer formation: Humidity effects and equilibrium shifts during analysis, Environ. Sci. Technol., 39, 8728-8735, 2005.

Heald, C. L., Henze, D. K., Horowitz, L. W., Feddema, J., Lamarque, J. F., Guenther, A., Hess, P. G., Vitt, F., Seinfeld, J. H., Goldstein, A. H., and Fung, I.: Predicted change in global secondary organic aerosol concentrations in response to future climate, emissions, and land use change, J. Geophys. Res., 113, D05211, doi:10.1029/2007JD009092, 2008.

Heald, C. L., Jacob, D. J., Park, R. J., Russell, L. M., Huebert, B. J., Seinfeld, J. H., Liao, H., and Weber, R. J.: A large organic aerosol source in the free troposphere missing from current models, Geophys. Res. Lett., 32, L18809, doi:10.1029/2005GL023831, 2005.

Heald, C. L., Jacob, D. J., Turquety, S., Hudman, R. C., Weber, R. J., Sullivan, A. P., Peltier, R. E., Atlas, E. L., de Gouw, J. A., Warneke, C., Holloway, J. S., Neuman, J. A., Flocke, F. M., and Seinfeld, J. H.: Concentrations and sources of organic carbon aerosols in the free troposphere over North America, J. Geophys. Res., 111, D23S47, doi:10.1029/2006JD007705, 2006.

Heald, C. L., Ridley, D. A., Kreidenweis, S. M., and Drury, E. E.: Satellite observations cap the atmospheric organic aerosol budget, Geophys. Res. Lett., 37, L24808, doi:10.1029/2010GL045095, 2010.

Heaton, K. J., Dreyfus, M. A., Wang, S., and Johnston, M. V.: Oligomers in the early stage of biogenic secondary organic aerosol formation and growth, Environ. Sci. Technol., 41, 6129-6136, 2007.

Henze, D. K., and Seinfeld, J. H.: Global secondary organic aerosol from isoprene oxidation, Geophys. Res. Lett., 33, L09812, doi:10.1029/2006GL025976, 2006.

Henze, D. K., Seinfeld, J. H., Ng, N. L., Kroll, J. H., Fu, T. M., Jacob, D. J., and Heald, C. L.: Global modeling of secondary organic aerosol formation from aromatic hydrocarbons: high- vs. low-yield pathways, Atmos. Chem. Phys., 8, 2405-2420, 2008.

Herzog, M., Weisenstein, D. K., and Penner, J. E.: A dynamic aerosol module for global chemical transport models: Model description, J. Geophys. Res., 109, D18202, doi:10.1029/2003JD004405, 2004.

Hodzic, A., Jimenez, J. L., Madronich, S., Canagaratna, M. R., DeCarlo, P. F., Kleinman, L., and Fast, J.: Modeling organic aerosols in a megacity: potential contribution of semi-volatile and intermediate volatility primary organic compounds to secondary organic aerosol formation, Atmos. Chem. Phys., 10, 5491-5514, 2010.

Hoyle, C. R., Berntsen, T., Myhre, G., and Isaksen, I. S. A.: Secondary organic aerosol in the global aerosol - chemical transport model Oslo CTM2, Atmos. Chem. Phys., 7, 5675-5694, 2007.

Hoyle, C. R., Boy, M., Donahue, N. M., Fry, J. L., Glasius, M., Guenther, A., Hallar, A. G., Hartz, K. H., Petters, M. D., Petaja, T., Rosenoern, T., and Sullivan, A. P.: A review of the anthropogenic influence on biogenic secondary organic aerosol, Atmos. Chem. Phys., 11, 321-343, 2011.

Hoyle, C. R., Myhre, G., Berntsen, T. K., and Isaksen, I. S. A.: Anthropogenic influence on SOA and the resulting radiative forcing, Atmos. Chem. Phys., 9, 2715-2728, 2009.

Huffman, J. A., Docherty, K. S., Aiken, A. C., Cubison, M. J., Ulbrich, I. M., DeCarlo, P. F., Sueper, D., Jayne, J. T., Worsnop, D. R., Ziemann, P. J., and Jimenez, J. L.: Chemically-resolved aerosol volatility measurements from two megacity field studies, Atmos. Chem. Phys., 9, 7161-7182, 2009.

Iinuma, Y., Boge, O., Gnauk, T., and Herrmann, H.: Aerosol-chamber study of the alpha-pinene/O-3 reaction: influence of particle acidity on aerosol yields and products, Atmos. Environ., 38, 761-773, 2004.

Iinuma, Y., Boge, O., Miao, Y., Sierau, B., Gnauk, T., and Herrmann, H.: Laboratory studies on secondary organic aerosol formation from terpenes, Faraday Discussions, 130, 279-294, 2005.

Iinuma, Y., Muller, C., Boge, O., Gnauk, T., and Herrmann, H.: The formation of organic sulfate esters in the limonene ozonolysis secondary organic aerosol (SOA) under acidic conditions, Atmos. Environ., 41, 5571-5583, 2007.

Ito, A. and Penner, J. E.: Historical emissions of carbonaceous aerosols from biomass and fossil fuel burning for the period 1870-2000, Global Biogeochemical Cycles, 19, GB2028, doi:10.1029/2004GB002374, 2005.

Ito, A., Sillman, S., and Penner, J. E.: Effects of additional nonmethane volatile organic compounds, organic nitrates, and direct emissions of oxygenated organic species on global tropospheric chemistry, J. Geophys. Res., 112, D06309, doi:10.1029/2005JD006556, 2007.

Ito, A., Sillman, S., and Penner, J. E.: Global chemical transport model study of ozone response to changes in chemical kinetics and biogenic volatile organic compounds emissions due to increasing temperatures: Sensitivities to isoprene nitrate chemistry and grid resolution, J. Geophys. Res., 114, D09301, doi:10.1029/2008JD011254, 2009.

Jang, M., Czoschke, N. M., and Northcross, A. L.: Atmospheric organic aerosol production by heterogeneous acid-catalyzed reactions, Chemphyschem, 5, 1647-1661, 2004.

Jang, M., Czoschke, N. M., Northcross, A. L., Cao, G., and Shaof, D.: SOA formation from partitioning and heterogeneous reactions: Model study in the presence of inorganic species, Environ. Sci. Technol., 40, 3013-3022, 2006.

Jang, M., Lee, S., and Kamens, R. M.: Organic aerosol growth by acid-catalyzed heterogeneous reactions of octanal in a flow reactor, Atmos. Environ., 37, 2125-2138, 2003a.

Jang, M. S., Carroll, B., Chandramouli, B., and Kamens, R. M.: Particle growth by acid-catalyzed heterogeneous reactions of organic carbonyls on preexisting aerosols, Environ. Sci. Technol., 37, 3828-3837, 2003b.

Jang, M. S., Czoschke, N. M., Lee, S., and Kamens, R. M.: Heterogeneous atmospheric aerosol production by acid-catalyzed particle-phase reactions, Science, 298, 814-817, 2002.

Jang, M. S., Czoschke, N. M., and Northcross, A. L.: Semiempirical model for organic aerosol growth by acid-catalyzed heterogeneous reactions of organic carbonyls, Environ. Sci. Technol., 39, 164-174, 2005.

Jang, M. S., and Kamens, R. M.: Characterization of secondary aerosol from the photooxidation of toluene in the presence of NOx and 1-propene, Environ. Sci. Technol., 35, 3626-3639, 2001.

Jimenez, J. L., Canagaratna, M. R., Donahue, N. M., Prevot, A. S. H., Zhang, Q., Kroll, J. H., DeCarlo, P. F., Allan, J. D., Coe, H., Ng, N. L., Aiken, A. C., Docherty, K. S., Ulbrich, I. M., Grieshop, A. P., Robinson, A. L., Duplissy, J., Smith, J. D., Wilson, K. R.,

Lanz, V. A., Hueglin, C., Sun, Y. L., Tian, J., Laaksonen, A., Raatikainen, T., Rautiainen, J., Vaattovaara, P., Ehn, M., Kulmala, M., Tomlinson, J. M., Collins, D. R., Cubison, M. J., Dunlea, E. J., Huffman, J. A., Onasch, T. B., Alfarra, M. R., Williams, P. I., Bower, K., Kondo, Y., Schneider, J., Drewnick, F., Borrmann, S., Weimer, S., Demerjian, K., Salcedo, D., Cottrell, L., Griffin, R., Takami, A., Miyoshi, T., Hatakeyama, S., Shimono, A., Sun, J. Y., Zhang, Y. M., Dzepina, K., Kimmel, J. R., Sueper, D., Jayne, J. T., Herndon, S. C., Trimborn, A. M., Williams, L. R., Wood, E. C., Middlebrook, A. M., Kolb, C. E., Baltensperger, U., and Worsnop, D. R.: Evolution of Organic Aerosols in the Atmosphere, Science, 326, 1525-1529, 2009.

Johnson, D., Utembe, S. R., and Jenkin, M. E.: Simulating the detailed chemical composition of secondary organic aerosol formed on a regional scale during the TORCH 2003 campaign in the southern UK, Atmos. Chem. Phys., 6, 419-431, 2006.

Kalberer, M., Paulsen, D., Sax, M., Steinbacher, M., Dommen, J., Prevot, A. S. H., Fisseha, R., Weingartner, E., Frankevich, V., Zenobi, R., and Baltensperger, U.: Identification of polymers as major components of atmospheric organic aerosols, Science, 303, 1659-1662, 2004.

Kalberer, M., Sax, M., and Samburova, V.: Molecular size evolution of oligomers in organic aerosols collected in urban atmospheres and generated in a smog chamber, Environ. Sci. Technol., 40, 5917-5922, 2006.

Kamens, R., Jang, M., Chien, C. J., and Leach, K.: Aerosol formation from the reaction of alpha-pinene and ozone using a gas-phase kinetics aerosol partitioning model, Environ. Sci. Technol., 33, 1430-1438, 1999.

Kanakidou, M., Seinfeld, J. H., Pandis, S. N., Barnes, I., Dentener, F. J., Facchini, M. C., Van Dingenen, R., Ervens, B., Nenes, A., Nielsen, C. J., Swietlicki, E., Putaud, J. P., Balkanski, Y., Fuzzi, S., Horth, J., Moortgat, G. K., Winterhalter, R., Myhre, C. E. L., Tsigaridis, K., Vignati, E., Stephanou, E. G., and Wilson, J.: Organic aerosol and global climate modelling: a review, Atmos. Chem. Phys., 5, 1053-1123, 2005.

Karl, T., Guenther, A., Turnipseed, A., Tyndall, G., Artaxo, P., and Martin, S.: Rapid formation of isoprene photo-oxidation products observed in Amazonia, Atmos. Chem. Phys., 9, 7753-7767, 2009.

Karl, T., Harley, P., Emmons, L., Thornton, B., Guenther, A., Basu, C., Turnipseed, A., and Jardine, K.: Efficient atmospheric cleansing of oxidized organic trace gases by vegetation, Science, 330, 816–819, 2010.

Kleindienst, T. E., Jaoui, M., Lewandowski, M., Offenberg, J. H., Lewis, C. W., Bhave, P. V., and Edney, E. O.: Estimates of the contributions of biogenic and anthropogenic hydrocarbons to secondary organic aerosol at a southeastern US location, Atmos. Environ., 41, 8288-8300, 2007.

Kleinman, L. I., Springston, S. R., Daum, P. H., Lee, Y. N., Nunnermacker, L. J., Senum, G. I., Wang, J., Weinstein-Lloyd, J., Alexander, M. L., Hubbe, J., Ortega, J.,

Canagaratna, M. R., and Jayne, J.: The time evolution of aerosol composition over the Mexico City plateau, Atmos. Chem. Phys., 8, 1559-1575, 2008.

Kroll, J. H., Ng, N. L., Murphy, S. M., Flagan, R. C., and Seinfeld, J. H.: Secondary organic aerosol formation from isoprene photooxidation under high-NOx conditions, Geophys. Res. Lett., 32, L18808, doi:10.1029/2005GL023637, 2005a.

Kroll, J. H., Ng, N. L., Murphy, S. M., Flagan, R. C., and Seinfeld, J. H.: Secondary organic aerosol formation from isoprene photooxidation, Environ. Sci. Technol., 40, 1869–1877, 2006.

Kroll, J. H., Ng, N. L., Murphy, S. M., Varutbangkul, V., Flagan, R. C., and Seinfeld, J. H.: Chamber studies of secondary organic aerosol growth by reactive uptake of simple carbonyl compounds, J. Geophys. Res., 110, D23207, doi:10.1029/2005JD006004, 2005b.

Kroll, J. H., and Seinfeld, J. H.: Chemistry of secondary organic aerosol: Formation and evolution of low-volatility organics in the atmosphere, Atmos. Environ., 42, 3593-3624, 2008.

Kubistin, D., Harder, H., Martinez, M., Rudolf, M., Sander, R., Bozem, H., Eerdekens, G., Fischer, H., Gurk, C., Klupfel, T., Konigstedt, R., Parchatka, U., Schiller, C. L., Stickler, A., Taraborrelli, D., Williams, J., and Lelieveld, J.: Hydroxyl radicals in the tropical troposphere over the Suriname rainforest: comparison of measurements with the box model MECCA, Atmos. Chem. Phys., 10, 9705-9728, 2010.

Lee-Taylor. J, S. Madronich, B. Aumont, M. Camredon, A. Hodzic, G. S. Tyndall, E. Apel, and R. A. Zaveri: Explicit modeling of organic chemistry and secondary organic aerosol partitioning for Mexico City and its outflow plume. Atmos. Chem. Phys. Discuss., 11, 17013-17070, doi:10.5194/acpd-11-17013-2011, 2011.

Lelieveld, J., Butler, T. M., Crowley, J. N., Dillon, T. J., Fischer, H., Ganzeveld, L., Harder, H., Lawrence, M. G., Martinez, M., Taraborrelli, D., and Williams, J.: Atmospheric oxidation capacity sustained by a tropical forest, Nature, 452, 737-740, 2008.

Lewis, C. W., Klouda, G. A., and Ellenson, W. D.: Radiocarbon measurement of the biogenic contribution to summertime PM-2.5 ambient aerosol in Nashville, TN, Atmos. Environ., 38, 6053-6061, 2004.

Liao, H., Henze, D. K., Seinfeld, J. H., Wu, S. L., and Mickley, L. J.: Biogenic secondary organic aerosol over the United States: Comparison of climatological simulations with observations, J. Geophys. Res., 112, D06201, doi:10.1029/2006JD007813, 2007.

Liggio, J., Li, S. M., and McLaren, R.: Reactive uptake of glyoxal by particulate matter, J. Geophys. Res., 110, D10304, doi:10.1029/2004JD005113, 2005a.

Liggio, J., Li, S. M., and McLaren, R.: Heterogeneous reactions of glyoxal on particulate matter: Identification of acetals and sulfate esters, Environ. Sci. Technol., 39, 1532-1541, 2005b.

Lim, Y. B., Tan, Y., Perri, M. J., Seitzinger, S. P., and Turpin, B. J.: Aqueous chemistry and its role in secondary organic aerosol (SOA) formation, Atmos. Chem. Phys., 10, 10521–10539, doi:10.5194/acp-10-10521-2010, 2010.

Liu, H. Y., Jacob, D. J., Bey, I., and Yantosca, R. M.: Constraints from Pb-210 and Be-7 on wet deposition and transport in a global three-dimensional chemical tracer model driven by assimilated meteorological fields, J. Geophys. Res., 106, 12109-12128, 2001.

Liu, X. H., and Penner, J. E.: Effect of Mount Pinatubo H2SO4/H2O aerosol on ice nucleation in the upper troposphere using a global chemistry and transport model, J. Geophys. Res., 107, D12, doi:10.1029/2001JD000455, 2002.

Liu, X. H., Penner, J. E., and Herzog, M.: Global modeling of aerosol dynamics: Model description, evaluation, and interactions between sulfate and nonsulfate aerosols, J. Geophys. Res., 110, D18206, doi:10.1029/2004JD005674, 2005.

Loeffler, K. W., Koehler, C. A., Paul, N. M., and De Haan, D. O.: Oligomer formation in evaporating aqueous glyoxal and methylglyoxal solutions, Environ. Sci. Technol., 40(20), 6318–6323, 2006.

Luo, G., and Yu, F.: A numerical evaluation of global oceanic emissions of alpha-pinene and isoprene, Atmos. Chem. Phys., 10, 2007-2015, 2010.

Malm,W. C., Pitchford, M. L., Scuggs, M., Sisler, J. F., Ames, R., Copeland, S., Gebhart, K. A., and Day, D. E.: Spatial and seasonal patterns and temporal variability of haze and its constituents in the United States, Rep. III, Coop. Inst. for Res., Colo. State Univ., Fort Collins, 2000.

Mari, C., Jacob, D. J., and Bechtold, P.: Transport and scavenging of soluble gases in a deep convective cloud, J. Geophys. Res., 105, 22255-22267, 2000.

Maria, S. F., Russell, L. M., Turpin, B. J., Porcja, R. J., Campos, T. L., Weber, R. J., and Huebert, B. J.: Source signatures of carbon monoxide and organic functional groups in Asian Pacific Regional Aerosol Characterization Experiment (ACE-Asia) submicron aerosol types, J. Geophys. Res., 108, D23, doi:10.1029/2003JD003703, 2003.

Martinez, M., Harder, H., Kubistin, D., Rudolf, M., Bozem, H., Eerdekens, G., Fischer, H., Klupfel, T., Gurk, C., Konigstedt, R., Parchatka, U., Schiller, C. L., Stickler, A., Williams, J., and Lelieveld, J.: Hydroxyl radicals in the tropical troposphere over the Suriname rainforest: airborne measurements, Atmos. Chem. Phys., 10, 3759-3773, 2010.

Minerath, E. C., and Elrod, M. J.: Assessing the potential for diol and hydroxy sulfate ester formation from the reaction of epoxides in tropospheric aerosols, Environ. Sci. Technol., 43, 1386-1392, 2009.

Minerath, E. C., Schultz, M. P., and Elrod, M. J.: Kinetics of the reactions of isoprene-derived epoxides in model tropospheric aerosol solutions, Environ. Sci. Technol., 43, 8133-8139, 2009.

Myrdal, P. B., and Yalkowsky, S. H.: Estimating pure component vapor pressures of complex organic molecules, Industrial & Engineering Chemistry Research, 36, 2494-2499, 1997.

Nannoolal, Y., Rarey, J., and Ramjugernath, D.: Estimation of pure component properties, Part 3, Estimation of the vapor pressure of non-electrolyte organic compounds via group contributions and group interactions, Fluid Phase Equilibr., 269, 117–133, 2008

Ng, N. L., Chhabra, P. S., Chan, A. W. H., Surratt, J. D., Kroll, J. H., Kwan, A. J., McCabe, D. C., Wennberg, P. O., Sorooshian, A., Murphy, S. M., Dalleska, N. F., Flagan, R. C., and Seinfeld, J. H.: Effect of NOx level on secondary organic aerosol (SOA) formation from the photooxidation of terpenes, Atmos. Chem. Phys., 7, 5159–5174, 2007.

Ng, N. L., Kroll, J. H., Keywood, M. D., Bahreini, R., Varutbangkul, V., Flagan, R. C., Seinfeld, J. H., Lee, A., and Goldstein, A. H.: Contribution of first- versus second-generation products to secondary organic aerosols formed in the oxidation of biogenic hydrocarbons, Environ. Sci. Technol., 40, 2283-2297, 2006.

Nozière, B., González, N. J.D., Borg-Karlson, A.-K., Pei, Y., Redeby, J. P., Krejci, R., Dommen, J., Prevot, A. S. H., and Anthonsen, T.,:, Atmospheric chemistry in stereo: A new look at secondary organic aerosols from isoprene, Geophys. Res. Lett., *38*, L11807, doi:10.1029/2011GL047323, 2011.

Odum, J. R., Hoffmann, T., Bowman, F., Collins, D., Flagan, R. C., and Seinfeld, J. H.: Gas/particle partitioning and secondary organic aerosol yields, Environ. Sci. Technol., 30, 2580-2585, 1996.

O'Donnell, D., Tsigaridis, K., and Feichter, J.: Estimating the influence of the secondary organic aerosols on present climate using ECHAM5-HAM, Atmos. Chem. Phys. Discuss., 11, 2407-2472, doi:10.5194/acpd-11-2407-2011, 2011.

O'Dowd, C. D., Langmann, B., Varghese, S., Scannell, C., Ceburnis, D., and Facchini, M. C.: A combined organic-inorganic sea-spray source function, Geophys. Res. Let., 35, L01801, doi:10.1029/2007GL030331, 2008.

Palmer, P. I., and Shaw, S. L.: Quantifying global marine isoprene fluxes using MODIS chlorophyll observations, Geophys. Res. Lett., 32, L09805, doi:10.1029/2005GL022592, 2005.

Pankow, J. F.: An absorption-model of the gas aerosol partitioning involved in the formation of secondary organic aerosol, Atmos. Environ., 28, 189-193, 1994.

Pankow, J. F. and Asher, W. E.: SIMPOL.1: a simple group contribution method for predicting vapor pressures and enthalpies of vaporization of multifunctional organic compounds, Atmos. Chem. Phys., 8, 2773–2796, doi:10.5194/acp-8-2773-2008, 2008.

Pankow, J. F., and Barsanti, K. C.: The carbon number-polarity grid: A means to manage the complexity of the mix of organic compounds when modeling atmospheric organic particulate matter, Atmos. Environ., 43, 2829-2835, 2009.

Park, R. J., Jacob, D. J., Chin, M., and Martin, R. V.: Sources of carbonaceous aerosols over the United States and implications for natural visibility, J. Geophys. Res., 108(D12), 4355, doi:10.1029/2002JD003190, 2003.

Paulot, F., Crounse, J. D., Kjaergaard, H. G., Kurten, A., St Clair, J. M., Seinfeld, J. H., and Wennberg, P. O.: Unexpected epoxide formation in the gas-phase photooxidation of isoprene, Science, 325, 730-733, 2009.

Paulsen, D., Weingartner, E., Alfarra, M. R., and Baltensperger, U.: Volatility measurements of photochemically and nebulizer-generated organic aerosol particles, Journal of Aerosol Science, 37, 1025-1051, 2006.

Peeters, J., Nguyen, T. L., and Vereecken, L.: HO_x radical regeneration in the oxidation of isoprene, Phys. Chem. Chem. Phys., 11, 5935-5939, 2009.

Peeters, J. and Müller, J-F.: HO_x radical regeneration in isoprene oxidation via peroxy radical isomerisations. II: experimental evidence and global impact, Phys. Chem. Chem. Phys: 12, 14227-14235, 2010.

Penner, J. E., Chuang, C. C., and Grant, K.: Climate forcing by carbonaceous and sulfate aerosols, Climate Dynamics, 14, 839-851, 1998.

Perraud, V., Bruns, E. A., Eznll, M. J., Johnson, S. N., Yu, Y., Alexander, M. L., Zelenyuk, A., Imre, D., Chang, W. L., Dabdub, D., Pankow, J. F., and Finlayson-Pitts B. J.: Nonequilibrium atmospheric secondary organic aerosol formation and growth, Proc. Natl. Acad. Sci. USA., 109, 2836-2841, 2012.

Pugh, T. A. M., MacKenzie, A. R., Hewitt, C. N., Langford, B., Edwards, P. M., Furneaux, K. L., Heard, D. E., Hopkins, J. R., Jones, C. E., Karunaharan, A., Lee, J., Mills, G., Misztal, P., Moller, S., Monks, P. S., and Whalley, L. K.: Simulating atmospheric composition over a South-East Asian tropical rainforest performance of a chemistry box model, Atmos. Chem. Phys., 10, 279–298, doi:10.5194/acp-10-279-2010, 2010.

Pun, B. K., Seigneur, C., and Lohman, K.: Modeling secondary organic aerosol formation via multiphase partitioning with molecular data, Environ. Sci. Technol., 40, 4722-4731, 2006.

Pye, H. O. T., and Seinfeld, J. H.: A global perspective on aerosol from low-volatility organic compounds, Atmos. Chem. Phys., 10, 4377-4401, 2010.

Reid, R. C., Prausnitz, J. M., and Polling, B. E.: The properties of gases and liquids, Hill, New York, USA, 1987.

Robinson, A. L., Donahue, N. M., Shrivastava, M. K., Weitkamp, E. A., Sage, A. M., Grieshop, A. P., Lane, T. E., Pierce, J. R., and Pandis, S. N.: Rethinking organic aerosols: Semivolatile emissions and photochemical aging, Science, 315, 1259-1262, 2007.

Robinson, N. H., Hamilton, J. F., Allan, J. D., Langford, B., Oram, D. E., Chen, Q., Docherty, K., Farmer, D. K., Jimenez, J. L., Ward, M. W., Hewitt, C. N., Barley, M. H., Jenkin, M. E., Rickard, A. R., Martin, S. T., McFiggans, G., and Coe, H.: Evidence for a significant proportion of Secondary Organic Aerosol from isoprene above a maritime tropical forest, Atmos. Chem. Phys., 11, 1039-1050, doi:10.5194/acp-11-1039-2011, 2011.

Rotman, D. A., Atherton, C. S., Bergmann, D. J., Cameron-Smith, P. J., Chuang, C. C., Connell, P. S., Dignon, J. E., Franz, A., Grant, K. E., Kinnison, D. E., Molenkamp, C. R., Proctor, D. D., and Tannahill, J. R.: IMPACT, the LLNL 3-D global atmospheric chemical transport model for the combined troposphere and stratosphere: Model description and analysis of ozone and other trace gases, J. Geophys. Res., 109, D04303, doi:10.1029/2002JD003155, 2004.

Saathoff, H., Naumann, K. H., Mohler, O., Jonsson, A. M., Hallquist, M., Kiendler-Scharr, A., Mentel, T. F., Tillmann, R., and Schurath, U.: Temperature dependence of yields of secondary organic aerosols from the ozonolysis of alpha-pinene and limonene, Atmos. Chem. Phys., 9, 1551-1577, 2009.

Sato, K., Hatakeyama, S., and Imamura, T.: Secondary organic aerosol formation during the photooxidation of toluene: NOx dependence of chemical composition, J. Phys. Chem.. A, 111, 9796-9808, 2007.

Seinfeld, J. H., and Pandis, S. N.: Atmospheric chemistry and physics: from air pollution to climate change, John Wiley, Hoboken, N. J., 1998.

Sillman, S.: A numerical-solution for the equations of tropospheric chemistry based on an analysis of sources and sinks of odd hydrogen, J. Geophys. Res., 96, 20735-20744, 1991.

Simpson, D., Yttri, K. E., Klimont, Z., Kupiainen, K., Caseiro, A., Gelencsér, A., Pio, C., Puxbaum, H., and Legrand, M.: Modeling carbonaceous aerosol over Europe: Analysis of the CARBOSOL and EMEP EC/OC campaigns, J. Geophys. Res., 112, D23S14, doi:10.1029/2006JD008158, 2007.

Slowik, J. G., Stroud, C., Bottenheim, J. W., Brickell, P. C., Chang, R. Y.-W., Liggio, J., Makar, P. A., Martin, R. V., Moran, M. D., Shantz, N. C., Sjostedt, S. J., van Donkelaar, A., Vlasenko, A., Wiebe, H. A., Xia, A. G., Zhang, J., Leaitch, W. R., and Abbatt, J. P. D.: Characterization of a large biogenic secondary organic aerosol event from eastern Canadian forests, Atmos. Chem. Phys., 10, 2825–2845, doi:10.5194/acp-10-2825-2010, 2010.

Song, C., Zaveri, R. A., Alexander, M. L., Thornton, J. A., Madronich, S., Ortega, J. V., Zelenyuk, A., Yu, X. Y., Laskin, A., and Maughan, D. A.: Effect of hydrophobic primary organic aerosols on secondary organic aerosol formation from ozonolysis of alpha-pinene, Geophys. Res. Lett., 34, L20803, doi:10.1029/2007GL030720, 2007.

Spracklen, D. V., Jimenez, J. L., Carslaw, K. S., Wrosnop, D. R., Evans, M. J., Mann, G. W., Zhang, Q., Canagaratna, M, R., Allan, J., Coe, H., McFiggans, G., Rap, A., and Forster, P.: Aerosol mass spectrometer constraint on the global secondary organic aerosol budget, Atmos. Chem. Phys. Discuss., 11, 5699-5755, 2011.

Stanier, C. O., Pathak, R. K., and Pandis, S. N.: Measurements of the volatility of aerosols from alpha-piniene ozonolysis, Environ. Sci. Technol., 41, 2756-2763, 2007.

Stavrakou, T., Muller, J. F., De Smedt, I., Van Roozendael, M., Kanakidou, M., Vrekoussis, M., Wittrock, F., Richter, A., and Burrows, J. P.: The continental source of glyoxal estimated by the synergistic use of spaceborne measurements and inverse modelling, Atmos. Chem. Phys., 9, 8431-8446, 2009.

Stavrakou, T., Peeters, J., and Muller, J. F.: Improved global modelling of HOx recycling in isoprene oxidation: evaluation against the GABRIEL and INTEX-A aircraft campaign measurements, Atmos. Chem. Phys., 10, 9863-9878, 2010.

Stone, D., Evans, M. J., Commane, R., Ingham, T., Floquet, C. F. A., McQuaid, J. B., Brookes, D. M., Monks, P. S., Purvis, R., Hamilton, J. F., Hopkins, J., Lee, J., Lewis, A. C., Stewart, D., Murphy, J. G., Mills, G., Oram, D., Reeves, C. E., and Heard, D. E.: HOx observations over West Africa during AMMA: impact of isoprene and NOx, Atmos. Chem. Phys., 10, 9415-9429, 2010.

Stroud, C. A., Makar, P. A., Moran, M. D., Gong, W., Song, S., Zhang, J., Hayden, K., Mihele, C., Brook, J. R., Abbatt, J. P. D., and Slowik, J. G.: Impact of model grid spacing on regional- and urban- scale air quality predictions of organic aerosol, Atmos. Chem. Phys., 11, 3107-3118, 2011.

Surratt, J. D., Chan, A. W. H., Eddingsaas, N. C., Chan, M. N., Loza, C. L., Kwan, A. J., Hersey, S. P., Flagan, R. C., Wennberg, P. O., and Seinfeld, J. H.: Reactive intermediates revealed in secondary organic aerosol formation from isoprene, Proc. Natl. Acad. Sci. USA., 107, 6640-6645, 2010.

Surratt, J. D., Lewandowski, M., Offenberg, J. H., Jaoui, M., Kleindienst, T. E., Edney, E. O., and Seinfeld, J. H.: Effect of acidity on secondary organic aerosol formation from isoprene, Environ. Sci. Technol., 41, 5363-5369, 2007.

Szidat, S.; Prévôt, A. S. H.; Sandradewi, J.; Alfarra, M. R.; Synal, H.-A.; Wacker, L. & Baltensperger, U. Dominant impact of residential wood burning on particulate matter in Alpine valleys during winter Geophys. Res. Lett., 34, L05820, 2007.

Szidat, S., Ruff, M., Perron, N., Wacker, L., Synal, H. A., Hallquist, M., Shannigrahi, A. S., Yttri, K. E., Dye, C., and Simpson, D.: Fossil and non-fossil sources of organic carbon

(OC) and elemental carbon (EC) in Goteborg, Sweden, Atmos. Chem. Phys., 9, 1521-1535, 2009.

Tan, Y., Carlton, A. G., Seitzinger, S. P., and Turpin, B. J.: SOA from methylglyoxal in clouds and wet aerosols: Measurement and prediction of key products, Atmos. Environ., 44, 5218–5226, 2010.

Tsigaridis, K. and Kanakidou, M.: Global modelling of secondary organic aerosol in the troposphere: a sensitivity analysis, Atmos. Chem. Phys., 3, 1849-1869, doi:10.5194/acp-3-1849-2003, 2003.

Tsigaridis, K., Krol, M., Dentener, F. J., Balkanski, Y., Lathière, J., Metzger, S., Hauglustaine, D. A., and Kanakidou, M.: Change in global aerosol composition since preindustrial times, Atmos. Chem. Phys., 6, 5143-5162, doi:10.5194/acp-6-5143-2006.

Tsigaridis, K., and Kanakidou, M.: Secondary organic aerosol importance in the future atmosphere, Atmos. Environ., 41, 4682-4692, 2007.

Trainic, M., Riziq, A. A., Lavi, A., Flores, J. M., and Rudich, Y.: The optical, physical and chemical properties of the products of glyoxal uptake on ammonium sulfate seed aerosols, Atmos. Chem. Phys. Discuss., 11, 19223-19252, doi:10.5194/acpd-11-19223-2011, 2011.

Utembe, S. R., Cooke, M. C., Archibald, A. T., Shallcross, D. E., Derwent, R. G., and Jenkin, M. E.: Simulating secondary organic aerosol in a 3-D Lagrangian chemistry transport model using the reduced Common Representative Intermediates mechanism (CRI v2-R5), Atmos. Environ., 45, 1604-1614, 2011.

Vaden, T. D., Imre, D., Beranek, J., Shrivastava, M., and Zelenyuk, A.: Evaporation kinetics and phase of laboratory and ambient secondary organic aerosol, Proc. Natl. Acad. Sci. USA., 108, 2190-2195, 2011.

Valorso, R., Aumont, B., Camredon, M., Raventos-Duran, T., Mouchel-Vallon, C., Ng, N. L., Seinfeld, J. H., Lee-Taylor, J., and Madronich, S.: Explicit modelling of SOA formation from α-pinene photooxidation: sensitivity to vapour pressure estimation, Atmos. Chem. Phys., 11, 6895–6910, doi:10.5194/acp-11-6895-2011, 2011.

Volkamer, R., Jimenez, J. L., San Martini, F., Dzepina, K., Zhang, Q., Salcedo, D., Molina, L. T., Worsnop, D. R., and Molina, M. J.: Secondary organic aerosol formation from anthropogenic air pollution: Rapid and higher than expected, Geophys. Res. Lett., 33, L17811, doi:10.1029/2006GL026899, 2006.

Volkamer, R., Martini, F. S., Molina, L. T., Salcedo, D., Jimenez, J. L., and Molina, M. J.: A missing sink for gas-phase glyoxal in Mexico City: Formation of secondary organic aerosol, Geophys. Res. Lett., 34, L19807, doi:10.1029/2007GL030752, 2007.

Volkamer, R., Ziemann, P. J., and Molina, M. J.: Secondary Organic Aerosol Formation from Acetylene (C2H2): seed effect on SOA yields due to organic photochemistry in the

aerosol aqueous phase, Atmos. Chem. Phys., 9, 1907–1928, doi:10.5194/acp-9-1907-2009, 2009.

Wang, M., and Penner, J. E.: Aerosol indirect forcing in a global model with particle nucleation, Atmos. Chem. Phys., 9, 239-260, 2009.

Wang, M. H., Penner, J. E., and Liu, X. H.: Coupled IMPACT aerosol and NCAR CAM3 model: Evaluation of predicted aerosol number and size distribution, J. Geophys. Res., 114, D06302, doi:10.1029/2008JD010459, 2009.

Wang, Y. H., Jacob, D. J., and Logan, J. A.: Global simulation of tropospheric O-3-NOx-hydrocarbon chemistry 1. Model formulation, J. Geophys. Res., 103, 10713-10725, 1998.

Wesely, M. L., Cook, D. R., Hart, R. L., and Speer, R. E.: Measurements and parameterization of particulate sulfur dry deposition over grass, J. Geophys. Res., 90, 2131-2143, 1985.

Xia, A. G., Michelangeli, D. V., and Makar, P. A.: Box model studies of the secondary organic aerosol formation under different HC/NOx conditions using the subset of the Master Chemical Mechanism for alpha-pinene oxidation, J. Geophys. Res., 113, D10301, doi:10.1029/2007JD008726, 2008.

Yoon, Y. J., Ceburnis, D., Cavalli, F., Jourdan, O., Putaud, J. P., Facchini, M. C., Decesari, S., Fuzzi, S., Sellegri, K., Jennings, S. G., and O'Dowd, C. D.: Seasonal characteristics of the physicochemical properties of North Atlantic marine atmospheric aerosols, J. Geophys. Res., 112, D04206, doi:10.1029/2005JD007044, 2007.

Yttri, K. E., Aas, W., Bjerke, A., Cape, J. N., Cavalli, F., Ceburnis, D., Dye, C., Emblico, L., Facchini, M. C., Forster, C., Hanssen, J. E., Hansson, H. C., Jennings, S. G., Maenhaut, W., Putaud, J. P., and Torseth, K.: Elemental and organic carbon in PM10: a one year measurement campaign within the European Monitoring and Evaluation Programme EMEP, Atmos. Chem. Phys., 7, 5711-5725, 2007.

Yu, F.: A secondary organic aerosol formation model considering successive oxidation aging and kinetic condensation of organic compounds: global scale implications, Atmos. Chem. Phys., 11, 1083-1099, doi:10.5194/acp-11-1083-2011, 2011.

Zhang, J. Y., Huff Hartz, K. E., Pandis S. N., and Donahue, N. M.: Secondary organic aerosol formation from limonene ozonolysis: Homogeneous and heterogeneous influences as a function of NOx, J. Phys. Chem. A, 110, 11053–11063, 2006.

Zhang, Q., Jimenez, J. L., Canagaratna, M. R., Allan, J. D., Coe, H., Ulbrich, I., Alfarra, M. R., Takami, A., Middlebrook, A. M., Sun, Y. L., Dzepina, K., Dunlea, E., Docherty, K., DeCarlo, P. F., Salcedo, D., Onasch, T., Jayne, J. T., Miyoshi, T., Shimono, A., Hatakeyama, S., Takegawa, N., Kondo, Y., Schneider, J., Drewnick, F., Borrmann, S., Weimer, S., Demerjian, K., Williams, P., Bower, K., Bahreini, R., Cottrell, L., Griffin, R. J., Rautiainen, J., Sun, J. Y., Zhang, Y. M., and Worsnop, D. R.: Ubiquity and dominance of oxygenated species in organic aerosols in anthropogenically-influenced Northern

Hemisphere midlatitudes, Geophys. Res. Lett., 34, L13801, doi:10.1029/2007GL029979, 2007.

Zhang, S., Penner, J. E., and Torres, O.: Inverse modeling of biomass burning emissions using total ozone mapping spectrometer aerosol index for 1997, J. Geophys. Res., 110, D21306, doi:10.1029/2004JD005738, 2005.

Zhang, Y., Pun, B., Vijayaraghavan, K., Wu, S. Y., Seigneur, C., Pandis, S. N., Jacobson, M. Z., Nenes, A., and Seinfeld, J. H.: Development and application of the model of aerosol dynamics, reaction, ionization, and dissolution (MADRID), J. Geophys. Res., 109, D01202, doi:10.1029/2003JD003501, 2007.

CHAPTER 3

Global modeling of SOA formation in the aqueous phase using different mechanisms

3.1 Introduction

Aqueous phase processing, as a complementary pathway to form secondary organic aerosol (SOA), has the potential to enhance both SOA mass and the oxygen-to-carbon (O/C) ratio in atmospheric OA. Water-soluble and polar gases are oxidized in the aqueous phase leading to the production of low volatility substances (e.g., organic acids, oligomers, and organosulfates) (Blando and Turpin, 2000; Warneck, 2003; Tan et al., 2009; Liggio et al, 2005). These low-volatile products stay in the particle phase after water evaporation (Blondo and Turpin, 2000; Haddad El et al., 2009) and thereby increase SOA concentrations. In addition, aqueous phase chemistry tends to form the products with higher O/C ratios than those that form in gas phase reactions (Hermann et al., 2005; Lim et al., 2010; Ervens and Volkamer, 2010), since the precursors for the aqueous phase reactions tend to be small compounds with low-molecule weight (MW) and high O/C ratios, and aqueous phase chemistry on these small compounds tend to add functional groups to the C-C bond (e.g., acid formation) or to react with themselves to keep the carbon structure (e.g., accretion reactions) (Ervens et al., 2011). These products with high O/C ratios may help to explain the high O/C ratios observed in atmospheric OA (Aiken et al. 2008; Altieri et al., 2009; Ng et al., 2010), which can't be reproduced by

models that only form SOA from gas-phase reactions (Jimenez et al., 2009; Dzepina et al., 2009).

Given the potential importance of SOA from aqueous phase processing, several models to date have been developed to estimate the role of the SOA formed in the aqueous phase (denoted aqSOA hereafter). Chen et al. (2007) investigated the SOA formation from aqueous phase reactions in clouds using an explicit aqueous mechanism including organic acid formation from glyoxal and methylglyoxal; they found that aqueous phase processing increased the SOA formation by 27% for a rural scenario, by 7% for an urban scenario, and by 9% at the surface in the eastern United States. Assuming a fixed yield of 4% for the conversion of glyoxal into aqSOA, Carlton et al. (2008) added in-cloud SOA formation into a regional air quality model and improved the model's ability to predict the concentrations of water soluble organic carbon (WSOC) from aircraft measurements over northeastern US. Myriokefalitakis et al. (2011) and Liu et al. (2012) employed a global model to study the in-cloud formation of SOA and found that its global production could be around 13-30 Tg/yr. In addition to the contribution of cloud droplets, the contribution of aerosol water to the aqueous phase SOA from glyoxal and methylglyoxal has also been estimated in global models (Fu et al., 2008, 2009; Stavrakou et al., 2009; Lin et al., 2012). The amount of irreversible uptake of glyoxal and methylglyoxal into aerosol water were predicted to be much smaller than that taken up by cloud droplets, when a same reactive uptake parameter (γ=0.0029), based on the laboratory studies of Liggio et al. (2005), was used (Fu et al., 2008, 2009). This same basic result was also found by Lin et al. (2012) using the same approach for the uptake of glyoxal and methylglyoxal. The study by Stavrakou et al. (2009), however, concluded that the global

continental SOA source from uptake of glyoxal by aerosol particles was at least as large as that from cloud droplets or even up to 60% larger. Instead of irreversible uptake, an in-cloud parameterization similar to Ervens et al. (2008) was applied to the uptake by cloud droplets in this study.

The summary of the above model studies shows that a high degree of uncertainty in the processes leading to the SOA formation from glyoxal and methylglyoxal still exists. In fact, while the use of a reactive uptake parameter γ for the rate-limiting step in SOA formation implies a surface-limited uptake process, Ervens and Volkamer (2010) argued that bulk phase processes might dominate. They fitted the observed glyoxal loss rates or observed SOA mass formation rates from different literature studies (i.e., Hastings et al., 2005; Liggio et al., 2005; Volkamer et al., 2009) to a bulk-limitation equation expressing the SOA formation rate. However, the very recent paper by Waxman et al. (2013) found that a surface-limited uptake process could explain the gap of gas-phase glyoxal mass in Mexico City between observations and a gas-phase-only model prediction much better than the bulk phase process did. In addition to the uncertainty associated with the uptake process, the use of an identical reactive uptake parameter for both cloud droplets and aerosol water cloud does not account for differences in the chemistry of carbonyl compounds between in-cloud water and in-aerosol water (Lim et al., 2010; Ervens and Volkamer, 2010). Based on recent laboratory studies, in this paper we tested both a detailed chemical mechanism using a bulk phase representation and a parameterized mechanism using the reactive uptake parameter γ in a 3-D chemical transport model to simulate the formation of aqSOA in both in-cloud water and in-aqueous aerosol water.

Iron chemistry in cloud water has been shown to be a major source of aqueous OH (Ervens et al., 2003; Deguillaume et al., 2005). However, no model, to our knowledge, included this chemistry in simulating in-cloud aqSOA formation. Therefore we also study the effect of iron chemistry on in-cloud aqSOA formation. Further, we compared two simulations with two different cloud fields to examine the extent to which changes in cloud water content could influence the production of SOA in-cloud.

This paper is organized as follows. The model and chemistry will be described in Sec. 3.2; global budgets and distributions of aqSOA predicted from five different mechanisms and one different cloud field will be analyzed in Sec. 3.3; to further evaluate these mechanisms, we will make comparisons with available measurements in Sec. 3.4; Sec. 3.5 will summarize our conclusions.

3.2 Model description

We used a global chemical transport model (IMPACT) to simulate the formation of SOA. The IMPACT model includes the microphysics of sulfate aerosol and the interactions between sulfate and non-sulfate aerosols based on the aerosol module developed by Herzog et al. (2004) (Liu et al., 2005). In this paper, we used the same microphysics module described in Liu et al. (2005), and prescribed the SOA size distribution to be the same as that for biomass burning OM in Liu et al. (2005), but allowed it to interact with sulfate through condensation of sulfuric acid, through coagulation with pure sulfate aerosols, and through aqueous formation of sulfate. We used the 1997 meteorological fields from the National Aeronautics and Space Administration (NASA) Data Assimilation Office (DAO) GEOS-STRAT model (Coy and Swinbank, 1997; Coy et al.,

1997). The meteorology was defined on a 4° latitude x 5° longitude horizontal grid with 46 vertical layers. Cloud water content was not available in our meteorological fields from the GEOS-STRAT model, and thus was diagnosed with a parameterization used in the NCAR CCM2 model (Hack, 1998); The large scale stratiform cloud fraction is determined based on the grid box mean relative humidity (RH) as calculated from the DAO meteorological data using the parameterization by Sundqvist et al. (1989). The convective cloud fraction is parameterized by using the convective mass flux (Xu and Krueger, 1991). The model was run for a 1-year time period with a 1-month spin up time. Global emissions of gases, aerosols and aerosol precursors and treatments of dry and wet deposition used here are the same as those used in Lin et al. (2012).

3.2.1 SOA formation through gas-particle partitioning in the gas phase

In this paper, we adopted the SOA formation mechanism through gas-particle partitioning described in Lin et al. (2012). In short, in Lin et al. (2012), a fully explicit gas-phase photochemical mechanism was used to predict the formation of semi-volatile organic compounds (SV-VOCs) which then partition to an aerosol phase. These condensed SV-VOCs were assumed to further undergo aerosol phase reactions to form oligomers. In addition, we also accounted for the SOA formation due to the heterogeneous reactions of epoxides on the surface of sulfate aerosol by assuming an uptake coefficient of 0.0029. Lin et al. (2012) carried out three different simulations with different gas-phase chemical mechanisms. Here, we used the most realistic mechanism ('Simulation C' in Table 1 in Lin et al. (2012)). This includes the chemical mechanism published by Ito et al. (2007) to represent the basic photochemistry of O_3, OH, NO_x and VOCs, epoxide formation from isoprene from Paulot et al. (2009), and HO_x regeneration through isoprene oxidation

proposed by Peeters et al. (2009) but with a reduced rate for the 1,5-H and 1,6-H shifts in isoprene radicals by a factor of 10.

3.2.2 SOA formation in the aqueous phase

In the presence of cloud droplets or aqueous particles, water-soluble gases (e.g., glyoxal, methylglyoxal, and glycolaldehyde) will be dissolved in the aqueous phase and be further oxidized by OH and NO_3 radicals to form products with lower volatility (e.g., carboxylic acids and oligomers). These low volatility products are assumed to remain entirely in the particulate phase as SOA, when water is evaporated or there is no cloud.

3.2.2.A Multiphase reactions scheme

The change of aqueous phase species and gas phase species due to the photochemical reactions and the exchange between the gas and the particle is expressed by the following equation,

$$\frac{dC_g}{dt} = P_g - \left(L_g + k_t Q\right)C_g + \frac{k_t}{HRT} C_a \qquad (1a)$$

$$\frac{dC_a}{dt} = P_a + k_t Q C_g - \left(L_a + \frac{k_t}{HRT}\right) C_a \qquad (1b)$$

Where C_a and C_g are aqueous and gas phase concentrations (molecules cm^{-3} air), P_a and P_g are aqueous and gas phase chemical production rates (molecules cm^{-3} air s^{-1}), L_a and L_g are aqueous and gas phase pseudo-first-order chemical loss rates (s^{-1}), K_H is the Henry's law coefficient (M atm^{-1}), R is the universal gas constant (L atm $mol^{-1}K^{-1}$), T is the temperature (K), Q is the liquid water content (cm^3 H_2O cm^{-3} air), and k_t (cm^3 air cm^{-3} H_2O s^{-1}) is a first-order rate constant that represents diffusion through the gas phase and

across the interface of the drop (see Schwartz (1986) and Lelieveld and Crutzen (1991) for details).

To solve Equation (1a) and (1b), we used the method described by Sillman et al. (2007), which was based on implicit (reverse Euler) equations but incorporated a number of the nonstandard treatments described by Sillman (1991) and Barth et al. (2003). The mass transfer rate across the gas-aqueous interface was assumed to be limited by diffusion and was determined for each gas by its molecular diffusion, mass accommodation coefficient and Henry's law constant, following methods described in Lelieveld and Crutzen (1991). A gas diffusivity of $0.1 cm^2\ s^{-1}$ was assumed for all gaseous species. Accommodation coefficients for each species are listed in Table S7 in Appendix B and assumed to be 0.05 for species for which no information is available. For situations in which the average concentration of an aqueous species is limited by the rate of diffusion within the aqueous phase, a correction is made as recommended by Lelieveld and Crutzen (1991). In addition, an effective cloud droplet radius of 10 μm is assumed for all clouds, while the effective radius for aqueous sulfate particles is calculated explicitly according to their relative humidity dependent size distributions. Aerosol water results from the water uptake by sulfate, which is based on the equilibrium Köhler theory (Ghan and Zaveri, 2007) using the RH and hygroscopicity of sulfate to calculate the wet volume mean radius from the dry volume mean radius of each mode.

A complete list of aqueous phase reactions and their corresponding rate constants are contained in from Table S1 and Table S8 in Appendix B. Aqueous reactions for sulfates, nitrates, H_2O_2, O_3, OH and related radicals have been taken from Jacob (1986), Pandis and Seinfeld, Lelieveld and Crutzen (1990) and Liu et al. (1997); Aqueous reactions for

water-soluble organic compounds are based on recently published box modeling studies (Lim et al., 2005; Carton et al., 2007; Ervens and Volkamer, 2010; Lim et al., 2010); Aqueous reactions for iron are drawn from Deguillaume et al. (2010) and Chemical Aqueous Phase Radical Mechanism (CAPRAM) 2.4 (Ervens et al., 2003).

While the chemistry of organic species taking place in cloud droplets is generally well established in experiments and box modeling studies, the chemistry of organic species occurring in wet particles is only now being developed and very few models have been extended to include them (Ervens et al., 2011). Ervens and Volkamer (2010) and Lim et al. (2010) proposed different schemes for SOA formation in aerosol water. Ervens and Volkamer (2010) parameterized the SOA formation using simple first order reaction rate constants to fit photochemical chamber experiments. Basically, the gas phase glyoxal is taken into aerosol water based on its Henry's law coefficient and is further hydrated to monohydrate and dihydrate glyoxal using explicit hydration coefficients. These dissolved glyoxal, monohydrate and dihydrate glyoxals can react with dissolved OH radicals to form organic acids, or undergo oligomerization using a parameterized photochemical coefficient (k), or react with ammonium. The reactions and kinetic coefficients used in this paper are listed in Table S3 in Appendix B, in which we extended the Erven and Volkamer model to include the bulk phase reactions of methylglyoxal adopting kinetic data from the literature. On the other hand, Lim et al. (2010) described SOA formation using a set of detailed radical-radical reactions that were based on bulk aqueous phase experiments. Gas-phase glyoxal is partitioned into aerosol water based on its effective Henry's law constant (implicitly accounting for its hydration) and then further reacts with dissolved OH radicals to form radical species by H-atom abstraction, which combine

with themselves to form dimers and further trimers through so called "radical-radical" reactions ((Lim et al., 2010)). These "radical-radical" reactions compete with reactions of radicals with dissolved O_2 to form organic acids. In aerosol-water relevant conditions (i.e., 1-10 mole/Liter (M) glyoxal concentrations and 10^{-12} – 10^{-11} M dissolved OH radicals), over 80% of total products are favored to oligomers. Since no kinetic data for methylglyoxal in-aerosol-water reactions were available in Lim et al. (2010), we assumed 80% of products from the reaction of dissolved methylglyoxal with OH are oligomers and the rest are oxalic acid, which is consistent with the recent work of Lim et al. (2013).

3.2.2.B Reaction probability method (surface-limited uptake process)

As an alternative approach to the method described above with detailed gas-phase and aqueous phase chemical mechanism coupled by gas-particle transfer, a simpler method has also been used by Fu et al. (2008) and Lin et al. (2012) to describe the uptake of a gas and its further reactions inside the particles. In this method, the loss of gas phase glyoxal or methylglyoxal on aqueous particles or cloud droplets was parameterized using the following equation:

$$\frac{d\,C_g}{dt} = \frac{1}{4} \cdot \gamma \cdot A \cdot < \nu > \cdot\, C_g \qquad (2)$$

Where A is the total surface area of aqueous sulfate aerosols [m^2/m^3], C_g is the concentration of gas phase glyoxal or methylglyoxal, γ is the reactive uptake coefficient, representing the reaction probability that a molecule impacting the particle surface undergoes reaction. The value of γ used in Fu et al. (2008) and Lin et al. (2012) was assumed to be 2.9E-3 for both glyoxal and methylglyoxal uptake on aqueous sulfate and

cloud droplets. $<\upsilon>$ is the mean molecular speed of glyoxal or methylglyoxal in the gas phase given by $(8RT/\pi MW)^{-1/2}$.

3.2.3 Case set up

As described above, there are still large uncertainties in simulating aqSOA formation both in cloud water and aerosol water. We thus set up six cases to study the sensitivity of aqSOA formation to different representations of gas-particle mass transfer, to the different schemes in aerosol water reactions, to the cloud water content, and to the inclusion of iron chemistry in the cloud. The descriptions of these six cases are presented here (also summarized in Table 3-1), and comparisons of sensitivity test simulations with Case 1 as well as with observations are shown in Sec. 3.3.

In Case 1, we used the detailed multiphase reactions scheme (Equations 1a and 1b) to predict the production of glyoxylic acid, oxalic acid and pyruvic acid both in cloud water and aerosol water. To simulate the formation of oligomers due to glyoxal in the aerosol water, we used the surface-limited uptake process (Equation 2) with a reactive uptake parameter γ of 0.0033, the parameter which best describe the amount of glyoxal uptake by particles in Mexico City (Waxman et al., 2013). We scaled the uptake parameter of methylglyoxal to that of glyoxal by the ratios of their effective henry's law constants (Table S7 in Appendix B) to account the formation of oligomers due to the uptake of methylglyoxal.

In Case 2, all aqSOA formation was simulated using the multiphase reaction scheme. The parameterized reactions proposed by Ervens and Volkamer (2010) in the bulk phase process scheme are used to simulate the formation of aqSOA in aerosol water.

Case 3 also used the multiphase reaction scheme, but used the reactions from Lim et al. (2010) to predict the formation of aqSOA in both clouds and aerosol water.

For Case 4, we employed the same chemical mechanism as in Case 1, but used the cloud field output from AM3, the atmospheric component of the coupled general circulation model (CM3) developed at the NOAA Geophysical Fluid Dynamics Laboratory (GFDL) (Donner et al., 2011).

In Case 5, we added iron chemistry in cloud water (Table S6 in Appendix B) to the chemistry used in Case1. The only source of aqueous Fe in the model is the dissolution of dust aerosol particles incorporated into cloud droplets. We assumed 3.5% mass of dust aerosol composed of Fe (Taylor and McLennan, 1985), only 5% of which could be dissolved into cloud water (Ito et al., 2013). The initial speciation of Fe(II)/Fe(III) was set to 4 (Deguillaume et al., 2010).

For Case 6, we used the surface-limited uptake process to simulate all aqSOA formation in both cloud water and aerosol water, exactly following the method of Fu et al (2008) and Lin et al. (2012).

3.3 Results

Table 3-2 shows the global budget of total aqSOA and each of its components (if available) for these six cases. We will focus on the detailed budget and global distributions of aqSOA for Case 1 in Sec. 3.3.1 and Sec. 3.3.2, and the difference between other cases with Case 1 will be analyzed in Sec. 3.3.3 to Sec. 3.3.6.

Table 3-1 Case descriptions

Case name	SOA formation in cloud	SOA formation in aerosol water	Cloud field	Iron chemistry
Case 1	Multiphase reactions; aqueous phase reactions are referred to Table S2 and S3 in Appendix B	Surface-limited process, using a reactive uptake parameter of 3.3E-3 for glyoxal and 2.9E-5 for methylglyoxal.	The diagnostic cloud field	N/A
Case 2	Multiphase reactions; aqueous phase reactions are referred to Table S2 and S3 in Appendix B	Multiphase reactions, using the parameterization by Ervens and Volkamer (2010) (Table S4 in Appendix B)	The diagnostic cloud field	N/A
Case 3	Multiphase reaction, using the detailed chemistry by Lim et al. (2010) (Table S2 and S5 in Appendix B)	Multiphase reaction, using the detailed chemistry by Lim et al. (2010) (Table S2 and S5 in Appendix B)	The diagnostic cloud field	N/A
Case 4	Multiphase reactions; aqueous phase reactions are referred to Table S2 and S3 in Appendix B	Surface-limited process, using a reactive uptake parameter of 3.3e-3 for glyoxal and 2.9e-5 for methylglyoxal	GFDL AM3 cloud field	N/A
Case 5	Multiphase reactions; aqueous phase reactions are referred to Table S2, S3 and S6 in Appendix B	Surface-limited process, using a reactive uptake parameter of 3.3e-3 for glyoxal and 2.9e-5 for methylglyoxal	The diagnostic cloud field	Include the aqueous iron chemistry (Table S6 in Appendix B)
Case 6	Surface-limited process, using a reactive uptake parameter of 2.9E-3 for both glyoxal and methylglyoxal	Surface-limited process, using a reactive uptake parameter of 2.9E-3 for both glyoxal and methylglyoxal	The diagnostic cloud field	N/A

Table 3-2 Global aqSOA budget analyses for all cases

Case name	Species name	Chemical production (Tg/yr)	Chemical destruction (Tg/yr)	Net production (Tg/yr)	Dry deposition (Tg/yr)	Wet deposition (Tg/yr)	Burden (Tg)
Case1	Glyoxylic acid	8.5	4.0	4.5	0.2	4.3	3.5E-2
	Pyruvic acid	6.9E-1	5.1E-1	1.8E-1	1.0E-2	1.8E-1	1.6E-3
	Oxalic acid	22.9	7.2	15.7	0.6	15.1	1.0E-1
	Glyoxal oligomer	6.1	--	6.1	0.4	5.7	8.5E-2
	Methylglyoxal oligomer	2.2E-1	--	2.2E-1	2.4E-2	2.0E-1	2.3E-3
Case 2	Glyoxylic acid	8.7	4.0	4.7	0.2	4.5	3.6E-2
	Pyruvic acid	6.8E-1	5.0E-1	1.8E-1	8.9E-3	1.7E-1	1.5E-3
	Oxalic acid	23.6	7.3	16.3	0.6	15.7	1.0E-1
	Glyoxal oligomer	2.5E-2	--	2.5E-2	4.4E-3	2.1E-2	2.0E-3
	Methylglyoxal oligomer	1.7E-2	--	1.7E-2	4.3E-3	1.3E-2	9.7E-4
Case 3	Glyoxylic acid	8.2	3.7	4.5	0.2	4.3	3.7E-2
	Pyruvic acid	5.6E-1	3.9E-1	1.7E-1	8.7E-3	1.6E-1	1.5E-3
	Oxalic acid	20.4	6.4	14.0	0.5	13.5	9.1E-2
	Glyoxal oligomer	4.6E-2	2.9E-2	1.7E-2	5.1E-4	1.7E-2	1.8E-3
	Methylglyoxal oligomer	2.1E-3	--	2.1E-3	1.2E-4	2.0E-3	1.4E-4
Case 4	Glyoxylic acid	4.8	3.2	1.6	0.2	1.4	2.6E-2
	Pyruvic acid	4.4E-1	3.3E-1	1.1E-1	1.0E-2	1.0E-1	1.9E-3
	Oxalic acid	11.8	5.6	6.2	0.4	5.8	8.6E-2
	Glyoxal oligomer	9.2	--	9.2	0.8	8.3	1.2E-1
	Methylglyoxal oligomer	4.1E-1	0	4.1E-1	5.7E-2	3.5E-1	5.2E-3
Case 5	Glyoxylic acid	12.7	8.1	4.6	0.2	4.4	3.7E-2
	Pyruvic acid	2.0	1.8	0.2	1.1E-2	1.9E-1	1.9E-3
	Oxalic acid	33.0	16.1	16.9	0.7	16.2	1.1E-1

	Glyoxal oligomer	5.7	--	5.7	0.4	5.3	8.1E-2
	Methylglyoxal oligomer	2.2E-1	--	2.2E-1	2.4E-2	0.2	2.3E-3
Case 6	Glyoxal oligomer	22.6	--	22.6	1.0	21.6	2.0E-1
	Methylglyoxal oligomer	36.9	--	36.9	1.6	35.3	3.0E-1

3.3.1 Global budget

In Case 1, the net global aqSOA source totals 26.7 Tg/yr, over 95% of which is removed by wet deposition while the rest is removed by dry deposition. The global annual mean aqSOA burden equals to 0.22 Tg, corresponding to a global mean life time of about 3.0 days due to deposition. Five aqSOA species are identified here: glyoxylic acid, pyruvic acid, oxalic acid, and two classes of oligomers formed from glyoxal and methylglyoxal. Among these five aqueous SOA components, oxalic acid accounts for about 58.8% of total aqueous SOA source, glyoxal oligomers accounts for about 22.9%, glyoxylic acid for about 16.8%, methylglyoxal oligomers for 0.8% and pyruvic acid for 0.7%. While all oligomers are assumed to be formed in the aerosol water, organic acids can be formed in both cloud and aerosol water. However, the contribution of aerosol water to the formation of organic acids formations is very small. The net production rate of glyoxylic acid in the aerosol water accounts for only 0.025 Tg/yr of the total 4.5 Tg/yr net production rate; 0.2% of pyruvic acid is formed in aerosol water; for oxalic acid, the net production rate in the aerosol water is -0.7 Tg/yr, since it is consumed by reaction with OH, compared to the net formation rate of 16.4 Tg/yr in cloud water.

Table 3-3 Global detailed in-cloud chemical reactions of organic acids for Case 1

	Source	Reaction rate (Tg/yr)	Sink	Reaction rate (Tg/yr)
Glyoxylic acid	Glyoxal + OH/NO_3	5.1	Reaction with OH	3.7
	Methylglyoxal +OH/NO_3	6.6e-2		
	Acetic acid + OH	1.3	Reaction with NO_3	3.5e-1
	Glycolaldhyde +OH	2.0		
Oxalic acid	Glyoxal + OH	18.0	Reaction with OH	5.6
	Glyoxylic acid +OH/NO_3	4.9	Reaction with NO_3	1.5
Pyruvic acid	Methylglyoxal + OH	6.8e-1	Reaction with OH	5.1e-1
	Methylglyoxal + NO_3	1.8e-2	Reaction with NO_3	1.7e-3

To further study the detailed budget for these organic acids, their reaction rates within cloud are listed in Table 3-3. The global glyoxylic acid production rate is 8.5 Tg/yr, which comes from the oxidation of glyoxal, glycolaldehyde, methylglyoxal and acetic acid. Glyoxal oxidation accounts for 60.0%, while the oxidation of glycolaldehyde, methylglyoxal and acetic acid account for 23.5%, 0.8% and 15.2%, respectively. 47.7% of glyoxylic acid is destroyed by reaction with OH and NO_3, and the rest is deposited to the surface. For oxalic acid, the global production rate is equal to 22.9 Tg/yr, which is close to the estimate by Myriokefalitakis et al. (2011) and the estimate by Liu et al. (2012). In our model, the direct reaction of glyoxal with OH contributes 78.6% to the total oxalic acid production; the reaction of glyoxylic acid with OH and NO_3 contributes the rest. Oxalic acid is removed from the atmosphere by OH and NO_3 radicals in aqueous

phase oxidation (31.0%) and by wet and dry deposition (69.0%). The only source of pyruvic acid is the reactions of methylglyoxal with OH and NO_3. Different from glyoxylic acid and oxalic acid, over half (73.3%) of pyruvic acid is removed by reactions with OH and NO_3 radicals. For glyoxal and methylglyoxal oligomers, no chemical destruction is included in the model.

The analysis above shows the importance of glyoxal, glycolaldehyde, methylglyoxal and acetic acid as precursors leading to aqueous SOA formation, the global budget of these four species are thus summarized in Table 3-4. While all of glyoxal, glycolaldehyde and methylglyoxal are generated by oxidation of VOCs in the gas phase and in the aqueous phase, around half of acetic acid is directly emitted into the atmosphere through biomass burning. The global glyoxal production in the gas phase is equal to 70.5 Tg/yr, and reactions in cloud contribute 3.3 Tg/yr production rate through the oxidation of dissolved glycolaldehyde. About 60.3% of this is consumed in the gas phase, 21.3% is oxidized in cloud, 8.3% is oxidized in aqueous aerosol, and the rest is deposited to the surface. The total source of methylglyoxal is 167.9 Tg/yr. Only 0.63 Tg/yr and 0.23 Tg/yr is absorbed and oxidized in cloud and in aqueous aerosol, respectively. Most of the methylglyoxal is destroyed in the gas phase or deposited to the surface. The net chemical production of glycolaldehyde in the gas phase is about 17.7 Tg/yr, of which 28.8% is dissolved into cloud and reacts with OH and NO_3. For acetic acid, the uptake rate by cloud is 0.36 Tg/yr, compared to its total source (60.7 Tg/yr). Aqueous aerosol contributes a negligible amount to the sink of both glycolaldehyde and acetic acid.

Table 3-4 Global budget of aqSOA precursors (Tg/yr) for Case 1

	Glyoxal	Methylglyoxal	Glycolaldehyde	Acetic Acid
Emission	0	0	0	31.4
Gas phase production	70.5	167.9	81.3	29.3
Aqueous phase production	3.3	0	0	3.6e-1
Gas phase consumption	44.0	157.7	63.6	25.8
Aqueous phase consumption	23.0	0.86	5.1	1.2
Deposition	6.8	9.3	12.6	34.1

3.3.2 Global distribution and seasonal variability

Figure 3-1 presents the global annual mean distributions of total aqSOA, total organic acids (i.e., glyoxylic acid, pyruvic acid and oxalic acid) which are mostly formed in cloud, and oligomers formed in aqueous aerosol at approximately 970 hPa. The zonal mean vertical distributions are also shown. The total aqSOA concentrations show large values over tropical Africa, the Amazon basin, Eastern Asia, Eastern United States and Europe. The SOA distributions are determined by their precursor (mainly glyoxal) distributions, oxidant (which is primarily dissolved OH radicals) distributions, and the availability of cloud water or aerosol water. The maximum SOA concentrations over tropical Africa and the Amazon basin reflect the large biogenic VOC emissions and the resulting glyoxal concentration to a great extent. The different pattern shown between

organic acid concentrations (Figure 3-1C) and in oligomer concentrations (Figure 3-1E) is due to the different patterns of cloud and aerosol water content (Figure 3-2). Aerosol water content is largely due to sulfate, which spreads over the industrial regions in the Northern Hemisphere because most of sulfate comes from the anthropogenic emissions. In contrast, most of cloud water is located over the tropical region and the Southern Hemisphere. This contrast is also reflected in the vertical zonal mean distributions of organic acids and oligomers (Figure 3-1D and Figure 3-1F). There is a hot spot in organic acids over the tropical region, most of which are formed in cloud, while the peak is located over the Northern Hemisphere for the oligomers, all of which are formed in aqueous aerosols.

The column burdens of organic acids and oligomers for winter (December, January and February) and for summer (June, July, and August) are presented in Figure 3-3. During the winter, the column burden of organic acids peaks over the tropical land because of the huge biogenic emissions over there. During the summer, a secondary column burden maximum arises in the Northern Hemisphere, which can be attributed to the enhanced photochemistry and biogenic emissions over these regions in the summer. Enhanced photochemistry combined with larger biogenic emissions can increase the production of aqSOA precursors (e.g., glyoxal) and aqueous OH radical through intensifying in-cloud H_2O_2 photolysis. For the same reason, the column burden of oligomers in the summer shows a larger value and spread over a wider area than that in the winter over the Northern Hemisphere (see the right panels in Figure 3-3).

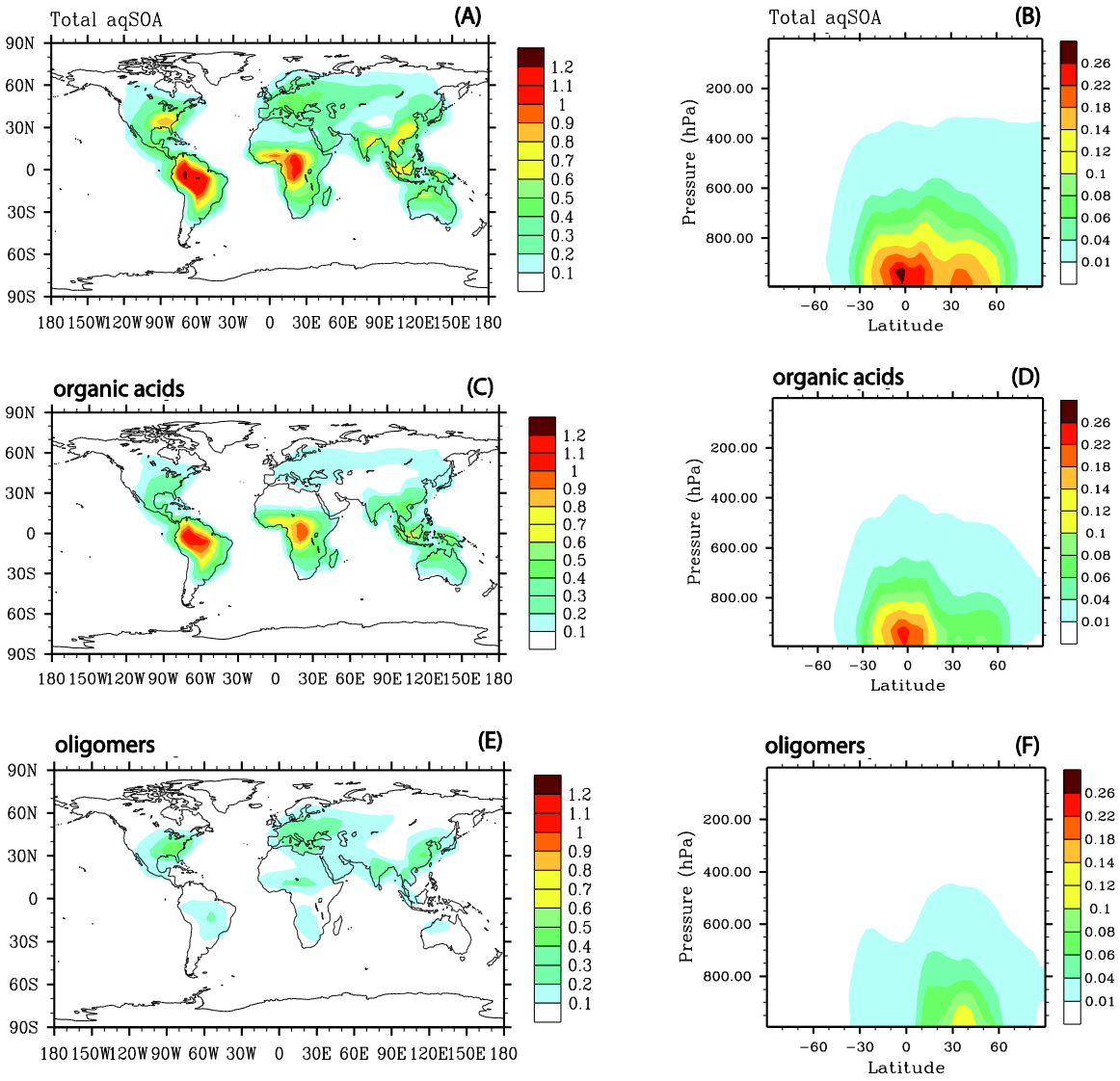

Figure 3-1. Annual mean simulated concentrations of total aqSOA (panel A and B), organic acids (the sum of glyoxylic acid, pyruvic acid and oxalic acid) (panel C and D), oligomers from glyoxal and methylglyoxal (panel E and F). The left column shows the global distributions at the level of around 971hPa in the model; the right column depicts the zonal mean distributions. All are simulated from Case 1. Units: $\mu g/m^3$.

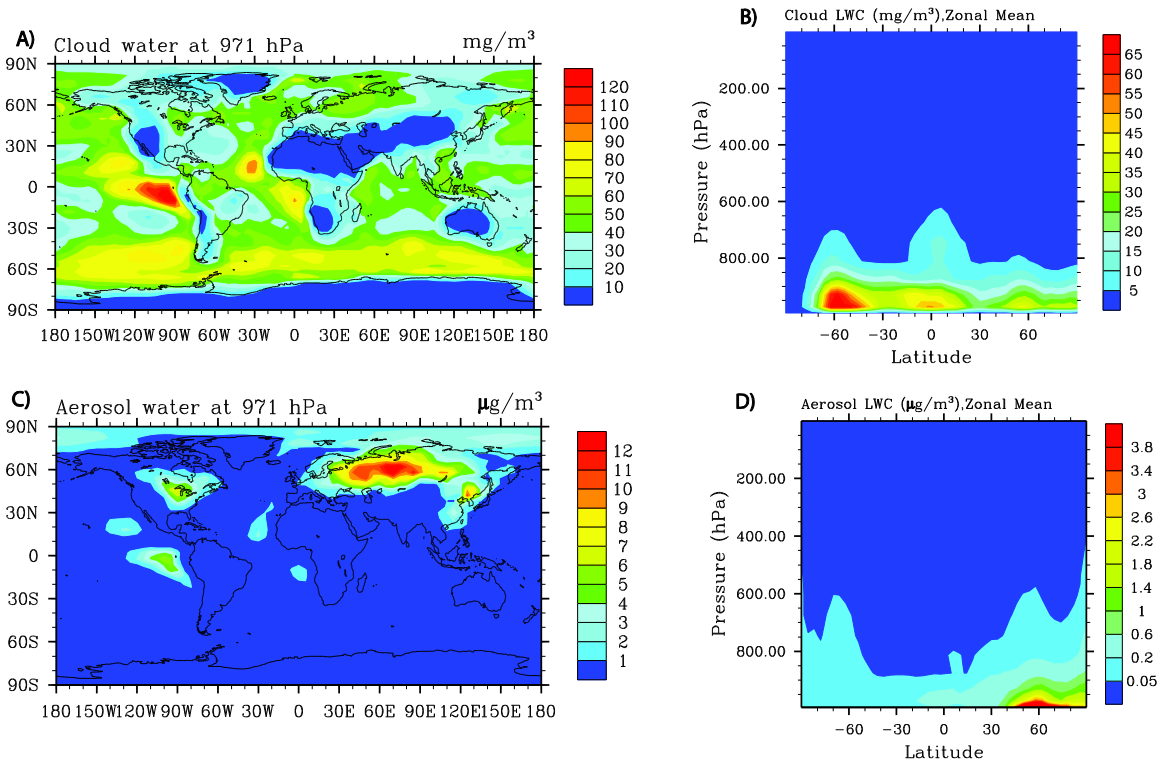

Figure 3-2. Annual mean grid-box averaged cloud liquid water content (LWC) in mg/m^3 at the level of approximately 971hPa in the model of Case 1(A) and zonal mean content (B), and annual mean aerosol LWC in μg/m^3 at the level of approximately 971 hPa in the model of Case 1 (C) and zonal mean content (D).

3.3.3 Reaction probability method

As shown in Table 3-2, the production rates of oligomers in Case 1 are higher than those in Case 2, which suggests that the value of reactive uptake probability γ adopted from Waxman et al. (2013) is higher than that implied by the simulation with detailed gas-phase and aqueous phase chemical mechanisms coupled by gas-to-droplet transfer. Indeed, we can derive a global averaged γ from the Equation (2) for the uptake of glyoxal or methlglyoxal into the cloud or the aqueous aerosol in Case 2. We integrated the left

side and the right side of Equation (2) globally and annually, and thus obtained the global averaged annual mean reactive uptake probability following the equation below

$$\bar{\gamma} = (\sum \frac{d\, C_g}{dt})/(\sum \frac{1}{4} \cdot A \cdot < \nu > \cdot C_g) \qquad (3)$$

The derived global averaged $\bar{\gamma}$ for the uptake of glyoxal into the aqueous aerosol is 1.24E-5, while the $\bar{\gamma}$ for the uptake of methylglyoxal into the aqueous aerosol is 1.70E-5. This value for glyoxal uptake is much smaller than 3.30E-3 as suggest by Waxman et al. (2013) and 2.90E-3 derived by Liggio et al. (2005). The value of 1.70E-5 for methylglyoxal uptake is comparable to the value of 2.92E-5 that we used in Case 1. The reason for this discrepancy might be that the actual value of uptake parameter in remote and rural regions may be smaller than that derived in urban region-Mexico city by Waxman et al. (2013) or/and might be that the bulk phase reactions adopted from Ervens and Volkamer (2010) may not include the surface reactions of glyoxal in the real atmosphere.

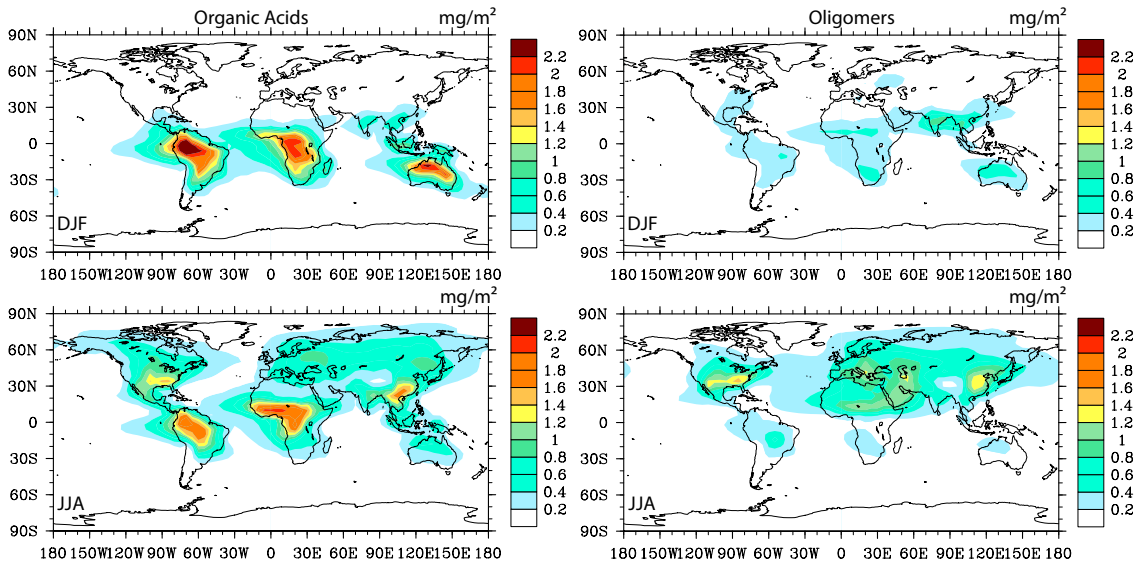

Figure 3-3. Seasonal averaged column concentrations (mg/m^2) of organic acids (the left column) and oligomers (the right column) in December, January and February (DJF) (the top row) and in June, July and August (JJA) (the bottom row). All are simulated from Case 1.

3.3.4 The effect of cloud water content

The global distributions at approximately 971 hPa in the model and zonal annual mean distribution of grid-box averaged cloud water content for Case 4 are shown in Figure 3-4(A) and (B). The cloud water content in Case 1 (Figure 3-2) is higher than that in Case 4 almost everywhere below about 900 hPa, leading to a larger global organic acids source and burden in Case 1 compared to those in Case 4 (Table 3-2). He et al. (2013) studied the relationship between the in-cloud SOA formation and the cloud water content and proposed a parameterization that its formation rate is linear proportional to the cloud water content. Therefore we present the ratio of cloud water content in Case1 to that in Case 4 and the ratio of in-cloud aqSOA formation rate between these two cases in Figure 3-4 (C) and (D). Comparing these two plots, both the pattern and value are generally

similar below around 900 hPa, but above 900hPa neither the pattern nor the value is similar, which might suggest that in-cloud aqSOA formation is not proportional to the cloud water content in the high altitudes.

The lifetime of oxalic acid in Case 4 is longer than that in Case 1 (5.0 days in Case 4 vs. 2.3 days in Case 1), because in Case 4 more oxalic acids are produced at high altitudes or high latitudes and much less (a factor of over 10) are formed in the low tropical region (Figure 3-4(D)). Given more precipitation, especially convective precipitation at low altitudes in tropical regions, oxalic acid can be precipitated out more easily than in other regions. Similarly, we have a longer lifetime of sulfate aerosol in Case 4 than that in Case 1. In addition, a slightly larger in-cloud production rate of sulfate aerosol (93.3 Tg/yr) is also found in Case 4 compared to that in Case 1 (91.6 Tg/yr). This results from the abundant cloud water in Case 4 in the Northern hemisphere, where most of sulfate is formed. The longer lifetime and larger in-cloud production rate of sulfate causes a larger sulfate burden and thus a larger oligomer formation rate in sulfate aerosol water.

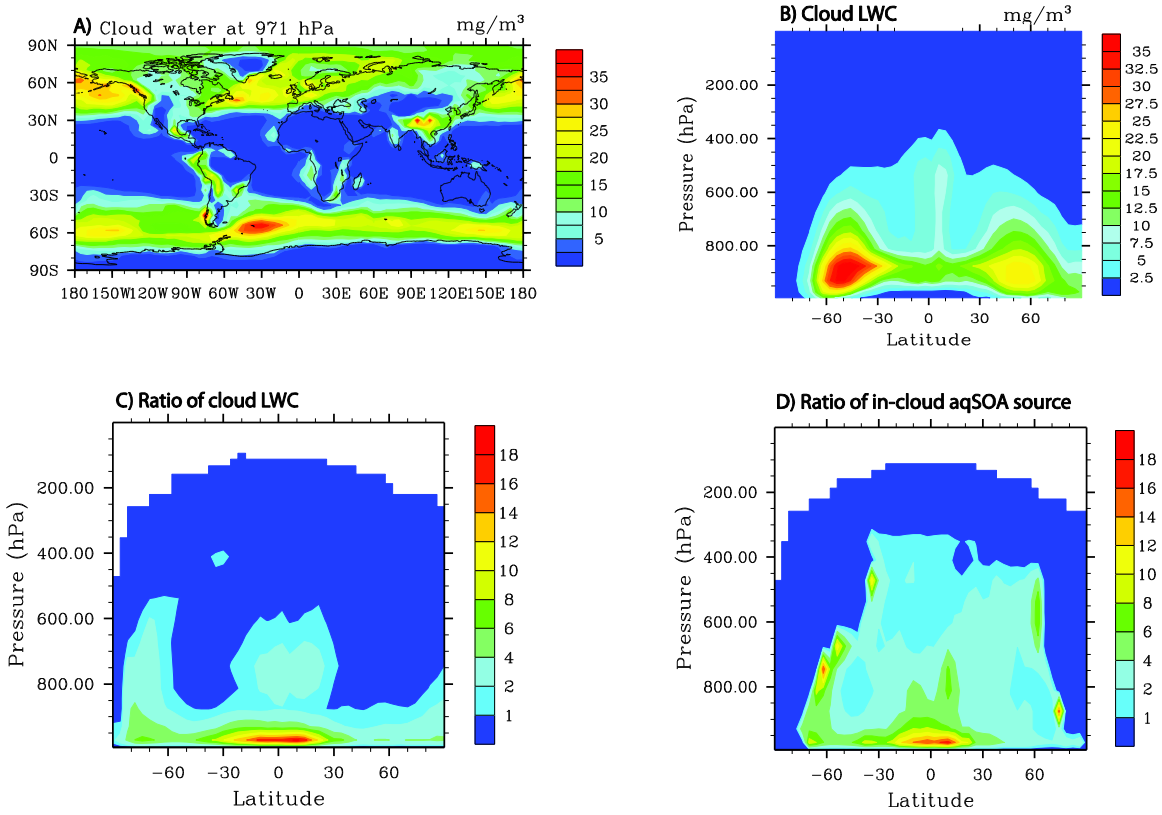

Figure 3-4. Annual mean grid-box averaged cloud liquid water content (LWC) in mg/m^3 from the GFDL AM3 cloud field at the level of approximately 971hPa in the model of Case 4 (A) and zonal mean content (B). Panel C shows the zonal mean distributions for the ratio of grid-box averaged cloud LWC in Case 1 to that in Case 4; panel D shows the zonal mean distributions for the ratio of in-cloud aqSOA source in Case 1 to that in Case 4.

3.3.5 The effect of iron chemistry in cloud

Inclusion of iron chemistry in cloud increases the net production of aqSOA only by 3.5% globally, although it increases both the chemical production and destruction of carboxylic acids in cloud (Table 3-2), which is due to the increase of the in-cloud OH radical source. The global in-cloud OH radical source in the troposphere (below approximately 200 hPa) in Case 5 is 2.6 times larger than that in Case 1 because of the formation of aqueous

phase OH radical through the reaction of Fe(II) with H_2O_2 and the photolysis of Fe(III). The largest increase occurs over the Sahara desert, Northwestern China and Mongolia regions where there are huge amounts of dust aerosol (Figure 3-5). The enhancement of in-cloud OH radical leads to an increase of 10.1 Tg/yr in the oxalic acid chemical production rate and an increase of 8.9 Tg/yr in the oxalic acid chemical destruction rate. These two increases cancel each other, leading to a small change in the net chemical production rate (1.2 Tg/yr), and thus a small variation in the burden as well. The inclusion of iron chemistry decreases the formation rate of glyoxal oligomers from 6.1 Tg/yr in Case 1 to 5.7 Tg/yr in Case 5, which is due to the increased absorption rate of glyoxal into cloud and thus less glyoxal uptake into aqueous aerosol.

3.3.6 SOA formation in clouds vs. SOA formation in aerosol water

On a global basis, the SOA production rate in cloud is larger than that in aerosol water in all simulations (Table 3-5), although the fraction of SOA formed in cloud varies from case to case. SOA formed in cloud water accounts for about 21% of total aqSOA in Case 1, Case 5 and Case 6; the SOA production rate in aerosol water even show negative values in Case 2 and Case 3, which means the aqSOA is consumed in aerosol water. This is because the oxalic acid formed in cloud dissolved into the aerosol water after cloud water evaporated and further reacted with high concentrated dissolved OH radicals inside the aerosol water, as we showed in Section 3.3.1. The amount of destruction rate of oxalic acid by reacting with OH is larger than that of production rate through the reaction of glyoxlic acid and glyoxal with OH. Nevertheless, oligomers still can be formed in the aerosol water, with a production rate of 4.2E-2 Tg/yr and 3.5E-2 Tg/yr for Case 2 and Case 3, respectively. The similar amount of SOA formed in the aerosol water between

Case 2 and Case 3 is consistent with the finding by Ervens et al. (2011), who claimed that their parameterized reaction system produce similar amount of SOA as that of Lim et al. (2010) in box model simulations. The relative importance of SOA formed in cloud water decreases to 50.3% in Case 4 when using the GFDL AM3 cloud field because of decreased cloud water content in the tropical regions but increased cloud water in the Northern Hemisphere.

Table 3-5. SOA formation in cloud vs. SOA formation in aerosol water

	SOA production rate in cloud (Tg/yr)	SOA production rate in aerosol water (Tg/yr)	Total aqSOA production rate (Tg/yr)	Fraction of SOA production in cloud
Case 1	21.1	5.6	26.7	79.0%
Case 2	22.0	-0.9	21.1	104.0%
Case 3	19.5	-0.8	18.7	104.3%
Case 4	8.8	8.7	17.5	50.3%
Case 5	21.9	5.7	27.6	79.3%
Case 6	46.8	12.6	59.4	78.8%

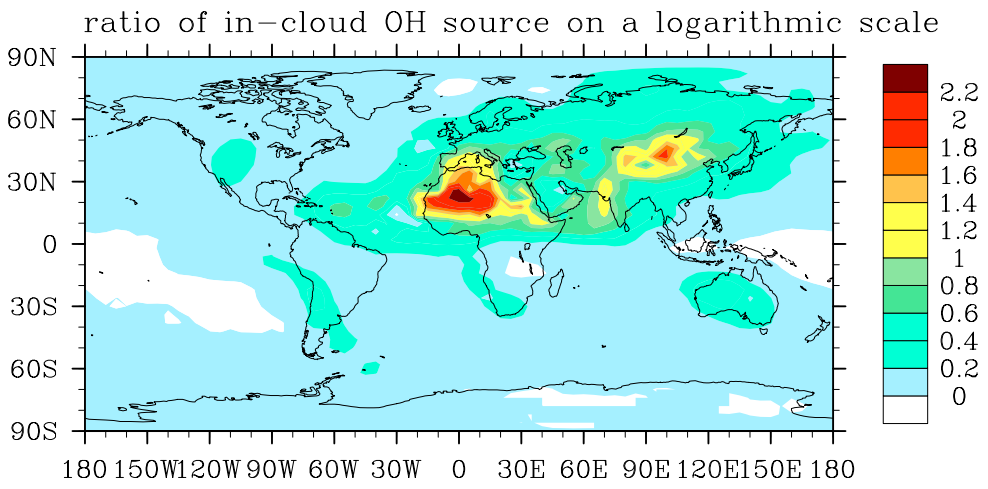

Figure 3-5. The ratio of annual mean in-cloud OH radical production rates in Case 5 (with Fe chemistry) to that in Case 1 (without Fe chemistry). The value shown is the logarithm of the ratio.

3.4 Comparison with measurements

First we compare the modeled oxalic acid with measured oxalate adopted from Myriokefalitakis et al. (2011) (Figure 3-6). We only show this comparison for Case 1 and Case 4, since the oxalic acid concentrations in other cases are similar to those in Case 1 (Table 3-2). Although oxalate measurements are sparse around the world, the observations listed here cover most of the continental regions: United States, Europe, China, Amazon basin and Africa, and all these measurements have long time sampling durations which span from several days to 2 years. To compare with the measurements, the monthly simulation data were sampled on the specific month and at the specific location corresponding to the measurements. It should be noted that due to the coarse resolution used in the model (4 degrees by 5 degrees), we don't expect the model can predict the high concentrations seen in urban regions. For completeness, however, we

also list these comparisons here and they indeed show a large underestimate by the model. Over rural areas, the model performance varies in different regions and different seasons. In Europe, while most of simulations lie within a factor of 2 of the observed concentrations during the summer (see green triangles in Figure 3-6), the model in Case 1 underestimates all observations in winter (black dots in Figure 3-6), the discrepancy of which can be as high as an order of magnitude at some sites (e.g., K-Pustza, Hungary). The different model performances between in summer and in winter may be attributed to different oxalate sources in these two seasons. According to Legand et al. (2007), the major oxalate sources at the CARBOSOL surface stations in winter are primary emissions from wood burning, vehicular exhausts and meat cooking and secondary production through the oxidation of toluene and ethane emitted from vehicles. In summer these anthropogenic emissions decrease and biogenic emissions (e.g., isoprene) increase and make an important contribution to the oxalate source via multiphase photochemical reactions. These four CARBOSOL sites are included in the comparison here and we suspect the other European sites that we included have similar oxalate sources to those at the CARBOSOL sites. Unlike what is expected for the measurements, the model only accounts for secondary source of oxalic acid formation through multiphase photo-oxidations; the oxalic acid formation from primary sources and local vehicle emissions is not represented. Therefore the model can predict the observed oxalate concentrations relatively well in summer, whereas in winter the model under-predicts them. Other factors might also contribute to this under-estimation, such as low cloud water content or high deposition rates in the model. When using the GFDL AM3 cloud field, the model prediction improves at some sites.

Case 1

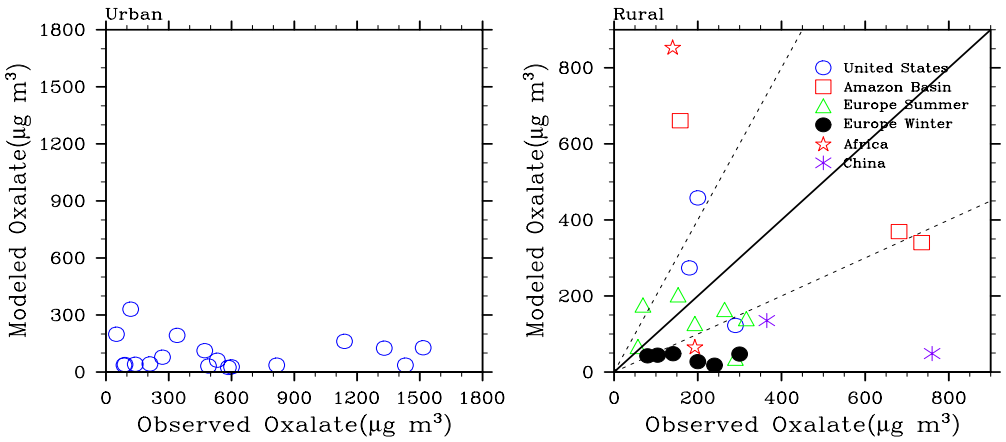

Case 4

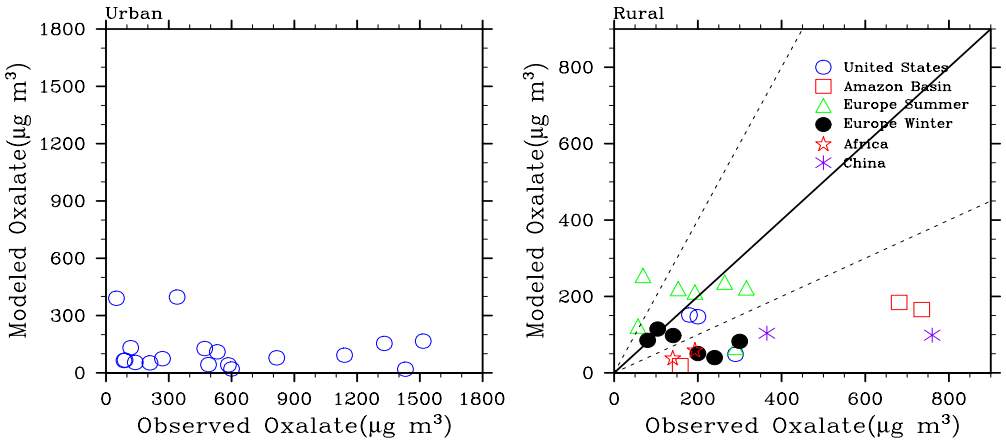

Figure 3-6. Comparison of oxalate mass concentrations observed at the urban and rural sites adopted from Myriokefalitakis et al. (2011) with oxalic acid concentrations simulated in Case 1 and Case 4. Solid lines show the 1:1 ratio, and dashed lines show the 1:2 and 2:1 ratios. The measurements at the various sites were made in different seasons and different years between 1980 and 2007 and most of them were reported with several-days sampling duration. The model results are the average values over the same months as the observations.

As shown by the red squares in Figure 3-6, the model also significantly underestimates the measured oxalate concentrations at 2 of the 3 sites in the Amazon basin. One possible

reason for this underestimation is that the model doesn't include the oxalate source from biomass burning either through direct emission or through secondary formation during aerosol aging (Gao et al., 2003). At these two sites, biomass burning is the major source of oxalate formation (Falkovich et al., 2005; Kundu et al., 2010; Granham et al., 2002). At the site where the aerosol samples were believed to be out of the influence of biomass burning (Talbot et al. 1988), the modeled oxalate concentration in Case 1 is even higher than the observation, but in Case 4 (using the GFDL AM3 cloud field) the model still underestimates the observation.

There are only two sites in China and three sites in US available to compare. The modeled oxalate concentration is 60% lower than the observation at the Mount Tai site reported by Wang et al. (2009), which is clean and free of local emissions. In contrast, the Mangshan site, 40 km north of Beijing, is polluted by air mass transported from Beijing (He and Kawamura, 2010), which leads to a high oxalate concentration of 760 ng/m^3. The model can't represent the local emissions and thus only captures less than 10% of the observation. Using GFDL AM3 cloud field doesn't improve the model performance. Overestimation of oxalate deposition in the model may also contribute to this under-prediction. The three blue circles in Figure 3-6 stand for the comparisons for the sites in United States, which indicates that the model predicts reasonably well the measured oxalate concentrations, except for the site in Florida Sydney. For the two sites in Africa (red stars in Figure 3-6), the model fails to predict the observations. The modeled oxalate concentration in Case 1 is 3 times higher than the observation at the site in Central Africa and at the site in South Africa it only predicts about 1/3 of measured concentration. This might suggest that the cloud water content in this simulation is inconsistent with the real

cloud water content or that the model doesn't represent well the sources and/or sinks of oxalate over this region. In Case 4, the model under-predicts the measurements at both of these two sites.

As shown above and in Sec. 3.3.4, cloud water has an important effect on oxalate formation. Therefore it is also valuable to compare the cloud water content in the model with that in measurements. However, there is no such information available in the literature where measured oxalate concentrations were also reported.

Table 3-6. Normalized mean bias (NMB) and correlation coefficient (R) between the predicted SOA for the simulation and observations. The number of sites in the comparison is in parentheses.

Case name	Urban sites (N=14)		Urban downwind sites (N=6)		Rural sites (N=17)	
	NMB	R	NMB	R	NMB	R
Case 1	-38.4%	0.68	-35.3%	0.87	-30.3%	0.24
Case 2	-46.4%	0.70	-44.7%	0.89	-40.0%	0.27
Case 3	-47.4%	0.72	-45.9%	0.89	-40.6%	0.27
Case 4	-25.8%	0.64	-23.2%	0.79	-11.4%	0.24
Case 5	-37.8%	0.68	-34.2%	0.86	-29.4%	0.24
Case 6	-12.5%	0.72	8.9%	0.86	20.0%	0.30

Although there are no measurements available that can separate aqSOA from the SOA formed in the gas phase, we can compare the modeled total SOA with the observed SOA from aerosol mass spectrometry (AMS) measurements. Zhang et al. (2007) present observational SOA data (measured by aerosol mass spectrometry, AMS) from a series of

surface measurements at multiple sites in the Northern Hemisphere, which were made in different seasons and different years between 2000 and 2006 and were reported for the average of varying durations spanning from 8 to 36 days. Here, we compare the model data at the corresponding grid in the corresponding month. Figure 3-7 shows the comparisons of SOA between observations and predictions in Case 1, Case 2, Case 4 and Case 6. The normalized mean bias (NMB) and correlation coefficient (R) of these comparisons are listed in Table 3-6. We don't show these statistics for Case 3 and Case 5 because the SOA concentrations in these 2 cases are close to those in Case 2 and Case 1, respectively (Table 3-2). Again, we do not expect the model with its low horizontal resolution to capture the POA emissions at urban sites, nor would we capture high local VOC and NO_x emissions, which have a very complex effect on SOA formation due to non-linear chemistry (Stroud et al., 2011). Nevertheless, the model-predicted SOA is subject to longer formation times than is POA, and is in reasonable agreement with the AMS observations. The NMB in Case 1 is -30.3% for rural sites (see the Table 3-6). The multiphase reactions scheme used for aqSOA in aerosol water in Case 2 leads to a bigger underestimation (a NMB of around -40.0%); Using the GFDL AM3 cloud fields allows the model predictions to become closer to the measurements; The model in Case 6 even overestimates the observations by around 20% when adopting the reactive uptake probability method to predict the aqSOA formation both in the cloud and the aerosol water.

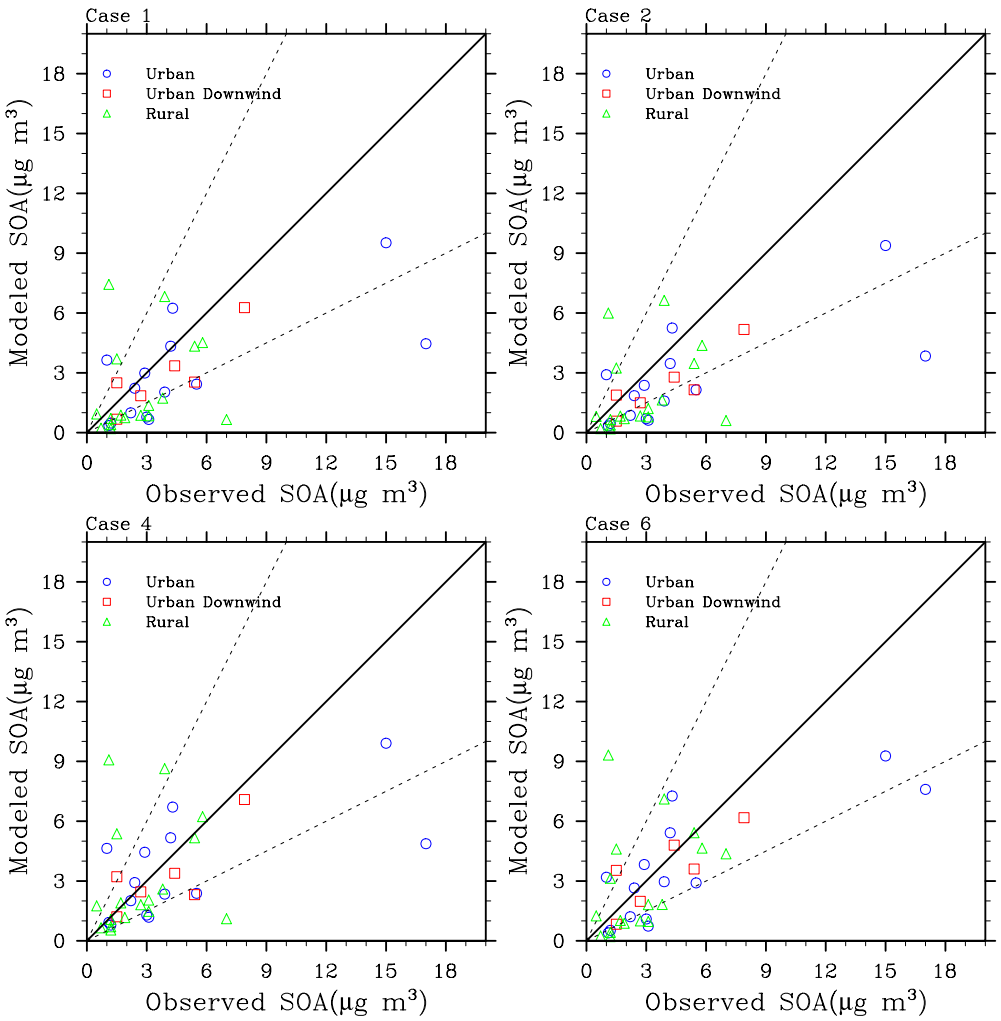

Figure 3-7. Comparison of SOA mass concentrations observed at the urban, urban-downwind and rural sites reported in Zhang et al. (2007) with those simulated in Case 1, Case 2, Case 4 and Case 6. Solid lines show the 1:1 ratio, and dashed lines show the 1:2 and 2:1 ratios. The measurements at the various sites were made in different seasons and different years between 2000 and 2006 and were reported for the average of varying durations spanning from 8 to 36 days. The model results are the average values over the same months as the observations.

In addition to the AMS measurements made in the Northern Hemisphere extra-tropics reported in Zhang et al. (2007), we also show the comparison with measurements from three different campaigns in tropical forested areas (Table 3-7). In contrast to the

Northern Hemisphere, the model simulation for Case 1 to Case 5 is about a factor of 2 too high over both West Africa and the Amazon basin, but is only slightly higher (less than 40% higher) than the observation over Borneo, Malaysia. Gilardoni et al. (2011) reported average $PM_{2.5}$ organic aerosol concentrations during the wet season (February-June) of 1.7 μg /m^3, larger than the wet season concentrations measured at the same site by Chen et al. (2009) by about 60-80%. In comparison with these measurements, our simulated concentrations are around 60% too high. The simulation in Case 6 overestimates the measurement at all these three sites by a factor of 2 to 3. As SOA dominated the total submicaron OA in Amazon basin (Chen et al., 2009) and in Malysian Borneo (Robinson et al., 2011), the comparison of OA in these two sites reflects the model performance of SOA to a large extent.

Table 3-7. Comparison of simulated OA with observed OA measured in tropical forested regions.

	West Africa (Below 2 km) (SOA in μg/m^3)	Amazon Basin (surface) (Total OA in μg/m^3)	Malysian Borneo (surface) (Total OA in μg/m^3)
Observations	1.18 (Capes et al., 2009)	0.7 (Chen et al., 2009) 1.70 (Gilardoni et al., 2011)	0.74 (Robinson et al., 2011)
Case 1	2.89	2.56	1.03
Case 2	2.62	2.33	0.92
Case 3	2.29	2.12	0.92
Case 4	2.82	2.48	0.85
Case 5	2.70	2.70	1.03
Case 6	4.47	4.45	1.57

3.5 Conclusions

In this paper, we simulated the formation of SOA in both cloud and aerosol water using multiphase processes with different chemical reactions and a surface-limited uptake process. We also conducted a simulation using the GFDL AM3 cloud fields and a simulation including iron chemistry in cloud. Using the surface-limited uptake process scheme with the reactive uptake parameter adopted from the laboratory studies leads to higher aqSOA production rates both in cloud and in aerosol water than using the multiphase process scheme does. The global glyoxal oligomers formed in sulfate aerosol water predicted by the parameterized photochemistry from Ervens and Volkamer (2010) are consistent with those predicted by the detailed "radical-radical" chemistry proposed from Lim et al. (2010). The annual average organic acids peak over the tropical regions due to the large biogenic emissions and abundant cloud water there, while the oligomers generally show maxima over industrialized areas in the Northern Hemisphere because of the large sulfate aerosol concentrations formed. During the summer, however, the large organic acids concentrations also show up in the Northern Hemisphere resulting from enhanced biogenic emissions and photochemistry in the summer. Similarly, the oligomer concentrations increase in the summer. When we changed the diagnostic cloud field to that simulated by the GFDL AM3 model, the organic acids production rate decreased by around 60% while sulfate formation rates increased slightly, because the GFDL AM3 cloud field has much smaller cloud water content in tropical regions but higher cloud water content in the Northern Hemisphere. The introduction of Fe chemistry in cloud has a large impact on the in-cloud HO_x budget, increasing the tropical in-cloud OH radical source by a factor of over 2 on a global basis. Despite the increase of in-cloud OH radical,

the net source of organic acids barely changes, because the in-cloud OH radical concentration increases by almost the same amount as does the chemical production and chemical destruction rate of organic acids.

We also compared the oxalic acid predicted from these different schemes and chemical mechanisms with measurements obtained in Europe, Amazon, Africa, China and US region. Over all, the model tends to underestimate observations in European winter, Amazon, Africa, and China, probably because the model doesn't account for the direct emission of oxalic acid from primary sources (e.g., wood burning, meat cooking and biomass burning) or that formed in the aging process associated with these direct emissions. However, this underestimation might also be due to a deposition rate that is too high or a cloud water content that is too low in the model. In fact, using the GFDL AM3 cloud field in Case 4 improved the model predictions at some sites in the Northern Hemisphere. Further comparisons are needed in the future when both the cloud water content and aqSOA in cloud are available.

Comparisons of total SOA (aqSOA combined with the SOA formed in the gas phase) in the model for all cases with the SOA measured by AMS in the Northern Hemisphere show a reasonable agreement, although the NMB of comparisons varies between +20% in Case 6 using the reaction probability method for aqSOA both in cloud and aerosol water to around -40% in Cases 2 and 3 using the multiphase reactions for aqSOA. On the other hand, Case 6 over-estimates the observations by a factor of 2 or 3 in all three tropical sites. Adopting the multiphase reaction scheme for in-cloud aqSOA can close the gap into within a factor of 2 in all three sites.

3.6 Reference

Aiken, A. C., DeCarlo, P. F., Kroll, J. H., Worsnop, D. R., Huffman, J. A., Docherty, K. S., Ulbrich, I. M., Mohr, C., Kimmel, J. R., Sueper, D., Sun, Y., et al.: O/C and OM/OC Ratios of Primary, Secondary, and Ambient Organic Aerosols with High-Resolution Time-of-Flight Aerosol Mass Spectrometry, Environ. Sci. Technol., 42(12), 4478–4485, doi:10.1021/es703009q, 2008.

Altieri, K. E., Turpin, B. J. and Seitzinger, S. P.: Composition of Dissolved Organic Nitrogen in Continental Precipitation Investigated by Ultra-High Resolution FT-ICR Mass Spectrometry, Environ. Sci. Technol., 43(18), 6950–6955, doi:10.1021/es9007849, 2009.

Blando, J. D. and Turpin, B. J.: Secondary organic aerosol formation in cloud and fog droplets: a literature evaluation of plausibility, Atmospheric Environment, 34(10), 1623–1632, 2000.

Carlton, A. G., Turpin, B. J., Altieri, K. E., Seitzinger, S., Reff, A., Lim, H. J. and Ervens, B.: Atmospheric oxalic acid and SOA production from glyoxal: Results of aqueous photooxidation experiments, Atmospheric Environment, 41(35), 7588–7602, doi:10.1016/j.atmosenv.2007.05.035, 2007.

Chen, J., Griffin, R. J., Grini, A. and Tulet, P.: Modeling secondary organic aerosol formation through cloud processing of organic compounds, Atmos. Chem. Phys., 7(20), 5343–5355, doi:10.5194/acp-7-5343-2007, 2007.

Chen, Q., Farmer, D. K., Schneider, J., Zorn, S. R., Heald, C. L., Karl, T. G., Guenther, A., Allan, J. D., Robinson, N., Coe, H., Kimmel, J. R., et al.: Mass spectral characterization of submicron biogenic organic particles in the Amazon Basin, Geophys. Res. Lett., 36, doi:10.1029/2009gl039880, 2009.

Coy, L. and Swinbank, R.: Characteristics of stratospheric winds and temperatures produced by data assimilation, J. Geophys. Res., 102(D22), 25763–25781, 1997.

Coy, L., Nash, E. R. and Newman, P. A.: Meteorology of the polar vortex: Spring 1997, Geophys. Res. Lett., 24(22), 2693–2696, 1997.

Deguillaume, L., Desboeufs, K. V., Leriche, M., Long, Y., & Chaumerliac, N.: Effect of iron dissolution on cloud chemistry: from laboratory measurements to model results, Atmos. Pollut. Res, 1(4), 220-228, 2010.

Deguillaume, L., Leriche, M. and Desboeufs, K.: Transition metals in atmospheric liquid phases: Sources, reactivity, and sensitive parameters, Chemical Reviews-Columbus, 105, 3388-3431, 2005.

Donner, L. J., Wyman, B. L., Hemler, R. S., Horowitz, L. W., Ming, Y., Zhao, M., Golaz, J.-C., Ginoux, P., Lin, S. J., Schwarzkopf, M. D., Austin, J., et al.: The Dynamical Core, Physical Parameterizations, and Basic Simulation Characteristics of the Atmospheric

Component AM3 of the GFDL Global Coupled Model CM3, J Climate, 24(13), 3484–3519, doi:10.1175/2011JCLI3955.1, 2011.

Dzepina, K., Volkamer, R. M., Madronich, S., Tulet, P., Ulbrich, I. M., Zhang, Q., Cappa, C. D., Ziemann, P. J. and Jimenez, J. L.: Evaluation of recently-proposed secondary organic aerosol models for a case study in Mexico City, Atmos. Chem. Phys., 9(15), 5681–5709, 2009.

Ervens, B.: CAPRAM 2.4 (MODAC mechanism): An extended and condensed tropospheric aqueous phase mechanism and its application, J. Geophys. Res., 108(D14), 4426–, doi:10.1029/2002JD002202, 2003.

Ervens, B. and Volkamer, R.: Glyoxal processing by aerosol multiphase chemistry: towards a kinetic modeling framework of secondary organic aerosol formation in aqueous particles, Atmos. Chem. Phys., 10(17), 8219–8244, doi:10.5194/acp-10-8219-2010, 2010.

Ervens, B., Turpin, B. J. and Weber, R. J.: Secondary organic aerosol formation in cloud droplets and aqueous particles (aqSOA): a review of laboratory, field and model studies, Atmos. Chem. Phys., 11(21), 11069–11102, doi:10.5194/acp-11-11069-2011, 2011.

Falkovich, A. H., Graber, E. R., Schkolnik, G., Rudich, Y., Maenhaut, W. and Artaxo, P.: Low molecular weight organic acids in aerosol particles from Rondônia, Brazil, during the biomass-burning, transition and wet periods, Atmos. Chem. Phys., 5(3), 781–797, 2005.

Fu, T. M., Jacob, D. J., Wittrock, F., Burrows, J. P., Vrekoussis, M. and Henze, D. K.: Global budgets of atmospheric glyoxal and methylglyoxal, and implications for formation of secondary organic aerosols, J. Geophys. Res., 113(D15), doi:10.1029/2007jd009505, 2008.

Gao, S.: Water-soluble organic components in aerosols associated with savanna fires in southern Africa: Identification, evolution, and distribution, J. Geophys. Res., 108(D13), 8491, doi:10.1029/2002JD002324, 2003.

Ghan, S. J. and Zaveri, R. A.: Parameterization of optical properties for hydrated internally mixed aerosol, J. Geophys. Res., 112(D10), D10201, doi:10.1029/2006JD007927, 2007.

Gilardoni, S., Vignati, E., Marmer, E., Cavalli, F., Belis, C., Gianelle, V., Loureiro, A. and Artaxo, P.: Sources of carbonaceous aerosol in the Amazon basin, Atmos. Chem. Phys., 11(6), 2747–2764, doi:10.5194/acp-11-2747-2011, 2011.

Graham, B.: Water-soluble organic compounds in biomass burning aerosols over Amazonia1. Characterization by NMR and GC-MS, J. Geophys. Res., 107(D20), 8047, doi:10.1029/2001JD000336, 2002.

Hack, J. J.: Sensitivity of the Simulated Climate to a Diagnostic Formulation for Cloud Liquid Water, J. Climate, 11(7), 1497–1515, 1998.

Haddad, El, I., Liu, Y. and Nieto-Gligorovski, L.: In-cloud processes of methacrolein under simulated conditions–Part 2: Formation of secondary organic aerosol, Atmos. Chem. Phys., 9, 5107–5117, 2009.

Hastings, W. P., Koehler, C. A., Bailey, E. L. and De Haan, D. O.: Secondary organic aerosol formation by glyoxal hydration and oligomer formation: Humidity effects and equilibrium shifts during analysis, Environ. Sci. Technol., 39(22), 8728–8735, doi:10.1021/es0504461, 2005.

He, C., Liu, J., Carlton, A. G. and Fan, S.: Evaluation of factors controlling global secondary organic aerosol production from cloud processes, Atmos. Chem. Phys, 13, 1913-1926, 2013.

He, N. and Kawamura, K.: Distributions and diurnal changes of low molecular weight organic acids and α-dicarbonyls in suburban aerosols collected at Mangshan, North China, Geochemical Journal, 44(4), e17–e22, 2010.

Herrmann, H., Tilgner, A., Barzaghi, P., Majdik, Z., Gligorovski, S., Poulain, L. and Monod, A.: Towards a more detailed description of tropospheric aqueous phase organic chemistry: CAPRAM 3.0, Atmospheric Environment, 39(23-24), 4351–4363, doi:10.1016/j.atmosenv.2005.02.016, 2005.

Herzog, M., Weisenstein, D. K. and Penner, J. E.: A dynamic aerosol module for global chemical transport models: Model description, J. Geophys. Res., 109(D18), doi:10.1029/2003jd004405, 2004.

Ito, A., Sillman, S. and Penner, J. E.: Effects of additional nonmethane volatile organic compounds, organic nitrates, and direct emissions of oxygenated organic species on global tropospheric chemistry, J. Geophys. Res., 112(D6), doi:10.1029/2005jd006556, 2007.

Ito, A., Xu, L., and Penner, J. E.: Projected response of soluble iron supply to improvement of air quality in the future, Journal of Geophysical Research, submitted, 2013.

Jacob, D. J.: Chemistry of OH in remote clouds and its role in the production of formic acid and peroxymonosulfate, J. Geophys. Res., 1986.

Jimenez, J. L., Canagaratna, M. R., Donahue, N. M., Prevot, A. S. H., Zhang, Q., Kroll, J. H., DeCarlo, P. F., Allan, J. D., Coe, H., Ng, N. L., Aiken, A. C., et al.: Evolution of Organic Aerosols in the Atmosphere, Science, 326(5959), 1525–1529, doi:10.1126/science.1180353, 2009.

Kundu, S., Kawamura, K., Lee, M., Andreae, T. W., Hoffer, A. and Andreae, M. O.: Comparison of Amazonian biomass burning and East Asian marine aerosols : Bulk organics, diacids and related compounds, water-soluble inorganic ions, stable carbon and nitrogen isotope ratios, Low Temperature Science, 68, 89–100, 2010.

Legrand, M., Preunkert, S., Oliveira, T., Pio, C. A., Hammer, S., Gelencsér, A., Kasper-Giebl, A. and Laj, P.: Origin of C 2–C 5dicarboxylic acids in the European atmosphere inferred from year-round aerosol study conducted at a west-east transect, J. Geophys. Res., 112(D23), D23S07, doi:10.1029/2006JD008019, 2007.

Lelieveld, J. and Crutzen, P. J.: The role of clouds in tropospheric photochemistry, J Atmos Chem, 12(3), 229–267, doi:10.1007/BF00048075, 1991.

Liggio, J., Li, S. M. and McLaren, R.: Heterogeneous reactions of glyoxal on particulate matter: Identification of acetals and sulfate esters, Environ. Sci. Technol., 39(6), 1532–1541, 2005.

Lim, H. J., Carlton, A. G. and Turpin, B. J.: Isoprene Forms Secondary Organic Aerosol through Cloud Processing: Model Simulations - Environmental Science & Technology (ACS Publications), Environ. Sci. Technol., 9(12), 4441-4446, 2005.

Lim, Y. B., Tan, Y. and Turpin, B. J.: Chemical insights, explicit chemistry and yields of secondary organic aerosol from methylglyoxal and glyoxal, Atmos. Chem. Phys. Discuss., 13(2), 4687–4725, doi:10.5194/acpd-13-4687-2013, 2013.

Lim, Y. B., Tan, Y., Perri, M. J., Seitzinger, S. P. and Turpin, B. J.: Aqueous chemistry and its role in secondary organic aerosol (SOA) formation, Atmos. Chem. Phys., 10(21), 10521–10539, doi:10.5194/acp-10-10521-2010, 2010.

Lin, G., Penner, J. E., Sillman, S., Taraborrelli, D. and Lelieveld, J.: Global modeling of SOA formation from dicarbonyls, epoxides, organic nitrates and peroxides, Atmos. Chem. Phys., 12(10), 4743–4774, doi:10.5194/acp-12-4743-2012, 2012.

Liu, J., Horowitz, L. W., Fan, S., Carlton, A. G. and Levy, H., II: Global in-cloud production of secondary organic aerosols: Implementation of a detailed chemical mechanism in the GFDL atmospheric model AM3, J. Geophys. Res., 117(D15), D15303, doi:10.1029/2012JD017838, 2012.

Liu, X. H., Penner, J. E. and Herzog, M.: Global modeling of aerosol dynamics: Model description, evaluation, and interactions between sulfate and nonsulfate aerosols, J. Geophys. Res., 110(D18), doi:10.1029/2004jd005674, 2005.

Liu, X., Mauersberger, G. and Möller, D.: The effects of cloud processes on the tropospheric photochemistry: An improvement of the eurad model with a coupled gaseous and aqueous chemical mechanism, Atmospheric Environment, 31(19), 3119–3135, doi:10.1016/S1352-2310(97)00057-5, 1997.

Myriokefalitakis, S. and Tsigaridis, K.: In-cloud oxalate formation in the global troposphere: a 3-D modeling study, Atmos. Chem. Phys, 11(12), 5761-5782, 2011.

Ng, N. L., Canagaratna, M. R., Zhang, Q., Jimenez, J. L., Tian, J., Ulbrich, I. M., Kroll, J. H., Docherty, K. S., Chhabra, P. S., Bahreini, R., Murphy, S. M., et al.: Organic aerosol components observed in Northern Hemispheric datasets from Aerosol Mass

Spectrometry, Atmos. Chem. Phys., 10(10), 4625–4641, doi:10.5194/acp-10-4625-2010, 2010.

Pandis, S. N. and Seinfeld, J. H.: Sensitivity analysis of a chemical mechanism for aqueous-phase atmospheric chemistry, J. Geophys. Res., 94(D1), 1105, doi:10.1029/JD094iD01p01105, 1989.

Paulot, F., Crounse, J. D., Kjaergaard, H. G., Kurten, A., St Clair, J. M., Seinfeld, J. H. and Wennberg, P. O.: Unexpected Epoxide Formation in the Gas-Phase Photooxidation of Isoprene, Science, 325(5941), 730–733, doi:10.1126/science.1172910, 2009.

Peeters, J., Nguyen, T. L. and Vereecken, L.: HOx radical regeneration in the oxidation of isoprene, Physical Chemistry Chemical Physics, 11(28), 5935–5939, doi:10.1039/b908511d, 2009.

Schwartz, S. E.: Mass-transport considerations pertinent to aqueous phase reactions of gases on liquid water clouds, in Chemistry of Multiphase Atmospheric Systems, NATO ASI Ser., edited by: Jaeschke, W., Springer, Berlin, Germany, 1986.

Sillman, S.: A numerical-solution for the equations of tropospheric chemistry based on an analysis of sources and sinks of odd hydrogen, J. Geophys. Res., 96(D11), 20735–20744, 1991.

Sillman, S., Marsik, F. J., Al-Wali, K. I., Keeler, G. J. and Landis, M. S.: Reactive mercury in the troposphere: Model formation and results for Florida, the northeastern United States, and the Atlantic Ocean, J. Geophys. Res., 112(D23), D23305, doi:10.1029/2006JD008227, 2007.

Stavrakou, T., Muller, J. F., De Smedt, I., Van Roozendael, M., Kanakidou, M., Vrekoussis, M., Wittrock, F., Richter, A. and Burrows, J. P.: The continental source of glyoxal estimated by the synergistic use of spaceborne measurements and inverse modelling, Atmos. Chem. Phys., 9(21), 8431–8446, 2009.

Stroud, C. A., Makar, P. A., Moran, M. D. and Gong, W.: Impact of model grid spacing on regional-and urban-scale air quality predictions of organic aerosol, Atmos. Chem. Phys, 11(7), 3107-3118, 2011.

Sundqvist, H., Berge, E. and Kristjánsson, J. E.: Condensation and Cloud Parameterization Studies with a Mesoscale Numerical Weather Prediction Model, Mon. Wea. Rev., 117(8), 1641–1657, 1989.

Talbot, R. W., Andreae, M. O., Andreae, T. W. and Harriss, R. C.: Regional aerosol chemistry of the Amazon Basin during the dry season, J. Geophys. Res., 93(D2), 1499, doi:10.1029/JD093iD02p01499, 1988.

Taylor, S. R. and McLennan S. M.: The Continental Crust: Its Composition and Evolution, 312 pp., Blackwell Sci., Oxford, U.K., 1985.

Tan, Y., Perri, M. J., Seitzinger, S. P. and Turpin, B. J.: Effects of Precursor Concentration and Acidic Sulfate in Aqueous Glyoxal−OH Radical Oxidation and

Implications for Secondary Organic Aerosol, Environ. Sci. Technol., 43(21), 8105–8112, doi:10.1021/es901742f, 2009.

Wang, G., Kawamura, K., Umemoto, N., Xie, M., Hu, S. and Wang, Z.: Water-soluble organic compounds in PM 2.5and size-segregated aerosols over Mount Tai in North China Plain, J. Geophys. Res., 114(D19), D19208, doi:10.1029/2008JD011390, 2009.

Warneck, P.: In-cloud chemistry opens pathway to the formation of oxalic acid in the marine atmosphere, Atmospheric Environment, 37(17), 2423–2427, doi:10.1016/S1352-2310(03)00136-5, 2003.

Waxman, E. M., Dzepina, K., Ervens, B., Lee-Taylor, J., Aumont, B., Jimenez, J. L., Madronich, S. and Volkamer, R.: Secondary organic aerosol formation from semi- and intermediate-volatility organic compounds and glyoxal: Relevance of O/C as a tracer for aqueous multiphase chemistry, Geophys. Res. Lett., VOL. 40, 1–5, doi:10.1002/grl.50203, 2013.

Xu, K.-M. and Krueger, S. K.: Evaluation of Cloudiness Parameterizations Using a Cumulus Ensemble Model, Mon. Wea. Rev., 119(2), 342–367, doi:10.1175/1520-0493, 1991.

Zhang, Q., Jimenez, J. L., Canagaratna, M. R., Allan, J. D., Coe, H., Ulbrich, I., Alfarra, M. R., Takami, A., Middlebrook, A. M., Sun, Y. L., Dzepina, K., et al.: Ubiquity and dominance of oxygenated species in organic aerosols in anthropogenically-influenced Northern Hemisphere midlatitudes, Geophys. Res. Lett., 34(13), L13801, doi:10.1029/2007GL029979, 2007.

CHAPTER 4

Radiative forcing of secondary organic aerosol and present-day radiative forcing of organic aerosol in snow

4.1 Introduction

Organic aerosols make up a large fraction of sub-micron particulate mass in the troposphere [*Jimenez et al.,* 2009]. Even though these aerosols are thought to be formed primarily from biogenic emissions, their formation rates can increase as a result of changes in gas-phase oxidation rates, and, therefore, they can enhance the direct and indirect climate forcing by aerosols. The change in formation rates for the present day (PD) versus pre-industrial (PI) conditions was first highlighted by *Kanakidou et al.* [2000], but the forcing associated with increases in aerosols from biogenic compounds has not yet been included in the IPCC reports [e.g. *Forster et al*., 2007]. Changes in climate can significantly change biogenic emissions, which could also have significant implications for future emissions regulations [*Hoyle et al.* 2011], but these changes are not included here.

In the present study, we employ a 3-D chemistry transport model (CTM) with an explicit chemical formation mechanism to calculate the change in the production and burden of SOA between PD and PI conditions and evaluate its potential influence on radiative forcing. We note that there are still gaps in our understanding of the formation

mechanisms for SOA [*Spracklen et al.*, 2011], however, the current model is able to reproduce observations reasonably well [*Lin et al.*, 2012; Lin, Chapter 3].

SOA particles are important not only for their scattering of visible radiation (which leads to cooling), but also because they may absorb light (Kirschstetter et al., 2004; Chen and Bond, 2010), which leads to warming. Absorption can lead to a net positive forcing if it is stronger than the scattering by the aerosols. Here, we make some simplified assumptions to understand the importance of this absorption on the amount of radiation absorbed within the atmospheric column. Also, absorption can be enhanced when the particles are deposited on land snow and sea ice. This can reduce the albedo of the snow because of its extremely high reflectivity, causing even larger short-wave absorption and warming. Black carbon, for example, is known to be an effective agent to reduce snow albedos, and has been estimated to increase the absorption of short-wave radiation by 0.01 W/m^2 to 0.09 W/m^2 on a global basis [Bond et al., 2013]. However, few studies have been conducted on the role of light-absorbing organic aerosol (OA) (also known as brown carbon) on the reduction of snow albedo. Thus, we also estimate the radiative effect from the organic aerosol in snow using a 3-D model.

4.2 Model description

We used the Integrated Massively Parallel Atmospheric Chemical Transport (IMPACT) model run at a 4° latitude x 5° longitude horizontal resolution with 46 vertical layers. The model includes the microphysics of sulfate aerosol and the interactions between sulfate and non-sulfate aerosols [*Liu et al.,* 2005] and was run using the 1997 meteorological fields from NASA Data Assimilation Office (DAO) GEOS-STRAT model [*Coy and*

Swinbank, 1997]. The same meteorological data was used for both the present day and the pre-industrial simulations.

The SOA module used in IMPACT accounts for the formation of SOA from organic nitrates and peroxides, dicarbonyls, and epoxides [*Lin et al*., 2012]. We employ traditional gas-particle partitioning to treat the formation of SOA from organic nitrates and peroxides which are predicted using an explicit full chemistry scheme that includes

Table 4-1 Global emissions of gases, aerosols and aerosol precursors

Species	PD	PI
SO_2		
Fossil fuel and industry	61.3 Tg S/yr	1.5 Tg S/yr
Volcanoes	4.8 Tg S/yr	4.8 Tg S/yr
DMS	26.1 Tg S/yr	26.1 Tg S/yr
NO		
Fossil Fuel	22.7 Tg N/yr	1.0 Tg N/yr
Biomass burning	9.3 Tg N/yr	4.8 Tg N/yr
Soil	5.5 Tg N/yr	2.9 Tg N/yr
Lighting	3.0 Tg N/yr	3.0 Tg N/yr
Aircraft	0.9 Tg N/yr	0
Ship	0.7 Tg N/yr	0
CO	426.0 Tg C/ yr	0
MEK(>C3 ketones)	5.8 Tg C/yr	0
C_2H_6	9.3 Tg C/yr	0
C_3H_8	7.3 Tg C/yr	0
ALK4(>=C4 alkanes)	15.3 Tg C/yr	0
Acetaldehyde	3.3Tg C/yr	0
CH_2O	2.4Tg C/yr	0
ALK7(C6-C8 alkanes)	11.3Tg C/yr	0
Benzene	3.2 Tg C/yr	0

Toluene	5.8 Tg C/yr	0
Xylene	3.9 Tg C/yr	0
Trans-2-butene	6.6 Tg C/yr	0
HCOOH	2.6 Tg C/yr	0
Acetic acid	12.4 Tg C/yr	0
Phenol	4.3 Tg C/yr	0
Ocean source of POA	34.5 Tg OM/yr	34.5 Tg OM/yr
DMS source of MSA	8.2 Tg/yr	8.2 Tg/yr
Fossil fuel + biofuel POA	15.7 Tg OM/yr	5.1 Tg OM/yr
Fossil fuel + biofuel BC	5.8 Tg BC/yr	0.8 Tg BC/yr
Biomass burning OC	47.4 Tg OM/yr	17.9 Tg OM/yr
Biomass burning BC	4.7 Tg BC/yr	1.8 Tg BC/yr
Isoprene	472.0 Tg C/yr	472.0 Tg C/yr
α-pinene	78.8 Tg C/yr	78.8 Tg/yr
Limonene	38.8 Tg C/yr	38.8 Tg C/yr
PRPE(>=C4 alkenes)	24.2 Tg C/yr	12.9 Tg C/yr
Methanol	42.9 TgC/yr	33.4 TgC/yr
Acetone	44.5 TgC/yr	20.2 TgC/yr
Ethene	28.2 Tg C/yr	10.3 TgC/yr

the HO_x recycling mechanism proposed by *Peeters et al.* [2009] but with a reduced rate for the 1,5-H and 1,6-H shifts in isoprene radicals by a factor of 10 (scheme "C" in *Lin et al.*, 2012). The condensed semi-volatile organic compounds (SVOCs) that form from gas-particle partitioning are assumed to undergo further aerosol-phase reactions to form oligomers with a 1-day e-folding lifetime. We also include SOA formation from the uptake of gas-phase glyoxal and methylglyoxal onto clouds and aqueous sulfate aerosol following the work of *Fu et al.* [2008] as well as a version with full aqueous phase chemistry following *Ervens et al.* [2011] [Case 1 in Lin, Chapter 3]. The formation of

gas-phase epoxides from isoprene oxidation following *Paulot et al.* [2009] is included in both versions together with their aerosol formation on aqueous sulfate aerosol following *Fu et al.* [2008]. A full description and a validation of the original SOA scheme against measurements is given in *Lin et al.* [2012], while *Lin et al*. [in preparation, 2013] compare the SOA formed in the aqueous phase with measurements.

We assume a standard set of emissions that are close to those estimated for the year 2000 for the PD and close to those estimated for 1870 for PI conditions (Table 4-1). The biogenic emissions were held constant but anthropogenic emissions increased with time. Terrestrial isoprene emissions are based on a modified version of the inventory of *Guenther et al.* [1995] by *Wang et al.* [1998] and *Bey et al*. [2001], and have a total source strength of 470.8 Tg C/yr. The total marine isoprene emissions, 0.9 Tg C/yr, are from the estimate by *Gantt et al.* [2009] based on satellite observations. The biogenic terpene source was 117.6 Tg C/yr and is based on the work of *Guenther et al.* [1995] as modified by *Wang et al.* [1998]. The other temperature-dependent BVOC emissions for ethane, propene, acetone, and methanol are distributed according to emissions of isoprene following *Ito et al.* [2007]. Methane mixing ratios for PD and PI conditions were set to 1770 ppb and 800 ppb similar to measurements summarized by *Forster et al.* [2007]. For the PI experiments, all fossil fuel related and industrial emissions of VOCs are set to zero. The primary sea spray organic source was estimated using the correlation between chlorophyll-*a* and the fractional water insoluble organic mass of sea salt, following *O' Dowd et al*. [2008], where the chlorophyll-*a* concentrations were those measured by the MODIS Aqua instrument averaged for the 5-years from 2004 to 2008. Anthropogenic and natural sulfur emissions for PD and PI were the same as those specified in *Wang and*

Penner [2009]. In particular, anthropogenic sulfur emissions were developed based on the emission data of *Smith et al.* [2001]; volcanic SO_2 emissions were from the work of *Andres and Kasgnoc* [1998]; marine DMS fluxes were based on the estimates from *Kettle and Andreae* [2000]. The anthropogenic NO_x emissions from fossil fuel combustion and soil emissions were adopted from *van Aardenne* et al. [2001] for year 1990, while those from biomass burning and lightning were based on the work of Ito et al. [2007] for the year 1990. Fossil fuel and biofuel emissions of organic matter (OM) and BC were those estimated by *Ito and Penner* [2005] but with the fossil fuel emissions adjusted as in *Wang et al.* [2009] to better fit surface observations. Open biomass burning BC and OM emissions were developed using the *Ito and Penner* [2005] emissions for BC as an a priori estimate together with the inverse model approach of *Zhang et al.* [2005].

We use an off-line radiative transfer model to calculate the optical properties of aerosols and their resulting radiative forcing [*Penner et al.* 2011a; *Wang and Penner,* 2009]. We use monthly average aerosol concentrations together with 6-hourly meteorological fields to estimate instantaneously varying aerosol optical depths. Daily averaged aerosol optical depth is calculated using a table lookup that included the Mie scattering refractive index as a function of wavelength and size parameter so that arbitrary internal mixtures and sizes could be included. Five types of aerosol populations (i.e., pure sulfate, fossil fuel OM/BC, biomass burning OM/BC, dust, and sea salt) are assumed to be externally mixed, but each non-sulfate aerosol type can include a sulfate coating. The refractive index for internally mixed aerosols (including mixing with water which is treated using the Köhler equation) is calculated from the volume mixture for each aerosol type. As noted above, the off-line radiative transfer model uses monthly average aerosol

concentrations, but the uptake of water with relative humidity is calculated based on the 6-hourly varying meteorological fields. This method provides a reasonable approximation of the radiative forcing calculated using hourly varying aerosol fields, and thus approximates an on-line calculation [*Penner et al*., 2011b]. Organic aerosols were treated with a "kappa" factor (a hygroscopicity parameter) of 0.14 for all source categories for both water uptake as well as droplet formation. The spectral variation of the refractive index for organic aerosols from biomass burning was that measured by *Kirchstetter et al.* [2004] (1.53–0.03i at 550 nm). The choice of refractive index of fossil fuel/biofuel OM, however, is not straightforward since part of this OM may be polymerized and/or oxidized and have the absorption characteristics of humic-like substances (HULIS) [*Sun et al*., 2007; *Cappa et al*., 2011]. Since the fraction of this material that is absorbing is not known with any precision, we followed *Zhou et al*. [2012] and made the expedient assumption that 50% of fossil fuel/biofuel OM has the refractive index from *Kirchstetter et al.* [2004] with the rest having the same refractive index of ammonium sulfate. Cloud droplet number concentrations were calculated using the cloud droplet activation parameterization of *Abdul-Razzak and Ghan* [2000; 2002]. The size distribution of the nucleated droplet population accounts for the effects of droplet dispersion [*Rotstayn and Liu,* 2003]. Then the cloud droplet effective radius was used to calculate the cloud optical depth and the first aerosol indirect forcing using an offline radiative transfer model taken from the NCAR CAM3 model [*Collins et al.,* 2006].

To compute the radiative forcing from organic aerosol deposited in snow and sea ice, we imported the organic aerosol dry and wet deposition field calculated in the IMPACT PD run into two offline models: the NCAR Community Land Model 4 (CLM4) [*Oleson et*

al., 2010; *Lawrence et al.,* 2011] for the land snow simulation and the Community Ice CodE 4 (CICE) [*Hunke and Lipscomb,* 2008; *Holland et al., 2012*] for the sea-ice simulation. Both simulations were run with prescribed meteorology data for the years 1994 to 2003. The treatments of size distributions and optical properties for OA in snow and sea ice were consistent with those specified for OA in the atmosphere. For the detailed descriptions for snow and sea ice treatments of aerosol processes and radiative transfer, readers are referred to *Flanner et al*. [2007], *Oleson et al*, 2010, *Lawrence et al*. [2011] and *Holland et al*. [2012].

Table 4-2 Burden in the boundary layer (below 900 hPa approximately in the model), in the troposphere (below 200 hPa approximately in the model), or in the whole atmosphere for PD and PI conditions and their relative difference.

Species	PD (Tg)	PI (Tg)	(PD-PI)/PI	Other work	
				PD (Tg)	(PD-PI)/PI
OH in boundary layer	1.78E-5	2.08E-5	-14.7%		
OH in troposphere	14.2 x 10^5 (molec cm^{-3})	17.9 x 10^5 (molec cm^{-3})	-21.1%	11.1 ±1.6 x 10^5 (molec cm^{-3}) [a]	-0.6 ±8.8%[a]
NO_x in boundary layer	1.04E-1	4.17E-2	150%		over 300%[b]
NO_x in troposphere	3.07E-1	1.91E-1	60.7%		108.0 ±75.4%[a]
CO in troposphere	288.3	110.6	160.8%		89.1 ±18.6%[a]
CH_4 (global)	4806	2262	112.4%	4813 ±81[a]	120.9%[a]
O_3 in boundary layer	25.3	16.6	52.6%		74%[b]
O_3 in troposphere	339	243	39.5%	337±23[c]	29% ± 17%[c]
Isoprene in boundary layer	1.10E-1	1.27E-1	-12.9%		-42%[b]
NO_3 in boundary layer	8.06E-4	2.12E-4	280%		
HO_2 in boundary layer	3.88E-3	3.40E-3	14.3%		
Sulfate in boundary layer	2.76E-1	8.70E-2	217%		
Sulfate (global)	2.70	1.11	141%	1.4[d]	338% [d]

				1.05[b]	160% [b]
				1.8[e]	114% [e]
POA in boundary layer	2.13E-1	7.52E-2	183%		
POA (global)	1.02	0.49	108%	1.27[d]	1220%[d]
				0.6[b]	120%[b]
				1.41[e]	178%[e]
				1.2[f]	991%[f]
PRN2 in boundary layer	7.12E-2	4.48E-2	58.9%		
Glyoxal in boundary layer	9.90E-3	1.08E-2	-8.69%		
Methylglyoxal in boundary layer	1.65E-2	1.65E-2	0		
Epoxide in boundary layer	6.34E-2	8.15E-2	-22.1%		
NMHCs in boundary layer	1.92E1	1.72E1	11.2%		
SOA (global)	1.54	1.00	54%	0.33[d]	43%[d]
				0.8[b]	25%[b]
				0.5-0.7[e]	56-59%[e]
				0.19[f]	217%[f]

[a] ACCMIP models (*Naik et al*. [2012])

[b] *Tsigaridis et al*. [2006]

[c] ACCMIP models (*Young et al*. [2013])

[d] *Liao and Seinfeld* [2005]

[e] *Hoyle et al*. [2009]

[f] *Chung and Seinfeld* [2002]

4.3 Changes in SOA production and burden between PD and PI simulations

The change in emissions from PI to PD leads to changes in the levels of oxidants (e.g., OH and O_3) which are important for the oxidation of VOC and therefore for the formation of SOA. As a result of the increase in emissions, there is an increase of a factor of 2.5 in the level of boundary layer NO_x, while NMHC concentrations increase by 11%

(Table 4-2). These changes result in an increase of boundary layer ozone of 53%, while there is a decrease in global average boundary layer OH of 15%, driven mainly by the changes in CO (increase of a factor of 2.8) and CH_4 (increase of a factor of 2.1). Over source regions, however, there is an increase in OH that is associated with the increase in NO_x, which is largest in the mid-latitude northern hemisphere (Figure 4-1). There is also a decrease in the global average boundary layer isoprene between PD and PI of 13% caused by the increases in OH over the continents, the increase in O_3, (see also *Tsigaridis et al.* [2006]), and an increase in NO_3 between PD and PI simulations of 280%.

The change in isoprene and oxidants alone, however, cannot fully explain the change in SOA. The boundary layer concentrations of SOA formed from glyoxal and methylglyoxal increase by 19.3% and 29.1%, respectively, since pre-industrial times, primarily as a result of the increased sulfate aerosol and its surface area, while the concentrations of gas phase glyoxal and methylglyoxal, most of which are formed from the OH-initiated oxidation of isoprene [*Fu et al.,* 2008], change very little in the boundary layer. The SOA formed from epoxide also increases as a result of the increased surface area of sulfate, by a factor of 1.2 in the boundary layer, even though the gas phase epoxide concentration decreases by 22.1% as a result of the significant increase of NO. The increase of NO causes more RIO2 (organic peroxy radicals from isoprene) to react with NO and therefore less RIO2 to react with HO_2 to form the epoxide [*Lin et al.,* 2012]. On the other hand, the concentration of PRN2 (isoprene-hydroxy-nitrate, the greatest contributor to the SOA formed from organic nitrates and peroxides), which mainly comes from the reaction of RIO2 with NO [*Lin et al.,* 2012], is enhanced by 58.9% in the boundary layer. This increase, together with the increase in the abundance of POA, upon

which the SOA can partition, causes the concentration of SOA from organic nitrates and peroxides to double in the boundary layer.

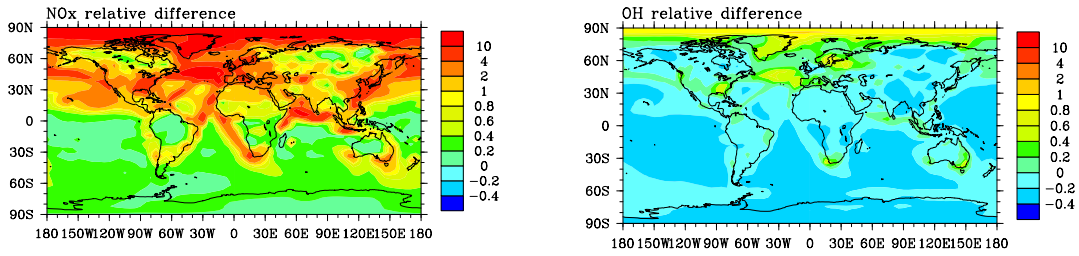

Figure 4-1 The relative difference (i.e., (PD-PI)/PI) between PD and PI conditions for NO_x (left panel) and OH (right panel) in the boundary layer.

Table 4-3 Summary of total burden and source of SOA for present day and pre-industrial conditions

	PD	PI
Burden (Tg)	1.54	1.00
Total source (Tg/yr)	119.3	84.3
Total biogenic source (Tg/yr)	105.6	84.3
Total anthropogenic source (Tg/yr)	13.7	0.0

Table 4-3 shows the global production rate and burden of SOA for PD and PI conditions. The global average formation of SOA is dominated by biogenic VOCs even for PD conditions. The SOA formed from anthropogenic VOCs (mainly aromatics) only accounts for 11.3% of the total SOA production. Although the biogenic VOC emissions do not change, the biogenic SOA production rate increases by 18.6 Tg/yr (23.3%) as a result of the anthropogenic emissions and reactions discussed here. The distribution of the changes in total SOA at the surface and for the total column are shown in Figure 4-2. The largest increase in SOA occurs over industrialized areas, such as South East Asia,

Europe and the eastern US, where the increases of NO_x, sulfate and OH account for most of the increase in SOA. Large increases in SOA are also evident in South America and West Africa, where the increase in biomass burning POA and sulfate are the major source of the SOA increase. Increases in SOA over the ocean, in the outflow of East Asia, Africa and South America, can also be seen in the column burden (Figure 4-2B).

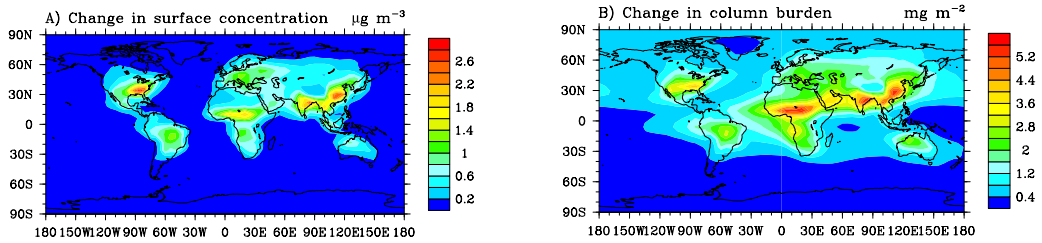

Figure 4-2 The change in annual mean SOA concentration between PD and PI conditions. Panel A shows changes at the surface and panel B shows changes for the total column integrated mass per square meter.

Table 4-4 Summary of estimated forcing (Wm^{-2}) in different simulations due to the change of SOA.

	Direct forcing				Indirect forcing	Other work	
	TOA clear-sky	TOA all-sky	Surface clear-sky	Surface all-sky		TOA all-sky	Indirect forcing
Case 1*	-0.36	-0.06	-0.69	-0.42	-0.32	-0.01 ~ -0.04 from other models in AEROCOM (*Myhre et al.* [2013]); -0.06 ~ -0.09 (*Hoyle et al.* [2009)]; -0.41 ~ -0.11 (*Spracklen et al.* [2012])	-0.36 ~ -0.74 (*Spracklen et al.* [2012])
Case 2*	-0.55	-0.21	-0.77	-0.46	-0.24		
Case 3	-0.41	-0.14	-0.59	-0.35	-0.32		
Case 4*	-0.48	-0.11	-0.88	-0.55	-0.24		
Case 5*	-0.54	-0.21	-0.75	-0.45	-0.23		

* Case 1: Median radius, r_g=0.08 mm and geometric standard deviation, s_g = 1.4. 100% of SOA is assumed to be light absorbing; Case 2: SOA median radius and standard deviation split into a nucleation mode and accumulation mode: (43% have r_g=0.005 mm, s_g = 1.5 and 50% have r_g=0.08 mm, s_g = 1.7). 50% of the SOA mass is light absorbing. Case 3: The same size SOA size distribution as Case 1, but 50% of SOA is assumed to be light absorbing; Case 4: The same SOA size distribution as Case 2, but 100% of the SOA mass is light absorbing; Case 5: using the SOA field output from the simulation with updated SOA formation in aqueous phase scheme, assuming the same size distribution and the same refractive index as Case 2.

4.4 Direct and indirect forcing due to the change in SOA

The forcing associated with SOA was calculated from the difference in the TOA radiation with all PD concentrations and that calculated assuming that all aerosols had their PD concentrations except those for SOA, which were specified at their PI concentrations. We set up five cases (Table 4-4) to investigate the radiative forcing due to SOA. For Case 1, we assume a log-normal size distribution for SOA which is similar to that of biomass burning aerosols with the majority of the number distribution having a median radius, r_g, near 0.08 mm and a geometric standard deviation, s_g, of 1.4 (Table 1 in *Wang and Penner,* 2009). However, if organics mainly condense on smaller aerosols, i.e., on freshly nucleated sulfate aerosols [*Metzger et al.,* 2010], their size might be considerably smaller. Thus, we also examine a second case where SOA is the sum of two log-normal size distributions where 43% of the number concentration has r_g=0.005 mm and s_g=1.5 and 57% has r_g=0.08 mm and s_g=1.7. We also varied the treatment of the refractive index for SOA in these two cases with one sensitivity case which assumed 100% of the SOA followed the spectral variation of the refractive index measured by *Kirchstetter et al.* [2004], while the 2nd sensitivity case assumed that 50% of SOA followed this same refractive index and the remainder had the refractive index of ammonium sulfate. The footnotes in Table 4-4 outlines the 4 cases treated using different size distributions and refractive indices. Finally, we note that *Lin et al*. [2012] were able to reproduce most measured concentrations of organic aerosols and SOA except for in the tropics, where their predicted concentrations were a factor of 3 – 4 too high. We have updated our SOA production mechanism to replace the production of SOA from glyoxal and methylglyoxal based on *Fu et al*. (2008) with that published by *Ervens et al*. (2011)

and *Waxman et al*. [2013]. When we do so, we obtain much better agreement with tropical observations. Thus Case 5 uses the SOA field with the updated SOA formation in the aqueous phase and with the same size distribution and the same treatment of refractive index of SOA as Case 2.

The difference in SOA between PD and PI conditions causes a global annual average direct radiative forcing of -0.36 W m^{-2} for clear sky and -0.06 W m^{-2} for all-sky conditions for Case 1 (Table 4-4). For Case 2, the direct forcing is -0.55 W m^{-2} for clear sky and -0.21 W m^{-2} for all-sky conditions. The direct forcing in Cases 3 and 4 lies between those in Cases 2 and 1 (Table 4-4). *Hoyle et al.* [2009] estimated the direct radiative forcing of anthropogenic SOA to be -0.06-0.09 Wm^{-2} which corresponded to an increase in the SOA production rate of 18-26 Tg/yr; *Spracklen et al.* [2011] reported a direct forcing of -0.26±0.15 Wm^{-2} resulting from a global anthropogenic SOA production rate that ranged from 40 Tg/yr to 160 Tg/yr. SOA were considered to be pure scattering aerosols in these two studies, but here we account for its absorbing properties [*Sun et al.*, 2007]. This absorption decreases the short wave radiative flux reaching the surface, leading to a stronger negative surface radiative forcing compared to that at the top of atmosphere (TOA) (shown below) for both clear sky and all-sky conditions. In addition, this absorption results in a weaker negative forcing at the TOA. For example, the TOA forcing in Case 4 is only half that in Case 2 (where only half of SOA is assumed to be light-absorbing). For the same reason, the direct radiative forcing at the TOA in Case 1 is larger than that in Case 3. Comparing Case 1 and Case 4, both of which use the same treatment of SOA refractive index but different SOA size distributions, shows that the

SOA that has a size distribution that is the sum of a nucleation mode and an accumulation mode scatters more short-wave radiation back to space than the SOA with a size distribution that is only in the accumulation mode. This stronger cooling shown in Case 4 than that in Case 1 indicates that the size of a particle is an important factor determining its mass extinction efficiency. For Case 5, the all-sky direct forcing is -0.21 Wm^{-2} and the indirect forcing is -0.23 Wm^{-2}, both of which are almost the same as those in Case 2.

The distribution of the direct radiative forcing at the TOA for all-sky and clear sky conditions and the all-sky radiative forcing at the surface associated with these changes in SOA is shown in Figure 4-3. The direct forcing at the TOA is dominated by changes of aerosols in the Northern Hemisphere with peaks over the source areas: southeast Asia, eastern US and Europe. The absorption by SOA within the atmospheric column is given by the difference between the forcing at the TOA and the surface (Figure 4-4). Assuming that all of the SOA are slightly absorbing, as in Case 1, leads to a positive direct forcing at the TOA for all-sky conditions the off west coast of Africa and South America (Figure 4-3A).

Figure 4-5 shows the first indirect effect at TOA due to the increased SOA since pre-industrial times. The spatial distribution of the forcing is determined by the change in the cloud drop number concentrations (CDNC). Case 1 shows a stronger indirect forcing than that for Case 2. The main cause of this difference is that more SOA is activated to cloud droplets in Case 1 since this case has more large SOA particles (that can therefore activate more easily) than does Case 2. The global mean indirect forcing is -0.32 Wm^{-2} for Case 1 and -0.24 Wm^{-2} for Case 2. Both of our estimates are smaller than the values reported by *Spracklen et al.* [2011] for the indirect forcing by so called

"anthropogenically controlled SOA" that was assumed to be spatially similar to anthropogenic CO emissions (i.e. -0.36 to -0.74 Wm^{-2}), based on fitting the results of a global chemical transport model to aerosol mass spectrometer (AMS) observations.

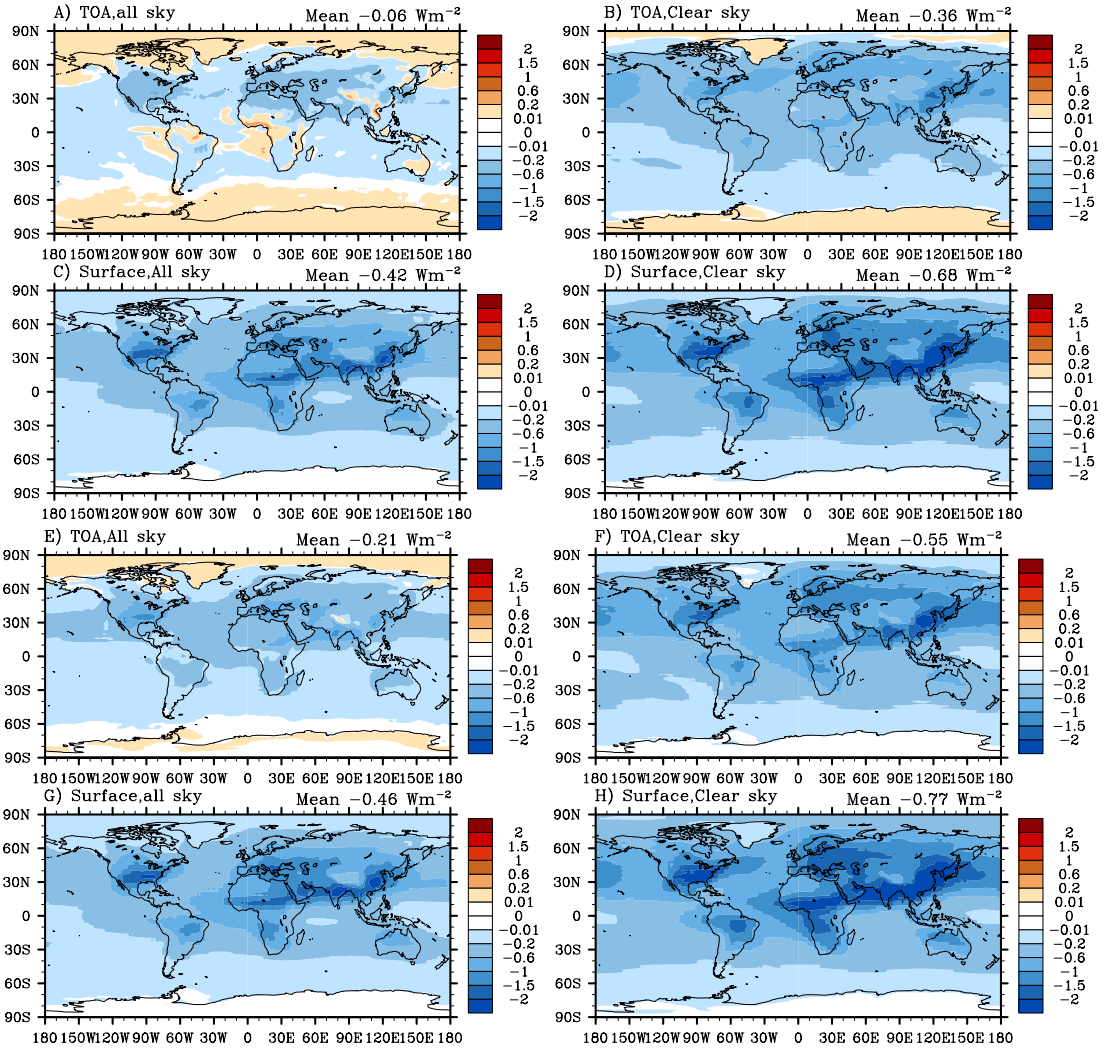

Figure 4-3 The direct forcing due to the change of SOA between PD and PI conditions at the TOA for all sky (panel A and E), and clear sky (panel B and F) conditions, and at the surface in all sky (panel C and G) and clear sky (panel D and H) conditions. We consider two cases here. Case 1 (Panels A-D): SOA median radius=0.08 mm with 100% of SOA assumed to be light absorbing; Case 2 (Panels E-H): SOA is the sum of two log-normal distributions (43% with r_g=0.005 mm and 50% with r_g=0.08 mm) with 50% of the mass assumed to be light absorbing.

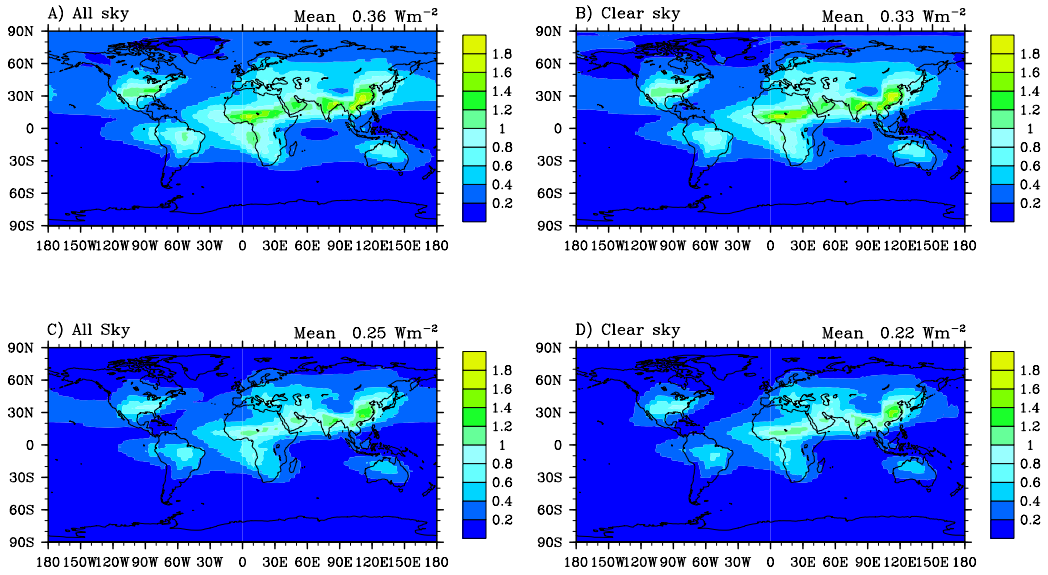

Figure 4-4 Atmospheric absorption due to the change in SOA for all-sky conditions in Case 1 (A), for clear-sky conditions in Case 1 (B), for all-sky conditions in Case 2 (C) and for clear-sky conditions in Case 2 (D).

4.5 Uncertainties of the radiative forcing

There are still substantial uncertainties associated with the radiative forcing of SOA, mainly resulting from the uncertainty in the mass budget and optical properties of SOA and their ability to act as cloud condensation nuclei (CCN). The sources, sinks and chemistry of SOA are uncertain [*Spracklen et al.,* 2011; *Lin et al*., 2012] due to the huge number of different atmospheric organic molecules and the complex physical and chemical processes controlling the conversion of gas phase organics to aerosol [*Hallquist et al*., 2009]. Our PD global SOA source is larger than that in other models, but consistent with the range estimated using top-down methods [*Lin et al.,* 2012]. In our model, the refractive index and the hygroscopicity are assumed to be constant for all SOA. Measurements, however, show that the refractive index of SOA depends on its source

and chemical age in the atmosphere and that its hygroscopicity is related to the particle O:C ratio or oxidation stage [*Cappa et al.,* 2011]. Thus, a more robust and sophisticated treatment for the optical properties and the hygroscopicity of SOA is needed in the future. In addition, recent laboratory studies and field measurements have shown the importance of organics in the nucleation of new particles [*Metzger et al.,* 2010]. *Metzger et al.* [2010] showed that the rate of nucleation of new particles is proportional to the product of sulfuric acid and organic concentration. The lack of the organics in the nucleation mechanism in this study, therefore, may not capture the real aerosol size distribution, which affects both the direct and indirect effects, and the aerosol number which affects the number of particles that can serve as CCN.

4.6 Radiative effect of OA in land snow and sea-ice

For Case 2 the calculated global mean radiative effect casued by OA in land snow is 0.026 Wm^{-2} averaged from year 1997 to year 2004, with a range from 0.024 to 0.028 Wm^{-2} due to the inter-annual variability of snow cover; The global mean radiative forcing by OA in sea ice is 0.0042 W m^{-2} with a range from 0.0037 to 0.0048 Wm^{-2}. Bond et al. (2013) gave a best estimate of 0.04 Wm^{-2} for all-source forcing by BC in snow and a best estimate of 0.012 Wm^{-2} for all-source forcing by BC in sea-ice based on the analysis of a suit of model studies. Therefore the role of OA in reducing snow and sea-ice albedo may be as important as that of BC. Although OA shows much weaker light-absorbing ability (smaller imaginary part of refractive index) than does BC, its global source is much larger than the source of BC (225 Tg/yr OA in this paper vs. 7.5 Tg/yr BC from the mean bottom-up estimates (Bond et al. 2013)). Using measurements of hundreds of snow

samples, *Doherty et al.* (2010) concluded that about 40% of the light absorption from impurities in Arctic snow and sea-ice is due to non-BC constituents.

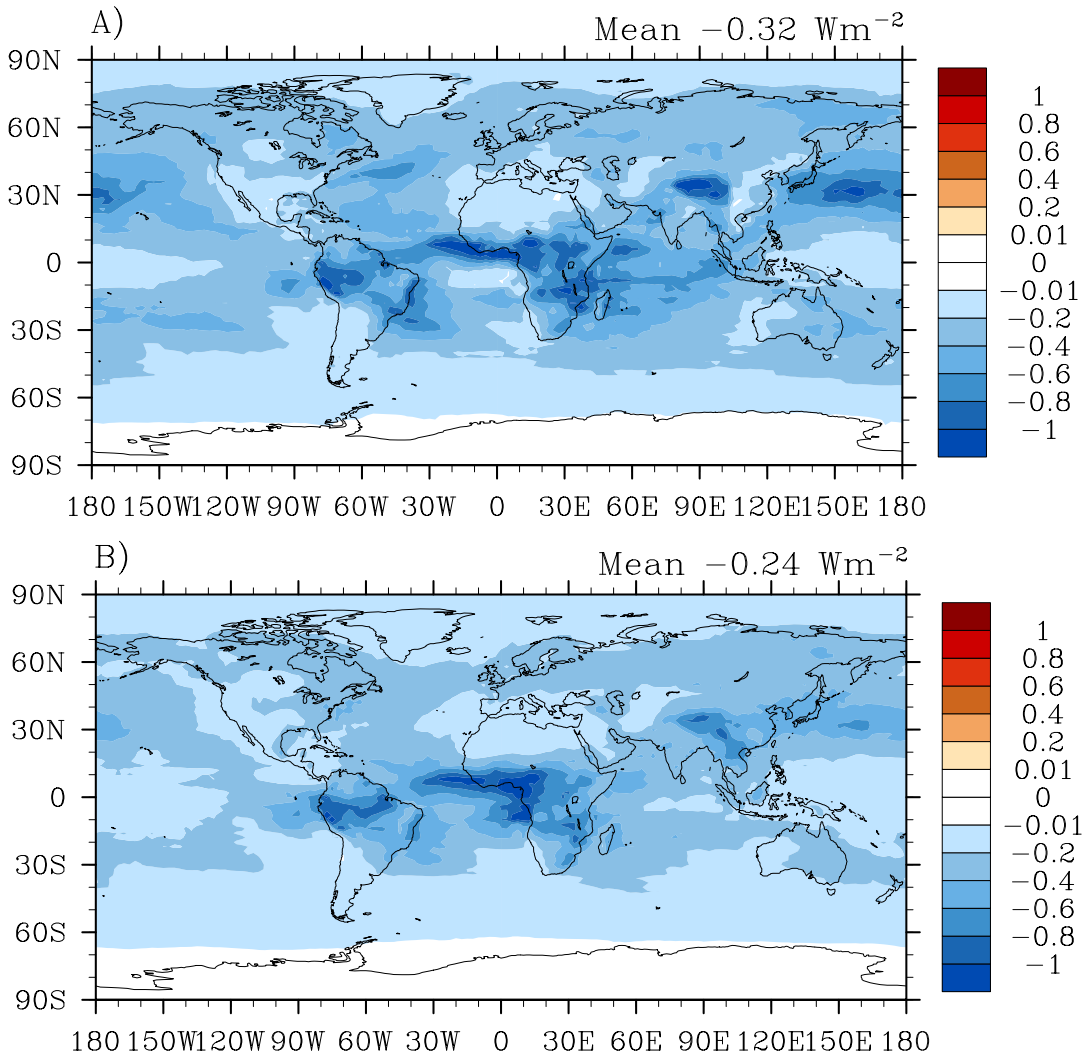

Figure 4-5 The first indirect forcing due to the PD-PI difference in SOA. (A): SOA is assumed to have the majority of particles with a median radius, r_g, equal to 0.08 μm; (B): SOA is assumed to have 43% with r_g=0.005 μm and 57% have r_g=0.08 μm.

Figure 4-6 depicts the global distribution of 10-year-mean radiative forcing by OA in land snow and sea-ice. The distribution reflects the combination of OA concentration in snow, snow cover and surface-incident solar flux. The forcing is distributed over high-latitude areas (40° N to 90° N and 60° S to 90° S). While the POA from ocean sources contributes most of the forcing in the Southern Hemisphere, fossil fuel, biofuel, and biomass burning POA and SOA play an important role in the Northern Hemisphere. There is a large forcing over Greenland primarily because of the all-year-long snow cover. There is a strip of large forcing over the Tibetan Plateau due to the strong surface-incident solar flux, the area of which is less than that shown by *Flanner et al*. (2007) for BC/snow forcing. The difference is mostly caused by the smaller amount of snow cover in the Tibetan Plateau (and also northern Asia) in this offline CLM simulation than that produced in the coupled land-atmosphere simulations applied by *Flanner et al.* (2007).

4.7 Summary

We used a global CTM (IMPACT), and calculated the change in SOA between present day and pre-industrial conditions. We show that the increase in anthropogenic emissions increases the biogenic SOA formation rate by 21.3 Tg/yr (25.3%), mostly as a result of increases in the emissions of NO_x and CO, anthropogenic NMHCs, and CH_4 which affect the formation of SOA precursors, through increasing POA on which SVOCs can condense, and through increases in sulfate aerosol where SOA-forming heterogenous reactions take place. The PD-PI change in SOA causes a direct radiative forcing of -0.21 Wm^{-2} if 50% of the SOA is light-absorbing and the size distribution includes a nucleation mode. Keeping the same size distribution but increasing the absorption fraction to 100% decreases the cooling to -0.14 Wm^{-2}. On the other hand, if the size of the SOA is assumed

to only include the accumulation mode, the direct forcing decreases to -0.11 Wm^{-2}. Combining these two changes together (i.e., increasing the absorption fraction to 100% and changing the size to only include the accumulation mode) decreases the cooling to -0.06 Wm^{-2}. The first aerosol indirect forcing of SOA can be as strong as -0.32 Wm^{-2} if most SOA particles are in the accumulation mode (r_g near 0.08 mm). If around half of SOA particles are assumed to have a peak in the nucleation mode, the first indirect forcing is -0.24 Wm^{-2}. Updating the SOA field with the new scheme for SOA formation in aqueous phase makes little difference to both the direct forcing and the first indirect forcing. The deposition of present-day SOA as well as POA onto the land snow and sea ice is shown, for the first time, to cause a warming of 0.03 Wm^{-2} at the TOA respectively, the magnitude of which is comparable to the warming caused by the BC in snow and ice.

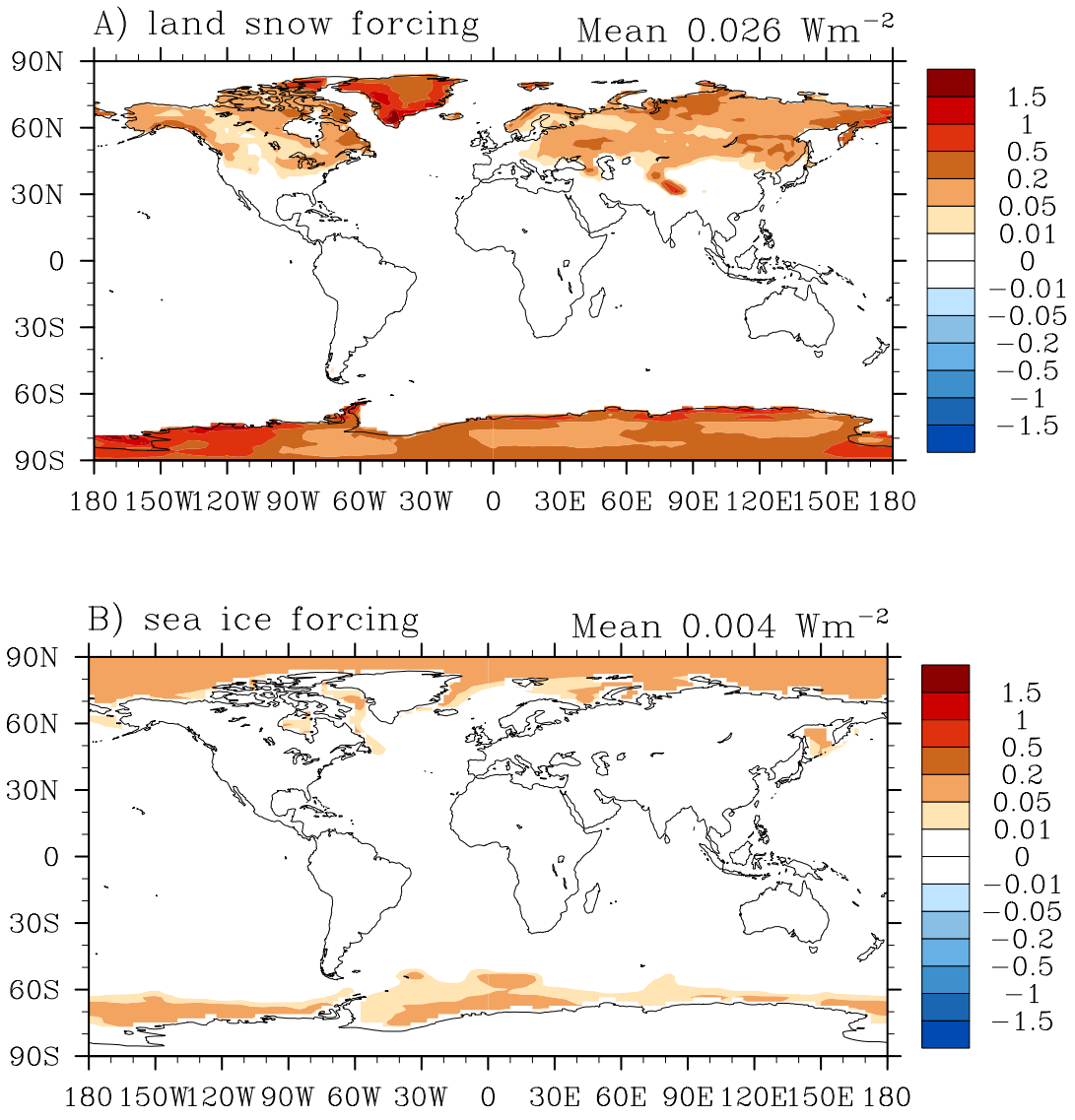

Figure 4-6 10-year-averaged grid-cell OA/snow forcing (A) and OA/sea-ice forcing (B).

4.8 References

Abdul-Razzak, H., and S. J. Ghan (2000), A parameterization of aerosol activation 2. Multiple aerosol types, *J. Geophys. Res.*, 105(D5), 6837-6844.

Abdul-Razzak, H., and S. J. Ghan (2002), A parameterization of aerosol activation - 3. Sectional representation, *J. Geophys. Res.*, 107(D3), 4026, doi:10.1029/2001JD000483.

Andres, R. J., and A. D. Kasgnoc (1998), A time-averaged inventory of subaerial volcanic sulfur emissions, *J. Geophys. Res.,* 103(D19), 25251–25,261, doi:10.1029/98JD02091.

Bey, I., D. J. Jacob, R. M. Yantosca, J. A. Logan, B. D. Field, A. M. Fiore, Q. B. Li, H. G. Y. Liu, L. J. Mickley, and M. G. Schultz (2001), Global modeling of tropospheric chemistry with assimilated meteorology: Model description and evaluation, *J. Geophys. Res.*, 106(D19), 23073-23095.

Bond T. C., et al. (2013), Bounding the role of black carbon in the climate system: A scientific assessment, *J. Geophys. Res*., doi:10.1002/jgrd.50171, in press.

Cappa, C. D., D. L. Che, S. H. Kessler, J. H. Kroll, and K. R. Wilson (2011), Variations in organic aerosol optical and hygroscopic properties upon heterogeneous OH oxidation, *J. Geophys. Res.,* 116, D15204, doi: 10.1029/2011JD015918.

Chung, S. H., and J. H. Seinfeld (2002), Global distribution and climate forcing of carbonaceous aerosols, *J. Geophys. Res.-Atmos.*, *107*(D19), doi:10.1029/2001jd001397.

Collins, W. D., P. J. Rasch, B. A. Boville, J. J. Hack, J. R. McCaa, D. L. Williamson, B. P. Briegleb, C. M. Bitz, S. J. Lin, and M. H. Zhang (2006), The formulation and atmospheric simulation of the Community Atmosphere Model version 3 (CAM3), *J. Clim.*, 19(11), 2144-2161.

Coy, L., and R. Swinbank (1997), Characteristics of stratospheric winds and temperatures produced by data assimilation, *J. Geophys. Res*., 102(D22), 25763-25781.

Doherty, S. J., Warren, S. G., Grenfell, T. C., Clarke, A. D., & Brandt, R. E. (2010). Light-absorbing impurities in Arctic snow. *Atmos. Chem. Phys*, *10*(23), 11647-11680.

Ervens, B., B. J. Turpin, and R. J. Weber (2011): Secondary organic aerosol formation in cloud droplets and aqueous particles (aqSOA): a review of laboratory, field and model studies, *Atmos. Chem. Phys.*, 11, 11069-11102, doi:10.5194/acp-11-11069-2011.

Flanner, M. G., C. S. Zender, J. T. Randerson, and P. J. Rasch (2007), Present-day climate forcing and response from black carbon in snow, *J. Geophys. Res.*, *112* (D11), 202, doi: 10.1029/2006JD008003.

Forster, P., et al. (2007), Changes in Atmospheric Constituents and in Radiative Forcing. In: Climate Change 2007: The Physical Science Basis. Contribution of Working Group I to the Fourth Assessment Report of the Intergovernmental Panel on Climate Change [Solomon, S., D. Qin, M. Manning, Z. Chen, M. Marquis, K.B. Averyt, M. Tignor and H. L. Miller (eds)]. Cambridge University Press, Cambridge, United Kingdom and New York, NY, USA.

Fu, T. M., D. J. Jacob, F. Wittrock, J. P. Burrows, M. Vrekoussis, and D. K. Henze (2008), Global budgets of atmospheric glyoxal and methylglyoxal, and implications for formation of secondary organic aerosols, *J. Geophys. Res.,* 113(D15), D15303, doi:10.1029/2007JD009505.

Gantt, B., N. Meskhidze, and D. Kamykowski (2009), A new physically-based quantification of marine isoprene and primary organic aerosol emissions, *Atmos. Chem. Phys.*, 9(14), 4915-4927.

Guenther, A., et al. (1995), A global-model of natural volatile organic-compound emissions, *J. Geophys. Res.,* 100(D5), 8873-8892.

Hallquist, M., et al. (2009), The formation, properties and impact of secondary organic aerosol: current and emerging issues, *Atmos. Chem. Phys.,* 9(14), 5155-5236.

Holland, M., D. A. Bailey, B. P. Briegleb, B. Light, and E. Hunke (2012), Improved sea ice shortwave radiation physics in CCSM4: The impact of melt ponds and aerosols on Arctic sea ice, *J. Clim.,* 25, 1413–1430, doi:10.1175/JCLI-D-11-00078.1.

Hoyle, C. R., et al. (2011), A review of the anthropogenic influence on biogenic secondary organic aerosol, *Atmos. Chem. Phys.*, 11(1), 321-343.

Hoyle, C. R., G. Myhre, T. K. Berntsen, and I. S. A. Isaksen (2009), Anthropogenic influence on SOA and the resulting radiative forcing, *Atmos. Chem. Phys.*, 9(8), 2715-2728.

Ito, A. and J. E. Penner (2005), Historical emissions of carbonaceous aerosols from biomass and fossil fuel burning for the period 1870–2000, *Global Biogeochem. Cy.*, 19, GB2028, doi:10.1029/2004GB002374.

Ito, A., S. Sillman, and J. E. Penner (2007), Effects of additional nonmethane volatile organic compounds, organic nitrates, and direct emissions of oxygenated organic species on global tropospheric chemistry, *J. Geophys. Res.,* 112(D6), D06309, doi:10.1029/2005JD006556.

Jimenez, J. L., et al. (2009), Evolution of Organic Aerosols in the Atmosphere, *Science*, 326(5959), 1525-1529.

Kanakidou, M., K. Tsigaridis, F. J. Dentener, and P. J. Crutzen (2000), Human-activity-enhanced formation of organic aerosols by biogenic hydrocarbon oxidation, *J. Geophys. Res*., 105(D7), 9243-9254.

Kirchstetter, T. W., T. Novakov, and P. V. Hobbs (2004), Evidence that the spectral dependence of light absorption by aerosols is affected by organic carbon, *J. Geophys. Res*., 109(D21).

Kettle, A. J., and M. O. Andreae (2000), Flux of dimethylsulfide from the oceans: A comparison of updated data seas and flux models, *J. Geophys. Res*., 105(D22), 26,793–26,808, doi:10.1029/2000JD900252.

Lawrence, D., et al. (2011), Parameterization improvements and functional and structural advances in version 4 of the Community Land Model, *J. Adv. Model. Earth Syst.,* 3, M03001, doi:10.1029/2011MS000045.

Liao, H., and J. H. Seinfeld (2005), Global impacts of gas-phase chemistry-aerosol interactions on direct radiative forcing by anthropogenic aerosols and ozone - *Journal of Geophysical Research: Atmospheres (1984–2012)*, *110*(D18).

Lin, G., J. E. Penner, S. Sillman, D. Taraborrelli, and J. Lelieveld (2012), Global modeling of SOA formation from dicarbonyls, epoxides, organic nitrates and peroxides, *Atmos. Chem. Phys.*, 12(10), 4743-4774.

Liu, X. H., J. E. Penner, and M. Herzog (2005), Global modeling of aerosol dynamics: Model description, evaluation, and interactions between sulfate and nonsulfate aerosols, *J. Geophys. Res.,* 110(D18), D18206, doi:10.1029/2004JD005674.

Metzger, A., et al. (2010), Evidence for the role of organics in aerosol particle formation under atmospheric conditions, *P. Natl. Acad. Sci. USA*, 107(15), 6646-6651.

Myhre, G. et al. (2013), Radiative forcing of the direct aerosol effect from AeroCom Phase II simulations, *Atmos. Chem. Phys.*, *13*(4), 1853–1877, doi:10.5194/acp-13-1853-2013.

Naik, V. et al. (2012), Preindustrial to present day changes in tropospheric hydroxyl radical and methane lifetime from the Atmospheric Chemistry and Climate Model Intercomparison Project (ACCMIP), *Atmos. Chem. Phys. Discuss.*, *12*(11), 30755–30804, doi:10.5194/acpd-12-30755-2012.

O'Dowd, C. D., et al. (2008), A combined organic inorganic sea-spray source function, *Geophys. Res. Let.*, 35, L01801, doi:10.1029/2007GL030331.

Paulot, F., J. D. Crounse, H. G. Kjaergaard, A. Kurten, J. M. St Clair, J. H. Seinfeld, and P. O. Wennberg (2009), Unexpected Epoxide Formation in the Gas-Phase Photooxidation of Isoprene, *Science*, 325(5941), 730-733.

Peeters, J., T. L. Nguyen, and L. Vereecken (2009), HOx radical regeneration in the oxidation of isoprene, *Phys. Chem. Chem. Phys*., 11(28), 5935-5939.

Penner, J. E, L. Xu, and M. Wang (2011a), Satellite methods underestimate indirect climate forcing by aerosols, *Proc. Natl. Acad. Sci. USA*, 108:13404–13408.

Penner, J.E., C. Zhou, L. Xu, M. Wang (2011b), Reply to Quaas et al.: Can satellites be used to estimate indirect climate forcing by aerosols?, Proc. Nat. Acad. Sci., Proc., www.pnas.org/cgi/doi/10.1073/pnas.1116135108.

Rotstayn, L. D., and Y. G. Liu (2003), Sensitivity of the first indirect aerosol effect to an increase of cloud droplet spectral dispersion with droplet number concentration, *J. Clim*., 16(21), 3476-3481.

Smith, S. J., H. Pitcher, and T. M. L. Wigley (2001), Global and regional anthropogenic sulfur dioxide emissions, *Global Planet. Change*, 29(1 – 2), 99 – 119, doi:10.1016/S0921-8181(00)00057-6.

Spracklen, D. V., et al. (2011), Aerosol mass spectrometer constraint on the global secondary organic aerosol budget, *Atmos. Chem. Phys*., 11(23), 12109-12136.

Sun, H., L. Biedermann, and T. C. Bond (2007), Color of brown carbon: A model for ultraviolet and visible light absorption by organic carbon aerosol, *Geophys. Res. Lett.,* 34, L17813, doi:10.1029/2007GL029797.

Tsigaridis, K., M. Krol, F. J. Dentener, Y. Balkanski, J. Lathiere, S. Metzger, D. A. Hauglustaine, and M. Kanakidou (2006), Change in global aerosol composition since preindustrial times, *Atmos. Chem. Phys*., 6, 5143-5162.

van Aardenne, J. A., F. J. Dentener, J.G. J. Olivier, C. G. M. Klein Gold- ewijk, and J. Lelieveld, (2001), A 1 × 1 degree resolution dataset of historical anthropogenic trace gas emissions for the period 1890–1990. *Global Biogeochem. Cy.,* 15, 909–928.

Wang, M., and J. E. Penner (2009), Aerosol indirect forcing in a global model with particle nucleation, *Atmos. Chem. Phys*., 9(1), 239-260.

Wang, M. H., J. E. Penner, and X. H. Liu (2009), Coupled IMPACT aerosol and NCAR CAM3 model: Evaluation of predicted aerosol number and size distribution, *J. Geophys. Res.*, 114, D06302, doi:10.1029/2008JD010459.

Wang, Y. H., D. J. Jacob, and J. A. Logan (1998), Global simulation of tropospheric O-3-NOx-hydrocarbon chemistry 1. Model formulation, *J. Geophys. Res.*, 103(D9), 10713-10725.

Young, P. J. et al. (2013), Pre-industrial to end 21st century projections of tropospheric ozone from the Atmospheric Chemistry and Climate Model Intercomparison Project (ACCMIP), *Atmos. Chem. Phys.*, *13*(4), 2063–2090, doi:10.5194/acp-13-2063-2013.

Zhou, C., J. E. Penner, Y. Ming, and X. Huang (2012) Aerosol forcing based on CAM5 and AM3 meteorological fields, Atmos. Phys. Chem. Disc., 12, 10679-10727, 2012.

CHAPTER 5

Conclusion and future work

5.1 Conclusion

The research presented in this thesis improves our understanding about the formation of secondary organic aerosol (SOA) and its radiative effect on climate. In this thesis, a new explicit model using detailed reactions is developed to simulate the formation of SOA. This new model is shown to predict ambient measurements reasonably well. Based on this model as well as a radiative transfer model, the global change in SOA since pre-industrial times and its resulting radiative effect on climate are assessed. Below, key results and conclusions from each chapter are summarized.

In Chapter 2, a basic framework to simulate the SOA formation, based on explicit photochemical reactions, is developed. A detailed gas phase chemical mechanism published by Ito et al. (2007) is used to represent the basic photochemistry of O_3, OH, NO_x and volatile organic compounds (VOCs). To determine what compounds are semi-volatile organic compounds (SVOCs), the criteria suggested by Griffin et al. (2002) are adopted, which are based on the chemical structures of each species. For each of these SVOCs, its gas-particle partitioning coefficient is calculated explicitly according to Pankow (1994) theory. Different from traditional gas-particle partitioning theory, here the condensed SVOCs are assumed to undergo further aerosol-phase reactions to form oligomers with a fixed time constant (assumed to be 1 day in the baseline model). I also

included SOA formation from the uptake of gas-phase glyoxal and methlyglyoxal onto clouds and aqueous sulfate aerosol following the work of Fu et al. (2008), and from the uptake of gas-phase epoxides onto aqueous sulfate aerosol following the work of Paulot et al. (2009). In addition, I examined the influence of including the HO_x recycling mechanism proposed by Peeters et al. (2009) for the oxidation of isoprene. These SOA formation mechanisms were evaluated by comparing global chemical transport model simulations with surface observations from the IMPROVE network in North America, the EMEP network in Europe and from a collection of AMS measurements. The results are also compared with vertical profiles of OC from aircraft measurements off of East Asia and over North America.

The total SOA source is predicted to be from 90.8 to 120.5 Tg yr^{-1}, much larger than that estimated by previous global chemical transport models, but within the range of recent top-down estimates that use satellite observations and AMS measurements (Heald et al., 2010; Spracklen et al., 2011). The introduction of the Peeters et al. (2009) HO_x recycling mechanism into the isoprene oxidation scheme has a strong impact on global SOA formation. It causes the total SOA source to decrease by 25 %. Comparison with the IMPROVE network and with AMS surface measurements in the Northern Hemisphere shows that the model can predict the surface organic aerosol concentrations reasonably well with low normalized mean biases ranging from −15 % to 15 % in rural regions. The comparison with the EMEP measurements demonstrates that the model under-predicts surface OC concentrations in Europe, which may be the result of an underestimation of POA in winter and of SOA in summer. In pristine tropical forest regions, the model over-estimates the OM burden by roughly a factor of three compared to three surface AMS

measurements made in West Africa, Amazon and Malaysia. In the free troposphere, the model reproduces the OC observed during the ITCT-2K4 aircraft campaign over North America relatively well, but clearly underestimates OC observations during ACE-Asia campaign off the coast of Japan. However, the model simulates Asian pollution layers above 3 km during the INTEX-B campaign very well.

Chapter 3 examines the SOA formation in aqueous phase by carrying out six simulations using different methods to represent uptake process of gaseous glyoxal and methylglyoxal into aqueous phase, different aqueous phase reactions in aerosol water, different cloud fields, and with/without iron chemistry in cloud. These different simulations lead to different total SOA production rates in the aqueous phase ranging from 17.5 Tg/yr to 59.4 Tg/yr, implying a high degree of uncertainty in SOA formation in the aqueous phase. Using the surface-limited uptake process scheme with the reactive uptake parameter adopted from the laboratory studies leads to higher aqSOA production rates both in cloud and in aerosol water than using the multiphase process scheme does. The global glyoxal oligomers formed in sulfate aerosol water predicted by the parameterized photochemistry from Ervens and Volkamer (2010) are consistent with those predicted by the detailed "radical-radical" chemistry proposed by Lim et al. (2010). After changing the diagnostic cloud field to that simulated by the GFDL AM3 model, the organic acids production rate decreased by around 60% while sulfate formation rates increased slightly, because the GFDL AM3 cloud field has much smaller cloud water content in tropical regions but higher cloud water content in the Northern Hemisphere. The introduction of Fe chemistry in cloud has a large impact on the in-cloud HO_x budget, increasing the tropical in-cloud OH radical source by a factor of over 2 on a global basis.

Despite the increase of in-cloud OH radical, the net source of organic acids barely changes, because the in-cloud OH radical concentration increases by almost the same amount as does the chemical production and chemical destruction rate of organic acids.

Over all, all simulations tend to underestimate the observations of oxalic acid in European winter, Amazon, Africa, and China, probably because the model doesn't account for the direct emission of oxalic acid from primary sources (e.g., wood burning, meat cooking and biomass burning) or that formed in the aging process associated with these direct emissions. However, this underestimation might also be due to a deposition rate that is too high or a cloud water content that is too low in the model. The multiphase process scheme improves the model's ability to predict the organic aerosol concentrations measured in the tropical regions, and this scheme is also shown to simulate the SOA concentrations measured by AMS in the northern hemisphere reasonably well.

In Chapter 4, global SOA burden is shown to increase by 0.54 Tg (54%) since preindustrial times, causing a direct radiative forcing ranging from -0.06 W/m2 to -0.21 W/m2 and a first indirect ratiative forcing from -0.24 W/m2 to -0.32 W/m2, depending on its size distribution and refractive index. Thus the potential radiative effect of SOA on climate can be as high as -0.53 W/m2, which is around one third of the radiative effect of all aerosols (excluding the SOA) reported in 2007 IPCC report. If considering the effect of SOA, the cooling effect of aerosols could be much stronger than we thought. In addition, the deposition of present-day SOA as well as POA onto the land snow and sea ice is shown, for the first time, to cause a warming of 0.026 Wm^{-2} and 0.0042 Wm^{-2} at the TOA, respectively, the magnitude of which is comparable to the warming caused by BC in snow and ice.

5.2 Future work

As demonstrated in Chapter 2, 3 and 4, there are still many gaps in our knowledge that limits our ability to simulate and predict SOA in the real atmosphere accurately and to assess the impact of SOA on climate. Therefore here I am discussing several major issues that need to be addressed in the future.

SOA from primary emissions of semi-volatile and intermediate volatility organic compounds. In this thesis, POA from diesel exhaust and biomass burning is assumed to be non-volatile, always existing as aerosol phase. However, recent studies showed that this POA can include low-volatility compounds that partition between the gas and aerosol phase, and further undergo gas-phase oxidation to form species of different volatilities that from SOA (Robinson et al., 2007; Huffman et al., 2009). There is still substantial uncertainty in the emissions, reaction rates, and SOA yields of these primary emitted aerosols (Pye and Seinfeld, 2010; Spracklen et al., 2010).

VOC oxidation mechanism. As shown in Chapter 2, the VOC oxidation mechanism has a large impact on the SOA budget. In addition to HOx recycling shown in Chapter 2, there is a high level of uncertainty for the oxidation of some complex SOA precursors (e.g., aromatics and terpenes) (Hallquist et al., 2009). It is poorly understood that what exact first-generation products can be formed through first initial oxidation sequences and how these first-generation products are further degraded in the atmosphere. Moreover, there is also lacking information on the chemical mechanisms for the atmospheric degradation of other potential SOA precursors, such as sesquiterpenes, long-chain alkanes and oxygenates.

Gas-particle partitioning. The gas-particle partitioning coefficient of one sVOC, which determines its fraction existing in the aerosol phase, strongly depends on its vapor pressure. But the vapor pressure is still difficult to measure or estimate, leading to a high degree of uncertainty on the vapor pressure (see the Chapter 2). Further work needs to be performed on decreasing this uncertainty. Moreover, this equilibrium gas-particle partitioning theory was challenged by recent laboratory studies carried on by Vaden et al. (2011). Vaden et al. (2011) found that the time scale for evaporating 75% of pure α-pinene SOA particles was about 1day, which was much shorter than the ~10 min time scale predicted by current gas-particle partitioning theory.

Aerosol phase reactions. This thesis assumes all aerosol phase reactions are first-order reactions with one-day e-folding lifetime without any explicit reactions, since the available data appears to be ambiguous (ambiguous chemical processes leading to oligomers and the ambiguous identification of oligomeric products). Further work is required to examine the key processes (e.g., oligomerization, organosulfate formation) under conditions relevant to the atmosphere.

Aqueous phase reactions. As shown in Chapter 3, the scientific knowledge of aqueous phase reactions leading to SOA is still very limited. Future studies should involve in investigating the major aqueous phase reactions responsible for the SOA formation in the bulk aerosol water and/or at the aqueous aerosol surface for both glyoxal and methylglyoxal and other potential aqueous phase SOA precursors (e.g., methyl vinyl ketone and methacrolein).

Optical properties. Size distributions and refractive indices of SOA particles are not well constrained, causing a large uncertainty associated with the direct forcing of SOA. Hence more measurements are needed to detect these missing properties.

Cloud condensation nuclei and ice nuclei. The activation of an aerosol particle into a cloud droplet is closely related to the hygroscopic properties of the aerosol. In our model, the hygroscopicity is assumed to be constant for all SOA. Measurements, however, show that the hygroscopicity of SOA depends on its source and chemical age in the atmosphere and is related to the particle O:C ratio or oxidation stage (Cappa et al., 2011). Thus, a more robust and sophisticated treatment for the hygroscopicity of SOA is needed in the future. In addition, recent laboratory studies and field measurements have shown the importance of organics in the nucleation of new particles (Metzger et al*.,* 2010). Finally, recent studies have shown that SOA generated from several biogenic and anthropogenic gas-phase precursors are characterized by an amorphous solid or semi-solid phase (Virtanen et al., 2010). The amorphous solid state of SOA particles may provide heterogeneous ice nucleation via the immersion or deposition mode by acting as IN (Wang et al., 2012). Certainly additional laboratory work and field measurements in clouds in the upper troposphere are needed in the future to understand the role of organics in ice nucleation.

5.3 Reference

Cappa, C. D., Che, D. L., Kessler, S. H., Kroll, J. H. and Wilson, K. R.: Variations in organic aerosol optical and hygroscopic properties upon heterogeneous OH oxidation, J. Geophys. Res., 116, doi:10.1029/2011jd015918, 2011.

Ervens, B., and Volkamer, R.: Glyoxal processing by aerosol multiphase chemistry: towards a kinetic modeling framework of secondary organic aerosol formation in

aqueous particles, Atmos. Chem. Phys., 10, 8219-8244, 2010.

Fu, T. M., Jacob, D. J., Wittrock, F., Burrows, J. P., Vrekoussis, M., and Henze, D. K.: Global budgets of atmospheric glyoxal and methylglyoxal, and implications for formation of secondary organic aerosols, J. Geophys. Res., 113, D15303, doi:10.1029/2007JD009505, 2008.

Griffin, R. J., Dabdub, D., and Seinfeld, J. H.: Secondary organic aerosol - 1. Atmospheric chemical mechanism for production of molecular constituents, J. Geophys. Res., 107, D17, doi:10.1029/2001JD000541, 2002.

Hallquist, M., Wenger, J. C., Baltensperger, U., Rudich, Y., Simpson, D., Claeys, M., Dommen, J., Donahue, N. M., George, C., Goldstein, A. H., Hamilton, J. F., Herrmann, H., Hoffmann, T., Iinuma, Y., Jang, M., Jenkin, M. E., Jimenez, J. L., Kiendler-Scharr, A., Maenhaut, W., McFiggans, G., Mentel, T. F., Monod, A., Prevot, A. S. H., Seinfeld, J. H., Surratt, J. D., Szmigielski, R. and Wildt, J.: The formation, properties and impact of secondary organic aerosol: current and emerging issues, Atmos. Chem. Phys., 9(14), 5155–5236, 2009.

Heald, C. L., Ridley, D. A., Kreidenweis, S. M., and Drury, E. E.: Satellite observations cap the atmospheric organic aerosol budget, Geophys. Res. Lett., 37, L24808, doi:10.1029/2010GL045095, 2010.

Huffman, J. A., Docherty, K. S., Aiken, A. C., Cubison, M. J., Ulbrich, I. M., DeCarlo, P. F., Sueper, D., Jayne, J. T., Worsnop, D. R., Ziemann, P. J. and Jimenez, J. L.: Chemically-resolved aerosol volatility measurements from two megacity field studies, Atmos. Chem. Phys., 9(18), 7161–7182, 2009.

Ito, A., Sillman, S., and Penner, J. E.: Effects of additional nonmethane volatile organic compounds, organic nitrates, and direct emissions of oxygenated organic species on global tropospheric chemistry, J. Geophys. Res., 112, D06309, doi:10.1029/2005JD006556, 2007.

Lim, Y. B., Tan, Y., Perri, M. J., Seitzinger, S. P., and Turpin, B. J.: Aqueous chemistry and its role in secondary organic aerosol (SOA) formation, Atmos. Chem. Phys., 10, 10521–10539, doi:10.5194/acp-10-10521-2010, 2010.

Metzger, A., Verheggen, B., Dommen, J., Duplissy, J., Prévôt, A. S. H., Weingartner, E., Riipinen, I., Kulmala, M., Spracklen, D. V., Carslaw, K. S. and Baltensperger, U.: Evidence for the role of organics in aerosol particle formation under atmospheric conditions, Proceedings of the National Academy of Sciences of the United States of America, 107(15), 6646–6651, doi:10.1073/pnas.0911330107, 2010.

Pankow, J. F.: An absorption-model of the gas aerosol partitioning involved in the formation of secondary organic aerosol, Atmos. Environ., 28, 189-193, 1994.

Paulot, F., Crounse, J. D., Kjaergaard, H. G., Kurten, A., St Clair, J. M., Seinfeld, J. H., and Wennberg, P. O.: Unexpected epoxide formation in the gas-phase photooxidation of isoprene, Science, 325, 730-733, 2009.

Peeters, J., Nguyen, T. L., and Vereecken, L.: HO_x radical regeneration in the oxidation of isoprene, Phys. Chem. Chem. Phys., 11, 5935-5939, 2009.

Pye, H. O. T. and Seinfeld, J. H.: A global perspective on aerosol from low-volatility organic compounds, Atmos. Chem. Phys., 10(9), 4377–4401, doi:10.5194/acp-10-4377-2010, 2010.

Robinson, A. L., Donahue, N. M., Shrivastava, M. K., Weitkamp, E. A., Sage, A. M., Grieshop, A. P., Lane, T. E., Pierce, J. R. and Pandis, S. N.: Rethinking organic aerosols: Semivolatile emissions and photochemical aging, Science, 315(5816), 1259–1262, doi:10.1126/science.1133061, 2007.

Spracklen, D. V., Jimenez, J. L., Carslaw, K. S., Wrosnop, D. R., Evans, M. J., Mann, G. W., Zhang, Q., Canagaratna, M, R., Allan, J., Coe, H., McFiggans, G., Rap, A., and Forster, P.: Aerosol mass spectrometer constraint on the global secondary organic aerosol budget, Atmos. Chem. Phys. Discuss., 11, 5699-5755, 2011.

Vaden, T. D., Imre, D., Beranek, J., Shrivastava, M. and Zelenyuk, A.: Evaporation kinetics and phase of laboratory and ambient secondary organic aerosol, Proceedings of the National Academy of Sciences of the United States of America, 108(6), 2190–2195, doi:10.1073/pnas.1013391108, 2011.

Wang, B., Lambe, A. T., Massoli, P., Onasch, T. B., Davidovits, P., Worsnop, D. R. and Knopf, D. A.: The deposition ice nucleation and immersion freezing potential of amorphous secondary organic aerosol: Pathways for ice and mixed-phase cloud formation, J. Geophys. Res., 117(D16), D16209, doi:10.1029/2012JD018063, 2012.

APPENDIX A

Supplementary material for "Global modeling of SOA formation from dicarbonyls, epoxides, organic nitrates and peroxides"

Table S1 SVOCs that partition to aerosol phase through gas-particle partitioning, parent VOCs, partitioning coefficients (K) at temperature 298K, oligomer formation rates for each SVOC species and its relative contribution (annual global mean) to total ne_oSOA in three different simulations.

Short name	Chemical formula	Parent VOC	K ($m^3/\mu g$)	Production (Tg/year)			% contribution to ne_oSOA		
				Simulation A	Simulation B	Simulation C	Simulation A	Simulation B	Simulation C
A-DI	C6H5OH(OH)CHO	aromatics	1.47E-03	8.11E-02	5.12E-02	6.32E-02	0.33	0.34	0.24
AD2P	C6H4(CH3)OH(OH)OOH	aromatics	1.01E-1	1.59E+00	1.47E+00	1.53E+00	6.47	9.71	5.74
AP	C6H5OH(OH)C(O)OOH	aromatics	8.34E-1	1.35E+00	1.26E+00	1.30E+00	5.52	8.35	4.87
APAN	C6H5OH(OH)CO3NO2	aromatics	1.76E-1	6.85E-01	6.43E-01	6.74E-01	2.80	4.26	2.53
DPAN	CHOCH=CHCO3NO2	aromatics	4.34E-07	3.79E-05	3.43E-05	3.83E-05	1.55E-04	2.27E-04	1.44E-04
GPAN	HOCH2C(O)OONO2	isoprene	6.33E-07	1.72E-03	1.05E-08	1.32E-08	7.04E-03	6.96E-08	4.94E-08
NITP	C6H5ONO2	aromatics	3.24E-07	7.76E-05	3.66E-05	5.05E-05	3.17E-04	2.42E-04	1.90E-04
XAP	CH3COCH=CHC(O)OOH	aromatics	1.12E-05	1.21E-04	7.09E-05	8.89E-05	4.93E-04	4.69E-04	3.34E-04
XPAN	CH3COCH=CHCO3NO2	aromatics	1.81E-06	4.56E-05	3.64E-05	4.20E-05	1.86E-04	2.41E-04	1.58E-04
YAP	CHOCH=C(CH3)C(O)OOH	aromatics	7.24E-06	8.54E-05	4.78E-05	6.10E-05	3.49E-04	3.16E-04	2.29E-04
YPAN	CHOCH=C(CH3)CO3NO2	aromatics	1.33E-06	3.43E-05	2.66E-05	3.10E-05	1.40E-04	1.76E-04	1.17E-04
ZAP	CHOC(CH3)=CHC(O)OOH	aromatics	7.54E-06	8.90E-05	4.97E-05	6.36E-05	3.63E-04	3.29E-04	2.39E-04
ZPAN	CHOC(CH3)=CHCO3NO2	aromatics	1.38E-06	3.56E-05	2.76E-05	3.22E-05	1.45E-04	1.83E-04	1.21E-04
IAP	HOCH2C(CH3)(OOH)CH(OH)CHO	isoprene	7.77E-02	4.58E+00	8.71E-01	2.12E+00	18.70	5.76	7.97
INPN	O2NOCH2C(OOH)(CH3)CH=CH2	Isoprene	1.83E-05	3.91E-03	2.77E-03	3.43E-03	1.60E-02	1.83E-02	1.29E-02
ISNP	HOCH2C(OOH)(CH3)CH(ONO2)CH2OH	Isoprene	3.39E+00	1.06E+00	4.51E-01	6.79E-01	4.32	2.98	2.55
LIP	HOC10H16OOH	Limonene	2.54E-02	8.10E-01	1.07E+00	1.07E+00	3.30	7.09	4.01

MRP	HOCH2C(OOH)(CH3)CHO	from MACR, isoprene, limonene, alpha pinene	6.15E-05	9.94E-03	2.00E-03	3.39E-03	4.06E-02	1.33E-02	1.27E-02
PINT	ONO2C10H16OOH	alpha pinene and limonene	1.55E-02	2.05E-01	1.11E-01	1.57E-01	0.84	0.74	0.60
PIP	HOC10H16OOH	alpha pinene	7.58E-03	7.87E-01	8.02E-01	8.63E-01	3.21	5.31	3.24
VRP	HOCH2CH(OOH)C(O)CH3	Isoprene	9.90E-05	2.01E-02	4.25E-03	7.75E-03	8.21E-02	2.81E-02	2.91E-02
DB1OOH	HOCH=C(CH3)CH(OOH)CH2OH + HOCH2C(CH3)(OOH)CH=CHOH	Isoprene	6.40E-03	-	5.22E-01	1.41E+00	-	3.45	5.30
DB2OOH	CHOC(CH3)(OOH)CHOHCH2OH + HOCH2C(CH3)(OH)CH(OOH)CH2OH	Isoprene	1.10E-01	-	2.47E+00	6.34E+00	-	16.3	23.8
TRIOL	HOCH=C(CH3)CH(OH)CH2OH + HOCH2C(CH3)(OH)CH=CHOH	isoprene	4.78E-06	-	1.67E-06	5.16E-06	-	1.10E-05	1.94E-05
PRN2	C4H7O6N	Isoprene	4.42E-02	1.34E+01	8.07E+00	1.04E+01	54.5	53.4	39.1
RIP	HOCH2C(OOH)(CH3)CH=CH2	isoprene	1.77E-05	7.04E-03	1.09E-03	3.28E-03	2.87E-02	7.21E-03	1.23E-02
Total anthropogenic sources			-	3.7	3.4	3.6	15.1	19.1	13.5
Total biogenic sources			-	20.8	14.4	23.0	84.9	80.9	86.5

Table S2 Additional species used in the HO_x recycling mechanism and in the epoxide formation mechanism.

Symbol	Formula	Description
RIPEEO2	Z-HOCH2C(CH3)=CHCH2O2 + Z-CH2O2C(CH3)=CHCH2OH	Z isomers of the internally double bonded isoprene peroxy radicals
RIPEEOOH	Z-HOCH2C(CH3)=CHCH2OOH + Z-CH2OOHC(CH3)=CHCH2OH	Hydroperoxide from RIPEEO2
DB1O2	HOCH=C(CH3)CH(O2)CH2OH +HOCH2C(CH3)(O2)CH=CHOH	first-generation RO2 from Dibble mechanism (Paulot et al., 2009a)
DB2O2	CHOC(CH3)(O2)CHOHCH2OH + HOCH2C(CH3)(OH)CH(O2)CH2OH	second-generation RO2 from Dibble mechanism (Paulot et al., 2009a)
DB1OOH	HOCH=C(CH3)CH(OOH)CH2OH +HOCH2C(CH3)(OOH)CH=CHOH	Hydroperoxide from DB1O2
DB2OOH	CHOC(CH3)(OOH)CHOHCH2OH +	Hydroperoxide from DB2O2

	HOCH2C(CH3)(OH)CH(OOH)CH2OH	
TRIOL	HOCH=C(CH3)CH(OH)CH2OH + HOCH2C(CH3)(OH)CH=CHOH	Triol from the molecular channel of DB1O2 permutation reaction
ZCO3HC23DBCOD	HOCH=C(CH3)CH(OH)CH2OH + HOCH2C(CH3)(OH)CH=CHOH	Acylhydroperoxyaldehydes (PACALD) predicted by Peeters et al., (2009)
ZCODC23DBCOOH	CHOC(CH3)=CHCH2OOH + HOOCH2C(CH3)CHCHO	Hydroperoxyaldehydes (HPALD) predicted by Peeters et al., (2009)
IEPOXO2		RO2 from isoprene epoxide
HAC	HOCH2C(O)CH3	Hydroxyacetone
GLYC	HOCH2CHO	Glyxoaldehyde
GLYX	CHOCHO	Glyoxal
MGLY	CH3COCHO	Methylglyoxal
HCHO	CH2O	Formaldehyde
ACO2	HCOOH	Formic acid

Table S3 Additional reactions for HO_x recycling mechanism.

	Reaction	Rate constant	References	Notes
1	RIPEEO2 => ZCODC23DBCOOH + HO2	9.82E8 * EXP(-6303/T)	Peeters et al. (2009)	1,6-H-shift
2	RIO2 => 0.864 HO2 + 0.690 HCHO + 0.402 MVK + 0.288 MACR + 0.136 RIO1 + 0.127 IALD	6.08E10 * EXP(-8893/T)	Peeters et al. (2009)	1,5-H-shift for MVK and MACR precursors; Although the parent RO2 of IALD do not undergo 1,5-H-shift, for simplicity the products of RIO2 + NO are taken except NO2
3	RIPEEO2 + HO2 => RIPEEOOH	2.91E-13 * EXP(1300./T) * 0.706		MCM rate constant
4	RIPEEO2 + MO2 => IAP + HO2 + HCHO + HO2	K same as for IAO2 + MO2		
5	RIPEEO2 + NO => IAP + HO2 + NO2	2.54E-12 * EXP(360./T)		Rate constant as for the others first-generation RO2 from isoprene
6	RIPEEOOH + hv => OH + IAP + HO2	J(CH3OOH)		

7	RIPEEOOH + OH => 0.5 IEPOX + 0.25MGLY + 0.25GLYX + 0.25HOOCH2CHO + 0.25CH3COCH2OOH	k= same as for RIP + OH		approximation: a carbonyl function should have been an -OH functional group
8	ZCODC23DBCOOH + OH => 0.5MGLY + 0.5 HOOCH2CHO + 0.5CH3COCH2OOH + 0.5GLYX	4.50E-11	SAR (Taraborrelli et al., 2012.)	rate constant calculated by SAR by and similar to the estimate of Peeter and Mueller, PCCP 2010
9	ZCODC23DBCOOH + hv => OH + IAO2	J(CH3OOH)+J(MACR)/0.004		J value for MACR photolysis assuming IMPACT has a quantum yield of 0.004 (as recommended by IUPAC). IAO2 should represent LHC4ACCO3 of MIM2
10	CH3COCH2OOH + OH => ATO2	1.90E-12 * EXP(190/T)	IUPAC	H-abstraction channel from the –OOH group
11	CH3COCH2OOH + OH => MGLY + OH	8.39E-12	SAR (Taraborrelli et al., 2012.)	H-abstraction from the –CH2OOH group with following prompt OH-elimination
12	CH3COCH2OOH + hv => MCO3 + HCHO + OH	J(MEK) + J(CH3OOH)		Structural analogy to methyl ethyl ketone and methyl hydroperoxide
13	IAO2 => ZCO3HC23DBCOD + HO2	7.32E8 * EXP(-5556./T)	Peeters et al. (2009)	1, 6-H-shift
14	ZCO3HC23DBCOD + hv => MCO3 + 2CO2 + 2OH + HO2 + CO	J(CH3OOH)+J(MACR)/0.004	Peeters et al. (2009)	enhanced photolysis
15	VRO2 => 0.7MGLY + 0.7HCHO + 0.3HOOCH2CHO + 0.3MCO3 + OH	5.1E10 * EXP(-8893/T)	Peeters et al. (2009)	1,5-H-shift
16	MRO2 => 0.830 HCHO + 0.830 MGLY1 + 0.170 + HAC + 0.170 CO + .17 HO2 + OH	4.5E10*EXP(-8893/T)	Peeters et al. (2009)	1,5-H-shift
17	HOOCH2CHO + OH => OH + 0.44HCHO + 0.44CO + 0.56GLYX	2.081E-11		0.29 HCOCH2O2 neglected and the other two yields re-scaled with a factor of 1/(1-.29)
18	HOOCH2CHO + hv => OH + HCHO + CO + HO2	J(CH3OOH)+J(GLYC)		Structural analogy to glycolaldehyde and methyl hydroperoxide
19	DB1O2 + MO2 => 0.8 DB2O2 + 0.2 TRIOL + HCHO + HO2	2.9E-12		MCM rata constant for a secondary RO2

20	DB1O2 + HO2 => DB1OOH	0.706 * 2.91E-13 * EXP(1300./T)		MCM rate constant
21	DB1O2 + NO => DB2O2 + NO2	2.54E-12 * EXP(360./T)		Rate constant as for the others first-generation RO2 from isoprene
22	DB2O2 + MO2 => 0.5 HAC + 0.5 GLYC + 0.5 MGLY + 0.5 GLYX + HO2 + HCHO + HO2	2.9E-12		MCM rata constant for a secondary RO2
23	DB2O2 + HO2 => DB2OOH	0.706 * 2.91E-13 * EXP(1300./T)		MCM Rate constants
24	DB2O2 + NO => 0.5 HAC + 0.5 GLYC + 0.5 MGLY + 0.5 GLYX + HO2 + NO2	2.54E-12 * EXP(360./T)		Rate constant as for the others first-generation RO2 from isoprene
25	DB1OOH + OH = >DB1O2	0.4*k_CH3OOH_OH		
26	DB1OOH + hv => DB2O2 + OH	J(CH3OOH)		Structural analogy to methyl hydroperoxide
27	DB2OOH + OH => DB2O2	0.4*k_CH3OOH_OH		
28	DB2OOH + hv => 0.5 HAC + 0.5 GLYC + 0.5 MGLY + 0.5 GLYX + HO2 + OH	J(CH3OOH)		Structural analogy to methyl hydroperoxide
29	TRIOL + OH => IAO2	1E-11	SAR (Taraborrelli et al., 2012.)	Triol from permutations reactions of DB1O2

Table S4 Modified reactions in HOx recycling mechanism.

	Modified reactions	Original reactions	References	Notes
1	MAO3 + HO2 => 0.44 OH + 0.44 HO2 + 1.76HCHO + 0.350 MAOP + 0.150 RCOH	MAO3 + HO2 => 0.7MAOP + 0.30 RCOH + 0.3O3		Structural analogy to MCO3
2	MCO3 + HO2 => 0.44 OH + 0.44 MO2 + 0.35 MAP + .15 ACTA + .15 O3	MCO3 + HO2 => O3 + ACTA MCO3 + HO2 => MAP	IUPAC, 2009	
3	RIO2 + NO => NO2 + 0.864 HO2 + 0.690 HCHO + 0.402 MVK + 0.288 MACR + 0.09 DB1O2 + 0.046 RIO1 + 0.127 IALD	RIO2 + NO => NO2 + 0.864 HO2 + 0.690 HCHO + 0.402 MVK + 0.288 MACR + 0.136 RIO1 + 0.127 IALD	Paulot et al., (2009a)	

4	MO2 + RIO2 => 1.864 HO2 + 1.690 HCHO + 0.402 MVK + 0.288 MACR + 0.09 DB1O2 + 0.046 RIO1 + 0.127 IALD	MO2 + RIO2 => 0.25MOH + 0.92HO2 + HCHO +0.2MVK + 0.14MACR +0.07RIO1 + 0.06IALD +0.25MEK +0.25ROH	This work	Consistent with Paulot et al., (2009a)
5	MCO3 + RIO2 => MO2 + 0.864 HO2 + 0.690 HCHO + 0.402 MVK + 0.288 MACR + 0.09 DB1O2 + 0.046 RIO1 + 0.127 IALD	MCO3 + RIO2 => MO2 + 0.864HO2 + 0.690HCHO + 0.402MVK + 0.288MACR + 0.136RIO1 + 0.127IALD	This work	Consistent with Paulot et al., (2009a)
6	RIO2 + RIO2 => 1.728 HO2 + 1.38 HCHO + 0.804 MVK + 0.576 MACR + 0.18 DB1O2 + 0.092 RIO1 + 0.254 IALD	RIO2 + RIO2 => 0.680MVK + 0.390MACR + 0.930IPRD +0.40HCHO + 1.380HO2	This work	Consistent with Paulot et al., (2009a)
7	RIO2 + HO2 => RIP	RIO2 + HO2 => 0.88RIP + 0.12OH + 0.047MACR + 0.073MVK + 0.120HCHO + 0.120HO2		the 12% yield of OH was used in Paulot et al., (2009b) in order to account for the initial NOx present in the "low-NOx" experiments
8	RIO1 + HO2 => RIP	RIO1 + HO2 => 0.88RIP + 0.12OH + 0.047MACR + 0.073MVK + 0.120HCHO + 0.120HO2		The same above
9	GLYX + OH => 1.8 CO + 0.8 HO2 + 0.2 OH	GLYX + OH => HO2 +2CO	This work	Combination of results from Orlando and Tyndall, (2001), Feierabend et al., (2008)
10	GLYC + OH => 0.75 HO2 + 0.25 OH + 0.13 GLYX + 0.52 CO + 0.16 HCOOH + 0.71 HCHO	GLYC + OH => 0.80GCO3 + 0.20 GLYX + 0.20HO2	Butkovskaya et al., (2006a)	
11	HAC + OH => 0.75 MGLY + 0.825 HO2 + 0.125 HCOOH + 0.1 OH +0.125 MO2 + 0.05 CO + 0.125 ACTA	HAC + OH => MGLY + HO2	Butkovskaya et al., (2006b)	
12	RIP + OH => 0.5 IAO2 + 0.50MGLY + 0.50GLYX + 0.50CH3COCH2OOH + 0.50HOOCH2CHO	RIP + OH => 0.50IAO2 + 0.4RIO2 + 0.2RIO1	This work	Approximation regarding the degradation products

References:

Butkovskaya, N. I., Pouvesle, N., Kukui, A., and Le Bra, G.: Mechanism of the OH-initiated oxidation of glycolaldehyde over the temperature range 233-296 K, J. Phys. Chem. A, 110, 13492-13499, 2006a.

Butkovskaya, N. I., Pouvesle, N., Kukui, A., Mu, Y. J., and Le Bras, G.: Mechanism of the OH-initiated oxidation of hydroxyacetone over the temperature range 236-298 K, J. Phys. Chem. A, 110, 6833-6843, 2006b.

Feierabend, K. J., Zhu, L., Talukdar, R. K., and Burkholder, J. B.: Rate Coefficients for the OH+HC(O)C(O)H (glyoxal) Reaction between 210 and 390, J. Phys. Chem. A, 112, 73-82, 2008.

IUPAC, 2009: http://www.iupac-kinetic.ch.cam.ac.uk/datasheets/pdf/HOx_VOC54_HO2_CH3CO3.pdf.

Orlando, J. J., and Tyndall, G. S.: The atmospheric chemistry of the HC(O)CO radical, Int. J. Chem. Kinet., 33, 149-156, 2001.

Paulot, F., Crounse, J. D., Kjaergaard, H. G., Kroll, J. H., Seinfeld, J. H., and Wennberg, P. O.: Isoprene photooxidation: new insights into the production of acids and organic nitrates, Atmos. Chem. Phys, 9, 1479-1501, 2009a.

Paulot, F., Crounse, J. D., Kjaergaard, H. G., Kurten, A., St Clair, J. M., Seinfeld, J. H., and Wennberg, P. O.: Unexpected epoxide formation in the gas-phase photooxidation of isoprene, Science, 325, 730-733, 2009b.

Peeters, J., and Muller, J.-F.: HO(x) radical regeneration in isoprene oxidation via peroxy radical isomerisations. II: experimental evidence and global impact, Physical Chemistry Chemical Physics, 12, 14227-14235, 2010.

Peeters, J., Nguyen, T. L., and Vereecken, L.: HOx radical regeneration in the oxidation of isoprene, Physical Chemistry Chemical Physics, 11, 5935-5939, 2009.

Taraborrelli D., Lawrence, M. G., Crowley, J. N., Dilon, T. J., Gromov, S., Groβ, C. B. M., Vereecken, L., and Lelieveld, J..: Hydroxyl radical buffered by isoprene oxidation over tropical forests, Nature Geosci., 5, 190-193, 2012.

APPENDIX B

Aqueous phase Reactions

Table S1. Abbreviations listed in the chemical mechanism tables below

Species number	Abbreviation	Species name
1	GLYC	Glycolaldehyde
2	GLYX	Glyoxal
3	MGLY	Methylglyoxal
4	GLYAC	Glyoxylic acid
5	OXLAC	Oxalic acid
6	PRV	Pyruvic acid
7	GLYX_MH	Glyoxal monohydrate
8	GLYX_DH	Glyoxal dehydrate
9	MGLY_MH	Methylglyoxal monohydrate
10	MGLY_DH	Methylglyoxal dehydrate
11	GLYOLI	Oligomers from glyoxal
12	MGLOLI	Oligomers from methylglyoxal
13	C4D	C_4 dimer
14	TA	Tartaric acid
15	C3D	C_3 dimer
16	MA	Malonic acid

Table S2. Non-organic chemistry used in the model.

Reaction Number	Aqueous phase Reactions	K_{298} (M^nS^{-1})	E/R (K)	References
1	H_2O_2+hv=>2OH	Using the gas phase photolysis rate, increased by a factor of 1.5		Barth et al., (2003)
2	H_2O_2+OH=>HO_2+H_2O	2.7E07		Lim et al., 2005
3	H_2O_2+HO_2=>OH+H_2O	3.7E00		Tan
4	HO_2+HO_2=>H_2O_2+O_2	9.7E05	2500	Lim et al., 2005
5	OH+HO_2=>H_2O + O_2	7.1E09		Lim et al., 2005
6	O_3 + hv => H_2O_2	Using the gas phase photolysis rate, increased by a factor of 1.5		Barth et al., (2003)
7	OH + O_3 => HO_2	2.0E+09		Pandis and Seinfeld, 1989
8	HO_2 + O_3 => OH	1.0E+04		Pandis and Seinfeld, 1989
9	O_2^- + O_3 => OH + OH^-	1.5E+09	1500	Pandis and Seinfeld, 1989
10	OH^- + O_3 => $O2^-$ + HO_2	7.0E+01		Pandis and Seinfeld, 1989
11	HO_2^- + O_3 => OH +O_2^-	2.8E+06		Pandis and Seinfeld, 1989
12	NO + NO_2 => $2NO_2^-$ + $2H^+$	2.0E+08	1500	Pandis and Seinfeld, 1989
13	NO_2 + NO_2 => NO_2^- + NO_3^- + $2H^+$	1.0E+08	1500	Pandis and Seinfeld, 1989
14	NO + OH => NO_2^- + H^+	2.0E+10	1500	Pandis and Seinfeld, 1989

15	$NO_2 + OH \Rightarrow NO_3^- + H^+$	1.3E+09	1500	Pandis and Seinfeld, 1989
16	HONO + hv => NO + OH	Using the gas phase photolysis rate, increased by a factor of 1.5		Pandis and Seinfeld, 1989
17	HNO_2^- + hv => NO + OH	Using the gas phase photolysis rate, increased by a factor of 1.5		Barth et al., (2003)
18	HONO+ OH => NO_2	1.0E+09	1500	Pandis and Seinfeld, 1989
19	NO_2^- + OH => NO_2 +OH^-	1.0E+10	1500	Pandis and Seinfeld, 1989
20	NO_2^- + O_3 => NO_3^-	5.0E+05	6950	Pandis and Seinfeld, 1989
21	NO_2^- + CO_3^- => NO_2 + CO_3^{2-}	4.0E+05	0.	Pandis and Seinfeld, 1989
22	NO_2^- + NO_3 => NO_2 +NO_3^-	1.2E+09	1500	Pandis and Seinfeld, 1989
23	NO_3^- + hv => NO_2 + OH + OH^-	Using the same as gas-phase HNO3 photolysis, increased a factor of 1.5		Barth et al., (2003)
24	NO_3 + hv => NO	Using the gas phase photolysis rate, increased by a factor of 1.5		Barth et al., (2003)
25	$NO_3 + HO_2 \Rightarrow NO_3^- + H^+$	1.2E+09	1500	Jacob, 1986
26	$NO_3 + O_2^- \Rightarrow NO_3^-$	1.0E+09	1500	Jacob, 1986
27	$NO_3 + H_2O_2 \Rightarrow NO_3^- + HO_2 + H^+$	1.0E+06	2800	Pandis and Seinfeld, 1989
28	$HO_2+O_2^-\Rightarrow H_2O_2 + OH^-$	1.0e8	1500	Pandis and Seinfeld, 1989
29	$SO_2+O_3\Rightarrow H_2SO_4$	2.4e4		Pandis and Seinfeld, 1989
30	HSO_3-+O_3=>HSO_4-	3.7e5	5530	Pandis and Seinfeld, 1989
31	$SO_3^{-2} + O_3 \Rightarrow SO_4^{-2}$	1.5e9	5280	Pandis and Seinfeld, 1989

32	$SO_2+H_2O_2 \Rightarrow H_2SO_4$	1.3e6	4430	Pandis and Seinfeld, 1989
33	$HSO_3- + H_2O_2 \Rightarrow HSO_4^-$	5.2e6	3650	Pandis and Seinfeld, 1989
34	$SO_3^{-2} + H_2O_2 \Rightarrow SO_4^{-2}$	5.2e6	3650	Pandis and Seinfeld, 1989
35	$SO_3^{-2} + OH \Rightarrow SO_5^- + OH^-$	4.6e9	1500	Pandis and Seinfeld, 1989
36	$HSO_3^-+OH \Rightarrow SO_5^-$	4.2e9	1500	Pandis and Seinfeld, 1989
37	$SO_5^- + HSO_3^- \Rightarrow SO_5^- + HSO_5^-$	3.0e5	3100	Pandis and Seinfeld, 1989
38	$SO_5^- + SO_3^{-2} \Rightarrow SO_4^{-2} + SO_4^-$	1.3e7	2000	Jacob, 1986
39	$SO_5^- + O_2^- \Rightarrow HSO_5^- + OH^-$	1.0e8	1500	Jacob, 1986
40	$SO_5^- + HCOOH \Rightarrow HSO_5^- + CO_2 + HO_2$	2.0E+02	5300	Jacob, 1986
41	$SO_5^- + HCOO^- \Rightarrow HSO_5^- + CO_2 + O_2^-$	1.4E+04	4000	Jacob, 1986
42	$SO_5^- + SO_5^- \Rightarrow 2SO_4^-$	2.0E+08	1500	Jacob, 1986
43	$HSO_5^- + OH \Rightarrow SO_5^-$	1.7E+07	1900	Jacob, 1986
44	$HSO_5^- + SO_4^- \Rightarrow SO_5^- + SO_4^{-2} + H^+$	1.0E+5	0.	Jacob, 1986
45	$HSO_5^- + NO_2^- \Rightarrow HSO_4^- + NO_3^-$	3.1E-01	6650	Jacob, 1986
46	$SO_4^- + HSO_3^- \Rightarrow SO_5^- + SO_4^{-2} + H^+$	1.3E+09	1500	Jacob, 1986
47	$SO_4^- + SO_3^{-2} \Rightarrow SO_5^- + SO_4^{-2}$	5.3E+08	1500	Jacob, 1986
48	$SO_4^- + HO_2 \Rightarrow SO_4^{-2} + H^+$	5.0E+09	1500	Jacob, 1986
49	$SO_4^- + O_2^- \Rightarrow SO_4^{-2}$	5.0E+09	1500	Jacob, 1986
50	$SO_4^- + OH^- \Rightarrow SO_4^{-2} + OH$	8.0E+07	1500	Jacob, 1986
51	$SO_4^- + H_2O_2^- \Rightarrow SO_4^{-2} + HO_2 + H^+$	1.2E+07	2000	Pandis and Seinfeld, 1989
52	$SO_4^- + NO_2^- \Rightarrow SO_4^{-2} + NO_2$	8.8E+08	1500	Jacob, 1986

53	$SO_4^- + HCO_3^- \Rightarrow SO_4^{-2} + CO_3^- + H^+$	9.1E+06	2100	Pandis and Seinfeld, 1989
54	$SO_4^- + HCOO^- \Rightarrow SO_4^{-2} + CO_2 + HO_2$	1.7E+08	1500	Jacob, 1986
55	$SO_4^- + HCOOH \Rightarrow SO_4^{-2} + CO_2 + HO_2 + H^+$	1.4E+06	2700	Jacob, 1986
56	$SO_2 + HO_2 \Rightarrow H_2SO_4 + OH$	1.0E+06	0.	Pandis and Seinfeld, 1989
57	$SO_4^- + CH_3OH \Rightarrow SO_4^{-2} + HCHO + HO_2 + H^+$	2.5E+07	1800	Pandis and Seinfeld, 1989

Table S3. Organic chemistry in cloud

Reaction Number	Aqueous phase Reactions	K_{298} (M^nS^{-1})	E/R (K)	References
1	$GLYX + OH \Rightarrow GLYAC + HO_2$	1.1E+09	1564	Lim et al. (2005)
2	$GLYAC + OH \Rightarrow OXLAC + H_2O$	3.62E+08	962	Herrmann (2003)
3	$GLYAC^- + OH \Rightarrow OXLAC^- + H_2O$	2.8E+09	4330	Herrmann (2003)
4	$OXLAC + OH \Rightarrow 2CO_2 + 2H_2O$	1.4E+06		Lim et al. (2005)
5	$OXLAC^- + OH \Rightarrow 2CO_2 + 2H_2O$	4.7E+07		Lim et al. (2005)
6	$OXLAC^{=} + OH \Rightarrow 2CO_2 + 2H_2O$	7.7E+06		Lim et al. (2005)
7	$H_2C(OH)_2 + OH \Rightarrow HCOOH + HO_2$	2.0E+09	1500	Pandis and Seinfeld, 1989
8	$HCOO^- + NO_3 \Rightarrow NO_3^- + CO_2 + HO_2$	6.0E+07	1500	Jacob, 1986
9	$HCOOH + O_3 \Rightarrow CO_2 + HO_2 + OH$	5.0E+00	0	Pandis and Seinfeld, 1989
10	$HCOO^- + O_3 \Rightarrow CO_2 + OH + O_2^-$	1.0E+02	0	Pandis and Seinfeld, 1989
11	$HCOO^- + CO_3^- \Rightarrow CO_2 + HCO_3^- + HO_2 + OH^-$	1.1E+05	3400	Pandis and Seinfeld, 1989
12	$CH_3O_2 + HO_2 \Rightarrow CH3OOH$	4.3E+05	3000	Jacob, 1986

13	$CH_3O_2 + O_2^- \Rightarrow$ CH3OOH+ OH-	5.0E+07	1600	Jacob, 1986
14	$CH_3OOH + hv \Rightarrow HCHO + OH + HO_2$	5.0E-4*j_{NO2}		Pandis and Seinfeld, 1989
15	CH3OOH + OH => CH3O2	2.7E+07	1700	Jacob, 1986
16	CH3OH + OH => $HCHO + HO_2$	4.5E+06	1500	Pandis and Seinfeld, 1989
17	$CH3OH + CO3^- \Rightarrow HCHO + HO_2 + HCO3^-$	2.6E+03	4500	Pandis and Seinfeld, 1989
18	CH3OOH + OH => HCHO + OH	1.9E+07	1800	Jacob, 1986
19	$CH3OH + NO_3 \Rightarrow NO_3^- + H^+ + HCHO + HO_2$	1.0E+06	2800	Pandis and Seinfeld, 1989
20	MGLY + OH => 0.92 PRV +0.08 GLYAC + $H_2O + HO_2$	1.1E+09	1600	Ervens et al. (2004)
21	PRV + OH => CH3C(O)OH + HO_2 + CO_2	1.2E+08	2766	Lim et al. (2005)
22	PRV- + OH => CH3COO- + HO_2 + CO_2	7.0E+08	2285	Lim et al. (2005)
23	CH3COO- + OH => 0.85GLYAC- + 0.15 HCOO-	1.9E+09	1800	Lim et al. (2005)
24	CH3COOH + OH => 0.85GLYAC + 0.15 HCOOH	1.5E+07	1800	Lim et al. (2005)
25	GLYX + OH => 0.03GLYAC +0.97 OXLAC	3.1E+09		Lumped reactions based on Carlton et al. (2007)
26	GLYC + OH => GLYX + HO_2	1.0E+09	1564	Lim et al. (2005)
27	GLYC +OH => GLYAC + $2HO_2$	5.0E+08	1564	Lim et al. (2005)
28	$GLYC + NO_3 \Rightarrow GLYAC + HO_2 + NO_3$-	1.1E+07		Herrmann et al. (2005)
29	$GLYC + NO_3 \Rightarrow GLYX + NO_3$- $+H_2O$	5.5E+06		Herrmann (2003)
30	$GLYX + NO_3 \Rightarrow GLYAC + NO_3$- + HO_2	6.3E+07		The same as for MGLY+NO3
31	$MGLY + NO_3 \Rightarrow$ 0.92 PRV +0.08 GLYAC + NO_3- + HO_2	6.3E+07		Herrmann et al. (2005)

32	PRV + NO_3 => CH3COOH + HO2 +CO_2 + NO_3-	4.8E+06		Herrmann et al. (2005)
33	PRV- + NO_3 => CH3COO- + HO_2 + CO_2 + NO_3-	4.8E+06		Herrmann et al. (2005)
34	GLYAC + NO_3 => OXLAC + HO_2 + NO_3-	3.0E+06		The same as glyxolic acid from Herrmann et al. (2005)
35	GLYAC- + NO_3 => OXLAC- + HO_2 + NO_3-	1.1E+08		The same as glyxolic acid from Herrmann et al. (2005)
36	OXLAC + NO_3 => 2CO_2 + NO_3-	6.8E+07		The same as OLAC- + NO_3
37	OXLAC- + NO_3 => 2CO_2 + NO_3-	6.8E+07		Herrmann et al. (2000)
38	OXLAC= + NO_3 => 2CO_2 + NO_3-	2.2E+08		Herrmann et al. (2000)

Table S4. Organic chemistry in aerosol water adopted from Ervens and Volkamer (2010)

Reaction Number	Aqueous phase Reactions	K_{298} (M^nS^{-1})	E/R (K)	References
1	GLYX + H_2O => GLYX_MH	7		Creighton et al., 1988
2	GLYX_MH=> GLYX	2.0E-2		Creighton et al., 1988
3	GLYX_MH + H2O =>GLYX_DH	4.0		Ervens and Volkamer, 2010
4	GLYX_DH=>GLYX_MH	2.0E-2		Ervens and Volkamer, 2010
5	GLYX+GLYX_MH=>GLYOLI	1.0E+2		Ervens and Volkamer, 2010
6	GLYOLI=>GLYX+GLYX_MH	5.556		Ervens and Volkamer, 2010
7	GLYX_MH+GLYX_MH=>GLYOLI	1.0E+2		Ervens and Volkamer, 2010

8	GLYOLI=>GLYX_MH+GLYX_MH	5.556		Ervens and Volkamer, 2010
9	GLYX_DH+GLYX_MH=>GLYOLI	1.0E+2		Ervens and Volkamer, 2010
10	GLYOLI=>GLYX_DH+GLYX_MH	5.556		Ervens and Volkamer, 2010
11	GLYX_DH=>GLYOLI	$0.8\ s^{-1} < k < 7 s^{-1}$		k scales with OH concentration with highest value at $[OH]=10^7\ cm^{-3}$ (Ervens and Volkamer, 2010)
12	GLYX_MH=>GLYOLI	$0.8\ s^{-1} < k < 7 s^{-1}$		k scales with OH concentration with highest value at $[OH]=10^7\ cm^{-3}$ (Ervens and Volkamer, 2010)
13	GLYX =>GLYOLI	$0.8\ s^{-1} < k < 7 s^{-1}$		k scales with OH concentration with highest value at $[OH]=10^7\ cm^{-3}$ (Ervens and Volkamer, 2010)
14	MGLY+ H2O => MGLY_MH	1.1E+1		Creighton et al., 1988
15	MGLY_MH => MGLY	2.0E-2		Creighton et al., 1988
16	MGLY_MH => MGLY_DH	9.6E-2		
17	MGLY_DH => MGLY_MH	2.0E-2		Assuming the same as monohydrate
18	MGLY +MGLY_MH => MGLOLI	1.0E2		Assuming the same as glyoxal
19	MGLOLI => MGLY_MH + MGLY	5.556E0		Assuming the same as glyoxal
20	MGLY_MH + MGLY_MH => MGLOLI	1.0E+2		Assuming the same as glyoxal
21	MGLOLI => MGLY_MH + MGLY_MH	5.556E0		Assuming the same as glyoxal

22	MGLY_DH + MGLY_MH => MGLOLI	1.0E+2		Assuming the same as glyoxal
23	MGLOLI => MGLY_MH + MGLY_DH	5.556E0		Assuming the same as glyoxal
24	MGLY_DH => MGLOLI	4.0		Ervens et al., 2011
25	MGLY_MH => MGLOLI	4.0		Ervens et al., 2011
26	MGLY => MGLOLI	4.0		Ervens et al., 2011
27	MGLY+ H2O => MGLY_MH	1.1E+1		Creighton et al., 1988
28	MGLY_MH => MGLY	2.0E-2		Creighton et al., 1988
29	MGLY_MH => MGLY_DH	9.6E-2		
30	MGLY_DH => MGLY_MH	2.0E-2		Assuming the same as monohydrate
31	MGLY +MGLY_MH => MGLOLI	1.0E2		Assuming the same as glyoxal
32	MGLOLI => MGLY_MH + MGLY	5.556E0		Assuming the same as glyoxal
33	MGLY_MH + MGLY_MH => MGLOLI	1.0E+2		Assuming the same as glyoxal
34	MGLOLI => MGLY_MH + MGLY_MH	5.556E0		Assuming the same as glyoxal
35	MGLY_DH + MGLY_MH => MGLOLI	1.0E+2		Assuming the same as glyoxal
36	GLYX+OH=> GLYAC+HO_2	1.1E+09	1564	Lim et al. (2005)
37	GLYAC+OH=>OXLAC+H_2O	3.62E+08	962	Herrmann (2003)
38	GLYAC- + OH => OXLAC- + H_2O	2.8E+09	4330	Herrmann (2003)
39	OXLAC +OH => $2CO_2$ + $2H_2O$	1.4E+06		Lim et al. (2005)
40	OXLAC- + OH => $2CO_2$ + 2 H_2O	4.7E+07		Lim et al. (2005)
41	OXLAC= + OH => $2CO_2$ + $2H_2O$	7.7E+06		Lim et al. (2005)
42	$H_2C(OH)_2$ + OH => HCOOH + HO_2	2.0E+09	1500	Pandis and Seinfeld, 1989
43	$HCOO^-$ + NO_3 => NO_3^- + CO_2 + HO_2	6.0E+07	1500	Jacob, 1986

44	$HCOOH + O_3 \Rightarrow CO_2 + HO_2 + OH$	5.0E+00	0	Pandis and Seinfeld, 1989
45	$HCOO^- + O_3 \Rightarrow CO_2 + OH + O_2^-$	1.0E+02	0	Pandis and Seinfeld, 1989
46	$HCOO^- + CO_3^- \Rightarrow CO_2 + HCO_3^- + HO_2 + OH^-$	1.1E+05	3400	Pandis and Seinfeld, 1989
47	$CH_3O_2 + HO_2 \Rightarrow CH3OOH$	4.3E+05	3000	Jacob, 1986
48	$CH_3O_2 + O_2^- \Rightarrow CH3OOH + OH^-$	5.0E+07	1600	Jacob, 1986
49	$CH_3OOH + hv \Rightarrow HCHO + OH + HO_2$	$5.0E\text{-}4 * j_{NO2}$		Pandis and Seinfeld, 1989
50	$CH3OOH + OH \Rightarrow CH3O2$	2.7E+07	1700	Jacob, 1986
51	$CH3OH + OH \Rightarrow HCHO + HO_2$	4.5E+06	1500	Pandis and Seinfeld, 1989
52	$CH3OH + CO3^- \Rightarrow HCHO + HO_2 + HCO3^-$	2.6E+03	4500	Pandis and Seinfeld, 1989
53	$CH3OOH + OH \Rightarrow HCHO + OH$	1.9E+07	1800	Jacob, 1986
54	$CH3OH + NO_3 \Rightarrow NO_3^- + H^+ + HCHO + HO_2$	1.0E+06	2800	Pandis and Seinfeld, 1989
55	$MGLY + OH \Rightarrow 0.92\ PRV + 0.08\ GLYAC + H_2O + HO_2$	1.1E+09	1600	Ervens et al. (2004)
56	$PRV + OH \Rightarrow CH3C(O)OH + HO_2 + CO_2$	1.2E+08	2766	Lim et al. (2005)
57	$PRV^- + OH \Rightarrow CH3COO^- + HO_2 + CO_2$	7.0E+08	2285	Lim et al. (2005)
58	$CH3COO^- + OH \Rightarrow 0.85GLYAC^- + 0.15\ HCOO^-$	1.9E+09	1800	Lim et al. (2005)
59	$CH3COOH + OH \Rightarrow 0.85GLYAC + 0.15\ HCOOH$	1.5E+07	1800	Lim et al. (2005)
60	$GLYX + OH \Rightarrow 0.03GLYAC + 0.97\ OXLAC$	3.1E+09		Lumped reactions based on Carlton et al. (2007)
61	$GLYC + OH \Rightarrow GLYX + HO_2$	1.0E+09	1564	Lim et al. (2005)
62	$GLYC + OH \Rightarrow GLYAC + 2HO_2$	5.0E+08	1564	Lim et al. (2005)
63	$GLYC + NO_3 \Rightarrow GLYAC + HO_2 + NO_3^-$	1.1E+07		Herrmann et al. (2005)

64	GLYC + NO_3 => GLYX + NO_3- +H_2O	5.5E+06		Herrmann (2003)
65	GLYX + NO_3 => GLYAC + NO_3- + HO_2	6.3E+07		The same as for MGLY+NO3
66	MGLY + NO_3 => 0.92 PRV +0.08 GLYAC + NO_3- + HO_2	6.3E+07		Herrmann et al. (2005)
67	PRV + NO_3 => CH3COOH + HO2 +CO_2 + NO_3-	4.8E+06		Herrmann et al. (2005)
68	PRV- + NO_3 => CH3COO- + HO_2 + CO_2 + NO_3-	4.8E+06		Herrmann et al. (2005)
69	GLYAC + NO_3 => OXLAC + HO_2 + NO_3-	3.0E+06		The same as glyxolic acid from Herrmann et al. (2005)
70	GLYAC- + NO_3 => OXLAC- + HO_2 + NO_3-	1.1E+08		The same as glyxolic acid from Herrmann et al. (2005)
71	OXLAC + NO_3 => 2CO_2 + NO_3-	6.8E+07		The same as OLAC- + NO_3
72	OXLAC- + NO_3 => 2CO_2 + NO_3-	6.8E+07		Herrmann et al. (2000)
73	OXLAC= + NO_3 => 2CO_2 + NO_3-	2.2E+08		Herrmann et al. (2000)

Table S5. Organic chemistry in cloud water and aerosol water adopted from Lim et al. (2010), which is used in Case 3

Reaction Number	Aqueous phase Reactions	K_{298} (M^nS^{-1})	E/R (K)	References
1	GLYX + OH => GLYXr *+ H_2O	1.1E+09	1564	Tan et al., 2009
2	GLYXr +O_2 => GLYXOOr	1.0E+06	0	Guzman et al., 2006
3	GLYXOOr => GLYAC + HO_2	5.0E+01	0	Carlter et al., 1979
4	GLYXOOr* + GLYXOOr => 2HFALDr + 2CO_2 + O_2 + 2HO_2	3.0E+08	0	Lim et al., 2010

5	HFALDr + O_2 => ACOL + HO_2	5.0E+06	0	Lim et al., 2010
6	HFALDr + GLYXr => C3D	1.3E+09	0	Guzman et al., 2006
7	GLYXr + GLYXr => TA	1.3E+09	0	Guzman et al., 2006
8	GLYAC + OH => GLYACr +H_2O	3.62E+08	962	Tan et al., 2009
9	GLYACr + O_2 => GACO2r	1.0E+06	0	Guzman et al., 2006
10	GACO2r => OXLAC + HO_2	5.0E+01	0	Carlter et al., 1979
11	GACO2r + GACO2r => 2CO_2 + HCOOHr	3.0E+08	0	Lim et al., 2010
12	HCOOHr + O_2 => CO_2 + HO_2	5.0E+06	0	Guzman et al., 2006
13	HCOOHr + GLYXr => C3D	1.3E+09	0	Guzman et al., 2006
14	HFALDr + GLYXr => C3D	1.3E+09	0	Guzman et al., 2006
15	GLYACr + GLYACr => C4D	1.3E+09	0	Guzman et al., 2006
16	GLYAC- + OH => GLYACr-	2.8E+09	4330	Tan et al., 2009
17	GLYACr+ GLYXr => C4D	1.3E+09	0	Guzman et al., 2006
18	GLYACr- + GLYXr => C4D	1.3E+09	0	Guzman et al., 2006
19	GLYACr- + GLYACr => C4D	1.3E+09	0	Guzman et al., 2006
20	GLYACr-+ GLYACr- => C3D	1.3E+09	0	Guzman et al., 2006
21	GLYACr- + HCOOHr => C3D	1.3E+09	0	Guzman et al., 2006
22	GLYACr- + HFALDr => C3D	1.3E+09	0	Guzman et al., 2006
23	GLYACr- + O_2 => GACO2r-	1.0E+06	0	Guzman et al., 2006

24	GACO2r- => OXLAC-	1.0E+02	0	Lim et al., 2010
25	GACO2r- + GACO2r- => $2CO_2$- + 2HCOOHr	3.0E+08	0	Lim et al., 2010
26	OXLAC + OH => HCOOHr + CO_2 + $2H_2O$	1.4E+06	2766	Tan et al., 2009
27	OXLAC- + OH => HCOOHr + CO_2- + $2H_2O$	1.9E+08	2766	Tan et al., 2009
28	OXLAC-2 + OH => HCOOHr + CO_2- + 2 H_2O	1.6E+08	4330	Tan et al., 2009
29	CO_2- + O_2 => O_2- + CO_2	2.4E+09	0	Tan et al., 2009
30	GLYAC + H_2O_2 => ACOL + CO_2 + H_2O	3.0E-01	0	Tan et al., 2009
31	ACOL + OH => HCOOHr + H_2O	1.0E+08	0	Tan et al., 2009
32	HCOO- + OH => CO_2- + H_2O	2.4E+09	0	Tan et al., 2009
33	O_2- + OH => OH- + O_2	1.0E+10	0	Tan et al., 2009
34	HCOO- + OH => CO_2- + H_2O	1.0E+07	0	Tan et al., 2009
35	CO_2- + O_2- => CO_2= + O2	6.5E+08	0	Tan et al., 2009
36	CO_3- + HCOO- => HCO_3- + CO_2-	1.5E+5	0	Tan et al., 2009
37	CO_3- +H_2O_2 => HCO_3- + HO_2	8.0E+05	0	Tan et al., 2009
38	C3D + OH => C3Dr + H2O	3.0E+08	0	Lim et al., 2010
39	C3Dr + O_2 => C3DOOr	1.0E+06	0	Lim et al., 2010
40	C3DOOr => HO_2	5.0E+01	0	Carlter et al., 1979
41	C3DOOr => 2HCOOHr + 2GLYAC	3.0E+08	0	Lim et al., 2010
42	C4D + OH => C4Dr + H_2O	1.1E+08	0	Ervens et al., 2003
43	C4Dr + O_2 => C4DOOr	1.0E+06	0	Guzman et al., 2006
44	C4DOOr => HO_2	5.0E+01	0	Carlter et al., 1979
45	C4DOOr + C4DOOr => 2GLYAC	3.0E+08	0	Lim et al., 2010
46	HFALDr + HFALDr => GLYX	1.3E+09		Guzman et al., 2006

47	HFALDr + HCOOHr => GLYAC	1.3E+09		Guzman et al., 2006
48	HCOOHr +HCOOHr => OXLAC	1.3E+09	0	Guzman et al., 2006
49	CO_2- + HCOOHr => OXLAC-	1.3E+09	0	Guzman et al., 2006
50	CO_2- + CO_2- => OXLAC=	1.3E+09	0	Guzman et al., 2006
51	C3D => MA	1.0E-03	0	Tan et al., 2009
52	MA => C3D	5.556E-07	0	Tan et al., 2009
53	MA + OH => C3Dr + H_2O	1.6E+08	0	Ervens et al., 2003
54	TA +OH => C4Dr + H_2O	3.1E+08	0	Monod et al., 2005; 2008

*: r= radical. For example, GLYXr = glyoxal radical; OOr = peroxy radical.

Table S6. Fe chemistry in cloud used in Case 5

Reaction Number	Aqueous phase Reactions	K_{298} (M^nS^{-1})	E/R (K)	References
1	H_2O_2+ Fe^{2+} => Fe^{3+} + OH + OH^-	52.4	5050	Deguillaume et al. (2010)
2	H_2O_2 + FeO^{2+} => Fe^{3+} + HO_2 + OH^-	9.5E+03	2800	Deguillaume et al. (2010)
3	O_2^- + Fe^{2+} + $2H^+$ => H_2O_2 + Fe^{3+}	1.0E+07		Deguillaume et al. (2010)
4	O_2^- + Fe^{3+} => Fe^{2+} + O_2	1.5E+08		Deguillaume et al. (2010)
5	O_2^- + $[Fe(OH)]^{2+}$ => Fe^{2+} + O_2 + OH^-	1.5E+08		Deguillaume et al. (2010)
6	O_2^- + $[Fe(OH)_2]^+$ => Fe^{2+} + O_2 + $2OH^-$	1.5E+08		Deguillaume et al. (2010)
7	HO_2 + Fe^{2+} + H^+ => Fe^{3+} + H_2O_2	1.2E+06	5050	Deguillaume et al. (2010)
8	HO_2 + FeO^{2+} => Fe^{3+} +O_2 + OH^-	2.0E+06		Deguillaume et al. (2010)

9	$OH + Fe^{2+} => [Fe(OH)]^{2+}$	4.6E+08	1100	Deguillaume et al. (2010)
10	$OH + FeO^{2+} + H^{+} => Fe^{3+} H_2O_2$	1.0E+07		Deguillaume et al. (2010)
11	$O_3 + Fe^{2+} => FeO^{2+} + O_2$	8.2E+05		Deguillaume et al. (2010)
12	$FeO^{2+} + H_2O => Fe^{3+} + OH + OH^{-}$	1.3E-02	4100	Deguillaume et al. (2010)
13	$FeO^{2+} + Fe^{2+} + H_2O => 2Fe^{3+} + 2OH^{-}$	7.2E+04	840	Deguillaume et al. (2010)
14	$FeO^{2+} + Fe^{2+} + H_2O => Fe(OH)_2Fe^{4+}$	1.8E+04	5050	Deguillaume et al. (2010)
15	$Fe(OH)_2Fe^{4+} => 2Fe^{3+} + 2OH^{-}$	0.49	8800	Deguillaume et al. (2010)
16	$Fe(OH)_2Fe^{4+} + 2H^{+} => 2Fe^{3+} + 2H_2O$	2	5650	Deguillaume et al. (2010)
17	$NO_3 + Fe^{2+} => Fe^{3+} + NO_3^{-}$	8.0E+06		Deguillaume et al. (2010)
18	$NO_2 + Fe^{2+} => Fe^{3+} + NO_2^{-}$	3.1E+04		Deguillaume et al. (2010)
19	$HNO_2 + FeO^{2+} => Fe^{3+} + NO_2 + OH^{-}$	1.1E+04	4150	Deguillaume et al. (2010)
20	$NO_2^{-} + FeO^{2+} + H^{+} => Fe^{3+} NO_2 + OH^{-}$	1.0E+05		Deguillaume et al. (2010)
21	$HSO_3^{-} + [Fe(OH)]^{2+} => Fe^{2+} + SO_3^{-} + H_2O$	30		Deguillaume et al. (2010)
22	$SO_5^{-} + Fe^{2+} H_2O => [Fe(OH)]^{2+} + HSO_5^{-}$	2.65E+07		Deguillaume et al. (2010)
23	$HSO_5^{-} + Fe^{2+} => [Fe(OH)]^{2+} + SO_4^{-}$	3.0E+04		Deguillaume et al. (2010)
24	$SO_4^{-} + Fe^{2+} + H_2O => [Fe(OH)]^{2+} + SO_4^{2-} + H^{+}$	4.1E+09	-2165	Deguillaume et al. (2010)
25	$O^{2-} + [Fe(SO_4)]^{+} => Fe^{2+} + SO_4^{2-} + O_2$	1.5E+08		Deguillaume et al. (2010)
26	$HSO^{3-} + FeO^{2+} => Fe^{3+} + SO^{3-} + OH^{-}$	2.5E+05		Deguillaume et al. (2010)
27	$HCOOH + FeO^{2+} + O_2 + H^{+} => Fe^{3+} + CO_2 + HO_2 + H_2O$	160	2680	Deguillaume et al. (2010)
28	$HCOO^{-} + FeO^{2+} + O_2 + H^{+} =>$	3.0E+05		Deguillaume et al. (2010)

	$Fe^{3+} + CO_2 + HO_2 + OH-$			
29	$CH_2(OH)_2 + FeO^{2+} + O_2 \Rightarrow Fe^{3+} + HCOOH + HO_2 + OH^-$	400	5350	Deguillaume et al. (2010)
30	$CO_3^- + Fe^{2+} \Rightarrow Fe^{3+} + CO_3^{2-}$	2.0E+07		Deguillaume et al. (2010)
31	$CH_3O_2 + Fe^{2+} \Rightarrow CH_3O_2Fe^{2+}$	8.6E+05		Deguillaume et al. (2010)
32	$CH_3O_2Fe^{2+} \Rightarrow CH_3O_2 + Fe^{2+}$	1.3E+03		Deguillaume et al. (2010)
33	$CH_3O_2Fe^{2+} + H_2O \Rightarrow Fe^{3+} + CH_3OOH + OH^-$	100		Deguillaume et al. (2010)
34	$CH_3O_2Fe^{2+} + H^+ \Rightarrow Fe^{3+} + CH_3OOH$	3.0E+04		Deguillaume et al. (2010)
35	$Fe^{3+} + SO_4^{2-} \Rightarrow [Fe(SO_4)]^+$	3.2E+03		Deguillaume et al. (2010)
36	$[Fe(SO_4)]^+ \Rightarrow Fe^{3+} + SO_4^{2-}$	27		Deguillaume et al. (2010)
37	$[Fe(C_2O_4)]^+ \Rightarrow Fe^{3+} + C_2O_4^{2-}$	3.0E-03		Ervens et al. (2003)
38	$Fe^{3+} + C_2O_4^{2-} \Rightarrow [Fe(C_2O_4)]^+$	7.5E+06		Ervens et al. (2003)
39	$[Fe(C_2O_4)_2]^- \Rightarrow [Fe(C_2O_4)]^+ + C_2O_4^{2-}$	3.0E-03		Ervens et al. (2003)
40	$[Fe(C_2O_4)]^+ + C_2O_4^{2-} \Rightarrow [Fe(C_2O_4)_2]^-$	1.89E+04		Ervens et al. (2003)
41	$[Fe(OH)]^{2+} + hv \Rightarrow Fe^{2+} + OH$	$263*J_{NO2-}$		Based on the photolysis rate given by Ervens et al. (2003)
42	$[Fe(OH)_2]^+ + hv \Rightarrow Fe^{2+} + OH + OH^-$	$336*J_{NO2-}$		Based on the photolysis rate given by Ervens et al. (2003)
43	$[Fe(SO_4)]^+ + hv \Rightarrow Fe^{2+} + SO_4^-$	$375*J_{NO2-}$		Based on the photolysis rate given by Ervens et al. (2003)
44	$[Fe(C_2O_4)_2]- + hv \Rightarrow Fe2+ + C_2O_4^{2-} + C_2O_4^-$			

Table S7. Henry's law constant

Species	H_{298} (mol L^{-1} atm^{-1})	ΔH/R (K)	Mass accommodation coefficient	References
CO_2	3.4E-02	-2420	5.0E-2	Pandis and Seinfeld, 1989
GLYX	4.19E+05*	7481	2.3E-2	Ip et al., 2009
MGLY	3.7E+03*	7481	2.3E-2	Lim et al., 2005
OH	3.0E+1	4500	5.0E-2	Lim et al., 2005
HO_2	4.6E3	4800	1.0E-2	Lim et al., 2005
H_2O_2	8.6E4	6500	1.1E-1	Lim et al., 2005
GLYAC	1.09E4	4811	1.9E-2	Ip et al., 2009
OXLAC	3.26E6		1.9E-2	Lim et al., 2009
HNO_3	2.1E5		5.0E-2	Pandis and Seinfeld, 1989
O_3	1.03E-2	2300	5.3E-4	Lelieveld, 1991, Sander, 1996
NO_2	1.0E-2	2500	6.3E-4	Pandis and Seinfeld, 1989
NO	1.9E-3	1480	5.0E-3	Pandis and Seinfeld, 1989
CH_3O_2	6.0E0	5600	5.0E-2	Pandis and Seinfeld, 1989
HCHO	6.3E3	6460	5.0E-2	Pandis and Seinfeld, 1989
HCOOH	3.5E3	5740	5.0E-2	Pandis and Seinfeld, 1989
CH_3OOH	2.27E2	5610	5.0E-2	Pandis and Seinfeld, 1989
NO_3	2.1E5	8700	1.0E-3	Pandis and Seinfeld, 1989
HONO	5.1E-4	-1260	5.0E-2	Pandis and Seinfeld, 1989

CH_3OH	2.2E2	4900	5.0E-2	Pandis and Seinfeld, 1989
PAN	2.9E0	5910	5.0E-2	Pandis and Seinfeld, 1989
CH_3CO_3	1.0E2		5.0E-2	Pandis and Seinfeld, 1989
CH_3CHO	1.14E+01	6460	5.0E-2	Hermann, 2000
CH_3COOH	3.5E3	5740	5.0E-2	Pandis and Seinfeld, 1989
PRV	3.09E5		1.9E-2	Lim et al., 2005
GLYC	4.10E4	4600	2.3E-2	Lim et al., 2005
SO2	1.23E0	3120	5.0E-2	Pandis and Seinfeld, 1989

*: when using the organic chemistry in aerosol water adopted from Ervens and Volkamer (2010), the Henry's law constant for glyoxal and methylglyoxal is 5.8 and 1.4.

Table S8. Aqueous equilibrium coefficients

Reaction number	Reactions	K_{aq298}	ΔH/R	Reference
1	$CO_2 = H^+ + HCO_3^-$	4.46E-07	1000	Pandis and Seinfeld, 1989
2	$HCO_3^- = H^+ + CO_3^{-2}$	4.68E-11	1760	Pandis and Seinfeld, 1989
3	$SO_2 = H^+ + HSO_3^-$	1.23E-02	1960	Pandis and Seinfeld, 1989
4	$HSO_3 = H^+ + SO_3^{-2}$	6.61E-08	-1500	Sander, 1996
5	$H_2SO_4 = H^+ + HSO4^-$	1.0E+03		Pandis and Seinfeld, 1989
6	$HSO4^- = H^+ + SO_4^{2-}$	1.02E-02	-2720	Pandis and Seinfeld, 1989
7	$H_2O_2 = H^+ + HO_2^-$	2.2E-12	3730	Pandis and Seinfeld, 1989
8	$HO_2 = H^+ + O2^-$	3.5E-05		
9	$HNO_3 = H^+ + NO_3^-$	1.54E+01	-8700	Pandis and Seinfeld, 1989

10	$HONO = H^+ + NO_2^-$	5.1E-04	1260	Pandis and Seinfeld, 1989
11	$NH_3 = OH^- + NH_4^+$	1.7E-05	-4325	Pandis and Seinfeld, 1989
12	$HCHO + H_2O = H_2C(OH)_2$	1.82E+03	-4020	Pandis and Seinfeld, 1989; Sander, 2004
13	$HCOOH = H^+ + HCOO-$	1.78E-04	20	Pandis and Seinfeld, 1989
14	$CH_3C(O)OOH = H^+ + CH3C(O)OO^-$	1.78E-04	0	Assumed equal to HCOOH
15	$CH3COOH = H^+ + CH3COO^-$	1.75E-05	0	Hermann, 2000
16	$GLYAC = GLYAC^- + H^+$	3.47E-04	267	Lim et al. 2005
17	$OXLAC = OXLAC^- + H^+$	5.60E-02	453	Lim et al. 2005
18	$OXLAC^- = OXLAC^{2-} + H^+$	5.42E-02	805	Lim et al. 2005
19	$PRV = PRV^- + H^+$	3.20E-03	0	Lim et al. 2005
20	$Fe^{3+} = Fe(OH)^{2+} + H^+$	1.10E-04	0	Ervens et al. (2003)
21	$Fe(OH)^{2+} = Fe(OH)_2^+ + H^+$	1.4E-07	0	Ervens et al. (2003)
22	$Fe^{2+} = Fe(OH)^+ + H^+$	3.22E-10	0	Deguillaume et al. (2005)

Reference

Barth, M. C., Sillman, S., Hudman, R., Jacobson, M. Z., Kim, C.-H., Monod, A., Liang, J.: Summary of the cloud chemistry modeling intercomparison: Photochemical box model simulation, J. Geophys. Res., 108, 4214, doi:10.1029/2002JD002673, 2003.

Carlton, A. G., Turpin, B. J., Altieri, K. E., Seitzinger, S., Reff, A., Lim, H. J. and Ervens, B.: Atmospheric oxalic acid and SOA production from glyoxal: Results of aqueous photooxidation experiments, Atmospheric Environment, 41(35), 7588–7602, doi:10.1016/j.atmosenv.2007.05.035, 2007.

Carter, W. P. L., Darnall, K. R., Graham, R. A., Winer, A. M., and Pittts, Jr., J.: Reactions of C2 and C4 α–Hydroxy radicals with Oxygen, J. Phys. Chem., 83, 2305-2311, 1979

Creighton, D. J., Migliorini, M., Pourmotabbed, T., and Guha, M. K.: Optimization of efficieny in the glyoxylase pathway, Biochem., 27, 7376–7384, 1988.

Deguillaume, L., Leriche, M. and Desboeufs, K.: Transition metals in atmospheric liquid phases: Sources, reactivity, and sensitive parameters, Chemical Reviews-Columbus, 105,

3388-3431, 2005.

Deguillaume, L., Desboeufs, K. V., Leriche, M., Long, Y., & Chaumerliac, N.: Effect of iron dissolution on cloud chemistry: from laboratory measurements to model results, Atmos. Pollut. Res, *1*(4), 220-228, 2010.

Ervens, B.: CAPRAM 2.4 (MODAC mechanism): An extended and condensed tropospheric aqueous phase mechanism and its application, J. Geophys. Res., 108(D14), 4426–, doi:10.1029/2002JD002202, 2003.

Ervens, B. and Volkamer, R.: Glyoxal processing by aerosol multiphase chemistry: towards a kinetic modeling framework of secondary organic aerosol formation in aqueous particles, Atmos. Chem. Phys., 10(17), 8219–8244, doi:10.5194/acp-10-8219-2010, 2010.

Ervens, B., Turpin, B. J. and Weber, R. J.: Secondary organic aerosol formation in cloud droplets and aqueous particles (aqSOA): a review of laboratory, field and model studies, Atmos. Chem. Phys., 11(21), 11069–11102, doi:10.5194/acp-11-11069-2011, 2011.

Guzman, M. I., Colussi, A. J., and Hoffman, M. R.: Photoinduced oligomerization of aqueous pyruvic acid. J. Phys. Chem. A., 110, 3619-3626, 2006.

Jacob, D. J.: Chemistry of OH in remote clouds and its role in the production of formic acid and peroxymonosulfate, J. Geophys. Res., 1986.

Lelieveld, J. and Crutzen, P. J.: The role of clouds in tropospheric photochemistry, J Atmos Chem, 12(3), 229–267, doi:10.1007/BF00048075, 1991.

Ip, H. S. S., Huang, X. H. H., Yu, J. Z.: Effective Henry's law constants of glyoxal, glyoxylic acid, and glycolic acid, Geophys. Res. Lett., 36, L01802, doi:10.1029/2008GL036212, 2009.

Lim, H. J., Carlton, A. G., and Turpin, B. J.: Isoprene forms secondary organic aerosol through cloud processing: Model simulations, Environ. Sci. Technol., 39, 4441–4446, 2005.

Liu, X., G. Mauersberger and Moeller D., The effects of cloud processes on the tropospheric photochemistry: an improvement of the EURAD model with a coupled gaseous and aqueous chemical mechanism. Atmospheric Environment. 31, 3119-3135, 1997.

Monod, A., Poulain, L., Grubert, S., Voisin, D., and Wortham, H.: Kinetics of OH-initiated oxidation of oxygenated organic compounds in the aqueous phase: new rate constants, structure-activity relationship and atmospheric implications, Atmos. Environ., 39, 7667-7688, 2005.

Monod, A. and Doussin, J. F.: Structure-activity relationship for the estimation of OH-oxidation rate constants of aliphatic organic compounds in the aqueous phase: alkanes, alcohols, organic acids and bases, Atmos. Environ., 42, 7611-7622, 2008.

Pandis, S. N. and Seinfeld, J. H.: Sensitivity analysis of a chemical mechanism for aqueous-phase atmospheric chemistry, J. Geophys. Res., 94(D1), 1105, doi:10.1029/JD094iD01p01105, 1989.

Sander, R and P.J. Crutzen, Modelstudy indicating halogen activation and ozone destruction in polluted air massestransported to the sea, J. Geophys. Res., 101, 9121-9138, 1996.

Sander, S. P., Friedl R. R., D. M. Golden, M.J. Kurylo, R. E. Huie, V. L. Orkin, G. K. Moortgaat, A. R. Ravishankara, C. E. Kolb,M.J. Molina, and B.J. Finlayson-Pitts. Chemical kinetics and photochemical data for use in stratospheric modeling, Evaluation No. 14. JPL 02-25,Jet Propulsion Laboratory, NASA, 2003, available from http://jpldataeval.jpl.nasa.gov/. (Abbrev: JPL 2003).

Tan, Y., Perri, M. J., Seitzinger, S. P., and Turpin, B. J.: Effects of precursor concentration and acidic surfate in aqueous glyoxal-OH radical oxidation and implications for secondary organic aerosol, Environ. Sci. Technol, 43, 8105-8112, 2009.

Warneck P.: The relative importance of various pathways for the oxidation of sulfur dioxide and nitrogen dioxide in sunlit continental fair weather clouds, Phys. Chem. Chem. Phys., 1, 5471-5483, 1999.